

Summary of the  
Bulletin of the  
International Seismological Centre

2021

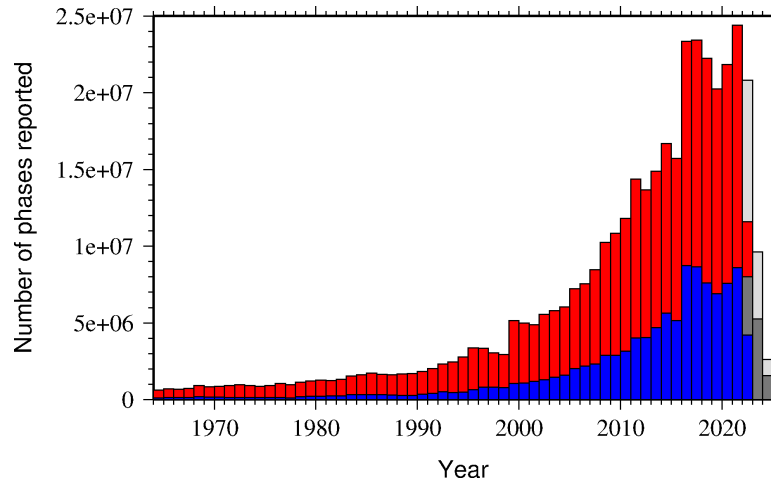
January – June

Volume 58 Issue I

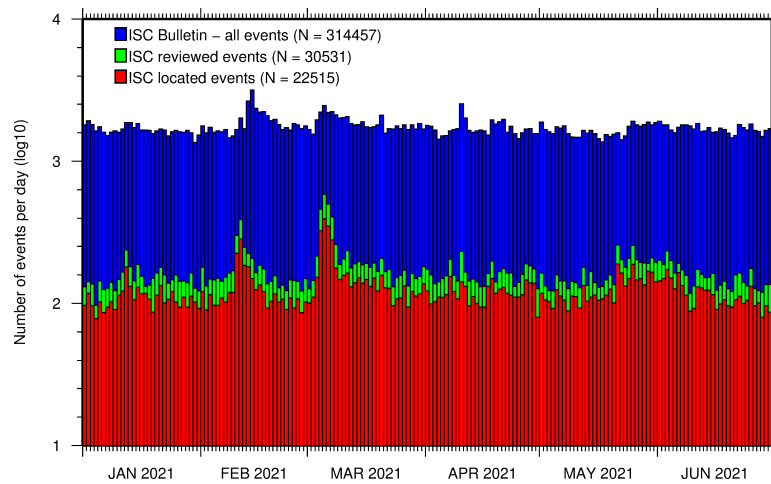
[www.isc.ac.uk](http://www.isc.ac.uk)

ISSN 2309-236X

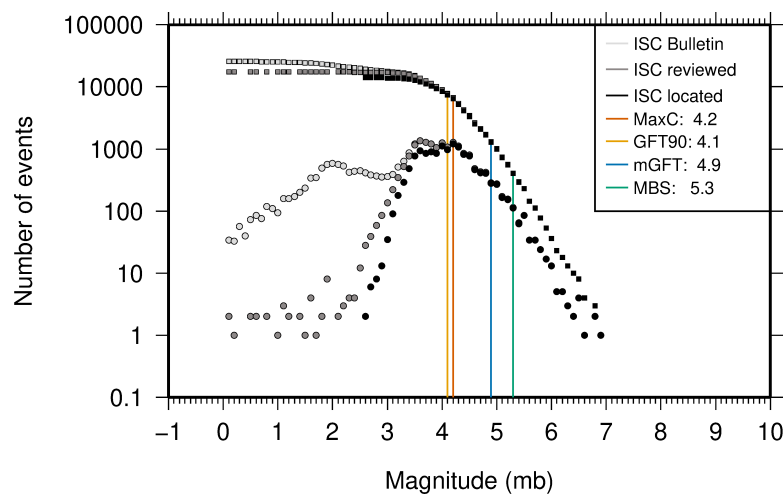
2024



The number of phases (red) and number of amplitudes (blue) collected by the ISC for events each year since 1964. The data in grey covers the current period where data are still being collected before the ISC review takes place and are accurate at the time of publication. See Section 7.3.



The number of events within the Bulletin for the current summary period. The vertical scale is logarithmic. See Section 8.1.



Frequency and cumulative frequency magnitude distribution for all events in the ISC Bulletin, ISC reviewed events and events located by the ISC. The magnitude of completeness ( $M_C$ ) is shown for the ISC Bulletin. Note: only events with values of  $m_b$  are represented in the figure. See Section 8.4.



# Summary of the Bulletin of the International Seismological Centre

2021

January - June

Volume 58 Issue I

Produced and edited by:

Kathrin Lieser, James Harris, Natalia Poiata and Dmitry Storchak



Published by  
International Seismological Centre

The International Seismological Centre (ISC) is a Charitable Incorporated Organization (CIO) registered with The Charity Commission for England and Wales. Registered charity number: 1188971.

## ISC Data Products

<http://www.isc.ac.uk/products/>

ISC Bulletin:

<http://www.isc.ac.uk/iscbulletin/search>

ISC Bulletin and Catalogue monthly files, to the last reviewed month in ISF2 format:

[http://download.isc.ac.uk/isf2/\[bulletin|catalogue\]/yyyy/yyyymm.gz](http://download.isc.ac.uk/isf2/[bulletin|catalogue]/yyyy/yyyymm.gz)

[ftp://www.isc.ac.uk/pub/isf2/\[bulletin|catalogue\]/yyyy/yyyymm.gz](ftp://www.isc.ac.uk/pub/isf2/[bulletin|catalogue]/yyyy/yyyymm.gz)

Datafiles for the ISC data before the rebuild in isf or ffb formats:

[http://download.isc.ac.uk/prerebuild/\[isf|ffb\]/\[bulletin|catalogue\]/yyyy/yyyymm.gz](http://download.isc.ac.uk/prerebuild/[isf|ffb]/[bulletin|catalogue]/yyyy/yyyymm.gz)

[ftp://www.isc.ac.uk/pub/prerebuild/\[isf|ffb\]/\[bulletin|catalogue\]/yyyy/yyyymm.gz](ftp://www.isc.ac.uk/pub/prerebuild/[isf|ffb]/[bulletin|catalogue]/yyyy/yyyymm.gz)

ISC-EHB Bulletin:

<http://www.isc.ac.uk/isc-ehb/search/>

IASPEI Reference Event List (GT bulletin):

<http://www.isc.ac.uk/gtevents/search/>

ISC-GEM Global Instrumental Earthquake Catalogue:

<http://www.isc.ac.uk/iscgem/download.php>

ISC Event Bibliography:

[http://www.isc.ac.uk/event\\_bibliography/bibsearch.php](http://www.isc.ac.uk/event_bibliography/bibsearch.php)

International Seismograph Station Registry:

<http://www.isc.ac.uk/registries/search/>

Seismological Contacts:

<http://www.isc.ac.uk/projects/seismocontacts/>

Copyright © 2024 by International Seismological Centre

Permission granted to reproduce for personal and educational use only. Commercial copying, hiring, lending is prohibited.

International Seismological Centre

Pipers Lane

Thatcham

RG19 4NS

United Kingdom

[www.isc.ac.uk](http://www.isc.ac.uk)

The International Seismological Centre (ISC) is a Charitable Incorporated Organization (CIO) registered with The Charity Commission for England and Wales. Registered charity number: 1188971.

ISSN 2309-236X

Printed and bound in Wales by Cambrian Printers.

# Contents

<b>1</b>	<b>Preface</b>	<b>1</b>
<b>2</b>	<b>The International Seismological Centre</b>	<b>2</b>
2.1	The ISC Mandate . . . . .	2
2.2	Brief History of the ISC . . . . .	3
2.3	Former Directors of the ISC and its U.K. Predecessors . . . . .	4
2.4	Member Institutions of the ISC . . . . .	5
2.5	Sponsoring Organisations . . . . .	10
2.6	Data Contributing Agencies . . . . .	11
2.7	ISC Staff . . . . .	19
<b>3</b>	<b>Availability of the ISC Bulletin</b>	<b>24</b>
<b>4</b>	<b>Citing the International Seismological Centre</b>	<b>25</b>
4.1	The ISC Bulletin . . . . .	25
4.2	The Summary of the Bulletin of the ISC . . . . .	26
4.3	The historical printed ISC Bulletin (1964-2009) . . . . .	26
4.4	The IASPEI Reference Event List . . . . .	26
4.5	The ISC-GEM Catalogue . . . . .	26
4.6	The ISC-EHB Dataset . . . . .	28
4.7	The ISC Event Bibliography . . . . .	28
4.8	International Registry of Seismograph Stations . . . . .	28
4.9	Seismological Dataset Repository . . . . .	28
4.10	Data transcribed from ISC CD-ROMs/DVD-ROMs . . . . .	28
<b>5</b>	<b>Operational Procedures of Contributing Agencies</b>	<b>29</b>
5.1	Regional Seismological Observation Network in Yakutia . . . . .	29
5.1.1	Introduction . . . . .	29
5.1.2	A Brief History of Instrumental Seismological Observations in Yakutia . . . . .	30
5.1.3	Current Status of Instrumental Seismic Observations . . . . .	30
5.1.4	General Characteristics of the Observed Seismicity . . . . .	33
5.1.5	Future Seismological Observation Development Project . . . . .	36
5.1.6	Conclusion . . . . .	36
<b>6</b>	<b>Summary of Seismicity, January – June 2021</b>	<b>38</b>

---

<b>7</b>	<b>Statistics of Collected Data</b>	<b>44</b>
7.1	Introduction . . . . .	44
7.2	Summary of Agency Reports to the ISC . . . . .	44
7.3	Arrival Observations . . . . .	49
7.4	Hypocentres Collected . . . . .	56
7.5	Collection of Network Magnitude Data . . . . .	58
7.6	Moment Tensor Solutions . . . . .	64
7.7	Timing of Data Collection . . . . .	67
<b>8</b>	<b>Overview of the ISC Bulletin</b>	<b>69</b>
8.1	Events . . . . .	69
8.2	Seismic Phases and Travel-Time Residuals . . . . .	78
8.3	Seismic Wave Amplitudes and Periods . . . . .	83
8.4	Completeness of the ISC Bulletin . . . . .	86
8.5	Magnitude Comparisons . . . . .	87
<b>9</b>	<b>The Leading Data Contributors</b>	<b>91</b>
9.1	The Largest Data Contributors . . . . .	91
9.2	Contributors Reporting the Most Valuable Parameters . . . . .	94
9.3	The Most Consistent and Punctual Contributors . . . . .	99
<b>10</b>	<b>Appendix</b>	<b>100</b>
10.1	ISC Operational Procedures . . . . .	100
10.1.1	Introduction . . . . .	100
10.1.2	Data Collection . . . . .	100
10.1.3	ISC Automatic Procedures . . . . .	101
10.1.4	ISC Location Algorithm . . . . .	105
10.1.5	Review Process . . . . .	115
10.1.6	Probabilistic Point Source Model (ISC-PPSM) . . . . .	117
10.1.7	The use of Network code for Arrivals at the ISC and in ISCLoc . . . . .	118
10.1.8	History of Operational Changes . . . . .	119
10.2	IASPEI Standards . . . . .	120
10.2.1	Standard Nomenclature of Seismic Phases . . . . .	120
10.2.2	Flinn-Engdahl Regions . . . . .	128
10.2.3	IASPEI Magnitudes . . . . .	135
10.2.4	The IASPEI Seismic Format (ISF) . . . . .	139
10.2.5	Ground Truth (GT) Events . . . . .	141
10.2.6	Nomenclature of Event Types . . . . .	143
10.3	Tables . . . . .	144
<b>11</b>	<b>Glossary of ISC Terminology</b>	<b>162</b>

---

<b>12 Acknowledgements</b>	<b>166</b>
<b>References</b>	<b>167</b>

# 1

## Preface

This publication contains information on the ISC, its staff, Members, Sponsors and Data providers. It offers analysis of the data contributed to the ISC by many seismological agencies worldwide as well as analysis of the data in the ISC Bulletin itself. This issue also includes seismological standards and procedures used by the ISC in its operations.

I would like to reiterate here that all ISC hypocenter solutions (1964-present) are now based on the *ak135* velocity model and all ISC magnitudes (1964-present) are based on the latest robust procedures.

As part of the series covering the Data Reporters to the ISC, we included an invited article from the Yakutia Branch of the Geophysical Survey of the Russian Academy of Sciences on the history, current status and monitoring procedures.

We hope that you find this publication useful in your work. If your home-institution or company is unable, for one reason or another, to support the long-term international operations of the ISC in full by becoming a Member or a Sponsor, then, please, consider subscribing to this publication by contacting us at [admin@isc.ac.uk](mailto:admin@isc.ac.uk).

With kind regards to our Data Contributors, Members, Sponsors and users,

Dr Dmitry A. Storchak  
Director  
International Seismological Centre (ISC)

*The ISC is a Charitable Incorporated Organization (CIO) registered with The Charity Commission for England and Wales. Registered charity number: 1188971.*

## 2

# The International Seismological Centre

## 2.1 The ISC Mandate

The International Seismological Centre (ISC) was set up in 1964 with the assistance of UNESCO as a successor to the International Seismological Summary (ISS) to carry forward the pioneering work of Prof. John Milne, Sir Harold Jeffreys and other British scientists in collecting, archiving and processing seismic station and network bulletins and preparing and distributing the definitive summary of world seismicity.

Under the umbrella of the International Association of Seismology and Physics of the Earth Interior (IASPEI/IUGG), the ISC has played an important role in setting international standards such as the International Seismic Bulletin Format (ISF), the IASPEI Standard Seismic Phase List (SSPL) and both the old and New IASPEI Manual of the Seismological Observatory Practice (NMSOP-2) (<https://doi.org/10.2312/GFZ.NMSOP-2>).

The ISC has contributed to scientific research and prominent scientists such as John Hodgson, Eugene Herrin, Hal Thirlaway, Jack Oliver, Anton Hales, Ola Dahlman, Shigeji Suehiro, Nadia Kondorskaya, Vit Karnik, Stephan Müller, David Denham, Bob Engdahl, Adam Dziewonski, John Woodhouse and Guy Masters all considered it an important duty to serve on the ISC Executive Committee and the Governing Council.

The current mission of the ISC is to maintain:

- the ISC **Bulletin** – the longest continuous definitive summary of World seismicity (collaborating with 150 seismic networks and data centres around the world). ([www.isc.ac.uk/iscbulletin/](http://www.isc.ac.uk/iscbulletin/))
- the International Seismographic Station Registry (**IR**, jointly with the World Data Center for Seismology, Denver). ([www.isc.ac.uk/registries/](http://www.isc.ac.uk/registries/))
- the IASPEI Reference Event List (Ground Truth, **GT**, jointly with IASPEI). ([www.isc.ac.uk/gtevents/](http://www.isc.ac.uk/gtevents/))

These are fundamentally important tasks. Bulletin data produced, archived and distributed by the ISC for almost 60 years are the definitive source of such information and are used by thousands of seismologists worldwide for seismic hazard estimation, for tectonic studies and for regional and global imaging of the Earth's structure. Key information in global tomographic imaging is derived from the analysis of ISC data. The ISC Bulletin served as a major source of data for such well known products as the ak135 global 1-D velocity model and the ISC-EHB (*Engdahl et al.*, 2020; 1998; *Weston et al.*, 2018) and Centennial (*Engdahl and Villaseñor*, 2002) catalogues. It presents an important quality-control benchmark for the Comprehensive Nuclear-Test-Ban Treaty Organization (CTBTO). Hypocentre parameters from

the ISC Bulletin are used by the Data Management Center of the Incorporated Research Institutions for Seismology (IRIS DMC) to serve event-oriented user-requests for waveform data. The ISC-GEM Bulletin is a cornerstone of the ISC-GEM Global Instrumental Reference Earthquake Catalogue for Global Earthquake risk Model (GEM).

The ISC Bulletin contains over 8 million seismic events: earthquakes, chemical and nuclear explosions, mine blasts and mining induced events. Almost 2 million of them are regional and teleseismically recorded events that have been reviewed by the ISC analysts. The ISC Bulletin contains approximately 255 million individual seismic station readings of arrival times, amplitudes, periods, SNR, slowness and azimuth, reported by approximately 19,000 seismic stations currently registered in the IR. Over 9,000 stations have contributed to the ISC Bulletin in recent years. This number includes the numerous sites of the USArray. The IASPEI GT List currently contains 10187 events for which latitude, longitude and depth of origin are known with high confidence (to 5 km or better) and seismic signals were recorded at regional and/or teleseismic distances.

## 2.2 Brief History of the ISC

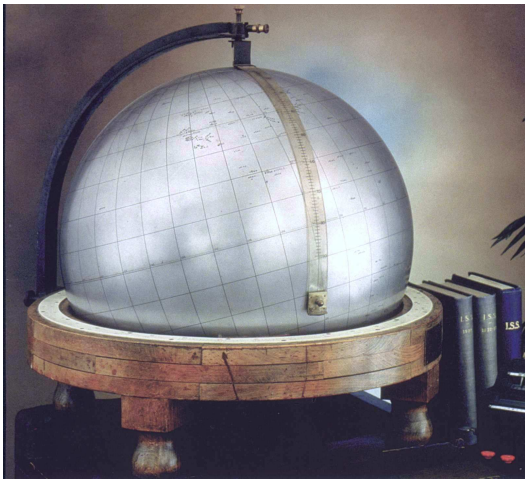


**Figure 2.1:** *The steel globe bearing positions of early seismic stations was used for locating positions of earthquakes for the International Seismological Summaries.*

(BCIS).

Following Milne's death in 1913, Seismological Bulletins of the BAAS were continued under Prof. H.H. Turner, later based at Oxford University. Upon formal post-war dissolution of the International Association of Seismology in 1922 the newly founded Seismological Section of the International Union of Geodesy and Geophysics (IUGG) set up the International Seismological Summary (ISS) to continue at Oxford under Turner, to produce the definitive global catalogues from the 1918 data-year onwards, under the auspices of IUGG and with the support of the BAAS.

ISS production, led by several professors at Oxford University, and Sir Harold Jeffreys at Cambridge



University, continued until it was superseded by the ISC Bulletin, after the ISC was formed in Edinburgh in 1964 with Dr P.L. Willmore as its first director.

During the period 1964 to 1970, with the help of UNESCO and other international scientific bodies, the ISC was reconstituted as an international non-governmental body, funded by interested institutions from various countries. Initially there were supporting members from seven countries, now there are almost 60, and member institutions include national academies, research foundations, government departments and research institutes, national observatories and universities. Each member, contributing a minimum unit of subscription or more, appoints a representative to the ISC's Governing Council, which meets every two years to decide the ISC's policy and operational programme. Representatives from the International Association of Seismology and Physics of the Earth's Interior also attend these meetings. The Governing Council appoints the Director and a small Executive Committee to oversee the ISC's operations.



*Figure 2.2: ISC building in Thatcham, Berkshire, UK.*

In 1975, the ISC moved to Newbury in southern England to make use of better computing facilities there. The ISC subsequently acquired its own computer and in 1986 moved to its own building at Pipers Lane, Thatcham, near Newbury. The internal layout of the new premises was designed for the ISC and includes not only office space but provision for the storage of extensive stocks of ISS and ISC publications and a library of seismological observatory bulletins, journals and books collected over many tens of years.

In 1997 the first set of the ISC Bulletin CD-ROMs was produced (not counting an earlier effort at USGS). The first ISC website appeared in 1998 and the first ISC database was put in day-to-day operations from 2001.

Throughout 2009-2011 a major internal reconstruction of the ISC building was undertaken to allow for more members of staff working in mainstream ISC operations as well as major development projects such as the CTBTO Link, ISC-GEM Catalogue and the ISC Bulletin Rebuild.

## 2.3 Former Directors of the ISC and its U.K. Predecessors



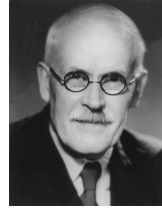
John Milne  
Publisher of the Shide Circular Reports on Earthquakes  
1899-1913



Herbert Hall Turner  
Seismological Bulletins of the BAAS  
1913-1922  
Director of the ISS  
1922-1930



Harry Hemley Plaskett  
Director of the ISS  
1931-1946



Harold Jeffreys  
Director of the ISS  
1946-1957



Robert Stoneley  
Director of the ISS  
1957-1963



P.L. (Pat) Willmore  
Director of the ISS  
1963-1970  
Director of the ISC  
1964-1970



Edouard P. Arnold  
Director of the ISC  
1970-1977



Anthony A. Hughes  
Director of the ISC  
1977-1997



Raymond J. Willemann  
Director of the ISC  
1998-2003



Avi Shapira  
Director of the ISC  
2004-2007

## 2.4 Member Institutions of the ISC

The ISC Constitution and Bye-laws stipulate that any national academy, agency, scientific institution or other non-profit organisation may become a Member of the ISC on payment to the ISC of a sum equal to at least one unit of subscription and the nomination of a voting representative to serve on the ISC's governing body. Membership shall be effective for one year from the date of receipt at the ISC of the annual contribution of the Member and is thereafter renewable for periods of one year.

The ISC is currently supported with funding from its 62 Member Institutions and Award 2414178 from the US National Science Foundation.

Figures 2.3 and 2.4 show major sectors to which the ISC Member Institutions belong and proportional

financial contributions that each of these sectors make towards the ISC’s annual budget.

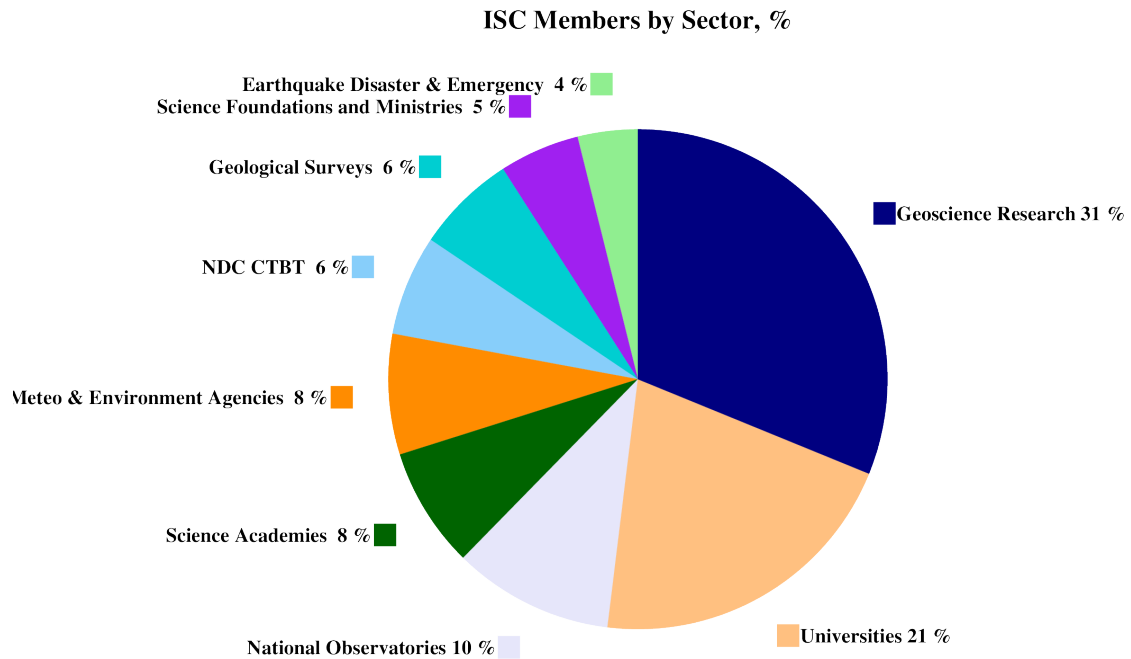



**Figure 2.3:** Distribution of the ISC Member Institutions by sector during the review of data in this Summary as a percentage of total number of Members.

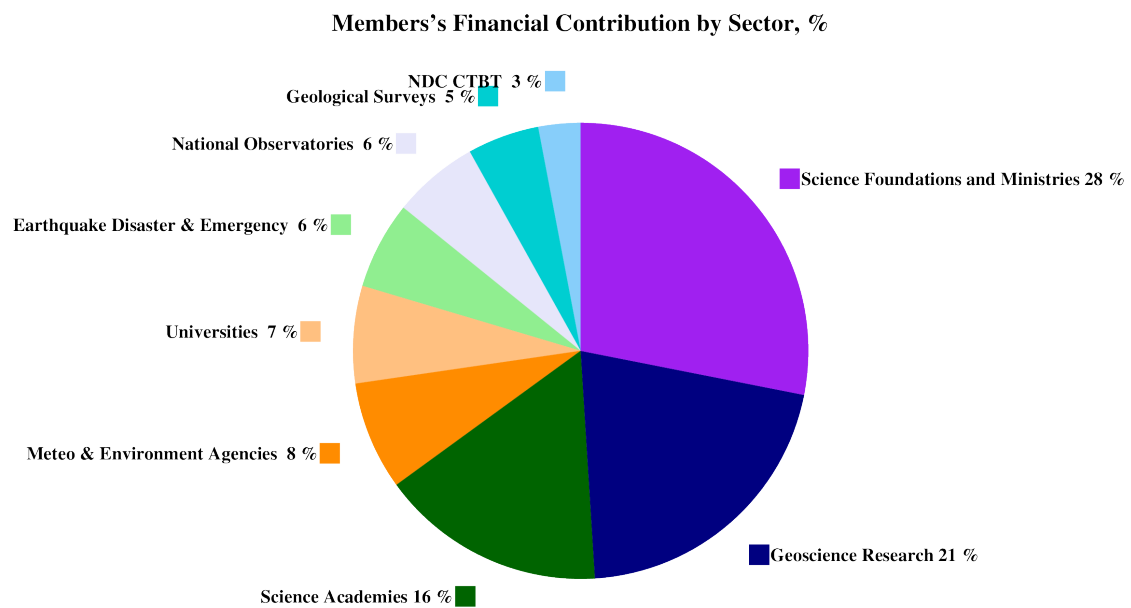


**Figure 2.4:** Distribution of Member’s financial contributions to the ISC by sector during the review of data in this Summary as a percentage of total annual Member contributions.

There follows a list of all current Member Institutions with a category (1 through 9) assigned according to the ISC Working Statutes. Each category relates to the number of membership units contributed.



Institute of Geosciences,  
Polytechnic University  
of Tirana  
Albania  
Category: 1



Centre de Recherche  
en Astronomie, As-  
trophysique et Géo-  
physique (CRAAG)  
Algeria  
www.craag.dz  
Category: 1



Geoscience Australia  
Australia  
www.ga.gov.au  
Category: 4



Geophysics, Research  
School of Earth Sci-  
ences, Australian  
National University  
Australia

Category: 1



Federal Ministry for  
Education, Science and  
Research  
Austria

Category: 2



Centre of Geophysical  
Monitoring (CGM) of  
the National Academy  
of Sciences of Belarus  
Belarus  
www.cgm.org.by  
Category: 1



Belgian Science Policy  
Office (BELSPO)  
Belgium

Category: 1



Universidade de São  
Paulo, Centro de Sis-  
mologia  
Brazil  
www.sismo.iag.usp.br  
Category: 1



Seismological Observa-  
tory, Institute of Geo-  
sciences, University of  
Brasilia  
Brazil  
www.obsis.unb.br  
Category: 1



Observatório Nacional  
Brazil  
www.on.br  
Category: 1



National Institute of  
Geophysics, Geodesy  
and Geography  
(NIGGG), Bulgarian  
Academy of Sciences  
Bulgaria  
www.niggg.bas.bg  
Category: 1



The Geological Survey  
of Canada  
Canada  
gsc.nrcan.gc.ca  
Category: 4



Centro Sismológico  
Nacional, Universidad  
de Chile  
Chile  
Category: 1



China Earthquake Ad-  
ministration  
China  
www.cea.gov.cn  
Category: 4



Institute of Earth Sci-  
ences, Academia Sinica  
Chinese Taipei  
www.earth.sinica.edu.tw  
Category: 1



Geological Survey De-  
partment  
Cyprus  
www.moa.gov.cy  
Category: 1



Institute of Geophysics,  
Czech Academy of Sci-  
ences  
Czech Republic  
Category: 1



Geological Survey of  
Denmark and Green-  
land (GEUS)  
Denmark  
www.geus.dk  
Category: 2



National Research Insti-  
tute for Astronomy and  
Geophysics (NRIAG),  
Cairo  
Egypt  
www.nriag.sci.eg  
Category: 1



The University of  
Helsinki  
Finland  
www.helsinki.fi  
Category: 2



Institute of Radiological  
and Nuclear Safety  
(IRSN), joint authority  
of the Ministries of De-  
fense, the Environment,  
Industry, Research, and  
Health  
France  
Category: 1



Institute National des  
Sciences de l'Univers  
France  
www.insu.cnrs.fr  
Category: 4



Laboratoire de Dé-  
tection et de Géo-  
physique/CEA  
France  
www-dase.cea.fr  
Category: 2



GeoForschungsZentrum  
Potsdam  
Germany  
www.gfz-potsdam.de  
Category: 2



Bundesanstalt für Ge-  
owissenschaften und  
Rohstoffe  
Germany  
www.bgr.bund.de  
Category: 4



The Seismological Insti-  
tute, National Observa-  
tory of Athens  
Greece  
www.noa.gr  
Category: 1



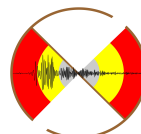
Institute of Earth  
Physics and Space Sci-  
ence (EPSS), Hungar-  
ian Research Network  
(ELKH)  
Hungary  
Category: 1



The Icelandic Meteor-  
ological Office  
Iceland  
www.vedur.is  
Category: 1



National Geophysical  
Research Institute  
(NGRI), Council of  
Scientific and Industrial  
Research (CSIR)  
India  
Category: 2



National Centre for  
Seismology, Ministry of  
Earth Sciences of India  
India  
www.moes.gov.in  
Category: 4



Iraqi Meteorological Organization and Seismology  
Iraq  
www.imos-tm.com  
Category: 1



DIAS  
Institute for Advanced Studies  
Dublin Institute for Advanced Studies  
Dublin Institute for Advanced Studies

Dublin Institute for Advanced Studies  
Ireland  
www.dias.ie  
Category: 1



Geological Survey of Israel  
Israel  
Category: 1



Soreq Nuclear Research Centre (SNRC)  
Israel  
www.soreq.gov.il  
Category: 1



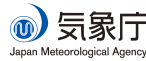
Istituto Nazionale di Oceanografia e di Geofisica Sperimentale  
Italy  
www.ogs.trieste.it  
Category: 1



Istituto Nazionale di Geofisica e Vulcanologia  
Italy  
www.ingv.it  
Category: 3



University of the West Indies at Mona  
Jamaica  
www.mona.uwi.edu  
Category: 1



気象庁  
Japan Meteorological Agency

The Japan Meteorological Agency (JMA)  
Japan  
www.jma.go.jp  
Category: 5



Japan Agency for Marine-Earth Science and Technology (JAMSTEC)  
Japan  
www.jamstec.go.jp  
Category: 2



National Institute of Polar Research (NIPR)  
Japan  
www.nipr.ac.jp  
Category: 1



EARTHQUAKE RESEARCH INSTITUTE  
UNIVERSITY OF TOKYO

Earthquake Research Institute, University of Tokyo  
Japan  
www.eri.u-tokyo.ac.jp  
Category: 3

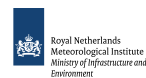


geofisica  
UNAM

Institute of Geophysics, National University of Mexico  
Mexico  
www.igeofcu.unam.mx  
Category: 1



Centro de Investigación Científica y de Educación Superior de Ensenada (CICESE)  
Mexico  
resnom.cicese.mx  
Category: 1



Royal Netherlands Meteorological Institute  
Ministry of Infrastructure and Environment

The Royal Netherlands Meteorological Institute (KNMI)  
Netherlands  
www.knmi.nl  
Category: 2



GNS SCIENCE  
TE PŪ AO

GNS Science  
New Zealand  
www.gns.cri.nz  
Category: 3



Stiftelsen NORSAR  
Norway  
www.norsar.no  
Category: 2



UNIVERSITAS BERGENSIS

The University of Bergen  
Norway  
www.uib.no  
Category: 2



Institute of Geophysics  
Polish Academy of Sciences

Institute of Geophysics, Polish Academy of Sciences  
Poland  
www.igf.edu.pl  
Category: 1



Instituto Português do Mar e da Atmosfera  
Portugal  
www.ipma.pt  
Category: 2



RED SISMICA DE PUERTO RICO  
GEOLOGIA UPR. MAYAGUEZ

Red Sismica de Puerto Rico  
Puerto Rico  
redsismica.uprm.edu  
Category: 1



KMA  
Korea Meteorological Administration

Korean Meteorological Administration  
Republic of Korea  
www.kma.go.kr  
Category: 1



National Institute for Earth Physics  
Romania  
www.infp.ro  
Category: 1



Russian Academy of Sciences

Russian Academy of Sciences  
Russia  
www.ras.ru  
Category: 5



EARTH OBSERVATORY OF SINGAPORE  
An autonomous institute of Nanyang Technological University

Earth Observatory of Singapore (EOS), an autonomous Institute of Nanyang Technological University  
Singapore  
www.earthobservatory.sg  
Category: 1



Environmental Agency of Slovenia  
Slovenia  
www.arso.gov.si  
Category: 1



Council for Geoscience  
Leaders in Applied Geoscience Solutions




















Council for Geoscience  
South Africa  
www.geoscience.org.za  
Category: 1



ICM-CSIC

Institute of Marine Sciences (ICM-CSIC)  
Spain  
Category: 1



	<p>Instituto Geografico Nacional Spain</p>		<p>Institut Cartogràfic i Geològic de Catalunya (ICGC) Spain www.icgc.cat Category: 1</p>		<p>National Defence Research Establishment (FOI) Sweden www.foi.se Category: 1</p>
	<p>Uppsala Universitet Sweden www.uu.se Category: 2</p>		<p>The Swiss Academy of Sciences Switzerland www.scnat.ch Category: 2</p>		<p>Disaster and Emergency Management Authority (AFAD) Turkey www.depem.gov.tr Category: 2</p>
	<p>Kandilli Observatory and Earthquake Research Institute Turkey www.koeri.boun.edu.tr Category: 1</p>		<p>AWE Blacknest United Kingdom www.blacknest.gov.uk Category: 1</p>		<p>British Geological Survey United Kingdom www.bgs.ac.uk Category: 2</p>
	<p>The Royal Society United Kingdom www.royalsociety.org Category: 6</p>		<p>University of Utah Seismograph Stations (UUSS) U.S.A.  Category: 1</p>		<p>The National Science Foundation of the United States. (NSF Award 2414178) U.S.A. www.nsf.gov Category: 5</p>
	<p>Texas Seismological Network (TexNet), Bureau of Economic Geology, J.A. and K.G. Jackson School of Geosciences, University of Texas at Austin U.S.A. www.beg.utexas.edu Category: 1</p>		<p>National Earthquake Information Center, U.S. Geological Survey U.S.A. www.neic.usgs.gov Category: 1</p>		<p>Lamont-Doherty Earth Observatory, Columbia Climate School, Columbia University U.S.A.  Category: 1</p>
	<p>Incorporated Research Institutions for Seismology U.S.A. www.iris.edu Category: 1</p>		<p>Pacific Northwest Seismic Network (PNSN) U.S.A.  Category: 1</p>		<p>Alaska Earthquake Center (AEC), University of Alaska Fairbanks U.S.A.  Category: 1</p>
	<p>Center for Earthquake Research and Information (CERI), the University of Memphis U.S.A.  Category: 1</p>		<p>Mavlyanov Institute of Seismology, Academy of Sciences, Republic of Uzbekistan  Category: 1</p>		

In addition the ISC is currently in receipt of grants from the International Data Centre (IDC) of the Preparatory Commission of the Comprehensive Nuclear-Test-Ban Treaty Organization (CTBTO), FM Global, Lighthill Risk Network, and AXA XL.



## 2.5 Sponsoring Organisations

Article 9.8.1 of the ISC Constitution stipulates that any organisation with an interest in the work of the ISC may at the discretion of the ISC Executive Committee become a Sponsoring Organisation (Sponsor) upon payment of a mutually agreed annual fee. In line with the Article VI of the ISC Bye-laws, the Sponsors are entitled to attend meetings of the ISC Governing Council without a vote.



GeoSIG provides earthquake, seismic, structural, dynamic and static monitoring and measuring solutions. As an ISO Certified company, GeoSIG is a world leader in design and manufacture of a diverse range of high quality, precision instruments for vibration and earthquake monitoring. GeoSIG instruments are at work today in more than 100 countries around the world with well-known projects such as the NetQuakes installation with USGS and Oresund Bridge in Denmark. GeoSIG offers off-the-shelf solutions as well as highly customised solutions to fulfil the challenging requirements in many vertical markets including the following:

- Earthquake Early Warning and Rapid Response (EEWRR)
- Seismic and Earthquake Monitoring and Measuring
- Industrial Facility Seismic Monitoring and Shutdown
- Structural Analysis and Ambient Vibration Testing
- Induced Vibration Monitoring
- Research and Scientific Applications



SARA designs and manufactures seismometers, accelerometers and portable multichannel seismographs for both seismology and applied geophysics. Since 2002 we provided over 5,000 seismic units, 15,000 acceleration transducers and 15,000 geophysical exploration channels, to thousands of professionals and researchers who are using our equipment with success. Providing low-cost instrumentation for developing countries is our main goal. We developed our seismological software SEISMOWIN which provides full support for all international file formats and communication standards like miniSEED, GSE, SeedLink and a number of tools for earthquake location and site assessment. The GEOEXPLORER software suite offers a number of modules for geological surveys.

In 2023 we introduced our new compact broadband seismometer to the market, suitable for surface, posthole and borehole installation, and new versions of our popular SL06 recorder with rack mount housing and ADC with PGA offering 24 or 32 bit streaming.

Visit our web site and download the free tools available at: [www.sara.pg.it](http://www.sara.pg.it)

The logo for MS&AD consists of the letters "MS&AD" in a white, bold, sans-serif font, centered within a dark green rectangular background.

<http://www.irric.co.jp/en/corporate/>

**MS&AD InterRisk Research & Consulting**

MS&AD InterRisk Research & Consulting, Inc. is responsible for the core of risk-related service businesses in the MS&AD group. We provide services which meet various expectations of the clients, including consulting, research and investigation, seminars and publications for risk management in addition to the think-tank functions.
























Gaiacode is a science based, forward looking, innovative company designing and building the next generation of seismic instrumentation.

## 2.6 Data Contributing Agencies

In addition to its Members and Sponsors, the ISC owes its existence and successful long-term operations to its 151 seismic bulletin data contributors. These include government agencies responsible for national



seismic networks, geoscience research institutions, geological surveys, meteorological agencies, universities, national data centres for monitoring the CTBT and individual observatories. There would be no ISC Bulletin available without the regular stream of data that are unselfishly and generously contributed to the ISC on a free basis.

	<p>East African Network EAF</p>		<p>Institute of Geosciences, Polytechnic University of Tirana Albania TIR</p>		<p>Centre de Recherche en Astronomie, As- trophysique et Géo- physique Algeria CRAAG</p>
	<p>Instituto Nacional de Prevención Sísmica Argentina SJA</p>		<p>Universidad Nacional de La Plata Argentina LPA</p>		<p>National Survey of Seis- mic Protection Armenia NSSP</p>
	<p>Geoscience Australia Australia AUST</p>		<p>Curtin University Australia CUPWA</p>		<p>Zentralanstalt für Me- teorologie und Geody- namik (ZAMG) Austria VIE</p>
	<p>International Data Cen- tre, CTBTO Austria IDC</p>		<p>Republican Seismic Sur- vey Center of Azerbai- jan National Academy of Sciences Azerbaijan AZER</p>		<p>Royal Observatory of Belgium Belgium UCC</p>
	<p>Observatorio San Cal- ixto Bolivia SCB</p>		<p>Republic Hydrometeo- rological Service, Seis- mological Observatory, Banja Luka Bosnia and Herzegovina RHSSO</p>		<p>Botswana Geoscience Institute Botswana BGSi</p>
	<p>Instituto Astronomico e Geofísico Brazil VAO</p>		<p>Observatory Seismologi- cal of the University of Brasilia Brazil OSUNB</p>		<p>National Institute of Geophysics, Geology and Geography Bulgaria SOF</p>
	<p>Canadian Hazards In- formation Service, Nat- ural Resources Canada Canada OTT</p>		<p>Centro Sismológico Na- cional, Universidad de Chile Chile GUC</p>		<p>China Earthquake Net- work Center China BJI</p>
	<p>Institute of Earth Sci- ences, Academia Sinica Chinese Taipei ASIES</p>		<p>Central Weather Bureau (CWB) Chinese Taipei TAP</p>		<p>Red Sismológica Na- cional de Colombia Colombia RSNC</p>



Sección de Sismología,  
Vulcanología y Exploración Geofísica  
Costa Rica  
UCR



Seismological Survey of  
the Republic of Croatia  
Croatia  
ZAG



Servicio Sismológico Na-  
cional Cubano  
Cuba  
SSNC



Cyprus Geological Sur-  
vey Department  
Cyprus  
NIC



The Institute of Physics  
of the Earth (IPEC)  
Czech Republic  
IPEC



Institute of Geophysics,  
Czech Academy of Sci-  
ences  
Czech Republic  
PRU



Institute of Geophysics,  
Czech Academy of Sci-  
ences  
Czech Republic  
WBNET



Korea Earthquake Ad-  
ministration  
Democratic People's Re-  
public of Korea  
KEA



Geological Survey of  
Denmark and Green-  
land  
Denmark  
DNK



Observatorio Sismo-  
logico Politecnico  
Loyola  
Dominican Republic  
OSPL



Universidad Autonoma  
de Santo Domingo  
Dominican Republic  
SDD



Servicio Nacional de Sis-  
mología y Vulcanología  
Ecuador  
IGQ



National Research Insti-  
tute of Astronomy and  
Geophysics  
Egypt  
HLW



Servicio Nacional de Es-  
tudios Territoriales  
El Salvador  
SNET



Institute of Seismology,  
University of Helsinki  
Finland  
HEL



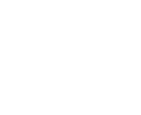
Laboratoire de Dé-  
tection et de Géo-  
physique/CEA  
France  
LDG



Institut de Physique du  
Globe de Paris  
France  
IPGP



EOST / RéNaSS  
France  
STR



Laboratoire de Géo-  
physique/CEA  
French Polynesia  
PPT



Institute of Earth Sci-  
ences/ National Seismic  
Monitoring Center  
Georgia  
TIF



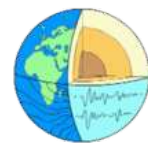
Seismological Observa-  
tory Berggießhübel, TU  
Bergakademie Freiberg  
Germany  
BRG



Alfred Wegener Insti-  
tute for Polar and Ma-  
rine Research  
Germany  
AWI



Bundesanstalt für Ge-  
owissenschaften und  
Rohstoffe  
Germany  
BGR



Geophysikalisches Ob-  
servatorium Collm  
Germany  
CLL



Helmholtz Centre Potsdam  
GFZ German Research Centre For Geosciences  
Germany  
GFZ



University of Patras,  
Department of Geology  
Greece  
UPSL



National Observatory of Athens  
Greece  
ATH



Department of Geophysics,  
Aristotle University of Thessaloniki  
Greece  
THE



INSIVUMEH  
Guatemala  
GCG



Hong Kong Observatory  
Hong Kong  
HKC



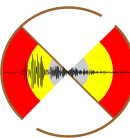
Geodetic and Geophysical Research Institute,  
Hungarian Academy of Sciences  
Hungary  
KRSZO



Icelandic Meteorological Office  
Iceland  
REY



National Geophysical Research Institute  
India  
HYB



National Centre for Seismology of the Ministry of Earth Sciences of India  
India  
NDI



Badan Meteorologi, Klimatologi dan Geofisika  
Indonesia  
DJA



Tehran University  
Iran  
TEH



International Institute of Earthquake Engineering and Seismology (IIEES)  
Iran  
THR



Iraqi Meteorological and Seismology Organisation  
Iraq  
ISN



Dublin Institute for Advanced Studies  
Ireland  
DIAS



The Geophysical Institute of Israel  
Israel  
GII



MedNet Regional Centroid - Moment Tensors  
Italy  
MED\_RCMT



Istituto Nazionale di Oceanografia e di Geofisica Sperimentale (OGS)  
Italy  
TRI



Dipartimento per lo Studio del Territorio e delle sue Risorse (RSNI)  
Italy  
GEN



SARA Electronic Instrument s.r.l.  
Italy  
SARA



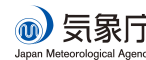
Istituto Nazionale di Geofisica e Vulcanologia  
Italy  
ROM



Laboratory of Research on Experimental and Computational Seismology  
Italy  
RISSC



Jamaica Seismic Network  
Jamaica  
JSN



Japan Meteorological Agency  
Japan  
JMA



National Research Institute for Earth Science and Disaster Resilience  
Japan  
NIED



National Institute of Polar Research  
Japan  
SYO



Jordan Seismological Observatory  
Jordan  
JSO



Seismological Experimental Methodological Expedition  
Kazakhstan  
SOME

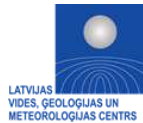


National Nuclear Center  
Kazakhstan  
NNC



Institute of Seismology, Academy of Sciences of Kyrgyz Republic  
Kyrgyzstan  
KRNET

Kyrgyz Seismic Network  
Kyrgyzstan  
KNET



Latvian Seismic Network  
Latvia  
LVSN



National Council for Scientific Research  
Lebanon  
GRAL



Geological Survey of Lithuania  
Lithuania  
LIT



Macao Meteorological and Geophysical Bureau  
Macao, China  
MCO

Antananarivo  
Madagascar  
TAN



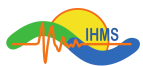
Geological Survey Department  
Malawi  
GSDM



Instituto de Geofísica de la UNAM  
Mexico  
MEX



Centro de Investigación Científica y de Educación Superior de Ensenada  
Mexico  
ECX



Institute of Hydrometeorology and Seismology of Montenegro  
Montenegro  
PDG



Centre National de Recherche  
Morocco  
CNRM



The Geological Survey of Namibia  
Namibia  
NAM



National Seismological Centre, Nepal  
Nepal  
DMN



IRD Centre de Nouméa  
New Caledonia  
NOU



Institute of Geological and Nuclear Sciences  
New Zealand  
WEL



Central American Tsunami Advisory Center  
Nicaragua  
CATAC



Seismological Observatory Skopje  
North Macedonia  
SKO



Stiftelsen NORSAR  
Norway  
NAO



University of Bergen  
Norway  
BER



Sultan Qaboos University  
Oman  
OMAN



Universidad de Panama  
Panama  
UPA



Philippine Institute of  
Volcanology and Seis-  
mology  
Philippines  
MAN



Manila Observatory  
Philippines  
QCP



Private Observatory of  
Pawel Jacek Wiejacz,  
D.Sc.  
Poland  
PjWWP



Institute of Geophysics,  
Polish Academy of Sci-  
ences  
Poland  
WAR



Sistema de Vigilância  
Sismológica dos Açores  
Portugal  
SVSA



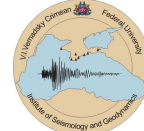
Instituto Dom Luiz,  
University of Lisbon  
Portugal  
IGIL



Instituto Português do  
Mar e da Atmosfera, I.P.  
Portugal  
INMG



Centre of Geophysical  
Monitoring of the Na-  
tional Academy of Sci-  
ences of Belarus  
Republic of Belarus  
BELR



Inst. of Seismology and  
Geodynamics, V.I. Ver-  
nadsky Crimean Federal  
University  
Republic of Crimea  
CFUSG



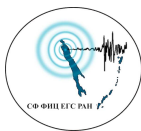
Korea Meteorological  
Administration  
Republic of Korea  
KMA



National Institute for  
Earth Physics  
Romania  
BUC



Yakutiya Regional Seis-  
mological Center, GS  
SB RAS  
Russia  
YARS



Sakhalin Experimental  
and Methodological  
Seismological Expedi-  
tion, GS RAS  
Russia  
SKHL



Kamchatka Branch of  
the Geophysical Survey  
of the RAS  
Russia  
KRSC



Baikal Regional Seismo-  
logical Centre, GS SB  
RAS  
Russia  
BYKL



Kola Branch, Geophys-  
ical Survey, Russian  
Academy of Sciences  
Russia  
KOGSR



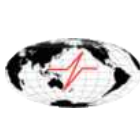
Altay-Sayan Branch,  
Geophysical Survey,  
Russian Academy of  
Sciences  
Russia  
ASGSR



Federal Center for Inte-  
grated Arctic Research  
Russia  
FCIAR



North Eastern Regional  
Seismological Centre,  
Magadan, GS RAS  
Russia  
NERS



Geophysical Survey of  
Russian Academy of Sci-  
ences  
Russia  
MOS



Mining Institute of the  
Ural Branch of the Rus-  
sian Academy of Sci-  
ences  
Russia  
MIRAS





Saudi Geological Survey  
Saudi Arabia  
SGS



Republički seizmoloski  
zavod  
Serbia  
BEO



Geophysical Institute,  
Slovak Academy of  
Sciences  
Slovakia  
BRA



Slovenian Environment  
Agency  
Slovenia  
LJU



Council for Geoscience  
South Africa  
PRE



Real Instituto y Obser-  
vatorio de la Armada  
Spain  
SFS



Instituto Geográfico Na-  
cional  
Spain  
MDD



Institut Cartogràfic i  
Geològic de Catalunya  
Spain  
MRB



University of Uppsala  
Sweden  
UPP



Swiss Seismological Ser-  
vice (SED)  
Switzerland  
ZUR



Thai Meteorological De-  
partment  
Thailand  
BKK



The Seismic Research  
Centre  
Trinidad and Tobago  
TRN



Institut National de la  
Météorologie  
Tunisia  
TUN



Kandilli Observatory and  
Earthquake Re-  
search Institute  
Turkey  
ISK



Disaster and Emergency  
Management Presidency  
Turkey  
AFAD



Pacific Tsunami Warn-  
ing Center  
U.S.A.  
PTWC



National Earthquake In-  
formation Center  
U.S.A.  
NEIC



The Global CMT  
Project  
U.S.A.  
GCMT



Red Sísmica de Puerto  
Rico  
U.S.A.  
RSPR



Texas Seismological  
Network, University of  
Texas at Austin  
U.S.A.  
TXNET



Pacific Northwest Sei-  
smic Network  
U.S.A.  
PNSN

Main Centre for Special  
Monitoring  
Ukraine  
MCSM



Subbotin Institute of  
Geophysics, National  
Academy of Sciences  
Ukraine  
SIGU



Dubai Seismic Network  
United Arab Emirates  
DSN



British Geological Sur-  
vey  
United Kingdom  
BGS



International Seismologi-  
cal Centre Probabilistic  
Point Source Model  
United Kingdom  
ISC-PPSM



International Seismologi-  
cal Centre  
United Kingdom  
ISC

Institute of Seismology,  
Academy of Sciences,  
Republic of Uzbekistan  
Uzbekistan  
ISU



Fundación Venezolana  
de Investigaciones Sis-  
mológicas  
Venezuela  
FUNV



Institute of Geophysics,  
Viet Nam Academy of  
Science and Technology  
Viet Nam  
PLV



Goetz Observatory  
Zimbabwe  
BUL

## 2.7 ISC Staff

Listed below are the staff (and their country of origin) who were employed at the ISC during the time period when the ISC worked on the data covered by this issue of the Summary.

- Dmitry Storchak
- Director
- Russia / United Kingdom



- Lynn Elms
- Administration Officer
- United Kingdom



- James Harris
- Senior System and  
Database Administrator
- United Kingdom





- Oliver Rea
- System Administrator
- United Kingdom



- Calum Clague
- Data Collection Officer
- South Africa



- Domenico Di Giacomo
- Senior Seismologist
- Italy/UK



- Tom Garth
- Seismologist / Senior Developer
- United Kingdom



- Ryan Gallacher
- Seismologist / Developer
- United Kingdom



- Natalia Poiata
- Seismologist / Developer
- Moldova



- Adrian Armstrong
- Software Engineer
- United Kingdom



- Rosemary Hulin
- Analyst
- United Kingdom





- Blessing Shumba
- Seismologist / Senior Analyst
- Zimbabwe



- Rebecca Verney
- Analyst
- United Kingdom



- Elizabeth Ayres
- Analyst / Historical Data Officer
- United Kingdom



- Kathrin Lieser
- Analyst Administrator /  
Summary Editor / Seismologist
- Germany



- Burak Sakarya
- Seismologist / Analyst
- Turkey



- Rian Harris
- Historical Data Officer
- United Kingdom



- Susana Carvalho
- Historical Data Officer
- Portugal



## 3

# Availability of the ISC Bulletin

The ISC Bulletin is available from the following sources:

- Web searches

The entire ISC Bulletin is available directly from the ISC website via tailored searches.

([www.isc.ac.uk/iscbulletin/search](http://www.isc.ac.uk/iscbulletin/search))

- Bulletin search - provides the most verbose output of the ISC Bulletin in ISF or QuakeML.
- Event catalogue - only outputs the prime hypocentre for each event, producing a simple list of events, locations and magnitudes.
- Arrivals - search for arrivals in the ISC Bulletin. Users can search for specific phases for selected stations and events.

- FTP site

The ISC Bulletin is also available to download from the ISC ftp site, which contains the Bulletin in PDF, ISF and FFB formats.

(<ftp://www.isc.ac.uk>)

and

(<http://download.isc.ac.uk>)

## 4

# Citing the International Seismological Centre

Data from the ISC should always be cited. This includes use by academic or commercial organisations, as well as individuals. A citation should show how the data were retrieved and may be in one of these suggested forms:

The ISC is named as a valid data centre for citations within American Geophysical Union (AGU) publications. As such, please follow the AGU guidelines when referencing ISC data in one of their journals. The ISC may be cited as both the institutional author of the Bulletin and the source from which the data were retrieved.

### 4.1 The ISC Bulletin

International Seismological Centre (2024), On-line Bulletin, <https://doi.org/10.31905/D808B830>

The procedures used for producing the ISC Bulletin have been described in a number of scientific articles. Depending on the use of the Bulletin, users are encouraged to follow the citation suggestions below:

a) For current ISC location procedure:

Bondár, I. and D.A. Storchak (2011). Improved location procedures at the International Seismological Centre, *Geophys. J. Int.*, 186, 1220-1244, <https://doi.org/10.1111/j.1365-246X.2011.05107.x>

b) For Rebuilt ISC Bulletin:

Storchak, D.A., Harris, J., Brown, L., Lieser, K., Shumba, B., Verney, R., Di Giacomo, D., Korger, E. I. M. (2017). Rebuild of the Bulletin of the International Seismological Centre (ISC), part 1: 1964–1979. *Geosci. Lett.* (2017) 4: 32. <https://doi.org/10.1186/s40562-017-0098-z>

Storchak, D.A., Harris, J., Brown, L., Lieser, K., Shumba, B., Di Giacomo, D. (2020) Rebuild of the Bulletin of the International Seismological Centre (ISC), part 2: 1980–2010. *Geosci. Lett.* (2020) 7: 18, <https://doi.org/10.1186/s40562-020-00164-6>

c) For principles of the ISC data collection process:

R J Willemann, D A Storchak (2001). Data Collection at the International Seismological Centre, *Seis. Res. Lett.*, 72, 440-453, <https://doi.org/10.1785/gssr1.72.4.440>

d) For interpretation of magnitudes:

Di Giacomo, D., and D.A. Storchak (2016). A scheme to set preferred magnitudes in the ISC Bulletin, *J. Seism.*, 20(2), 555-567, <https://doi.org/10.1007/s10950-015-9543-7>

e) For use of source mechanisms:

Lentas, K., Di Giacomo, D., Harris, J., and Storchak, D. A. (2020). The ISC Bulletin as a comprehensive source of earthquake source mechanisms, *Earth Syst. Sci. Data*, 11, 565-578, <https://doi.org/10.5194/essd-11-565-2020>

Lentas, K. (2018). Towards routine determination of focal mechanisms obtained from first motion P-wave arrivals, *Geophys. J. Int.*, 212(3), 1665–1686. <https://doi.org/10.1093/gji/ggx503>

f) For use of the original (pre-Rebuild) ISC Bulletin as a historical perspective:

Adams, R.D., Hughes, A.A., and McGregor, D.M. (1982). Analysis procedures at the International Seismological Centre. *Phys. Earth Planet. Inter.* 30: 85-93, [https://doi.org/10.1016/0031-9201\(82\)90093-0](https://doi.org/10.1016/0031-9201(82)90093-0)

## 4.2 The Summary of the Bulletin of the ISC

International Seismological Centre (2024), Summary of the Bulletin of the International Seismological Centre, January - June 2021, 58(I), <https://doi.org/10.31905/F3BUR770>

## 4.3 The historical printed ISC Bulletin (1964-2009)

International Seismological Centre, Bull. Internatl. Seismol. Cent., 46(9-12), Thatcham, United Kingdom, 2009.

## 4.4 The IASPEI Reference Event List

International Seismological Centre (2024), IASPEI Reference Event (GT) List, <https://doi.org/10.31905/32NSJF7V>

Bondár, I. and K.L. McLaughlin (2009). A New Ground Truth Data Set For Seismic Studies, *Seismol. Res. Lett.*, 80, 465-472, <https://doi.org/10.1785/gssr1.80.3.465>

Bondár, E. Engdahl, X. Yang, H. Ghalib, A. Hofstetter, V. Kirichenko, R. Wagner, I. Gupta, G. Ekström, E. Bergman, H. Israelsson, and K. McLaughlin (2004). Collection of a reference event set for regional and teleseismic location calibration, *Bull. Seismol. Soc. Am.*, 94, 1528-1545, <https://doi.org/10.1785/012003128>

Bondár, E. Bergman, E. Engdahl, B. Kohl, Y.-L. Kung, and K. McLaughlin (2008). A hybrid multiple event location technique to obtain ground truth event locations, *Geophys. J. Int.*, 175, <https://doi.org/10.1111/j.1365-246X.2011.05011.x>

## 4.5 The ISC-GEM Catalogue

International Seismological Centre (2024), ISC-GEM Earthquake Catalogue, <https://doi.org/10.31905/d808b825>, 2024.

---



Depending on the use of the Catalogue, to quote the appropriate scientific articles, as suggested below.

a) For a general use of the catalogue, please quote the following three papers (Storchak et al., 2013; 2015; Di Giacomo et al., 2018):

Storchak, D.A., D. Di Giacomo, I. Bondár, E.R. Engdahl, J. Harris, W.H.K. Lee, A. Villaseñor and P. Bormann (2013). Public Release of the ISC-GEM Global Instrumental Earthquake Catalogue (1900-2009). *Seism. Res. Lett.*, *84*, 5, 810-815, <https://doi.org/10.1785/0220130034>

Storchak, D.A., D. Di Giacomo, E.R. Engdahl, J. Harris, I. Bondár, W.H.K. Lee, P. Bormann and A. Villaseñor (2015). The ISC-GEM Global Instrumental Earthquake Catalogue (1900-2009): Introduction, *Phys. Earth Planet. Int.*, *239*, 48-63, <https://doi.org/10.1016/j.pepi.2014.06.009>

Di Giacomo, D., E.R. Engdahl and D.A. Storchak (2018). The ISC-GEM Earthquake Catalogue (1904-2014): status after the Extension Project, *Earth Syst. Sci. Data*, *10*, 1877-1899, <https://doi.org/10.5194/essd-10-1877-2018>

b) For use of location parameters, please quote (Bondár et al., 2015):

Bondár, I., E.R. Engdahl, A. Villaseñor, J. Harris and D.A. Storchak, 2015. ISC-GEM: Global Instrumental Earthquake Catalogue (1900-2009): II. Location and seismicity patterns, *Phys. Earth Planet. Int.*, *239*, 2-13, <https://doi.org/10.1016/j.pepi.2014.06.002>

c) For use of magnitude parameters, please quote (Di Giacomo et al., 2015a; 2018):

Di Giacomo, D., I. Bondár, D.A. Storchak, E.R. Engdahl, P. Bormann and J. Harris (2015a). ISC-GEM: Global Instrumental Earthquake Catalogue (1900-2009): III. Re-computed MS and mb, proxy MW, final magnitude composition and completeness assessment, *Phys. Earth Planet. Int.*, *239*, 33-47, <https://doi.org/10.1016/j.pepi.2014.06.005>

Di Giacomo, D., E.R. Engdahl and D.A. Storchak (2018). The ISC-GEM Earthquake Catalogue (1904-2014): status after the Extension Project, *Earth Syst. Sci. Data*, *10*, 1877-1899, <https://doi.org/10.5194/essd-10-1877-2018>

d) For use of station data from historical bulletins, please quote (Di Giacomo et al., 2015b; 2018):

Di Giacomo, D., J. Harris, A. Villaseñor, D.A. Storchak, E.R. Engdahl, W.H.K. Lee and the Data Entry Team (2015b). ISC-GEM: Global Instrumental Earthquake Catalogue (1900-2009), I. Data collection from early instrumental seismological bulletins, *Phys. Earth Planet. Int.*, *239*, 14-24, <https://doi.org/10.1016/j.pepi.2014.06.005>

Di Giacomo, D., E.R. Engdahl and D.A. Storchak (2018). The ISC-GEM Earthquake Catalogue (1904-2014): status after the Extension Project, *Earth Syst. Sci. Data*, *10*, 1877-1899, <https://doi.org/10.5194/essd-10-1877-2018>

e) For use of direct values of  $M_0$  from the literature, please quote (Lee and Engdahl, 2015):

Lee, W.H.K. and E.R. Engdahl (2015). Bibliographical search for reliable seismic moments of large earthquakes during 1900-1979 to compute MW in the ISC-GEM Global Instrumental Reference Earthquake Catalogue (1900-2009), *Phys. Earth Planet. Int.*, *239*, 25-32, <https://doi.org/10.1016/j.pepi.2014.06.004>



## 4.6 The ISC-EHB Dataset

International Seismological Centre (2024), ISC-EHB Dataset, <https://doi.org/10.31905/PY08W6S3>

Engdahl, E.R., R. van der Hilst, and R. Buland (1998). Global teleseismic earthquake relocation with improved travel times and procedures for depth determination, *Bull. Seism. Soc. Am.*, 88, 3, 722-743. <http://www.bssaonline.org/content/88/3/722.abstract>

Weston, J., Engdahl, E.R., Harris, J., Di Giacomo, D. and Storchack, D.A. (2018). ISC-EHB: Reconstruction of a robust earthquake dataset, *Geophys. J. Int.*, 214, 1, 474-484, <https://doi.org/10.1093/gji/ggy155>

Engdahl, E. R., Di Giacomo, D., Sakarya, B., Gkarlaoui, C. G., Harris, J., and Storchak, D. A. (2020). ISC-EHB 1964-2016, an Improved Data Set for Studies of Earth Structure and Global Seismicity, *Earth and Space Science*, 7(1), e2019EA000897, <https://doi.org/10.1029/2019EA000897>

## 4.7 The ISC Event Bibliography

International Seismological Centre (2024), On-line Event Bibliography, <https://doi.org/10.31905/EJ3B5LV6>

Also, please reference the following SRL article that describes the details of this service:

Di Giacomo, D., Storchak, D.A., Safronova, N., Ozgo, P., Harris, J., Verney, R. and Bondár, I., 2014. A New ISC Service: The Bibliography of Seismic Events, *Seismol. Res. Lett.*, 85, 2, 354-360, <https://doi.org/10.1785/0220130143>

## 4.8 International Registry of Seismograph Stations

International Seismological Centre (2024), International Seismograph Station Registry (IR), <https://doi.org/10.31905/EL3FQQ40>

## 4.9 Seismological Dataset Repository

International Seismological Centre (2024), Seismological Dataset Repository, <https://doi.org/10.31905/6TJZECEY>

## 4.10 Data transcribed from ISC CD-ROMs/DVD-ROMs

International Seismological Centre, Bulletin Disks 1-30 [CD-ROM], Internatl. Seismol. Cent., Thatcham, United Kingdom, 2024.

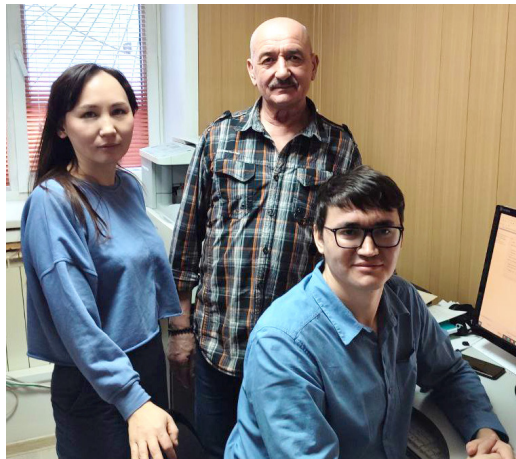
## 5

# Operational Procedures of Contributing Agencies

## 5.1 Regional Seismological Observation Network in Yakutia

Albina Semyonovna Kulyandina, Rustam Mingulovich Tuktarov, Sergey Valentinovich Shibaev

Yakutia Branch of the Geophysical Survey of the Russian Academy of Sciences (GS RAS), Yakutsk, Russia



Team of Yakutia Branch of GS RAS

The article gives a brief history of the development of instrumental seismic observations in the territory of the Republic of Sakha (Yakutia). We describe the current state of seismic observations and data processing in the Yakutia Branch of the Geophysical Survey of the Russian Academy of Sciences (GS RAS), ISC agency code YAGSR, as well as the results of the seismic activity monitoring on the territory of Yakutia for the last 66 years. The article also describes the organizational structure of the data collection centre at central seismic station Yakutsk (YAK) and presents the configuration and development of the seismic observation network in Yakutia.

### 5.1.1 Introduction

The first seismological studies in the Republic of Sakha (Yakutia) began in Tiksi (1956) and Yakutsk (1957) (see Fig. 5.1). The first seismogram recordings had already showed that the territory of Yakutia is seismically active, as seismic stations recorded not only earthquakes from known seismically active regions of the globe (Kamchatka, Kurils, Japan, etc.), but also local seismic events. This was especially evident following two catastrophic earthquakes (Nyukzhinsky and Olekminsky), which took place in the South of the republic in the Olekma river region in 1958 (*Imaev et al.*, 2000), a year after the seismic

station in Yakutsk had been opened. Instruments clearly recorded ground motions associated to the two events, making it possible to determine the coordinates of their epicentres reliably for the first time (see Fig. 5.2).

The MS 6.3 Nyukzhinsky earthquake (*International Seismological Centre, 2024a*) occurred on 5 January, 1958, and had an intensity at the epicenter of 9 points (MSK-64 scale). The event generated landslides, rockfalls and expanding ground cracks, which were found in the area most affected. In the village closest to the epicenter, Ust-Nyukzha (40 km epicentral distance), the earthquake was felt with an intensity of 7-8. Its macroseismic effects have been observed in Yakutia, Buryatia, Transbaikalia, and the Amur region over an area of about 800,000 – 900,000 km<sup>2</sup> (*Imaev et al., 2000*).

The second large event, the MS 6.4 Olekminsky earthquake (*International Seismological Centre, 2024b*), occurred in the Olekma river region on 14 September 1958, where the intensity at the epicenter reached 9 points on the MSK-64 scale. In the zone of strongest impact, tensile cracks were revealed in the ground, rockslides occurred and trees fell down. In the village of Ust-Nyukzha, macroseismic effects corresponding to the intensity 7 were observed. The total area of perceptible shaking in Yakutia, Buryatia, Transbaikalia and the Amur region amounted to more than 500,000 km<sup>2</sup> (*Imaev et al., 2000*).

### 5.1.2 A Brief History of Instrumental Seismological Observations in Yakutia

In 1964, a network of five seismic stations was running in Yakutia (Yakutsk, Tiksi, Ust-Nera, Chulman and Ust-Nyukzha), and additional seismic stations were installed in Chagda in 1968 and Batagai in 1975. By 1980 the seismic network included 12 stations, and reached 22 by 1990. Following this, due to difficulties in financing, their number was gradually reduced by half. All stations during the second half of the 20th century were equipped with domestic devices: SKM-3 seismographs and GK-VII galvanometers, designed for analogue recording of earthquakes on photographic paper. From 1999 to 2006, the seismic observation network was considerably extended with new digital devices of domestic manufacture (Seismic Distributed Acoustic Sensing (SDAS), Obninsk), which were installed in Aldan (1999), Chulman (2000), Tynda (2001), Batagai (2001) and Ust-Mai (2006).

### 5.1.3 Current Status of Instrumental Seismic Observations

At present, the Yakutia Branch of GS RAS carries out seismicity monitoring in Yakutia and neighboring regions based on a system of instrumental observations. The system includes 20 seismic stations, located in the North and North-East (7 stations), in the centre of the region (3 stations), in the West (3 stations) and in South Yakutia (7 stations) (Tab. 5.1, Fig. 5.1).

This regional network covers an area of over 4,107,735 km<sup>2</sup>. In addition to Yakutia, the network's area of responsibility also includes a small part of the Amur Region (about 2,500 km<sup>2</sup>), Khabarovsk Territory (80,000 km<sup>2</sup>) and part of the Krasnoyarsk Territory (240,000 km<sup>2</sup>) (Fig. 5.1). The seismic network is capable of registering local and regional events of magnitude  $M_w \geq 2.0$ –3.0. Continuous observations from the network stations are sent to the data collection and processing centre in a near real-time regime (*Shibaev et al., 2007*). The Yakutsk station has access to the internet through a dedicated optical communication channel at a speed of 40 Mb and a backup satellite channel. Station Tiksi has internet

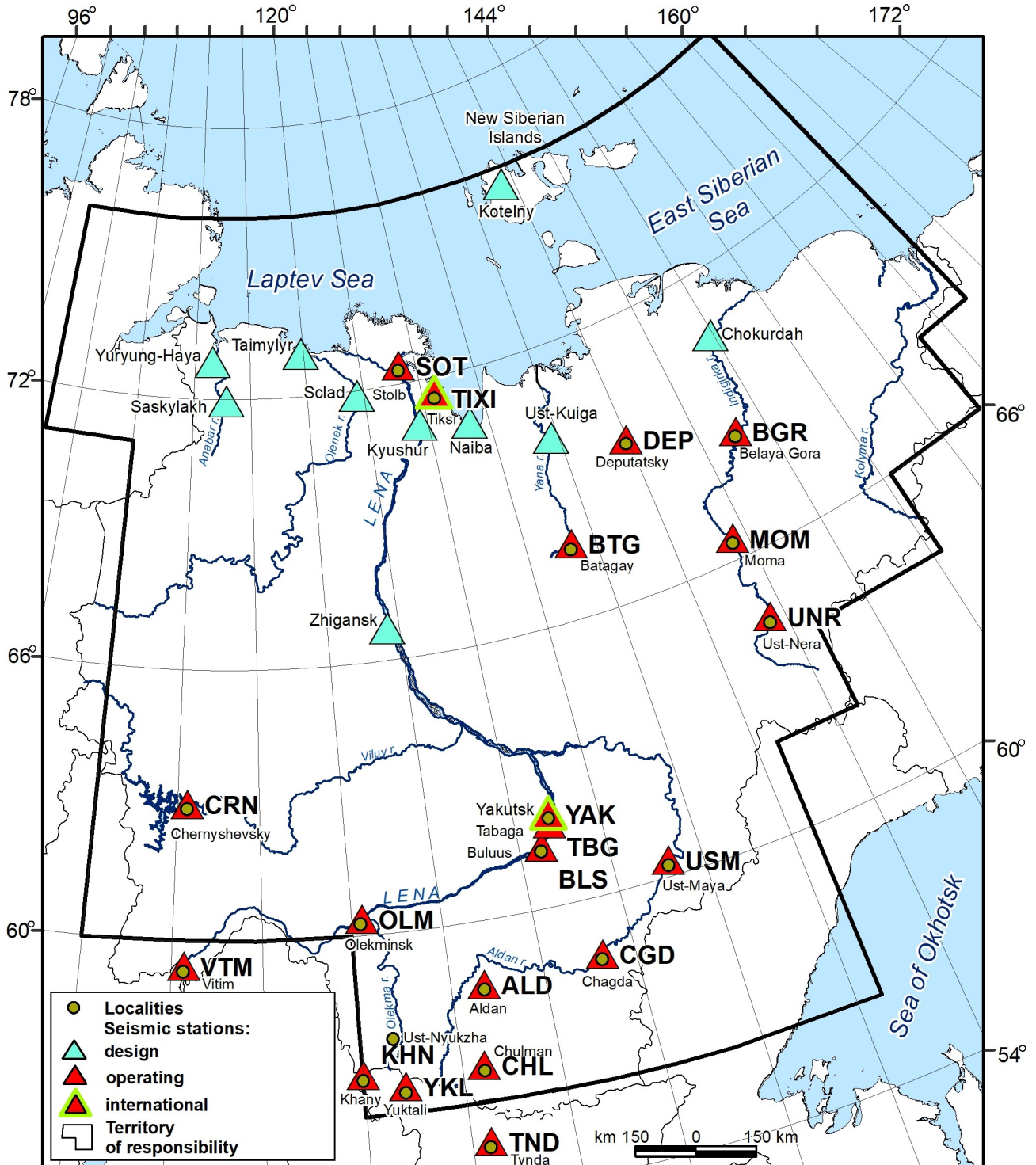


Figure 5.1: Map of active (red triangles) and planned (cyan triangles) seismic stations in Yakutia.

access via an ADSL modem and a backup satellite channel. Two more stations of the regional network (Chagda and Vitim) transmit data via satellite communication channels. The remaining stations of the regional network transmit data to the data collection server in Yakutsk through the network of the Megafon mobile operator.

Seismic data collection is carried out by the Yakutsk central reference station. It further sends digital data to the GS RAS (in Obninsk), local events to the Siberian branch of the GS RAS (in Novosibirsk) and Yakutsk ministry of emergency.

Over the last ten years, work has been carried out to equip seismic stations of Yakutia with digital equipment. Stations Yakutsk (YAK) and Tiksi (TIXI) were included into the International Monitoring System (IMS) of the Comprehensive Nuclear-Test-Ban Treaty Organization (CTBTO). The stations are equipped with broadband seismometers (STS and Trillium, Tab. 5.1), providing seismic wave recordings in the frequency range of 0.003 - 5.0 Hz. In addition, these stations are also equipped with short-period transducers extending the frequency range to higher frequencies of up to 40 Hz. The 120-140 dB dynamic range of the instruments allows them to record waveforms from the local earthquakes with magnitudes of 1-2 to 7-8 on the Richter scale in the near-field distances without distortion.

**Table 5.1:** *Seismic stations of the Yakutia Branch of the GS RAS (YAGSR) network in 2022.*

	Name	Code	Starting Date	Lat / deg	Lon / deg	Elev. / m	Site condition	Equipment
1	Aldan	ALDR	01/10/1999	58.61	125.41	662	Large gravel, clay, permafrost	CME-6211, Baikal-8
2	Batagay	BTGS	12/03/1975	67.656	134.625	127	Clay, gravel, permafrost	CME-6011, Baikal-8
3	BelayaGora	YBGR	12/08/2011	68.532	146.193	36	Clay, permafrost	KS-2000, Baikal-8
4	Buluus	BLSR	27/03/2012	61.36	129.03	90	Pebble	CME-6211, Baikal-8
5	Vitim	VTMR	16/06/2003	59.44	112.55	188	Loams	CMG-3ESPC, CD-24
6	Deputatsky	DEPR	27/08/2003	69.39	139.9	320	Permafrost	CME-6011, Baikal-8
7	Moma	MOMR	05/03/1983	66.467	143.217	192	Lay, gravel, permafrost	KS-2000, Baikal-8
8	Olekminsk	OLMR	11/06/2010	60.376	120.463	45	Sand, permafrost	CME-6211, Baikal-8
9	Stolb	SOTR	13/08/2021	72.403	126.812	50	Siltstones, permafrost	CME-6011, Baikal-8
10	Tabaga	TBGR	24/06/2003	61.821	129.637	98	Permafrost	Baikal-8 until 06/22, then Centaur
11	Tiksi	TIXI	02/03/1956 15/08/1995 (IRIS)	71.649	128.867	50	Dolomites, quartzites, permafrost	STS-1, STS-2, since 2023 Trillium Compact Q330
12	Tynda	TNDR	20/06/2001	55.147	124.721	530	Pebbles, clay	CME-6011, Baikal-8

Continued on next page



	Name	Code	Starting Date	Lat / deg	Lon / deg	Elev. / m	Site condition	Equipment
13	Ust-Maya	USM	08/04/2006	60.367	134.458	170	Clay, permafrost	KS-2000, Baikal-8
14	Ust-Nera	UNR	21/11/1961	64.566	143.228	485	Loams, permafrost	CME-6211, Baikal-8
15	Khany	KHNR	11/12/2005	56.921	119.979	690	Granitic gneisses	KS-2000, Baikal-8
16	Chagda	CGD	01/08/1968	58.752	130.609	195	Pebbles, clay, permafrost	CM3-KB, Baikal 11
17	Chernyshevsky	YCRN	14/07/2011	63.021	112.486	319	Pebbles, clay	KS-2000, Baikal-8
18	Chulman	CLNS	01/07/1963	56.837	124.893	745	Sandstone	CMG-3ESPC, CD-24
19	Yuktali	YKLR	04/07/2004	56.5915	121.654	417	Loams	CMG-3ESPC, CD-24
20	Yakutsk	YAK	04/10/1957 31/08/1993 (IRIS)	62.031	129.68	91	Sandstone, permafrost	STS-1, STS-2, Q330

The Yakutia Branch of GS RAS uses the Seismic Data Processing System WSG (<http://www.gsras.ru/new/soft/WSG/>), designed to analyse seismic signals and obtain estimates for hypocenter parameters of seismic events, both from the records of a single station as well as multiple stations. To store processing results, a SQL-compatible database with an ODBC driver is used. The authors of the program are Akimov Andrey Petrovich and Krasilov Sergey Alexandrovich (*Akimov and Krasilov, 2020*). In the processing routine we use the IASPEI-91 (*Kennet and Engdahl, 1991*) and Baikal (*Golenetsky, 1990*) travel time curves.

Integrated processing of the instrumentally-recorded data from the territory of Yakutia and neighboring regions, is performed by the instrumental observation interpretation and processing group of the Yakutia Branch of the GS RAS in the city of Yakutsk, as the digital earthquake records arrive from the local seismic stations (in near real-time). After a preliminary assessment of the records' quality, fixing of gaps in recorded data, analysing the operation of the individual channel components (EW, NS, UD) and timing, as well as assessing background interference (noise), the data is transferred to a group of regional stations to add to their processing procedures. The result of the this data-processing workflow provides the annual catalogue and map of earthquake epicenters in Yakutia (Fig. 5.2), which is sent to the Geophysical Service of the Russian Academy of Sciences in the city of Obninsk.

#### 5.1.4 General Characteristics of the Observed Seismicity

As a result of seismic monitoring, it has been established that earthquakes on the territory of Yakutia are concentrated along two extended seismic belts: the Arctic-Asian belt in the north-east, and the Baial-Stanovoy belt in the south (Fig. 5.2) (*Imaev et al., 2000*).

The Arctic-Asian earthquake belt traces across the Arctic Ocean, northeast Yakutia, the Sea of Okhotsk and the Kamchatka peninsula to the Aleutian island arc, and connects seismicity manifestations in the

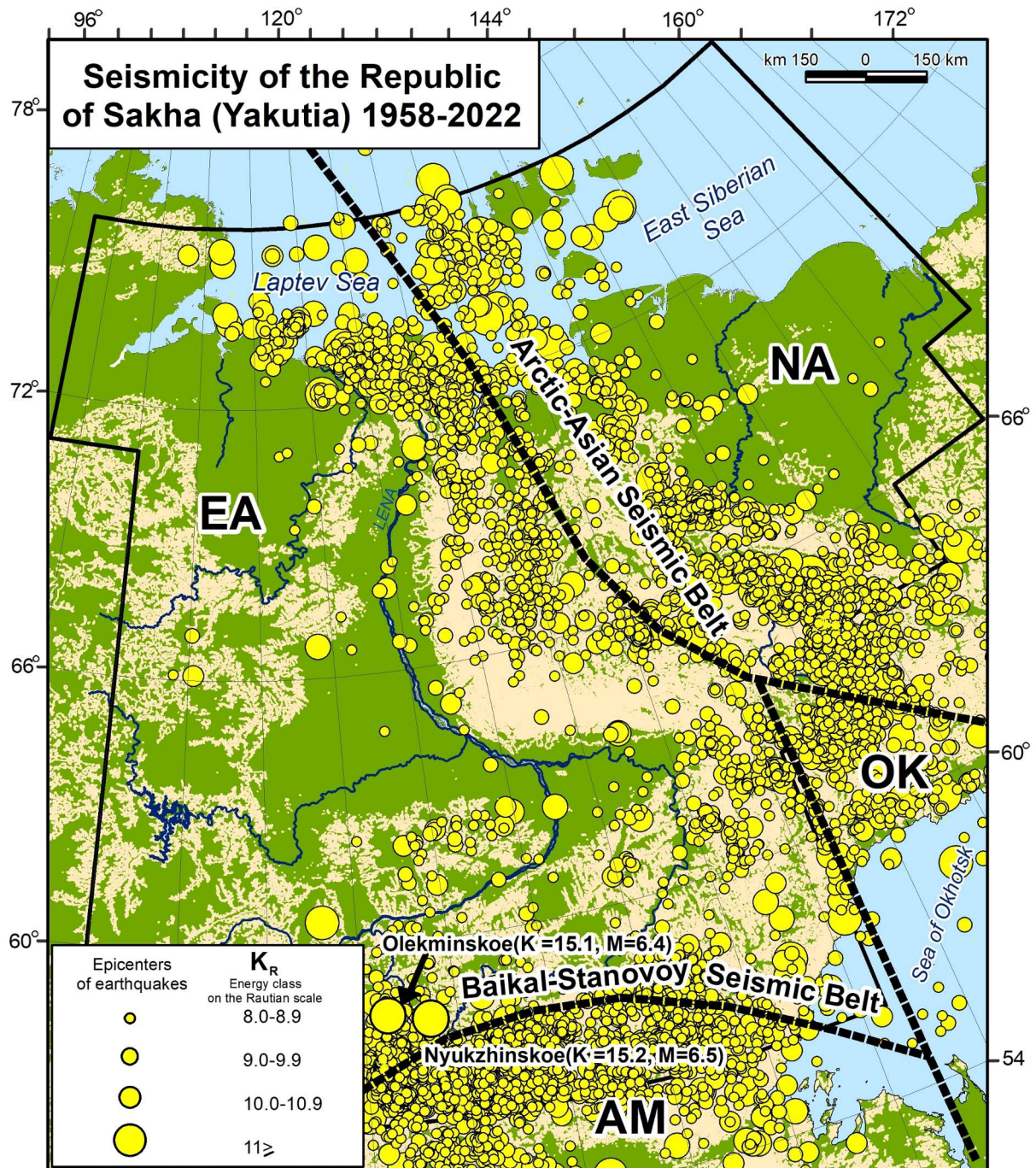


**Figure 5.2:** Map of seismic activity on the territory of the Republic of Sakha (Yakutia). Dotted lines show the boundaries of lithospheric plates and blocks traced by seismicity (circles) of the Arctic-Asian belt in the northeast and Baikal-Stanovoy belt in the south (Imaev et al., 2000). NA - North American, EA - Eurasian, OK - Okhotomorskaya, AM - Amurskaya lithospheric plates. See Section 5.1.4 for information on energy class  $K_R$ .

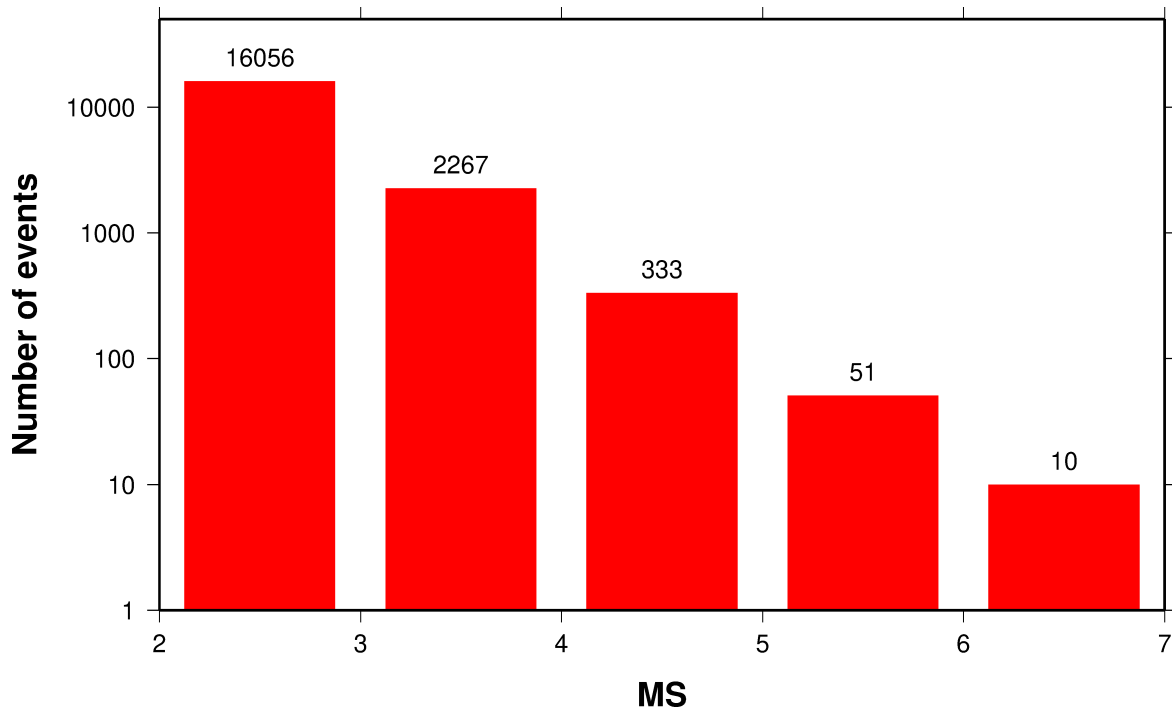


**Figure 5.3:** Earthquakes recorded at seismic stations of the Yakutia Branch of the GS RAS for the time period of 1960 to 2022. Magnitudes ( $MS$ ) were calculated from the Rautian energy classes ( $K_R$ ), see Section 5.1.4.

Arctic and Pacific regions. The Arctic-Asian belt separates the North American (NA), Eurasian (EA), Okhotomor (OK) and Pacific lithospheric plates, and is more than 10,000 km long (*Imaev et al.*, 2000).

The Baikal-Stanovoy belt in southern Siberia extends from Lake Baikal to the Sea of Okhotsk. It combines the Baikal rift zone and the Olekmo-Stanovaya seismic zone, which continues sub latitudinally from the Olekma River eastward to the Udskeya Bay of the Sea of Okhotsk, along a distance of over 3,000 km. This belt serves as the boundary between the Eurasian and Amur (Chinese) lithospheric plates and is reflected in the map of modern geodynamics of Northeast Asia (*Chemezov et al.*, 2007; Fig. 5.2).

Over the 66-year period of instrumental observations in Yakutia, more than 18,000 local earthquakes with  $MS \geq 2$  have been recorded (Fig. 5.3), where  $MS$  was calculated from the energy class  $K_R$  (*Rautian*, 1960). Equivalent to magnitude, the energy class  $K_R$  is a measure of the size of an earthquake and was defined as  $K = \log E$ , where  $E$  is the released seismic energy in Joules. The relation of magnitude  $M$  and energy class  $K$  can be approximated as  $K = 1.8M + 4$  (*Rautian*, 1960). More information on the relation of the energy class  $K_R$  to magnitudes  $mb$  and  $MS$  can be found in *Rautian et al.* (2007) and *Bormann et al.* (2013).

Currently, the seismic network of Yakutia annually records 1,000 - 5,000 local and regional earthquakes. Their spatial distribution covers more than 1.5 million  $km^2$ , which corresponds to almost half of the territory of the Republic of Sakha (Yakutia), and constitutes about one third of the total area of seismic risk zones in all of Russia (*Alekseev and Kozmin*, 2005).



### 5.1.5 Future Seismological Observation Development Project

In order to ensure an adequate level of safety for the population living in seismically hazardous areas of Russia, and reduce the casualties and material damage from natural and man-made earthquakes, as well as to ensure the functioning and further development of the federal system of seismological observations and earthquake prediction (FSSN), a federal decree on the target program “Development of the federal system of seismological observations and earthquake prediction for 2024-2028” is prepared and submitted to the Ministry of the Russian Federation. Within the framework of this program “Development of FSSN”, the Yakutia Branch of the GS RAS proposes to implement the strategy of developing seismic observations in the Arctic regions of Yakutia by modernising and expanding the representative coverage area (Fig. 5.1). The installation of the additional four to ten seismic stations (planned by 2025) in the the river Lena delta region and New Siberian Islands will make it possible to monitor the low seismicity of the Arctic coast and the Gakkel mid-ocean ridge, and also increase the efficiency the Yakutia Branch of the GS RAS seismic network.

### 5.1.6 Conclusion

After over 60 years of operation and development of the Yakutia seismic network, some areas are still poorly covered by seismic stations, especially the Arctic regions of Yakutia. Therefore, the planned development and extension of the seismic network in Yakutia aims to equip additional stations with modern digital instrumentation, as well as to modernise the data processing center. The expansion of the seismic network of the Yakutia Branch of the GS RAS will enable the recording of smaller seismic events. In addition, with the development of the seismological network, we will be able to build 3D velocity models of the Russian Arctic.

### Acknowledgement

The work was carried out with the support of the Ministry of Education and Science of the Russian Federation (within the framework of state assignment No. 075-00682-24) and using data obtained from the unique scientific installation “Seismic infrasound array for monitoring Arctic cryolitozone and continuous seismic monitoring of the Russian Federation, neighbouring territories and the world” (<http://www.gsras.ru/unu/>).

### References

- Akimov, A.P. and S.A. Krasilov (2020), Software complex WSG “System of seismic data processing”, Certificate of state registration of computer program no. 2020664678 (16/11/2020).
- Alekseev, N.N. and B.M. Kozmin (2005), Issues of hydrocarbon resources development in Eastern Siberia and Yakutia based on consideration of modern subsurface geodynamics, *Natural resources of Arctic and Subarctic*, <https://cyberleninka.ru/article/n/voprosy-osvoeniya-uglevodorodnyh-resursov-vostochnoy-sibiri-i-yakutii-na-osnove-ucheta-sovremennoy-geodinamiki-nedr/viewer>, (In Russian).

- Bormann, P., S. Wendt and D. Di Giacomo (2013) Chapter 3: Seismic Sources and Source Parameters, In: *New Manual of Seismological Observatory Practice 2 (NMSOP-2)*, [https://doi.org/10.2312/GFZ.NMSOP-2\\_ch3](https://doi.org/10.2312/GFZ.NMSOP-2_ch3).
- Chemezov, E.N., A.F. Petrov and T.E. Blinova (2007), On seismic hazard on the territory of Yakutia, *Vestnik of MK Ammosov North-Eastern Federal University*, 4(3), pp.33-38.
- Golenetsky, S.I. (1990), Problems of the seismicity of the Baikal rift zone, *J. Geodynamics*(11), 293–307, [https://doi.org/10.1016/0264-3707\(90\)90013-K](https://doi.org/10.1016/0264-3707(90)90013-K).
- Imaev, V.S., L.P. Imaeva and B.M. Kozmin (2000), Seismotectonics of Yakutia, *GEOS*, Moscow (In Russian).
- International Seismological Centre (2024a), On-line Bulletin, <https://doi.org/10.31905/D808B830>, [http://www.isc.ac.uk/cgi-bin/web-db-run?event\\_id=883651](http://www.isc.ac.uk/cgi-bin/web-db-run?event_id=883651).
- International Seismological Centre (2024b), On-line Bulletin, <https://doi.org/10.31905/D808B830>, [http://www.isc.ac.uk/cgi-bin/web-db-run?event\\_id=885127](http://www.isc.ac.uk/cgi-bin/web-db-run?event_id=885127).
- Kennett, B.L.N. and E.R. Engdahl (1991), Travel times for global earthquake location and phase association, *Geophys. J. Int.*, 105, 429 – 465, <https://doi.org/10.17611/DP/9991809>.
- Rautian T.G. (1960), Earthquake energy, Methods for detailed study of seismicity, *Proceedings of the USSR Academy of Sciences*, 75 – 114, (In Russian).
- Rautian, T.G., V.I. Khalturin, K. Fujita, K.G. Mackey and A.D. Kendall (2007), Origins and methodology of the Russian energy K-class system and its relationship to magnitude scales, *Seismol. Res. Lett.*, 78(6), 579–590, <https://doi.org/10.1785/gssrl.78.6.579>.
- Shibaev, S.V., A.F. Petrov and K.V. Timirshin (2007), Current state of seismic observations in the territory of Sakha Republic (Yakutia), *Modern methods of processing and interpretation of seismological data* In: *Proceedings of the Second International Seismological School*, Geophysical Service of the Russian Academy of Sciences, 218 – 223, (In Russian).

## 6

# Summary of Seismicity, January – June 2021

The first six months of 2021 saw eight earthquakes with magnitudes  $M_W \geq 7$ ; these are listed in Table 6.1. Two of these earthquakes, including the largest for this Summary's time period, were doublet earthquakes near Kermadec Islands where the Pacific Plate subducts under the Indo-Australian Plate. Both events were tsunamigenic thrust earthquakes occurring within two hours and 55 km of each other (First earthquake:  $M_W$  7.4, 2021/03/04 17:41:23.89 UTC, 29.6892°S, 177.8138°W, 40 km depth, 3467 stations (ISC); second earthquake:  $M_W$  8.1, 2021/03/04 19:28:34.63 UTC, 29.4424°S, 177.0912°W, 20 km depth, 3222 stations (ISC)). Large earthquakes consistently occur in doublets in the Kermadec region and the 2021 event likely re-ruptured the same asperity as another set of doublet earthquakes from 1976 ( $M_W$  7.8 and  $M_W$  8.0), although the detailed slip distribution differs (*Lythgoe et al.*, 2023). The tsunami generated by the larger 2021 event propagated across the Pacific Ocean up to South America, and oscillations of the first tsunami could still be detected during the second tsunami (*Wang et al.*, 2022).

The most discussed earthquake in the scientific community during this Summary's time period was the  $M_W$  7.4 Maduo earthquake, Tibetan Plateau, (2021/05/21 18:04:13.39 UTC, 34.5574°N, 98.3478°E, 5 km depth, 3634 stations (ISC)) with currently 174 entries in the ISC Event Bibliography (*Di Giacomo et al.*, 2014; *International Seismological Centre*, 2024). Its rupture propagated bilaterally for a length of about 170 km along the Jianguo fault, with a complicated structural geometry (e.g. *Yao et al.*, 2024; *Yuan et al.*, 2022; *Wang et al.*, 2021). Studies revealed that the Maduo earthquake was a supershear event, where the rupture velocity exceeded the shear-wave velocity (*Zhang et al.*, 2022; *Yue et al.*, 2022).

A devastating non-tectonic event that could be observed on teleseismic stations up to 75 degrees epicentral distance was the Chamoli landslide on 7 February 2021 (04:52:03.00 UTC, 30.8033°N, 80.4205°E, depth fixed to surface, 9 stations (ISC)). A massive rock and ice avalanche descended the Ronti Gad valley in Chamoli, Uttarakhand, India, rapidly transforming into a highly mobile debris flow that caused widespread devastation, severely damaged two hydropower plants and left more than 200 people dead or missing (*Shugar et al.*, 2021).

The number of events in this Bulletin Summary categorised by type are given in Table 6.2.

Figure 6.1 shows the number of moderate and large earthquakes in the first half of 2021. The distribution of the number of earthquakes should follow the Gutenberg-Richter law.

Figures 6.2 to 6.6 show the geographical distribution of moderate and large earthquakes in various magnitude ranges.

**Table 6.1:** Summary of the earthquakes of magnitude  $M_w \geq 7$  between January and June 2021.

Date	lat	lon	depth	$M_w$	Flinn-Engdahl Region
2021-03-04 19:28:34	-29.44	-177.09	20	8.1	Kermadec Islands
2021-02-10 13:19:57	-22.91	171.64	13	7.7	Southeast of Loyalty Islands
2021-05-21 18:04:13	34.56	98.35	5	7.5	Qinghai
2021-03-04 17:41:23	-29.69	-177.81	40	7.4	Kermadec Islands
2021-03-04 13:27:36	-37.41	179.41	21	7.3	Off east coast of North Island
2021-02-13 14:07:50	37.67	141.72	52	7.1	Near east coast of eastern Honshu
2021-03-20 09:09:45	38.47	141.53	53	7.1	Near east coast of eastern Honshu
2021-01-21 12:23:05	4.95	127.47	106	7.0	Talud Islands

**Table 6.2:** Summary of events by type between January and June 2021.

damaging earthquake	1
felt earthquake	2616
known earthquake	162044
known chemical explosion	4213
known induced event	3194
known landslide	3
known mine explosion	8571
known rockburst	535
known experimental explosion	132
suspected collapse	1
suspected earthquake	121011
suspected chemical explosion	5416
suspected induced event	83
suspected mine explosion	6081
suspected rockburst	260
suspected experimental explosion	241
suspected ice-quake	123
unknown	7
total	314532

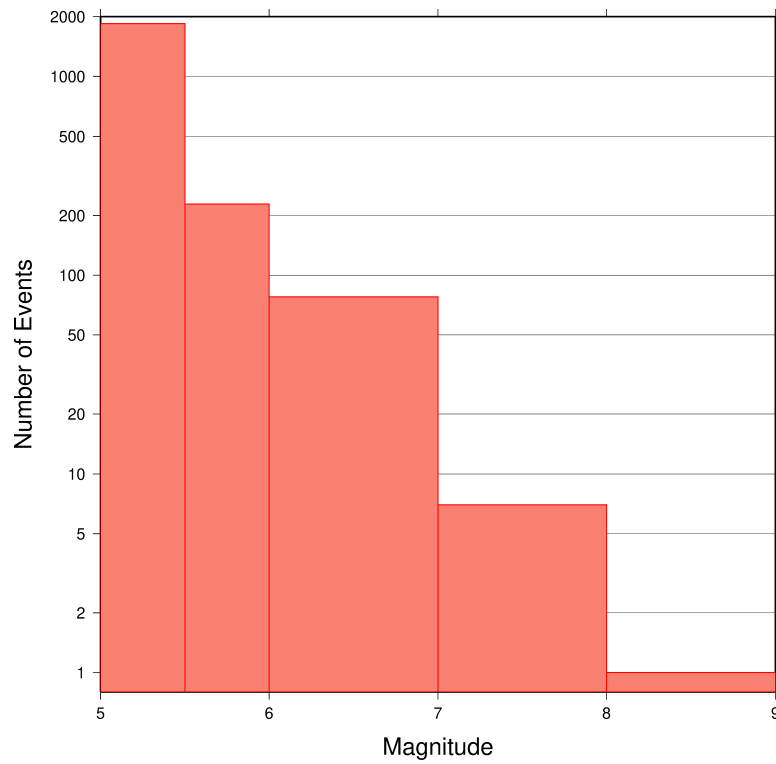


**Figure 6.1:** Number of moderate and large earthquakes between January and June 2021. The non-uniform magnitude bias here correspond with the magnitude intervals used in Figures 6.2 to 6.6.

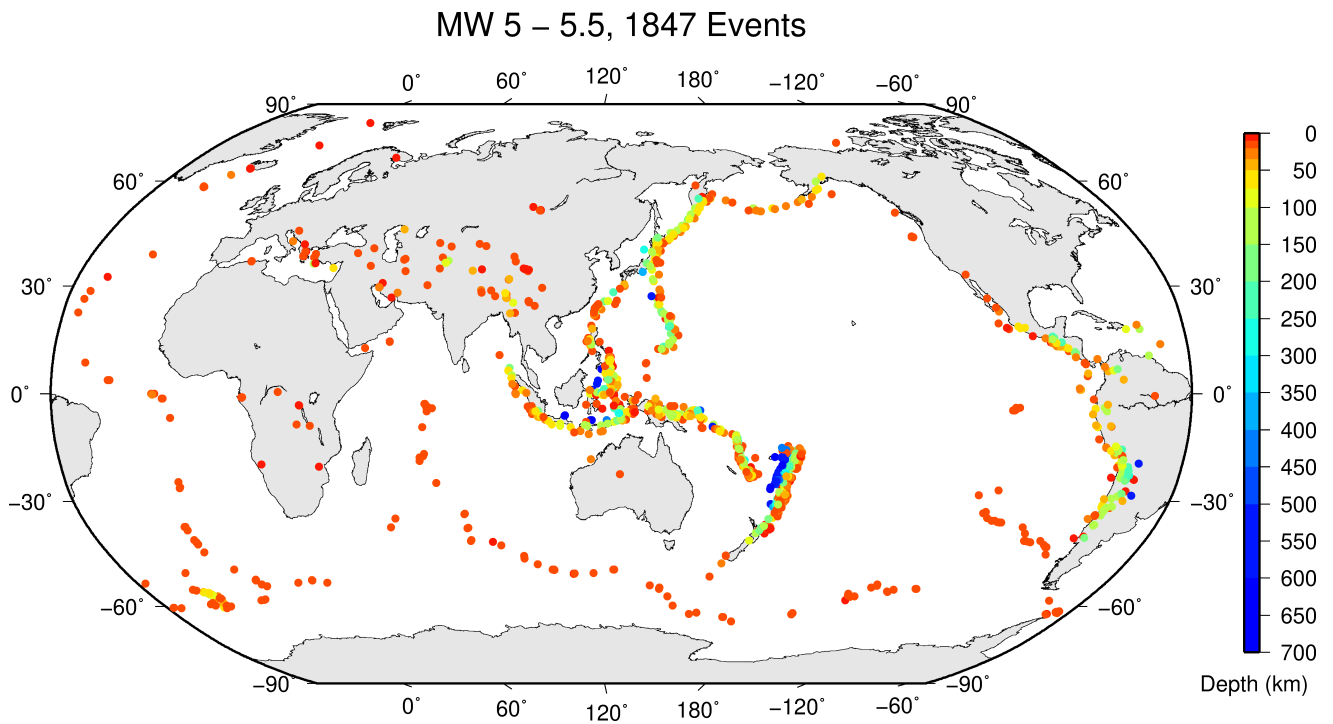


**Figure 6.2:** Geographic distribution of magnitude 5-5.5 earthquakes between January and June 2021.

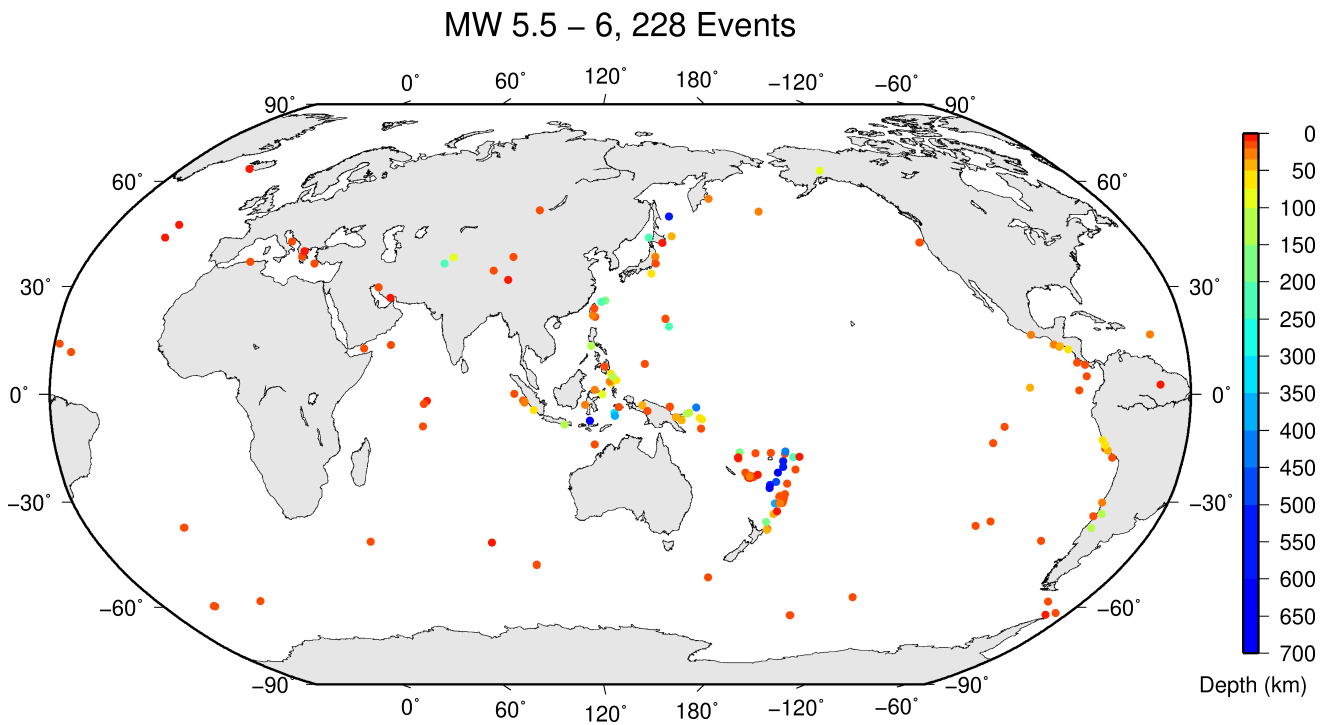


*Figure 6.3: Geographic distribution of magnitude 5.5-6 earthquakes between January and June 2021.*

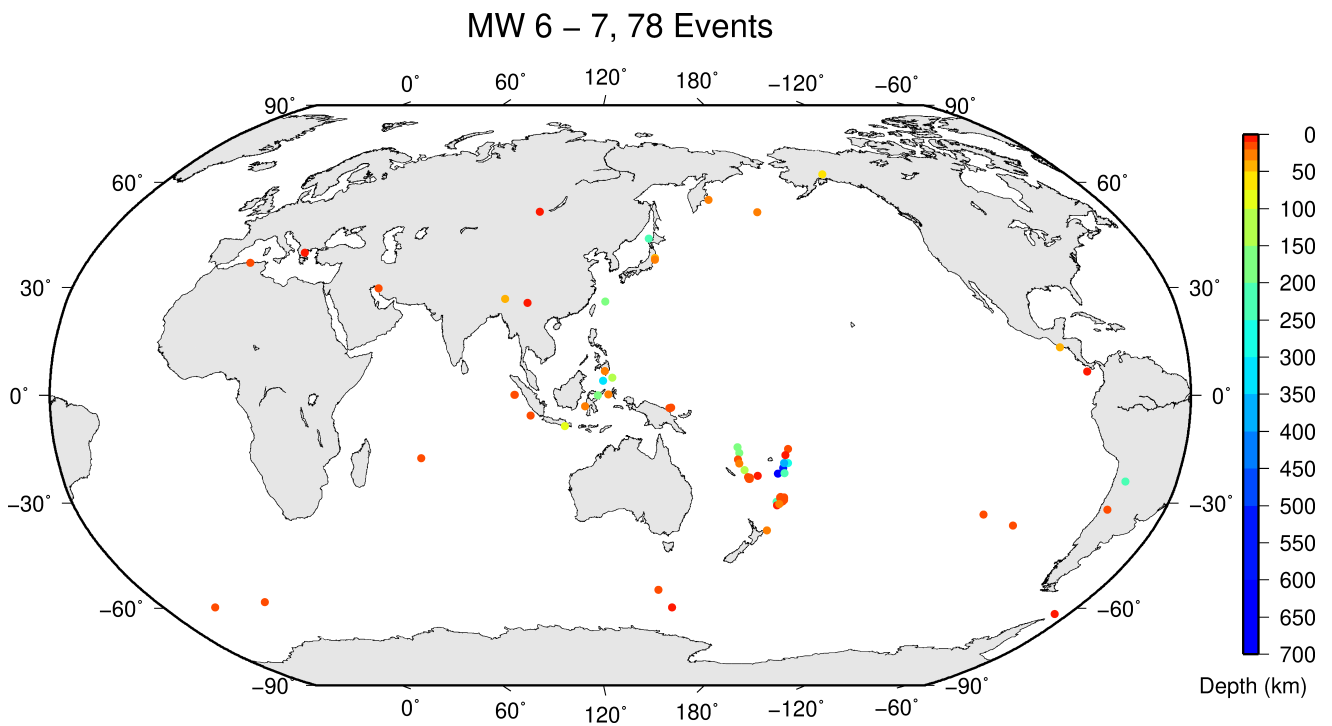


*Figure 6.4: Geographic distribution of magnitude 6-7 earthquakes between January and June 2021.*



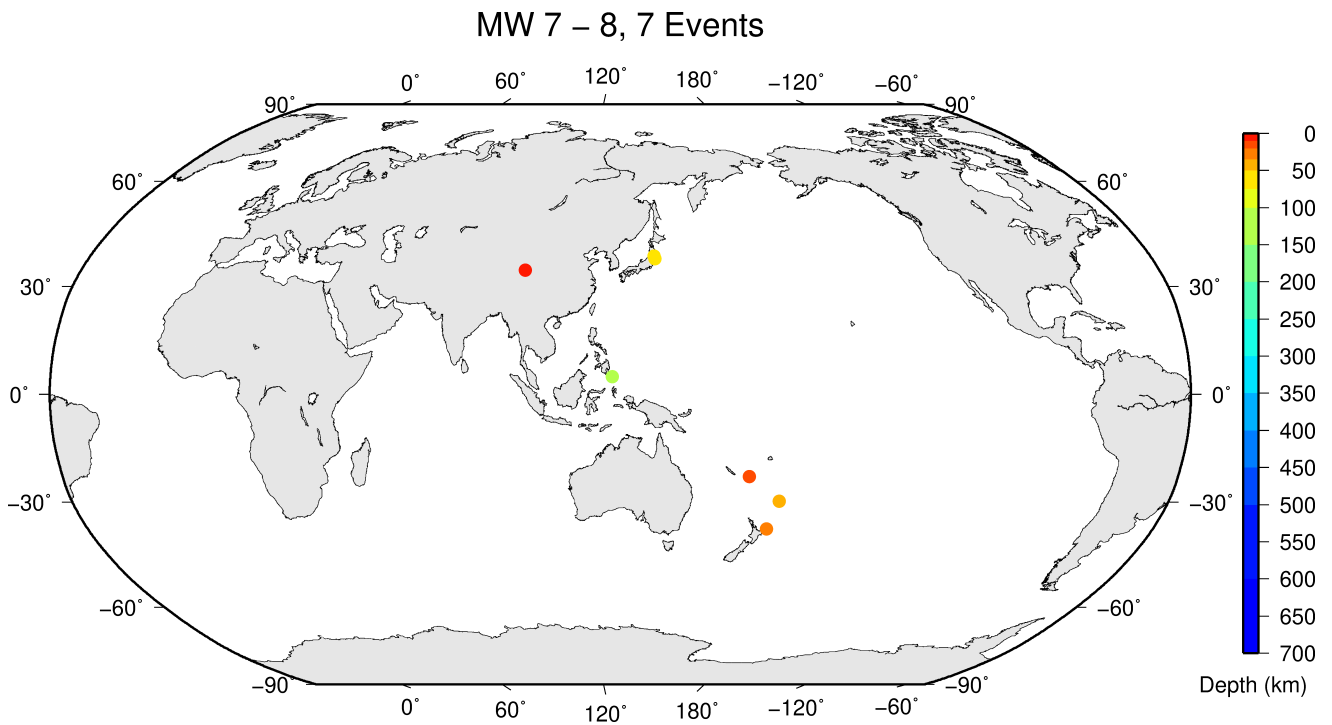


*Figure 6.5: Geographic distribution of magnitude 7-8 earthquakes between January and June 2021.*

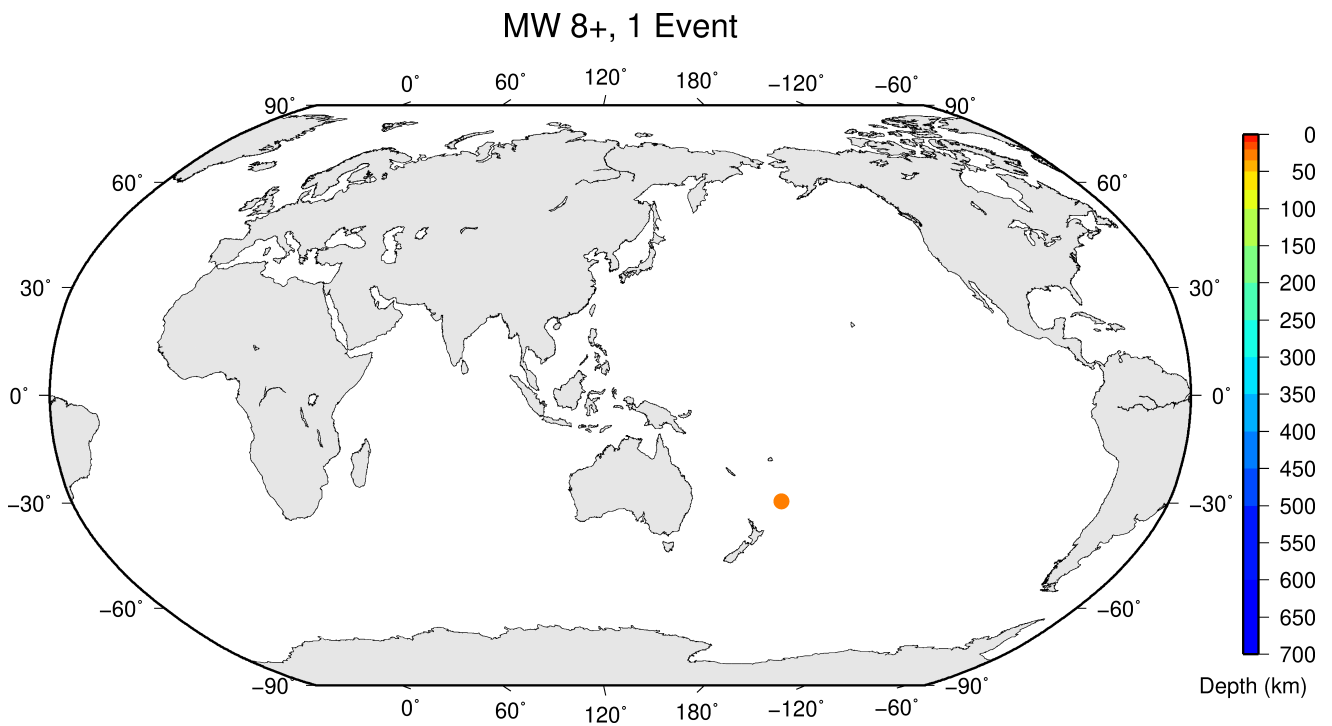


*Figure 6.6: Geographic distribution of magnitude 8+ earthquakes between January and June 2021.*

## References

- Di Giacomo, D., D.A. Storchak, N. Safronova, P. Ozgo, J. Harris, R. Verney and I. Bondár (2014), A New ISC Service: The Bibliography of Seismic Events, *Seismol. Res. Lett.*, 85(2), 354–360, <https://doi.org/10.1785/0220130143>.
- International Seismological Centre (2024), On-line Event Bibliography, <https://doi.org/10.31905/EJ3B5LV6>.
- Lythgoe, K., K. Bradley, H. Zeng, and S. Wei (2023), Persistent asperities at the Kermadec subduction zone controlled by changes in forearc structure: 1976 and 2021 doublet earthquakes, *Earth Planet. Sci. Lett.*, 624, 118465, <https://doi.org/10.1016/j.epsl.2023.118465>.
- D. H. Shugar et al. (2021), A massive rock and ice avalanche caused the 2021 disaster at Chamoli, Indian Himalaya, *Science*, 373, 300–306, <https://doi.org/10.1126/science.abh4455>.
- Wang, W., L. Fang, J. Wu, H. Tu, L. Chen, G. Lai and L. Zhang (2021), Aftershock sequence relocation of the 2021 MS7.4 Maduo earthquake, Qinghai, China, *Science China Earth Sciences*, 64(8), 1371–1380, <https://doi.org/10.1007/s11430-021-9803-3>.
- Wang, Y., M. Heidarzadeh, K. Satake and G. Hu (2022), Characteristics of two tsunamis generated by successive Mw 7.4 and Mw 8.1 earthquakes in the Kermadec Islands on 4 March 2021, *Nat. Hazards Earth Syst. Sci.*, 22, 1073–1082, <https://doi.org/10.5194/nhess-22-1073-2022>.
- Yao, W., J. Liu-Zeng, X. Shi, Z. Wang, A.R. Padilla, K. Qin, L. Han, Y. Shao, X. Liu, J. Xu, Y. Wang and Y. Gao (2024), Rupture branching, propagation, and termination at the eastern end of the 2021 Mw 7.4 Maduo earthquake, northern Tibetan plateau, *Tectonophysics*, 876, 230262, <https://doi.org/10.1016/j.tecto.2024.230262>.
- Yuan, Z., T. Li, P. Su, H. Sun, G. Ha, P. Guo, G. Chen and J.T. Jobe (2022), Large surface-rupture gaps and low surface fault slip of the 2021 Mw 7.4 Maduo earthquake along a low-activity strike-slip fault, Tibetan Plateau, *Geophys. Res. Lett.*, 49(6), e2021GL096874, <https://doi.org/10.1029/2021GL096874>.
- Yue, H., Z.-K. Shen, Z. Zhao, T. Wang, B. Cao, Z. Li, X. Bao, L. Zhao, X. Song, Z. Ge, C. Ren, W. Lu, Y. Zhang, J. Liu-Zeng, M. Wang, Q. Huang, S. Zhou and L. Xue (2022), Rupture process of the 2021 M7.4 Maduo earthquake and implication for deformation mode of the Songpan-Ganzi terrane in Tibetan Plateau, *Proc. Nat. Academy of Science*, 119(23), e2116445119, <https://doi.org/10.1073/pnas.2116445119>.
- Zhang, X., W. Feng, H. Du, S. Samsonov and L. Yi (2022) Supershear rupture during the 2021 Mw 7.4 Maduo, China, earthquake, *Geophys. Res. Lett.*, 49(6), e2022GL097984, <https://doi.org/10.1029/2022GL097984>.

# 7

## Statistics of Collected Data

### 7.1 Introduction

The ISC Bulletin is based on the parametric data reports received from seismological agencies around the world. With rare exceptions, these reports include the results of waveform review done by analysts at network data centres and observatories. These reports include combinations of various bulletin elements such as event hypocentre estimates, moment tensors, magnitudes, event type and felt and damaging data as well as observations of the various seismic waves recorded at seismic stations.

Data reports are received in different formats that are often agency specific. Once an authorship is recognised, the data are automatically parsed into the ISC database and the original reports filed away to be accessed when necessary. Any reports not recognised or processed automatically are manually checked, corrected and re-processed. This chapter describes the data that are received at the ISC before the production of the reviewed Bulletin.

Notably, the ISC integrates all newly received data reports into the automatic ISC Bulletin (available on-line) soon after these reports are made available to ISC, provided it is done before the submission deadline that currently stands at 12 months following an event occurrence.

With data constantly being reported to the ISC, even after the ISC has published its review, the total data shown as collected, in this chapter, is limited to two years after the time of the associated reading or event, i.e. any hypocentre data collected two years after the event are not reflected in the figures below.

### 7.2 Summary of Agency Reports to the ISC

A total of 151 agencies have reported data for January 2021 to June 2021. The parsing of these reports into the ISC database is summarised in Table 7.1.

**Table 7.1:** Summary of the parsing of reports received by the ISC from a total of 151 agencies, containing data for this summary period.

	Number of reports
Total collected	8430
Automatically parsed	7260
Manually parsed	1170

Data collected by the ISC consists of multiple data types. These are typically one of:

- Bulletin, hypocentres with associated phase arrival observations.

- Catalogue, hypocentres only.
- Unassociated phase arrival observations.

In Table 7.2, the number of different data types reported to the ISC by each agency is listed. The number of each data type reported by each agency is also listed. Agencies reporting indirectly have their data type additionally listed for the agency that reported it. The agencies reporting indirectly may also have ‘hypocentres with associated phases’ but with no associated phases listed - this is because the association is being made by the agency reporting directly to the ISC. Summary maps of the agencies and the types of data reported are shown in Figure 7.1 and Figure 7.2.

**Table 7.2:** Agencies reporting to the ISC for this summary period. Entries in bold are for new or renewed reporting by agencies since the previous six-month period.

Agency	Country	Directly or indirectly reporting (D/I)	Hypocentres with associated phases	Hypocentres without associated phases	Associated phases	Unassociated phases	Amplitudes
TIR	Albania	D	2793	802	48320	6	13683
CRAAG	Algeria	D	344	0	3036	0	0
LPA	Argentina	D	0	0	0	757	0
SJA	Argentina	D	967	2	43977	7	13342
NSSP	Armenia	D	48	2	1064	0	0
AUST	Australia	D	3045	11	305548	0	303908
CUPWA	Australia	D	38	0	594	0	0
IDC	Austria	D	19854	0	689142	0	598044
VIE	Austria	D	7319	162	82088	1474	83227
AZER	Azerbaijan	D	2466	0	44306	0	0
UCC	Belgium	D	1805	0	11224	8	3122
SCB	Bolivia	D	583	0	8271	0	1142
RHSSO	Bosnia and Herzegovina	D	1287	0	19140	5746	0
BGSI	Botswana	D	562	0	8833	0	2870
OSUNB	Brazil	D	199	0	4220	0	0
VAO	Brazil	D	876	13	19720	0	0
SOF	Bulgaria	D	389	0	4555	1951	0
OTT	Canada	D	1478	39	34341	0	5131
PGC	Canada	I OTT	711	0	17928	0	0
GUC	Chile	D	3443	696	101323	19166	33919
BJI	China	D	1632	6	124535	27525	83710
ASIES	Chinese Taipei	D	0	41	0	0	0
TAP	Chinese Taipei	D	11191	0	714856	0	0
RSNC	Colombia	D	11957	7	274305	293	26137
UCR	Costa Rica	D	499	3	19851	0	0
ZAG	Croatia	D	1	0	0	91614	0
SSNC	Cuba	D	2419	39	38179	17	14727
NIC	Cyprus	D	234	0	7063	0	2879
IPEC	Czech Republic	D	595	0	8974	25812	2884
PRU	Czech Republic	D	6032	0	73227	395	16724
WBNET	Czech Republic	D	1977	1	43430	41	43464
KEA	Democratic People's Republic of Korea	D	191	0	2282	0	1125
DNK	Denmark	D	2094	1113	29264	23133	7308
OSPL	Dominican Republic	D	619	0	8660	0	2561
SDD	Dominican Republic	D	1332	0	30944	93	11203
IGQ	Ecuador	D	159	0	7770	0	0
HLW	Egypt	D	320	0	2986	0	0
SNET	El Salvador	D	9499	215	64389	360	0
EST	Estonia	I HEL	223	9	0	0	0
HEL	Finland	D	6745	1265	187055	0	35950
CSEM	France	I AWI	2602	733	0	0	0
IPGP	France	D	0	129	0	0	0
LDG	France	D	1634	57	28818	0	9660
STR	France	D	3888	1	74388	58	0

Table 7.2: (continued)

Agency	Country	Directly or indirectly reporting (D/I)	Hypocentres with associated phases	Hypocentres without associated phases	Associated phases	Unassociated phases	Amplitudes
PPT	French Polynesia	D	1464	77	10271	14	9814
TIF	Georgia	D	0	102	0	1832	0
AWI	Germany	D	2427	0	9654	365	9779
BGR	Germany	D	759	394	21429	0	6101
BNS	Germany	I BGR	7	38	0	0	0
BRG	Germany	D	0	0	0	13523	4700
CLL	Germany	D	2998	0	18606	3328	7388
GDNRW	Germany	I BGR	0	1	0	0	0
GFZ	Germany	D	2725	922	193093	0	592670
HLUG	Germany	I BGR	1	1	0	0	0
LEDBW	Germany	I BGR	27	3	0	0	0
ATH	Greece	D	11861	30	576323	0	142853
THE	Greece	D	6025	116	192957	4419	103226
UPSL	Greece	D	0	13	0	0	0
GCG	Guatemala	D	1231	0	11176	0	463
HKC	Hong Kong	D	0	0	0	29	0
KRSZO	Hungary	D	781	100	19840	0	7785
REY	Iceland	D	239	0	11155	0	0
HYB	India	D	931	2	3374	0	119
NDI	India	D	807	6	20731	1129	4864
DJA	Indonesia	D	5902	4	266128	0	202202
TEH	Iran	D	1555	0	33845	0	12834
THR	Iran	D	27	0	646	0	231
ISN	Iraq	D	185	3	1727	0	435
DIAS	Ireland	D	0	0	0	987	0
GII	Israel	D	2517	0	48268	0	0
GEN	Italy	D	646	0	16298	8	0
MED_RCMT	Italy	D	0	88	0	0	0
RISSC	Italy	D	12	0	245	0	0
ROM	Italy	D	8393	279	745850	248779	491481
SARA	Italy	D	215	0	2744	0	0
TRI	Italy	D	0	0	0	8649	0
JSN	Jamaica	D	156	2	1241	8	0
JMA	Japan	D	100714	14285	660946	0	12472
NIED	Japan	D	0	652	0	0	0
SYO	Japan	D	0	0	0	889	0
JSO	Jordan	D	692	0	12381	0	4053
NNC	Kazakhstan	D	8328	0	77946	0	71969
SOME	Kazakhstan	D	4108	92	51612	0	44881
KNET	Kyrgyzstan	D	1170	0	9918	0	4530
KRNET	Kyrgyzstan	D	5111	0	72618	7	0
LVSN	Latvia	D	528	0	9923	346	6643
GRAL	Lebanon	D	97	0	928	1102	0
LIT	Lithuania	D	793	792	4659	423	0
MCO	Macao, China	D	0	0	0	31	0
TAN	Madagascar	D	921	146	8566	6	0
GSDM	Malawi	D	0	0	0	98	0
ECX	Mexico	D	612	0	16520	0	3132
MEX	Mexico	D	13293	176	227094	0	9
PDG	Montenegro	D	632	2	15297	60	6653
CNRM	Morocco	D	4505	0	50124	0	0
NAM	Namibia	D	147	0	1664	0	470
DMN	Nepal	D	1741	0	17606	13	14248
DBN	Netherlands	I BGR	0	3	0	0	0
NOU	New Caledonia	D	2405	1263	46952	0	29286
WEL	New Zealand	D	14099	134	753687	86796	275769
CATAC	Nicaragua	D	2253	0	82423	0	0
SKO	North Macedonia	D	0	603	8634	4116	1669
BER	Norway	D	2192	1361	48772	4954	10931
NAO	Norway	D	2761	604	6538	0	2500
OMAN	Oman	D	695	0	31466	0	0
UPA	Panama	D	600	1	9259	23	38
ARE	Peru	I RSNC	7	0	0	0	0
MAN	Philippines	D	20	2543	2270	81508	14890
QCP	Philippines	D	0	0	0	174	0
PJWWP	Poland	D	116	1	256	0	15

Table 7.2: (continued)

Agency	Country	Directly or indirectly reporting (D/I)	Hypocentres with associated phases	Hypocentres without associated phases	Associated phases	Unassociated phases	Amplitudes
WAR	Poland	D	0	0	0	19468	704
IGIL	Portugal	D	809	0	3149	0	899
INMG	Portugal	D	2069	2	100306	8161	49977
SVSA	Portugal	D	488	0	15070	2274	10349
BELR	Republic of Belarus	D	0	0	0	24990	7986
CFUSG	Republic of Crimea	D	99	0	2373	11	1433
KMA	Republic of Korea	D	9	0	217	0	0
BUC	Romania	D	526	0	22407	129629	7481
ASGSR	Russia	D	900	4561	26182	0	9110
BYKL	Russia	D	381	0	35163	0	12174
DAGSR	Russia	I MOS	181	160	0	0	0
FCIAR	Russia	D	79	0	818	149	202
IDG	Russia	I MOS	0	33	0	0	0
IGKRC	Russia	I MOS	0	26	0	0	0
KOGSR	Russia	D	1900	968	16936	64	0
KRSC	Russia	D	648	1	23235	0	0
MIRAS	Russia	D	142	0	3684	0	1881
MOS	Russia	D	2535	6235	287621	0	95083
NERS	Russia	D	138	142	2917	0	1430
NOGSR	Russia	I MOS	86	130	0	0	0
SKHL	Russia	D	676	779	14941	2	6046
YARS	Russia	D	201	82	5079	0	3000
SGS	Saudi Arabia	D	1560	0	24277	0	0
BEO	Serbia	D	1206	0	30581	0	0
BRA	Slovakia	D	0	0	0	19154	0
LJU	Slovenia	D	1362	4	15657	7441	7168
PRE	South Africa	D	1801	33	33215	274	9922
MDD	Spain	D	7258	57	151788	0	41504
MRB	Spain	D	647	0	26071	0	7527
SFS	Spain	D	1608	0	34323	12	0
UPP	Sweden	D	1849	935	23489	0	0
ZUR	Switzerland	D	538	21	22301	0	8505
BKK	Thailand	D	254	10	3576	0	3768
TRN	Trinidad and Tobago	D	3487	2732	20561	34549	0
TUN	Tunisia	D	35	0	205	0	0
AFAD	Turkey	D	12128	0	323810	1	114785
ISK	Turkey	D	13077	0	284747	1552	100237
AEIC	U.S.A.	I NEIC	1	2399	75329	0	0
BUT	U.S.A.	I NEIC	0	208	3010	0	0
GCMT	U.S.A.	D	0	2886	0	0	0
HVO	U.S.A.	I NEIC	0	660	25397	0	0
NCEDC	U.S.A.	I NEIC	1	370	29883	0	0
NEIC	U.S.A.	D	22804	8621	1728716	0	880419
PAS	U.S.A.	I NEIC	0	404	33266	0	0
PNSN	U.S.A.	D	0	93	0	0	0
PTWC	U.S.A.	D	214	0	3162	0	0
REN	U.S.A.	I NEIC	0	228	9214	0	0
RSPR	U.S.A.	D	5309	505	80313	0	0
SEA	U.S.A.	I NEIC	0	53	3357	0	0
SLM	U.S.A.	I NEIC	0	54	1180	0	0
TXNET	U.S.A.	D	3321	1	153381	0	42644
USSS	U.S.A.	I NEIC	0	67	1424	0	0
MCSM	Ukraine	D	1979	327	63070	61261	105369
SIGU	Ukraine	D	37	37	771	0	375
DSN	United Arab Emirates	D	509	0	6754	0	0
BGS	United Kingdom	D	350	9	9701	56	3801
ISC-PPSM	United Kingdom	D	0	101	0	0	0
EAF	Unknown	D	710	0	4618	4486	369
ISU	Uzbekistan	D	762	0	6208	21	0
FUNV	Venezuela	D	1014	0	10956	0	0
PLV	Viet Nam	D	69	3	362	0	114



**Table 7.2:** (continued)

Agency	Country	Directly or indirectly reporting (D/I)	Hypocentres with associated phases	Hypocentres without associated phases	Associated phases	Unassociated phases	Amplitudes
BUL	Zimbabwe	D	89	0	600	77	0

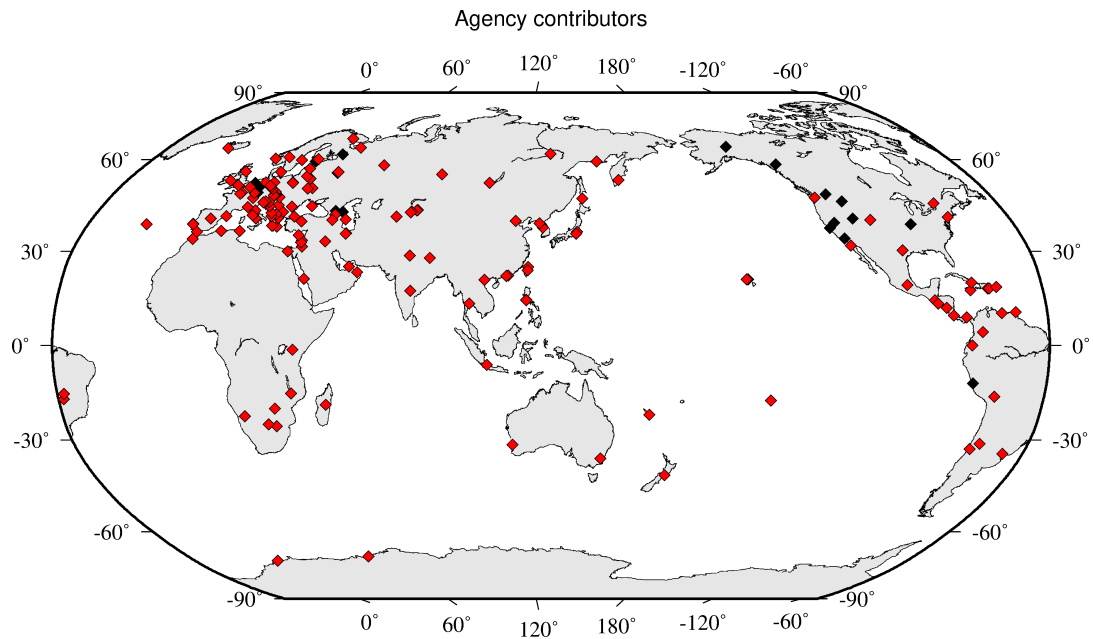


**Figure 7.1:** Map of agencies that have contributed data to the ISC for this summary period. Agencies that have reported directly to the ISC are shown in red. Those that have reported indirectly (via another agency) are shown in black. Any new or renewed agencies, since the last six-month period, are shown by a star. Each agency is listed in Table 7.2.

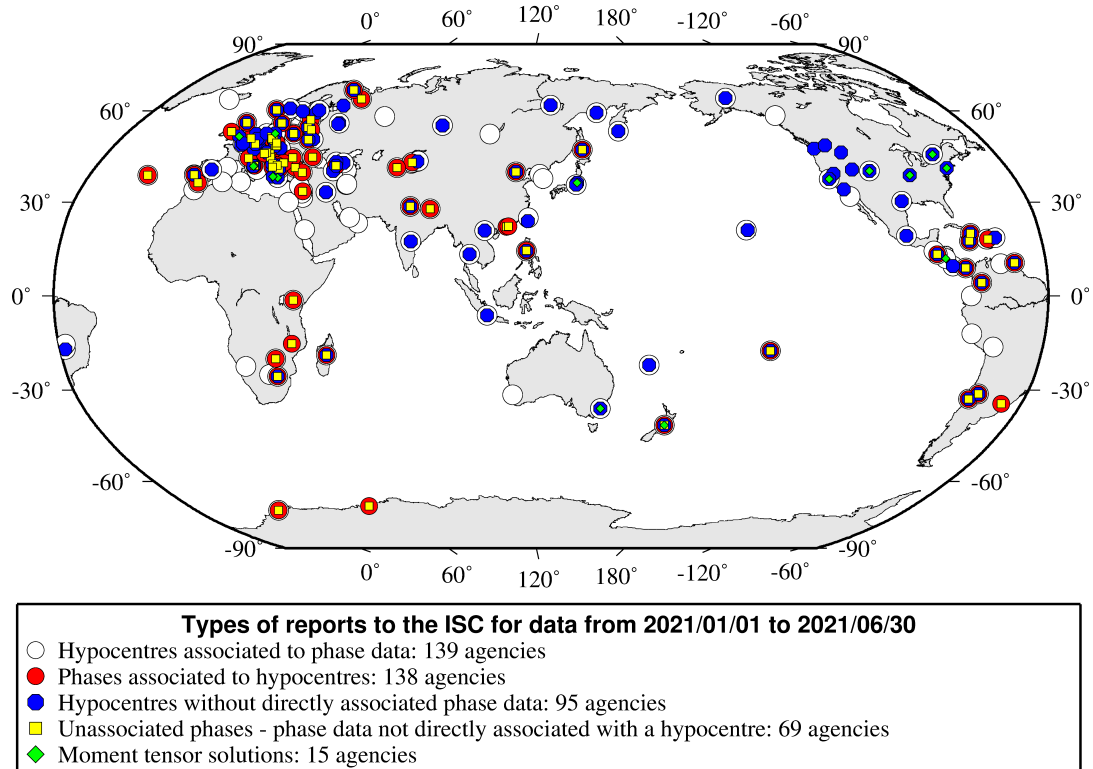


*Figure 7.2: Map of the different data types reported by agencies to the ISC. A full list of the data types reported by each agency is shown in Table 7.2.*

### 7.3 Arrival Observations

The collection of phase arrival observations at the ISC has increased dramatically with time. The increase in reported phase arrival observations is shown in Figure 7.3.

The reports with phase data are summarised in Table 7.3. This table is split into three sections, providing information on the reports themselves, the phase data, and the stations reporting the phase data. A map of the stations contributing these phase data is shown in Figure 7.4.

The ISC encourages the reporting of phase arrival times together with amplitude and period measurements whenever feasible. Figure 7.5 shows the percentage of events for which phase arrival times from each station are accompanied with amplitude and period measurements.

Figure 7.6 indicates the number of amplitude and period measurement for each station.

Together with the increase in the number of phases (Figure 7.3), there has been an increase in the number of stations reported to the ISC. The increase in the number of stations is shown in Figure 7.7. This increase can also be seen on the maps for stations reported each decade in Figure 7.8.

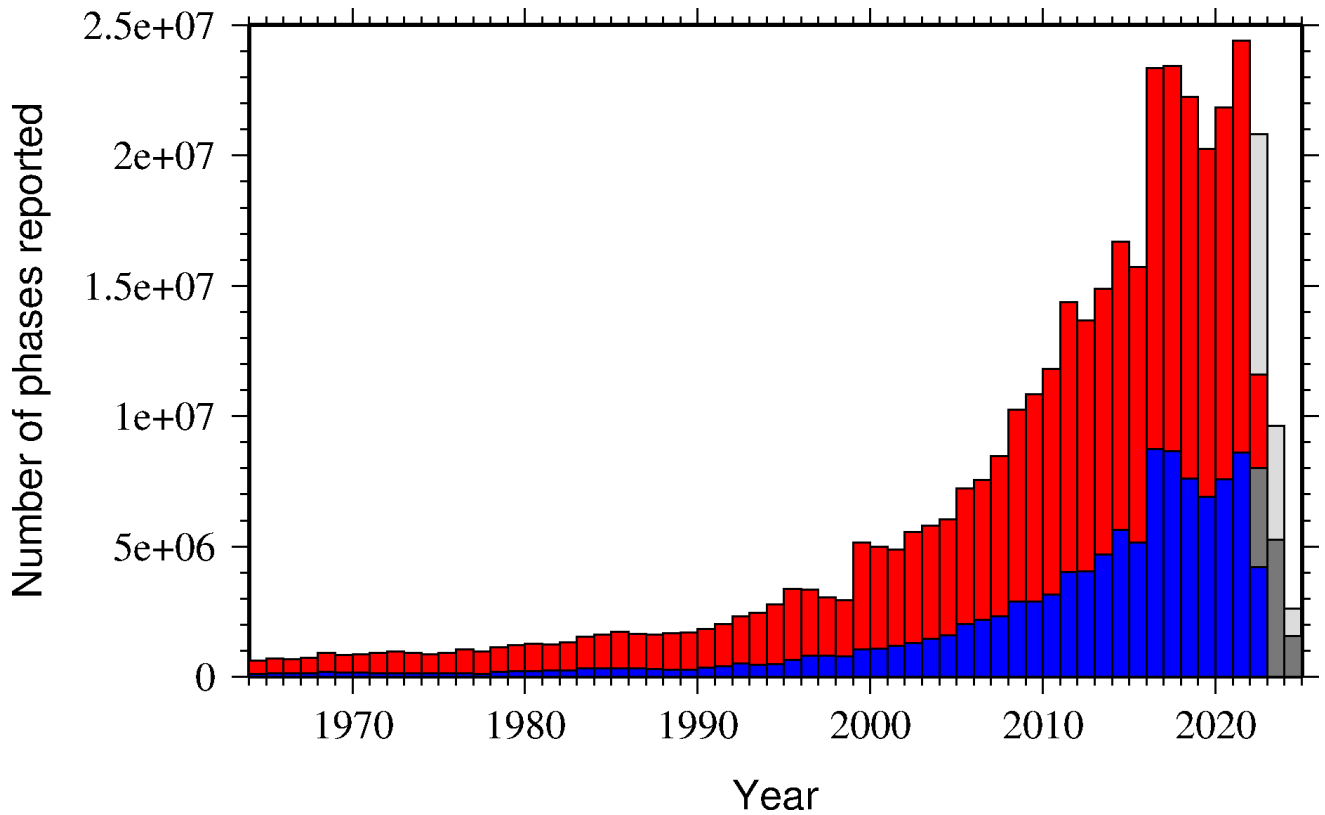
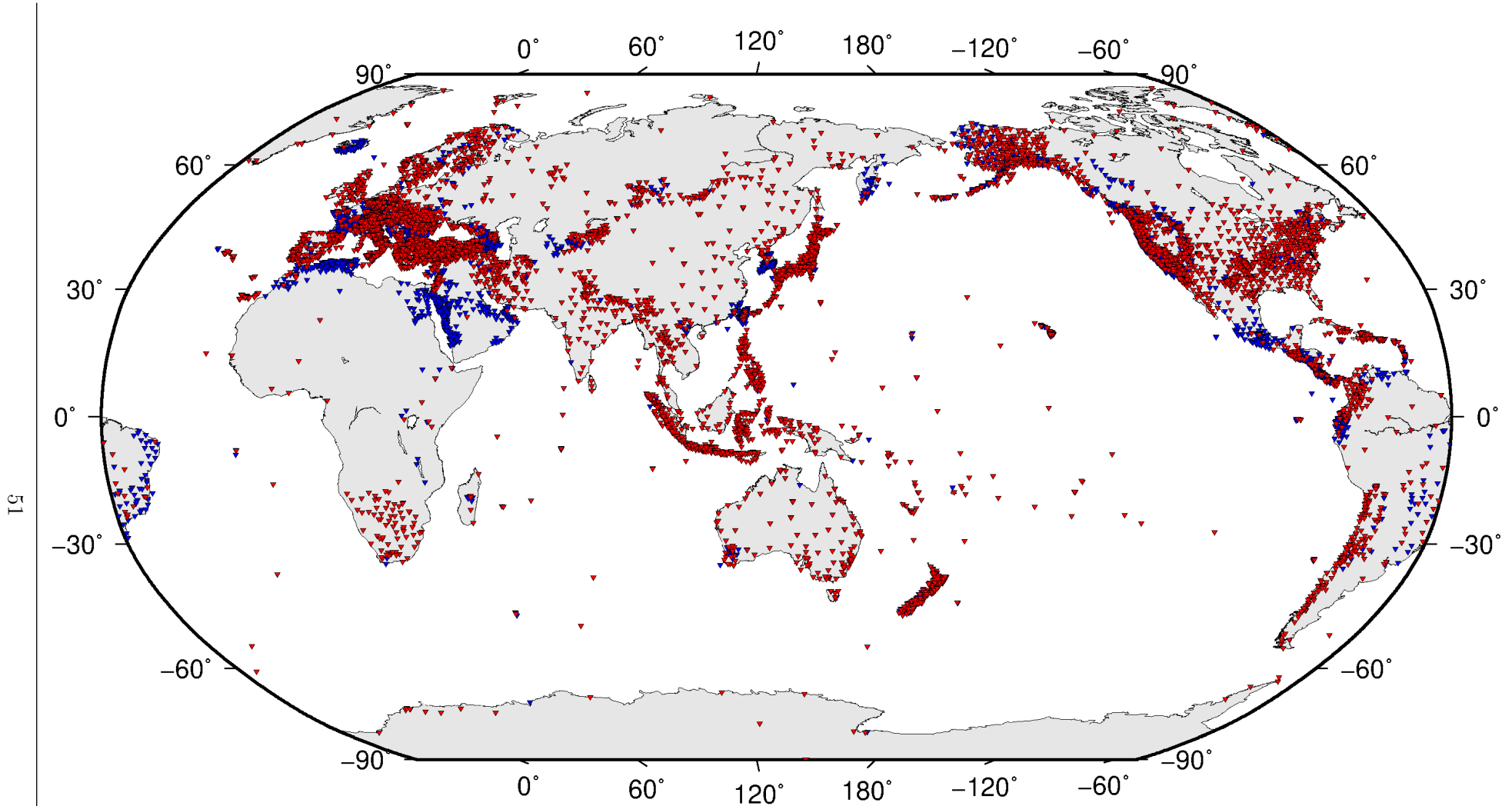


**Figure 7.3:** Histogram showing the number of phases (red) and number of amplitudes (blue) collected by the ISC for events each year since 1964. The data in grey covers the current period where data are still being collected before the ISC review takes place and is accurate at the time of publication.

**Table 7.3:** Summary of reports containing phase arrival observations.

Reports with phase arrivals	7921
Reports with phase arrivals including amplitudes	7277
Reports with only phase arrivals (no hypocentres reported)	182
Total phase arrivals received	12028061
Total phase arrival-times received	10541622
Number of duplicate phase arrival-times	874066 (8.3%)
Number of amplitudes received	4952087
Stations reporting phase arrivals	13587
Stations reporting phase arrivals with amplitude data	7668
Max number of stations per report	3105



Phase arrival data were collected by the ISC from **13587** stations for readings from **2021/01/01** to **2021/06/30**

**Figure 7.4:** Stations contributing phase data to the ISC for readings from January 2021 to the end of June 2021. Stations in blue provided phase arrival times only; stations in red provided both phase arrival times and amplitude data.

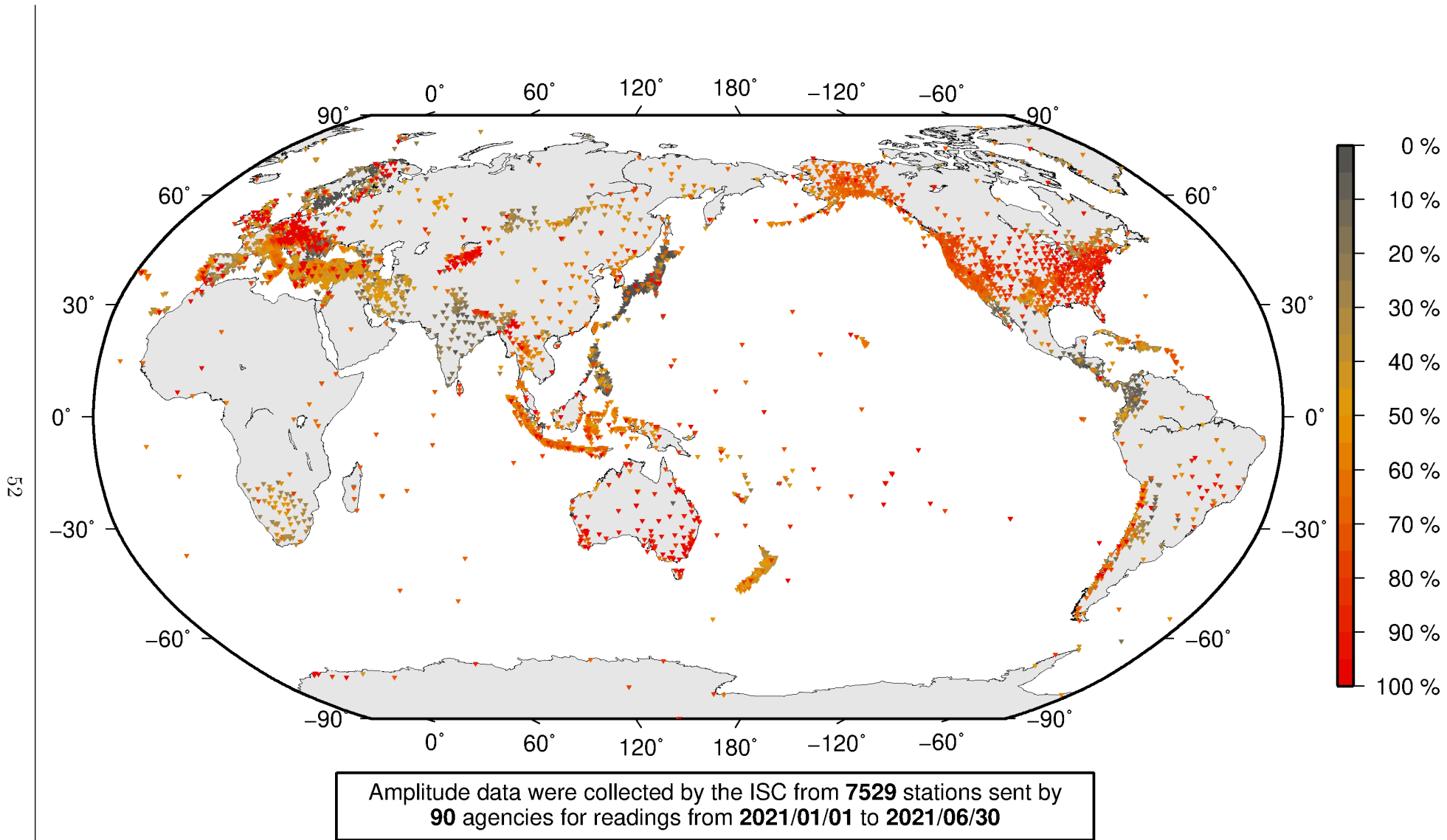
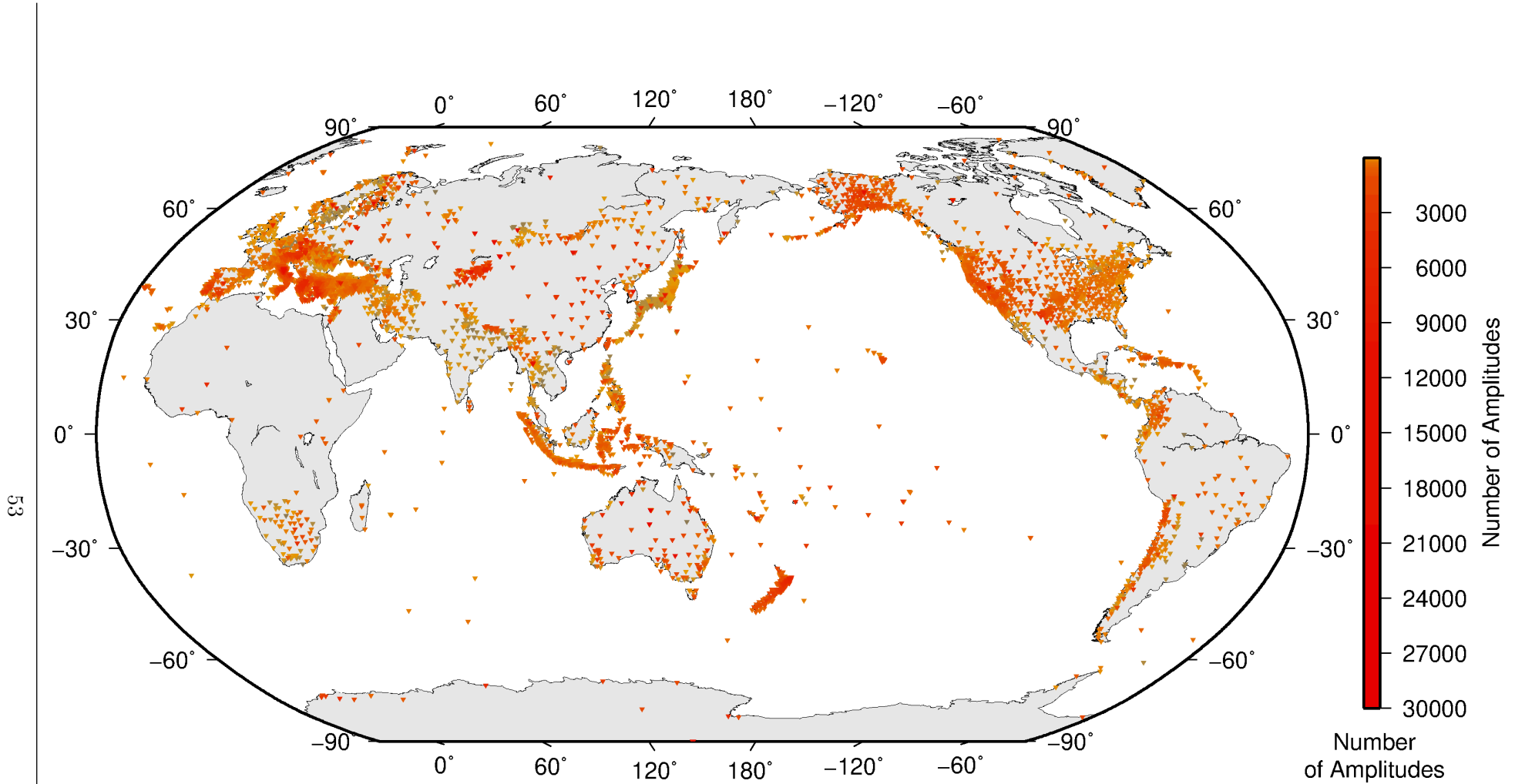


*Figure 7.5: Percentage of events for which phase arrival times from each station are accompanied with amplitude and period measurements.*





Amplitude data were collected by the ISC from **7529** stations sent by **90** agencies for readings from **2021/01/01** to **2021/06/30**

*Figure 7.6: Number of amplitude and period measurements for each station.*

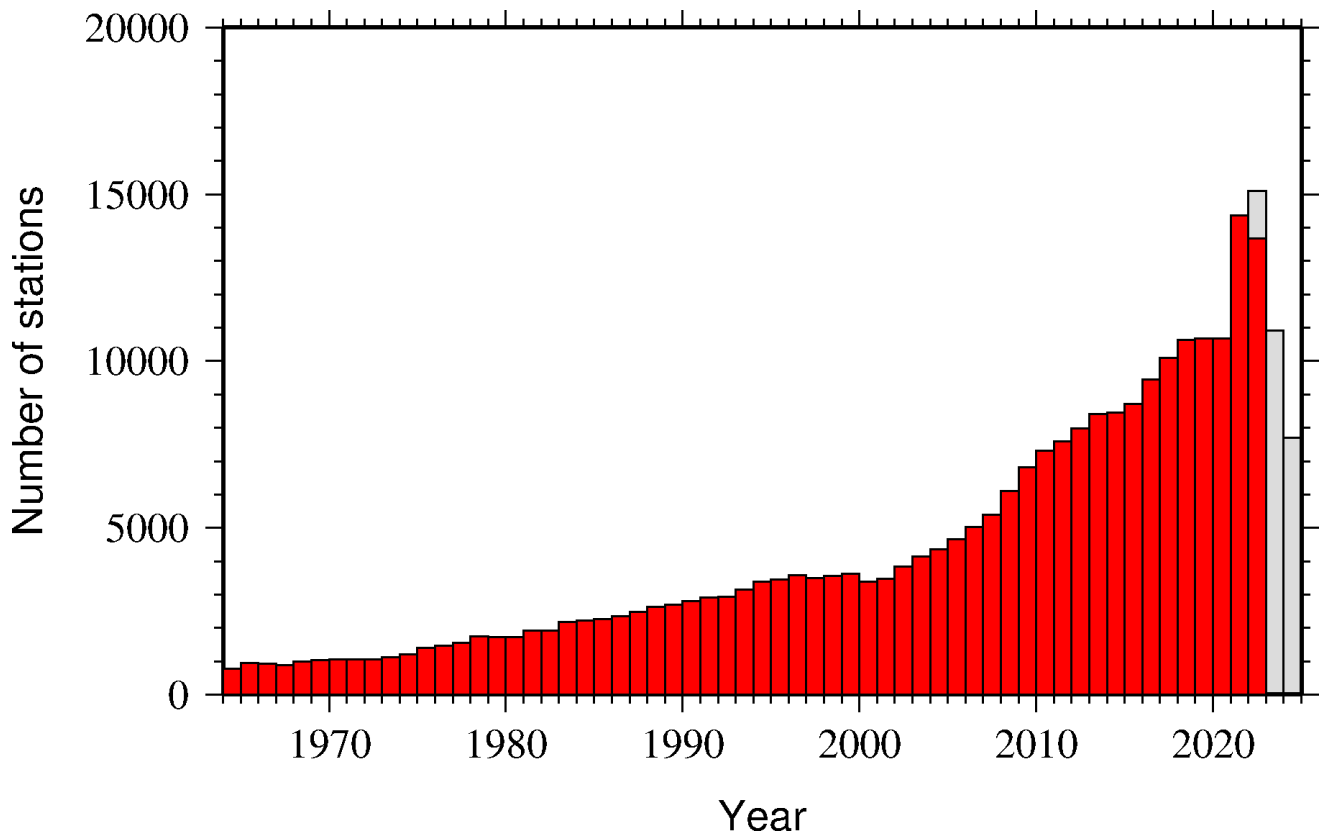


**Figure 7.7:** Histogram showing the number of stations reporting to the ISC each year since 1964. The data in grey covers the current period where station information is still being collected before the ISC review of events takes place and is accurate at the time of publication.

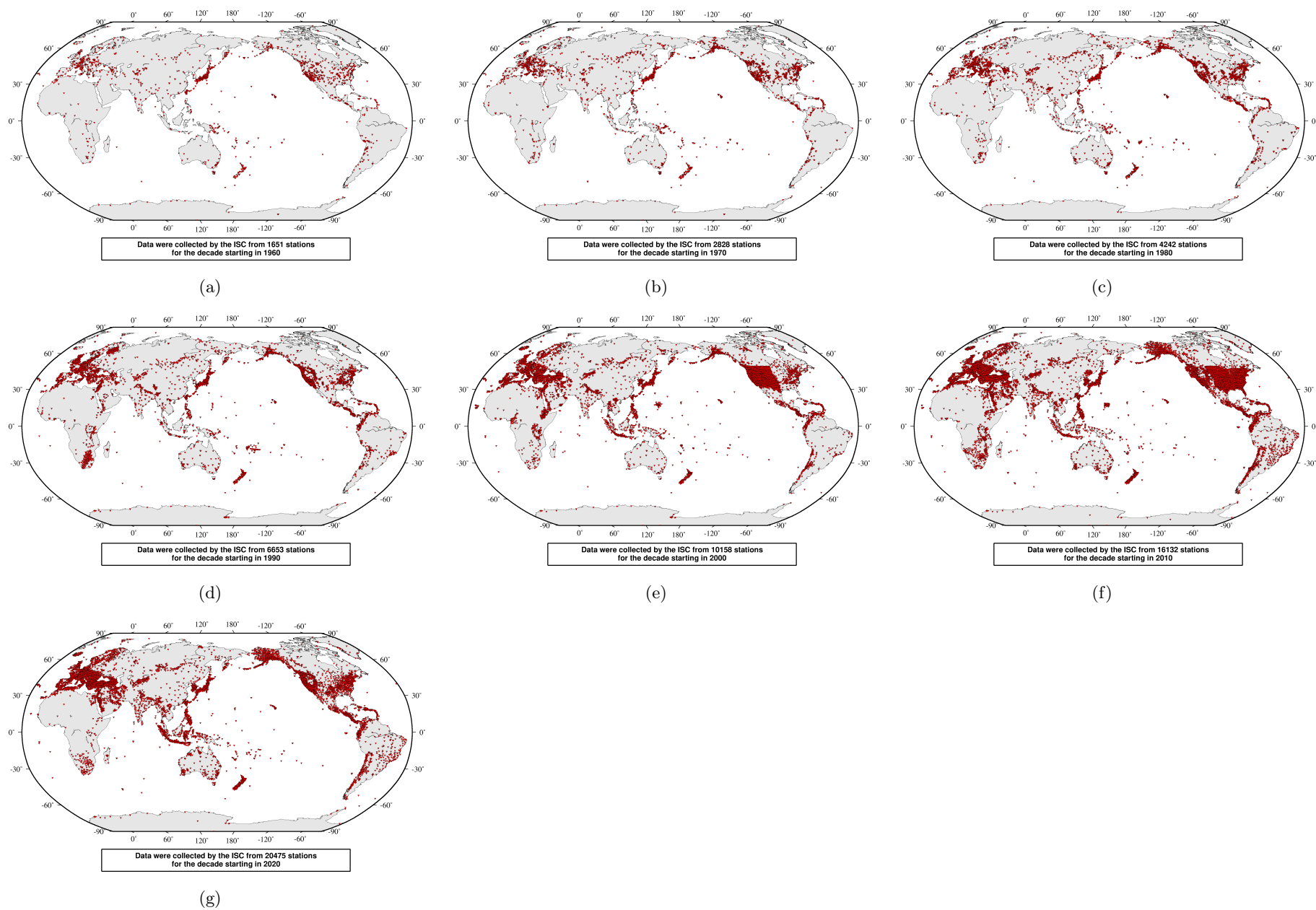


**Figure 7.8:** Maps showing the stations reported to the ISC for each decade since 1960. Note that the last map covers a shorter time period.

## 7.4 Hypocentres Collected

The ISC Bulletin groups multiple estimates of hypocentres into individual events, with an appropriate prime hypocentre solution selected. The collection of these hypocentre estimates are described in this section.

The reports containing hypocentres are summarised in Table 7.4. The number of hypocentres collected by the ISC has also increased significantly since 1964, as shown in Figure 7.9. A map of all hypocentres reported to the ISC for this summary period is shown in Figure 7.10. Where a network magnitude was reported with the hypocentre, this is also shown on the map, with preference given to reported values, first of  $M_W$  followed by  $M_S$ ,  $m_b$  and  $M_L$  respectively (where more than one network magnitude was reported).

**Table 7.4:** Summary of the reports containing hypocentres.

Reports with hypocentres	8248
Reports of hypocentres only (no phase readings)	509
Total hypocentres received	463851
Number of duplicate hypocentres	8128 (1.8%)
Agencies determining hypocentres	160

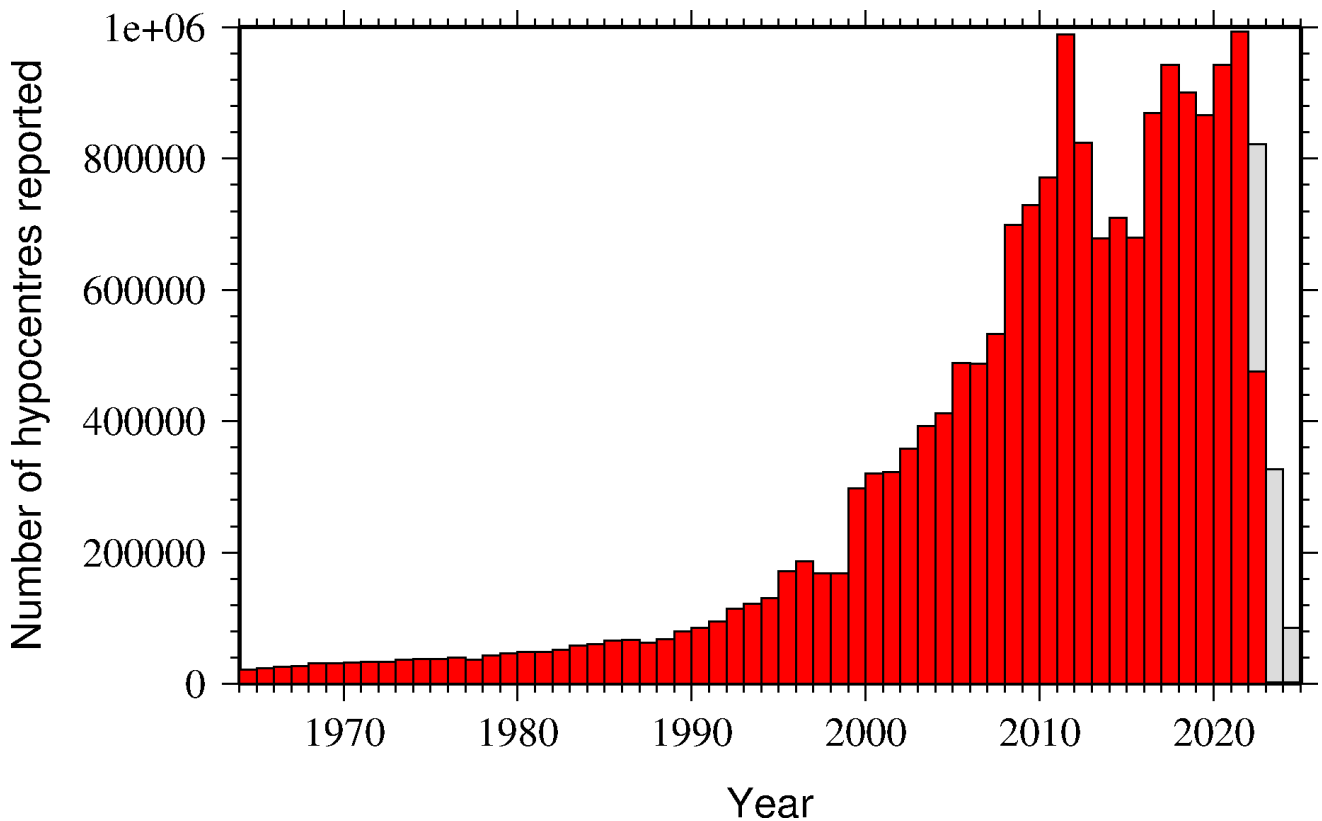


**Figure 7.9:** Histogram showing the number of hypocentres collected by the ISC for events each year since 1964. For each event, multiple hypocentres may be reported.

All the hypocentres that are reported to the ISC are automatically grouped into events, which form the basis of the ISC Bulletin. For this summary period 487026 hypocentres (including ISC) were grouped

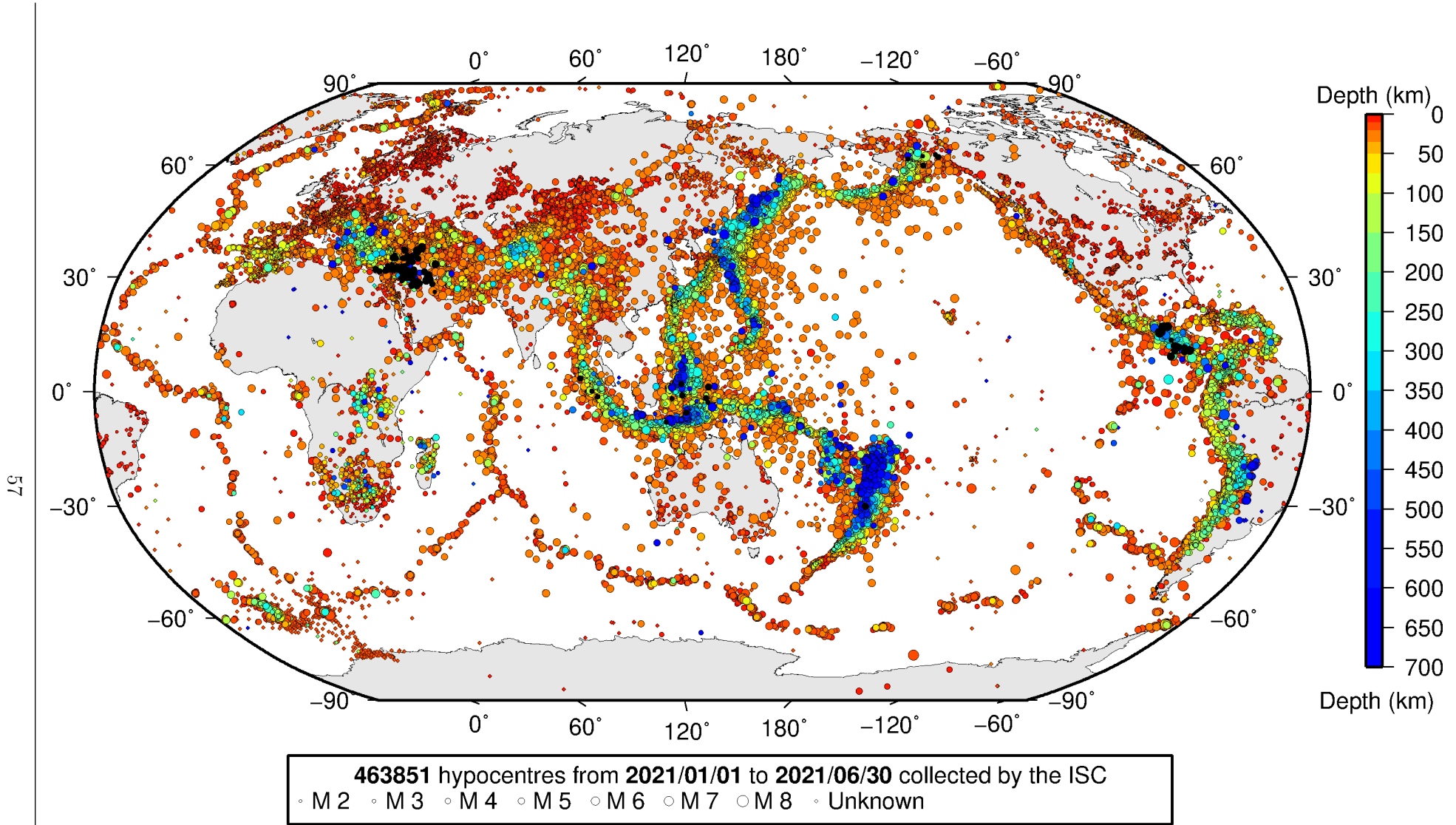


**Figure 7.10:** Map of all hypocenters collected by the ISC. The scatter shows the large variation of the multiple hypocenters that are reported for each event. The magnitude corresponds with the reported network magnitude. If more than one network magnitude type was reported, preference was given to values of  $M_W$ ,  $M_S$ ,  $m_b$  and  $M_L$  respectively. Compare with Figure 8.2



into 327834 events, the largest of these having 60 hypocentres in one event. The total number of events shown here is the result of an automatic grouping algorithm, and will differ from the total events in the published ISC Bulletin, where both the number of events and the number of hypocentre estimates will have changed due to further analysis. The process of grouping is detailed in Section 10.1.3. Figure 8.2 on page 71 shows a map of all prime hypocentres.

## 7.5 Collection of Network Magnitude Data

Data contributing agencies normally report earthquake hypocentre solutions along with magnitude estimates. For each seismic event, each agency may report one or more magnitudes of the same or different types. This stems from variability in observational practices at regional, national and global level in computing magnitudes based on a multitude of wave types. Differences in the amplitude measurement algorithm, seismogram component(s) used, frequency range, station distance range as well as the instrument type contribute to the diversity of magnitude types. Table 7.5 provides an overview of the complexity of reported network magnitudes reported for seismic events during the summary period.

**Table 7.5:** Statistics of magnitude reports to the ISC;  $M$  – average magnitude of estimates reported for each event.

	$M < 3.0$	$3.0 \leq M < 5.0$	$M \geq 5.0$
Number of seismic events	249350	47924	790
Average number of magnitude estimates per event	1.4	3.2	20.2
Average number of magnitudes (by the same agency) per event	1.2	1.9	2.9
Average number of magnitude types per event	1.2	2.5	11.1
Number of magnitude types	25	40	37

Table 7.6 gives the basic description, main features and scientific paper references for the most commonly reported magnitude types.

**Table 7.6:** Description of the most common magnitude types reported to the ISC.

Magnitude type	Description	References	Comments
M	Unspecified		Often used in real or near-real time magnitude estimations
mB	Medium-period and Broad-band body-wave magnitude	<i>Gutenberg</i> (1945a); <i>Gutenberg</i> (1945b); <i>IASPEI</i> (2005); <i>IASPEI</i> (2013); <i>Bormann et al.</i> (2009); <i>Bormann and Dewey</i> (2012)	
mb	Short-period body-wave magnitude	<i>IASPEI</i> (2005); <i>IASPEI</i> (2013); <i>Bormann et al.</i> (2009); <i>Bormann and Dewey</i> (2012)	Classical mb based on stations between 21°-100° distance

Table 7.6: continued

Magnitude type	Description	References	Comments
mb1	Short-period body-wave magnitude	<i>IDC</i> (1999) and references therein	Reported only by the IDC; also includes stations at distances less than 21°
mb1mx	Maximum likelihood short-period body-wave magnitude	<i>Ringdal</i> (1976); <i>IDC</i> (1999) and references therein	Reported only by the IDC
mbtmp	short-period body-wave magnitude with depth fixed at the surface	<i>IDC</i> (1999) and references therein	Reported only by the IDC
mbLg	Lg-wave magnitude	<i>Nuttli</i> (1973); <i>IASPEI</i> (2005); <i>IASPEI</i> (2013); <i>Bormann and Dewey</i> (2012)	Also reported as MN
Mc	Coda magnitude		
MD (Md)	Duration magnitude	<i>Bisztricsany</i> (1958); <i>Lee et al.</i> (1972)	
ME (Me)	Energy magnitude	<i>Choy and Boatwright</i> (1995)	Reported only by NEIC
MJMA	JMA magnitude	<i>Tsuboi</i> (1954)	Reported only by JMA
ML (Ml)	Local (Richter) magnitude	<i>Richter</i> (1935); <i>Hutton and Boore</i> (1987); <i>IASPEI</i> (2005); <i>IASPEI</i> (2013)	
MLSn	Local magnitude calculated for Sn phases	<i>Balfour et al.</i> (2008)	Reported by PGC only for earthquakes west of the Cascadia subduction zone
MLv	Local (Richter) magnitude computed from the vertical component		Reported only by DJA and BKK
MN (Mn)	Lg-wave magnitude	<i>Nuttli</i> (1973); <i>IASPEI</i> (2005)	Also reported as mbLg
MS (Ms)	Surface-wave magnitude	<i>Gutenberg</i> (1945c); <i>Vaněk et al.</i> (1962); <i>IASPEI</i> (2005)	Classical surface-wave magnitude computed from station between 20°-160° distance
Ms1	Surface-wave magnitude	<i>IDC</i> (1999) and references therein	Reported only by the IDC; also includes stations at distances less than 20°
ms1mx	Maximum likelihood surface-wave magnitude	<i>Ringdal</i> (1976); <i>IDC</i> (1999) and references therein	Reported only by the IDC

**Table 7.6:** *continued*

Magnitude type	Description	References	Comments
Ms7	Surface-wave magnitude	<i>Bormann et al. (2007)</i>	Reported only by BJI and computed from records of a Chinese-made long-period seismograph in the distance range 3°-177°
MW (Mw)	Moment magnitude	<i>Kanamori (1977); Dziewonski et al. (1981)</i>	Computed according to the <i>IASPEI (2005)</i> and <i>IASPEI (2013)</i> standard formula
Mw(mB)	Proxy Mw based on mB	<i>Bormann and Saul (2008)</i>	Reported only by DJA and BKK
Mwp	Moment magnitude from P-waves	<i>Tsuboi et al. (1995)</i>	Reported only by DJA and BKK and used in rapid response
mbh	Unknown		
mbv	Unknown		
MG	Unspecified type		Contact contributor
Mm	Unknown		
msh	Unknown		
MSV	Unknown		

Table 7.7 lists all magnitude types reported, the corresponding number of events in the ISC Bulletin and the agency codes along with the number of earthquakes.

**Table 7.7:** *Summary of magnitude types in the ISC Bulletin for this summary period. The number of events with values for each magnitude type is listed. The agencies reporting these magnitude types are listed, together with the total number of values reported.*

Magnitude type	Events	Agencies reporting magnitude type (number of values)
M	22165	WEL (12085), MOS (5266), GFZ (2139), CATAAC (2055), SNET (1055), BKK (213), JSO (145), IGQ (99), PRU (29), INMG (20), OTT (2), TAN (2), OSUNB (2)
mb	29650	IDC (18077), NEIC (8774), KRNET (5103), NNC (3654), VIE (3462), GFZ (2621), BJI (1428), MOS (1397), DJA (1309), VAO (337), NOU (274), CATAAC (271), BGR (237), OMAN (196), MDD (168), MCSM (126), MAN (101), BKK (98), AUST (89), CFUSG (67), SFS (36), INMG (33), SIGU (31), DSN (20), PDG (14), YARS (12), OSUNB (10), SNET (8), NDI (8), IGQ (7), PTWC (6), ROM (6), THE (5), UCC (3), SSNC (3), CRAAG (2), IGIL (2), GUC (1), BGS (1), DNK (1), WEL (1), DMN (1), AZER (1), THR (1)
MB	220	NAO (184), SCB (34), SSNC (2)
mB	2225	BJI (1271), DJA (761), WEL (242), CATAAC (194), GFZ (86), BKK (84), SNET (5), IGQ (4), OSUNB (1), MCSM (1)
mB_BB	24	BGR (24)
mb_Lg	7754	MDD (7109), NEIC (612), OTT (35)

**Table 7.7: Continued.**

Magnitude type	Events	Agencies reporting magnitude type (number of values)
mbR	110	VAO (110)
mbtmp	19542	IDC (19542)
Mc	38	KRSC (38)
MD	12008	RSPR (2939), SSNC (2169), LDG (1452), SDD (1321), GCG (1185), TRN (1173), ECX (517), SOF (359), JMA (353), EAF (271), NCEDC (262), ROM (151), MEX (137), JSN (100), GRAL (95), CFUSG (85), PDG (82), PNSN (81), GII (55), SLM (53), HVO (44), TUN (34), HLW (22), UPA (12), TIR (6), UUSS (3), OSPL (1), FUNV (1), STR (1), BER (1)
Mjma	1250	SNET (967), BKK (189), IGQ (95), RSNC (1), WEL (1)
ML	131293	ISK (13076), AFAD (11870), ATH (11849), RSNC (11670), TAP (11189), IDC (11136), WEL (9660), ROM (8286), HEL (6898), VIE (6191), NEIC (6076), GUC (3988), TXNET (3318), CNRM (2872), SFS (2554), UPP (2500), AEIC (2494), AZER (2465), SSNC (2134), INMG (1997), WBNET (1975), PRE (1776), SGS (1555), TEH (1554), SDD (1321), RHSSO (1287), BER (1226), KOGSR (1221), BEO (1203), LDG (1148), DNK (1147), LJU (1139), TIR (957), SJA (914), TAN (868), KRSC (648), MRB (645), OSPL (619), HVO (616), KRSZO (615), GEN (597), IPEC (593), SKO (586), PDG (583), SCB (573), PGC (563), ECX (545), BUC (526), BGSJ (486), IGIL (460), UCC (427), NAO (385), PAS (373), KNET (370), NDI (368), CRAAG (326), DJA (289), OMAN (287), SNET (256), LVSJ (242), NIC (234), REN (228), BGR (222), BUT (208), SARA (206), AUST (201), YARS (199), BJI (191), ISN (188), DSN (187), HLW (175), GCG (154), BKK (153), MIRAS (142), MAN (127), CLL (121), SKHL (100), BGS (91), PPT (83), NCEDC (72), SEA (68), PLV (66), UUSS (64), KEA (48), BNS (45), IGQ (43), DMN (40), PTWC (29), EAF (28), THR (26), CUPWA (25), OTT (21), GFZ (19), UPA (16), RSPR (11), NAM (9), RISSC (8), STR (6), PMR (2), VAO (2), CSEM (1)
MLh	6874	THE (5987), ASGSR (886), RSNC (1)
MLhc	491	ZUR (491)
MLSn	145	PGC (145)
MLv	24808	WEL (11002), DJA (5270), STR (3882), CATAC (2093), SFS (1270), SNET (1069), NOU (546), RSNC (466), BKK (237), IGQ (226), MCSM (144), AUST (29), GFZ (21), OSUNB (4), ASGSR (3), OTT (2)
MN	746	OTT (746)
mpv	4074	NNC (4074)
MPVA	253	NOGSR (213), MOS (164)
mR	138	OSUNB (138)

**Table 7.7:** *Continued.*

Magnitude type	Events	Agencies reporting magnitude type (number of values)
MS	10952	IDC (8514), MAN (2538), BJI (1015), MOS (421), BGR (157), NSSP (50), GCMT (45), VIE (31), INMG (25), OMAN (24), SOME (18), GUC (7), KEA (5), DSN (4), IGIL (3), SSNC (2), DNK (2), YARS (1), EAF (1), NDI (1), MEX (1)
Ms(BB)	92	IGQ (87), SNET (2), RSNC (1), BKK (1), WEL (1)
Ms7	1019	BJI (1019)
Ms_20	217	NEIC (217)
Ms_VX	2	NEIC (2)
MSH	85	CFUSG (85)
MV	110198	JMA (110198)
MW	7421	GCMT (1443), SDD (1268), SJA (897), FUNV (845), NIED (649), GFZ (643), UPA (555), UCR (417), BER (397), TIR (264), AFAD (247), NDI (240), PGC (147), IPGP (129), WEL (129), SSNC (116), DJA (109), MED_RCMT (88), JMA (80), ASIES (41), MEX (23), INMG (14), UPSL (13), OSPL (9), ATH (8), ROM (7), SNET (6), GUC (6), RSNC (3), OSUNB (1), AUST (1), NEIC (1)
Mw(mB)	568	WEL (212), CATAC (184), GFZ (98), BKK (82), SNET (5), IGQ (4)
Mwb	190	NEIC (190)
Mwc	5	NEIC (5)
MwMwp	85	CATAC (47), NOU (29), SNET (5), BKK (4), AUST (1)
Mwp	547	SARA (206), PTWC (177), DJA (142), CATAC (48), GFZ (40), RSNC (24), OMAN (8), ROM (6), SNET (5), BKK (4), NEIC (1), IGQ (1), AUST (1)
Mwr	378	NEIC (266), GUC (112), NCEDC (36), PAS (31), SLM (20), OTT (1)
Mws	613	GII (613)
Mww	642	NEIC (641), GUC (14)

The most commonly reported magnitude types are short-period body-wave, surface-wave, local (or Richter), moment, duration and JMA magnitude type. For a given earthquake, the number and type of reported magnitudes greatly vary depending on its size and location. The large earthquake of October 25, 2010 gives an example of the multitude of reported magnitude types for large earthquakes (Listing 7.1). Different magnitude estimates come from global monitoring agencies such as the IDC, NEIC and GCMT, a local agency (GUC) and other agencies, such as MOS and BJI, providing estimates based on the analysis of their networks. The same agency may report different magnitude types as well as several estimates of the same magnitude type, such as NEIC estimates of Mw obtained from W-phase, centroid and body-wave inversions.

**Listing 7.1:** *Example of reported magnitudes for a large event*

```

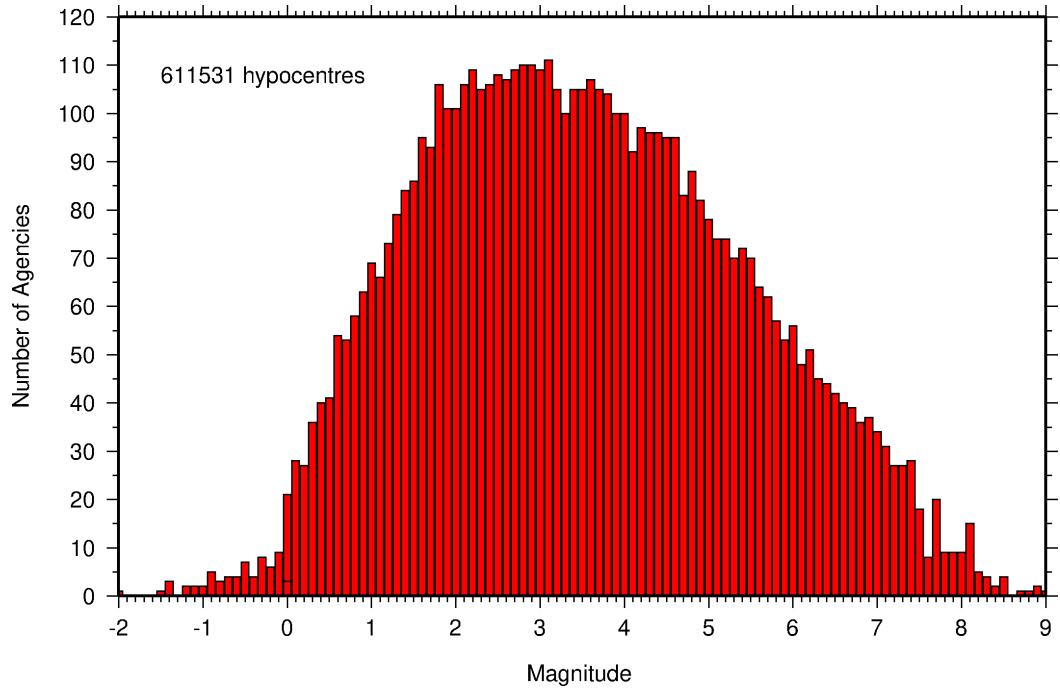
Event 15264887 Southern Sumatra
Date      Time      Err  RMS  Latitude Longitude  Smaj  Smin  Az  Depth  Err  Ndef  Nsta  Gap  mdist  Mdlist  Qual  Author  OrigID
2010/10/25 14:42:22.18  0.27  1.813  -3.5248  100.1042  4.045  3.327  54  20.0  1.37  2102  2149  23  0.76  176.43  m  i  de  ISC  01346132
(#PRIME)

```





**Figure 7.11:**  
*Histogram showing the number of agencies that reported network magnitude values. All magnitude types are included.*



## 7.6 Moment Tensor Solutions

The ISC Bulletin publishes moment tensor solutions, which are reported to the ISC by other agencies. The collection of moment tensor solutions is summarised in Table 7.8. A histogram showing all moment tensor solutions collected throughout the ISC history is shown in Figure 7.12. Several moment tensor solutions from different authors and different moment tensor solutions calculated by different methods from the same agency may be present for the same event.

**Table 7.8:** *Summary of reports containing moment tensor solutions.*

Reports with Moment Tensors	2297
Total moment tensors received	11476
Agencies reporting moment tensors	15

The number of moment tensors for this summary period, reported by each agency, is shown in Table 7.9. The moment tensor solutions are plotted in Figure 7.13.

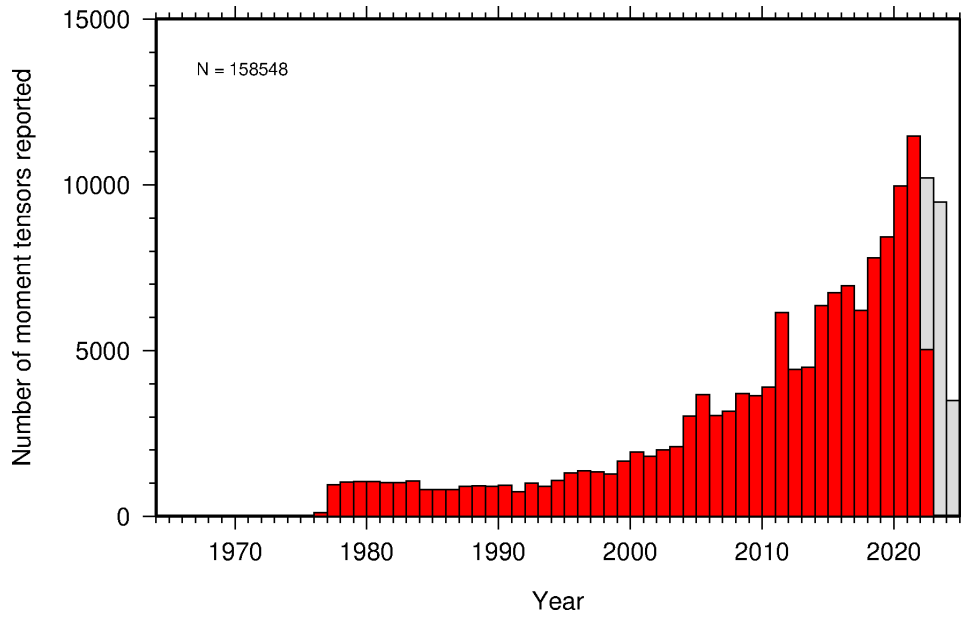
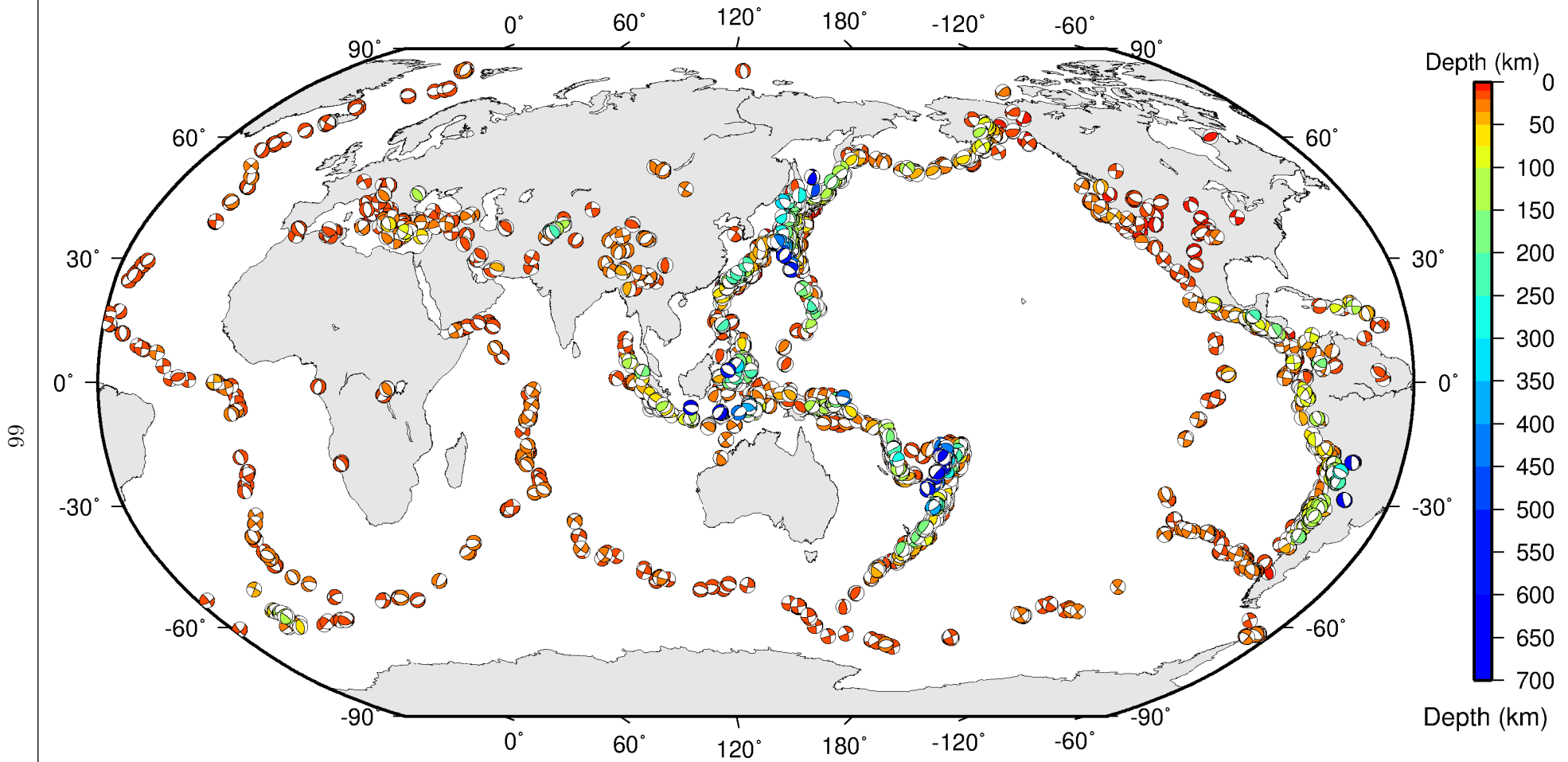


**Figure 7.12:** Histogram showing the number of moment tensors reported to the ISC since 1964. The regions in grey represent data that are still being actively collected.

**Table 7.9:** Summary of moment tensor solutions in the ISC Bulletin reported by each agency.

Agency	Number of moment tensor solutions
GCMT	1443
TAN	861
NEIC	854
NIED	649
GFZ	544
CATAC	422
IPGP	256
WEL	129
ISC-PPSM	101
MED_RCMT	88
ASIES	82
PNSN	81
UPA	24
SLM	20
MOS	20
UCR	19
MEX	16
ECX	16
UPSL	13
ATH	8
GCG	7
ROM	7
NCEDC	2
SDD	2
AUST	1
OTT	1
TIR	1



ISC Bulletin: **4282** focal mechanism solutions for **2423** events from **2021/01/01** to **2021/06/30**

*Figure 7.13: Map of all moment tensor solutions in the ISC Bulletin for this summary period.*

## 7.7 Timing of Data Collection

Here we present the timing of reports to the ISC. Please note, this does not include provisional alerts, which are replaced at a later stage. Instead, it reflects the final data sent to the ISC. The absolute timing of all hypocentre reports, regardless of magnitude, is shown in Figure 7.14. In Figure 7.15 the reports are grouped into one of six categories - from within three days of an event origin time, to over one year. The histogram shows the distribution with magnitude (for hypocentres where a network magnitude was reported) for each category, whilst the map shows the geographic distribution of the reported hypocentres.

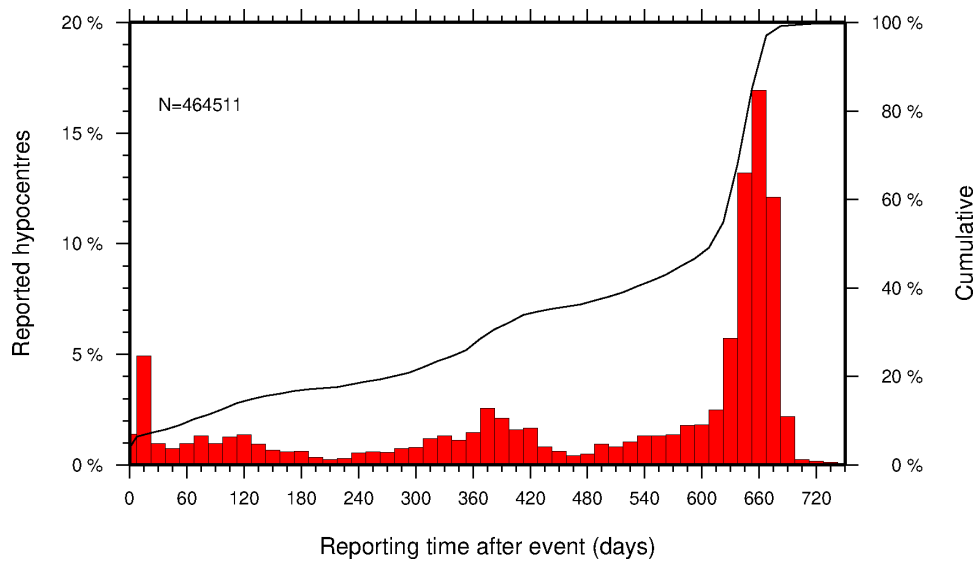


**Figure 7.14:** Histogram showing the timing of final reports of the hypocentres (total of  $N$ ) to the ISC. The cumulative frequency is shown by the solid line.

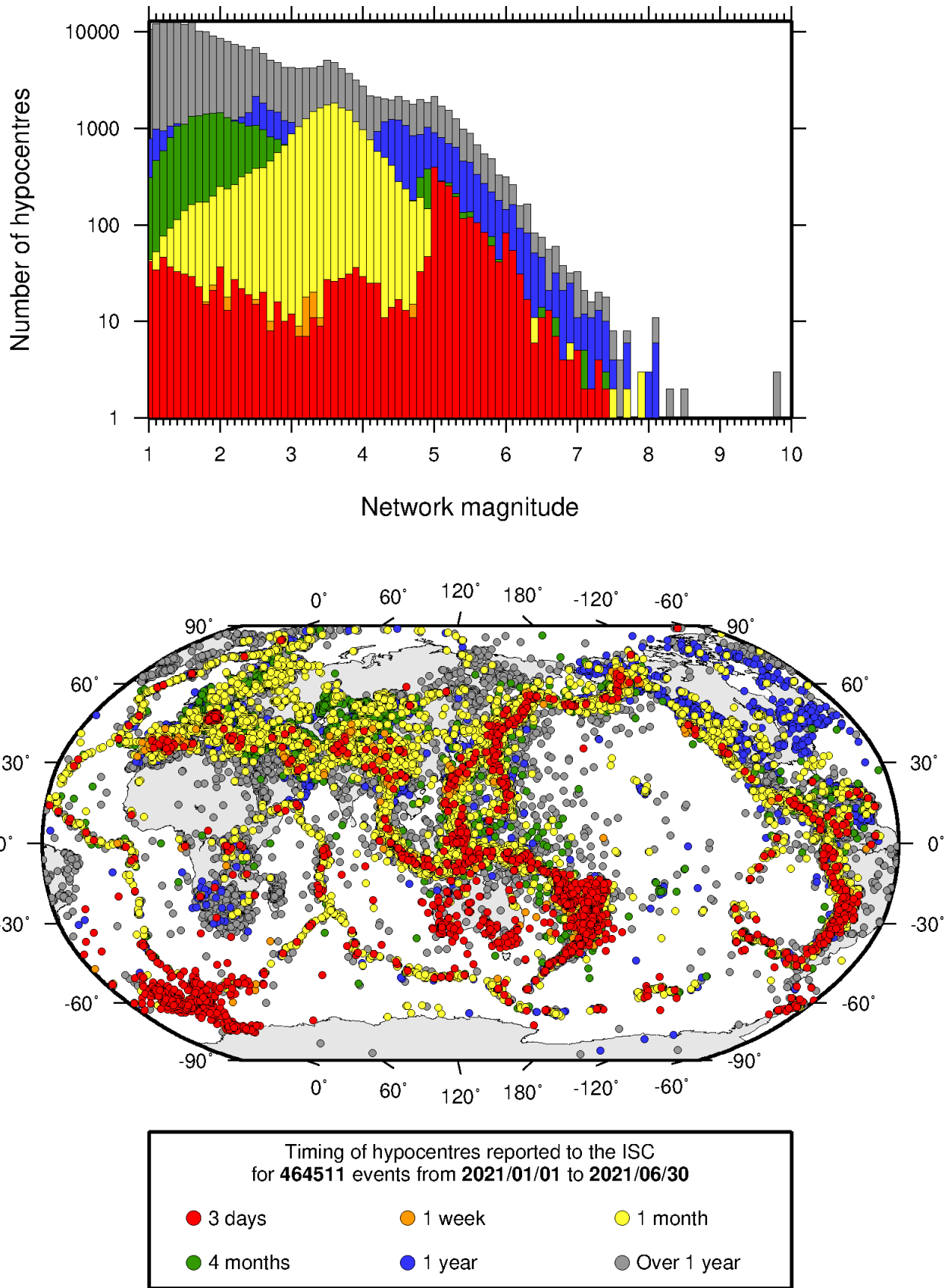


**Figure 7.15:** Timing of hypocentres reported to the ISC. The colours show the time after the origin time that the corresponding hypocentre was reported. The histogram shows the distribution with magnitude. If more than one network magnitude was reported, preference was given to a value of  $M_W$  followed by  $M_S$ ,  $m_b$  and  $M_L$  respectively; all reported hypocentres are included on the map. Note: early reported hypocentres are plotted over later reported hypocentres, on both the map and histogram.

## 8

# Overview of the ISC Bulletin

This chapter provides an overview of the seismic event data in the ISC Bulletin. We indicate the differences between all ISC events and those ISC events that are reviewed or located. We describe the wealth of phase arrivals and phase amplitudes and periods observed at seismic stations worldwide, reported in the ISC Bulletin and often used in the ISC location and magnitude determination. Finally, we make some comparisons of the ISC magnitudes with those reported by other agencies, and discuss magnitude completeness of the ISC Bulletin.

### 8.1 Events

The ISC Bulletin had 314544 reported events in the summary period between January and June 2021. Some 90% (285683) of the events were identified as earthquakes, the rest (28861) were of anthropogenic origin (including mining and other chemical explosions, rockbursts and induced events) or of unknown origin. As discussed in Section 10.1.3. In this summary period 9% of the events were reviewed and 7% of the events were located by the ISC. For events that are not located by the ISC, the prime hypocentre is identified according to the rules described in Section 10.1.3.

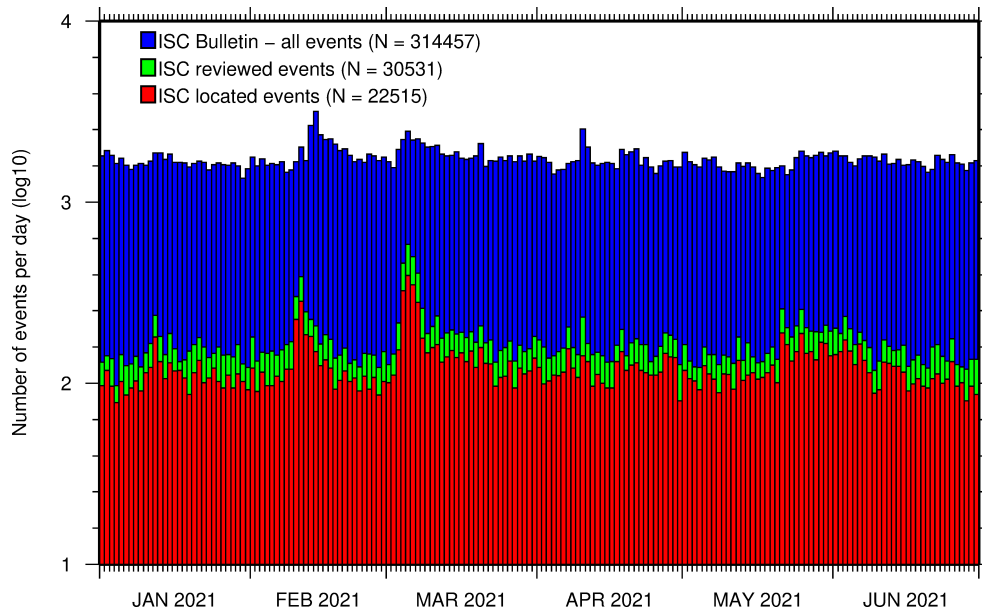
Of the 12170691 reported phase observations, 36% are associated to ISC-reviewed events, and 34% are associated to events selected for ISC location. Note that all large events are reviewed and located by the ISC. Since large events are globally recorded and thus reported by stations worldwide, they will provide the bulk of observations. This explains why only a small percentage of the events in a month is reviewed although the number of phases associated to reviewed events has increased nearly exponentially in the past decades.

Figure 8.1 shows the daily number of events throughout the summary period. Figure 8.2 shows the locations of the events in the ISC Bulletin; the locations of ISC-reviewed and ISC-located events are shown in Figures 8.3 and 8.4, respectively.

Figure 8.5 shows the hypocentral depth distributions of events in the ISC Bulletin for the summary period. The vast majority of events occur in the Earth's crust. Note that the peaks at 0, 10, 35 km, and at every 50 km intervals deeper than 100 km are artifacts of analyst practices of fixing the depth to a nominal value when the depth cannot be reliably resolved.

Figure 8.6 shows the depth distribution of free-depth solutions in the ISC Bulletin. The depth of a hypocentre reported to the ISC is assumed to be determined as a free parameter, unless it is explicitly labelled as a fixed-depth solution. On the other hand, as described in Section 10.1.4, the ISC locator attempts to get a free-depth solution if, and only if, there is resolution for the depth in the data, i.e. if there is a local network and/or sufficient depth-sensitive phases are reported.





**Figure 8.1:** Histogram showing the number of events in the ISC Bulletin for the current summary period. The vertical scale is logarithmic.

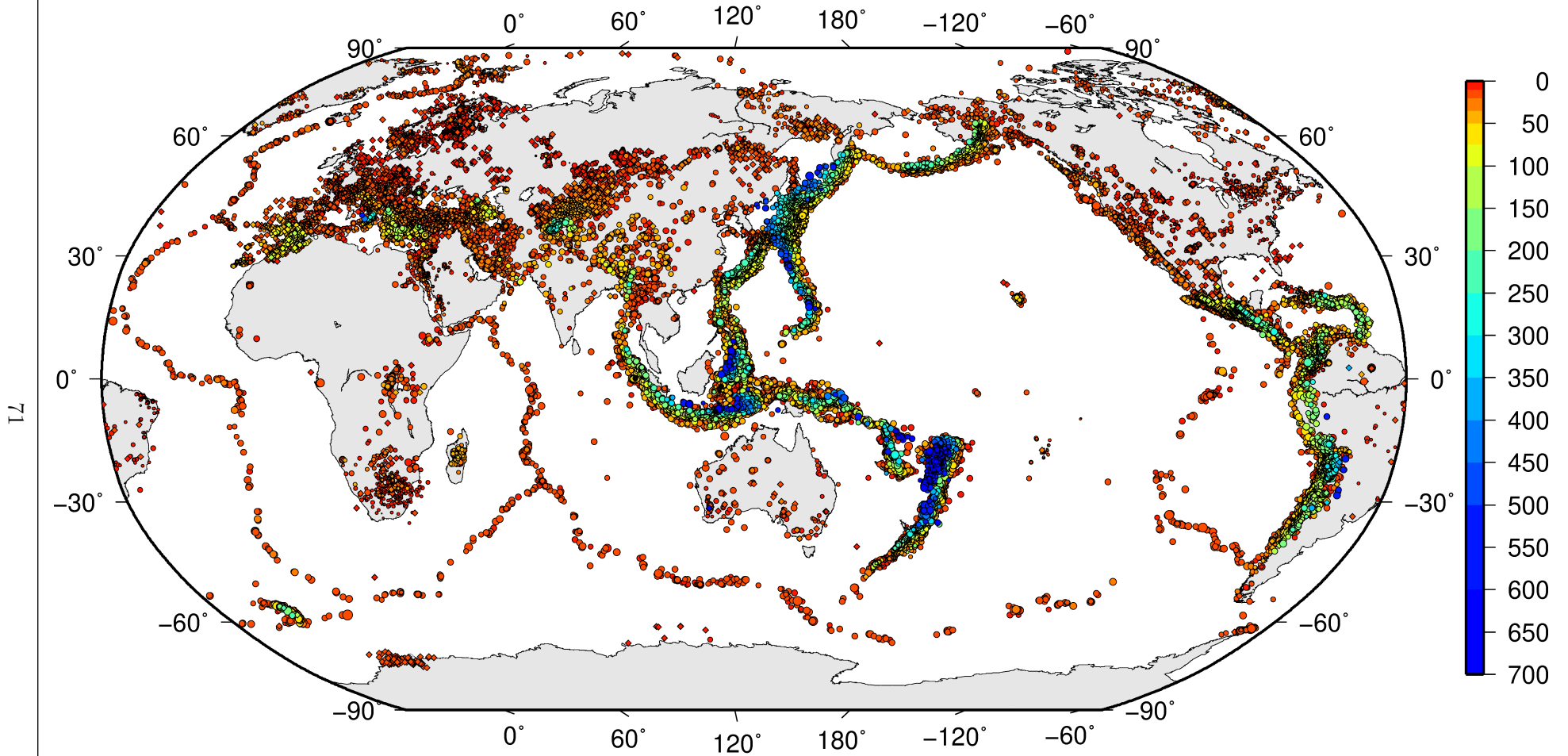
Figure 8.7 shows the depth distribution of fixed-depth solutions in the ISC Bulletin. Except for a fraction of events whose depth is fixed to a shallow depth, this set comprises mostly ISC-located events. If there is no resolution for depth in the data, the ISC locator fixes the depth to a value obtained from the ISC default depth grid file, or if no default depth exists for that location, to a nominal default depth assigned to each Flinn-Engdahl region (see details in Section 10.1.4). If during review the ISC analysts find these depth to be a poor fit, the depth will usually be fixed to a round number, preferably divisible by 50.

For events selected for ISC location, the number of stations typically increases as arrival data reported by several agencies are grouped together and associated to the prime hypocentre. Consequently, the network geometry, characterised by the secondary azimuthal gap (the largest azimuthal gap a single station closes), is typically improved. Figure 8.8 illustrates that the secondary azimuthal gap is indeed generally smaller for ISC-located events than that for all events in the ISC Bulletin. Figure 8.9 shows the distribution of the number of associated stations. For large events the number of associated stations is usually larger for ISC-located events than for any of the reported event bulletins. On the other hand, events with just a few reporting stations are rarely selected for ISC location. The same is true for the number of defining stations (stations with at least one defining phase that were used in the location). Figure 8.10 indicates that because the reported observations from multiple agencies are associated to the prime, large ISC-located events typically have a larger number of defining stations than any of the reported event bulletins.

The formal uncertainty estimates are also typically smaller for ISC-located events. Figure 8.11 shows the distribution of the area of the 90% confidence error ellipse for ISC-located events during the summary period. The distribution suffers from a long tail indicating a few poorly constrained event locations. Nevertheless, half of the events are characterised by an error ellipse with an area less than  $164 \text{ km}^2$ , 90% of the events have an error ellipse area less than  $1171 \text{ km}^2$ , and 95% of the events have an error ellipse area less than  $2214 \text{ km}^2$ .

Figure 8.12 shows one of the major characteristic features of the ISC location algorithm (Bondár and

# ISC Bulletin – all events

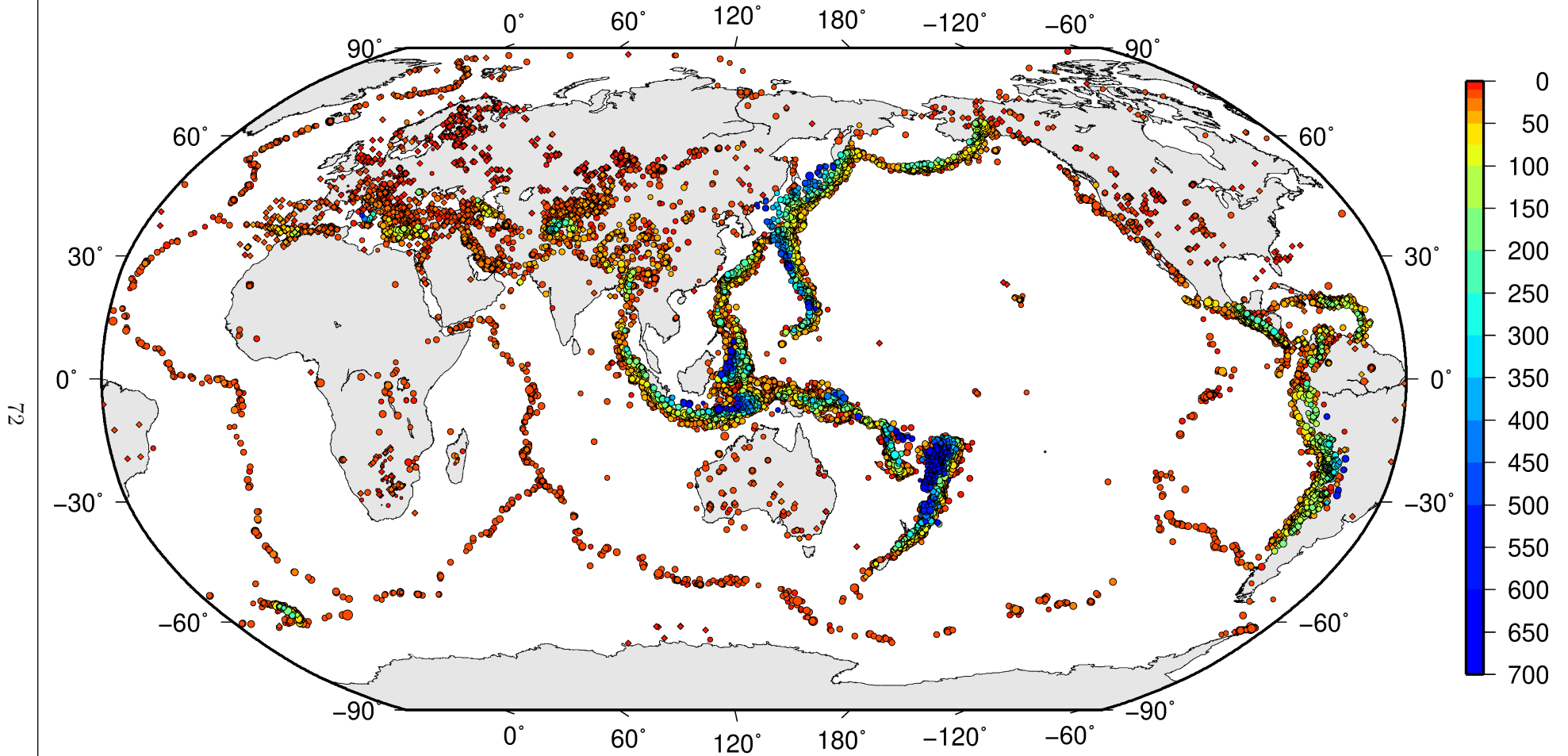


ISC Bulletin: **314457** reported events from **2021/01/01** to **2021/06/30**

◦ M 2   ◦ M 3   ◦ M 4   ◦ M 5   ◦ M 6   ◦ M 7   ◦ M 8   ◊ Unknown

*Figure 8.2: Map of all events in the ISC Bulletin. Prime hypocentre locations are shown. Compare with Figure 7.10.*

## ISC Bulletin – reviewed events



ISC Bulletin: **30531** reviewed events from **2021/01/01** to **2021/06/30**

◦ M 2 ◦ M 3 ◦ M 4 ◦ M 5 ◦ M 6 ◦ M 7 ◦ M 8 ◦ Unknown

*Figure 8.3: Map of all events reviewed by the ISC for this time period. Prime hypocentre locations are shown.*

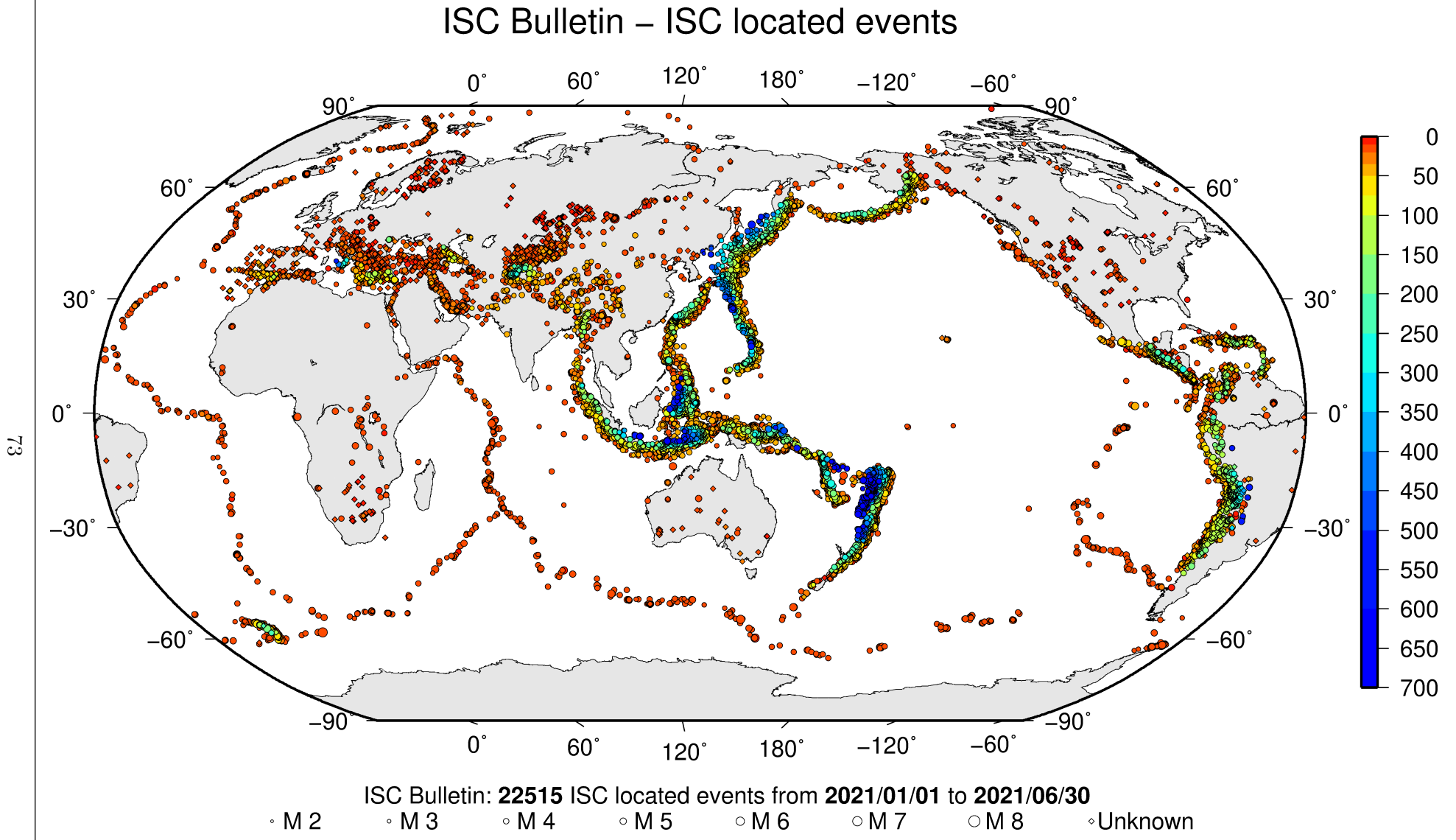


*Figure 8.4: Map of all events located by the ISC for this time period. ISC determined hypocentre locations are shown.*

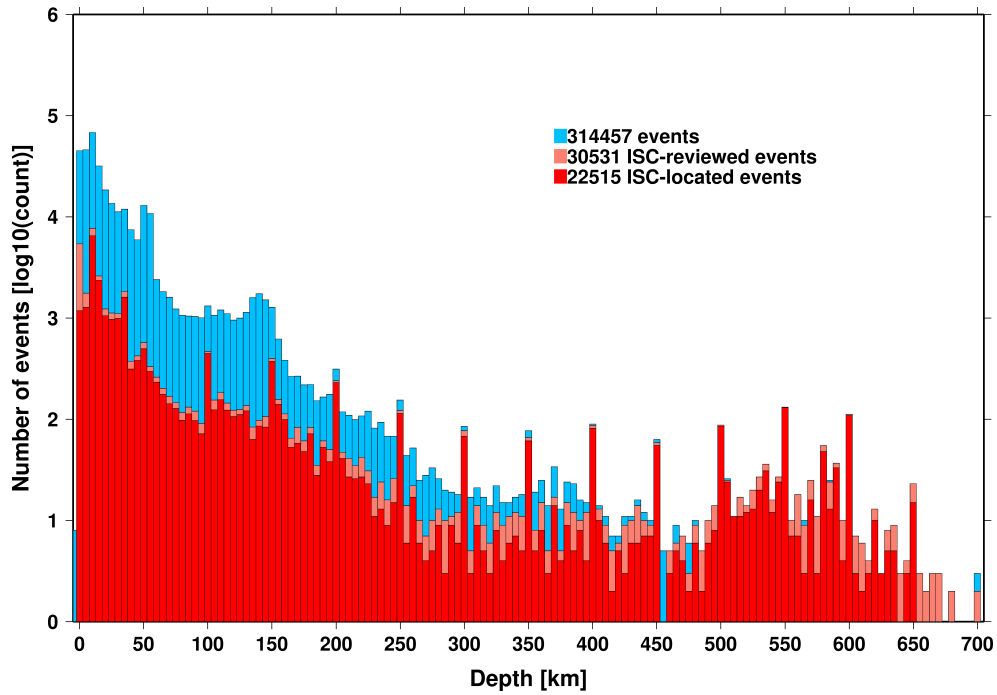


*Figure 8.5: Distribution of event depths in the ISC Bulletin (blue) and for the ISC-reviewed (pink) and the ISC-located (red) events during the summary period. All ISC-located events are reviewed, but not all reviewed events are located by the ISC. The vertical scale is logarithmic.*

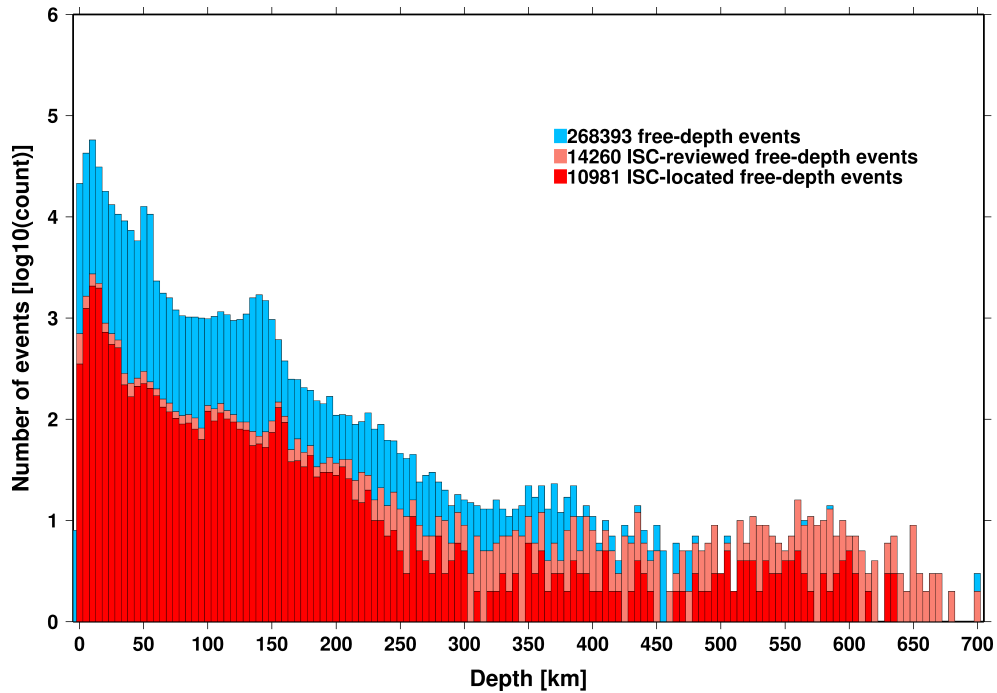


*Figure 8.6: Hypocentral depth distribution of events where the prime hypocentres are reported/located with a free-depth solution in the ISC Bulletin. The vertical scale is logarithmic.*

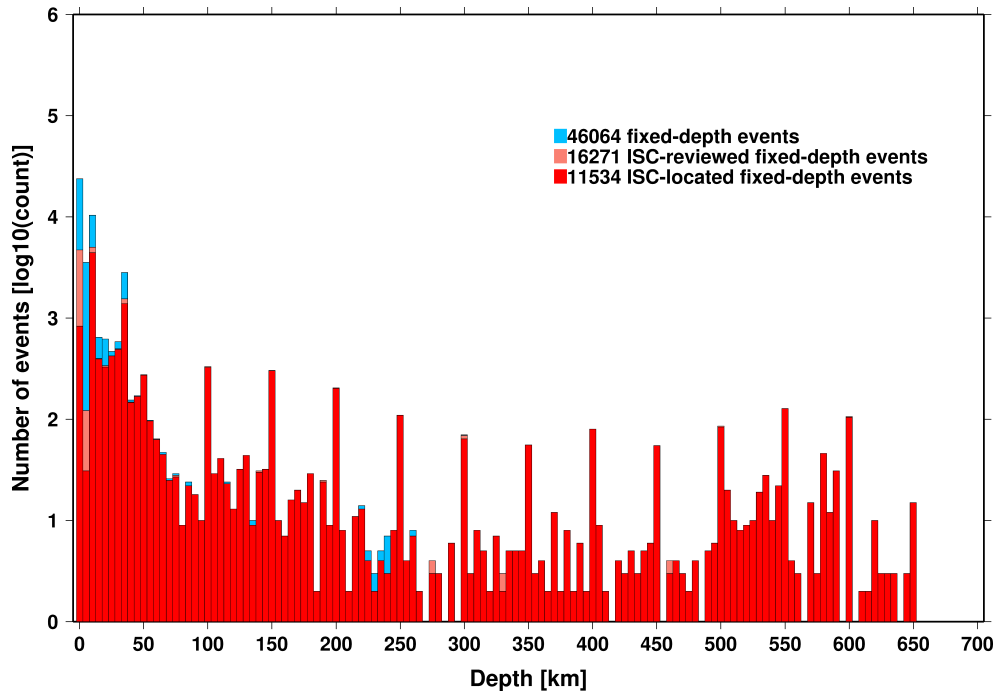


*Figure 8.7: Hypocentral depth distribution of events where the prime hypocentres are reported/located with a fixed-depth solution in the ISC Bulletin. The vertical scale is logarithmic.*

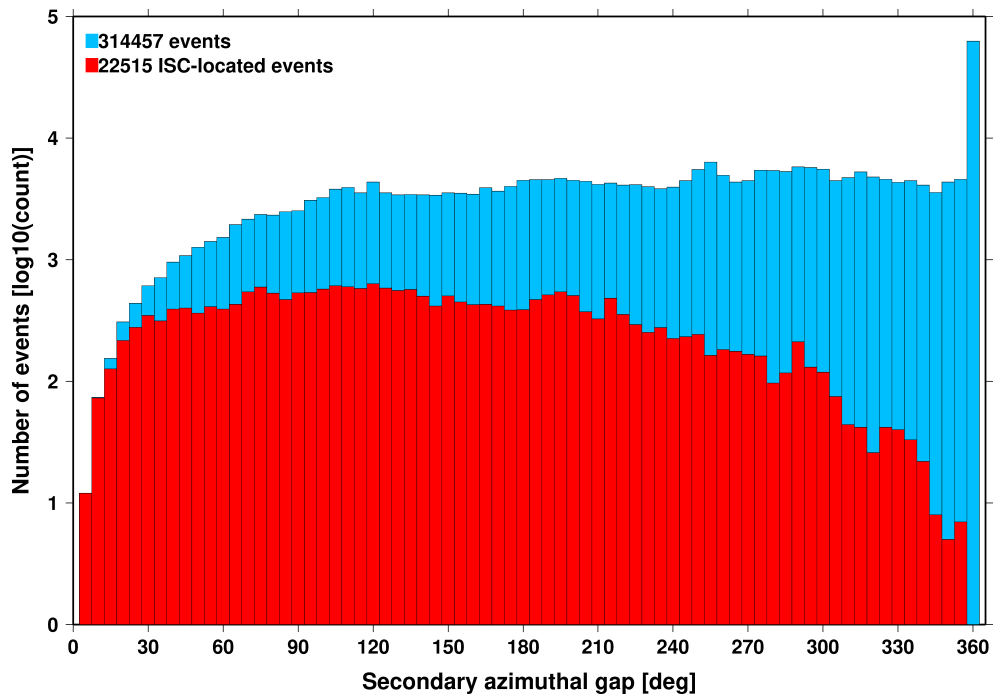


*Figure 8.8: Distribution of secondary azimuthal gap for events in the ISC Bulletin (blue) and those selected for ISC location (red). The vertical scale is logarithmic.*



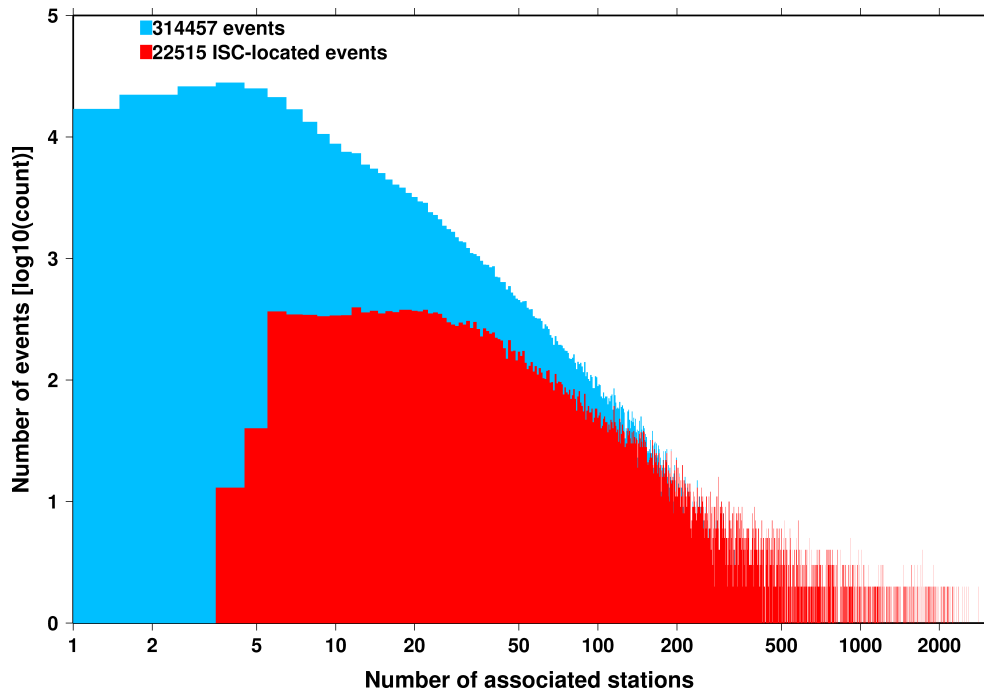


*Figure 8.9: Distribution of the number of associated stations for events in the ISC Bulletin (blue) and those selected for ISC location (red). The vertical scale is logarithmic.*

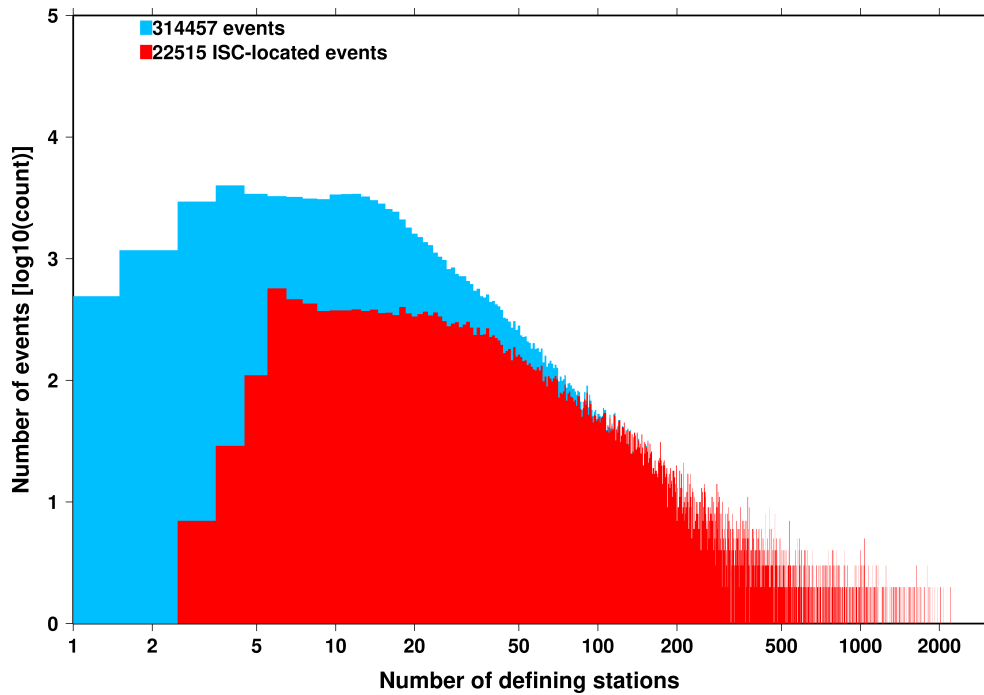


*Figure 8.10: Distribution of the number of defining stations for events in the ISC Bulletin (blue) and those selected for ISC location (red). The vertical scale is logarithmic.*

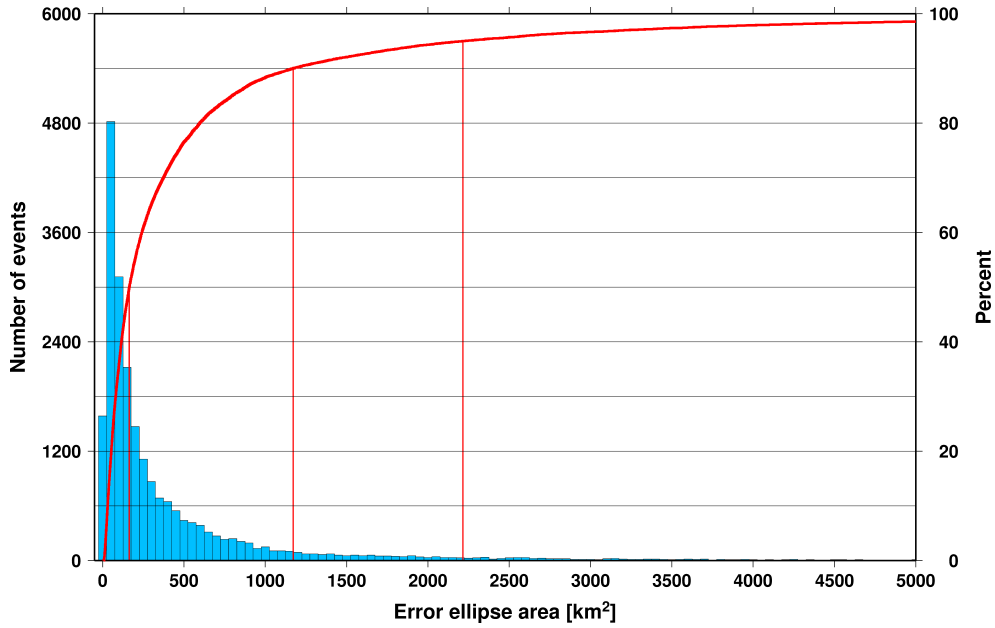


**Figure 8.11:** Distribution of the area of the 90% confidence error ellipse of the ISC-located events. Vertical red lines indicate the 50th, 90th and 95th percentile values.

Storchak, 2011). Because the ISC locator accounts for correlated travel-time prediction errors due to unmodelled velocity heterogeneities along similar ray paths, the area of the 90% confidence error ellipse does not decrease indefinitely with increasing number of stations, but levels off once the information carried by the network geometry is exhausted, thus providing more realistic uncertainty estimates.

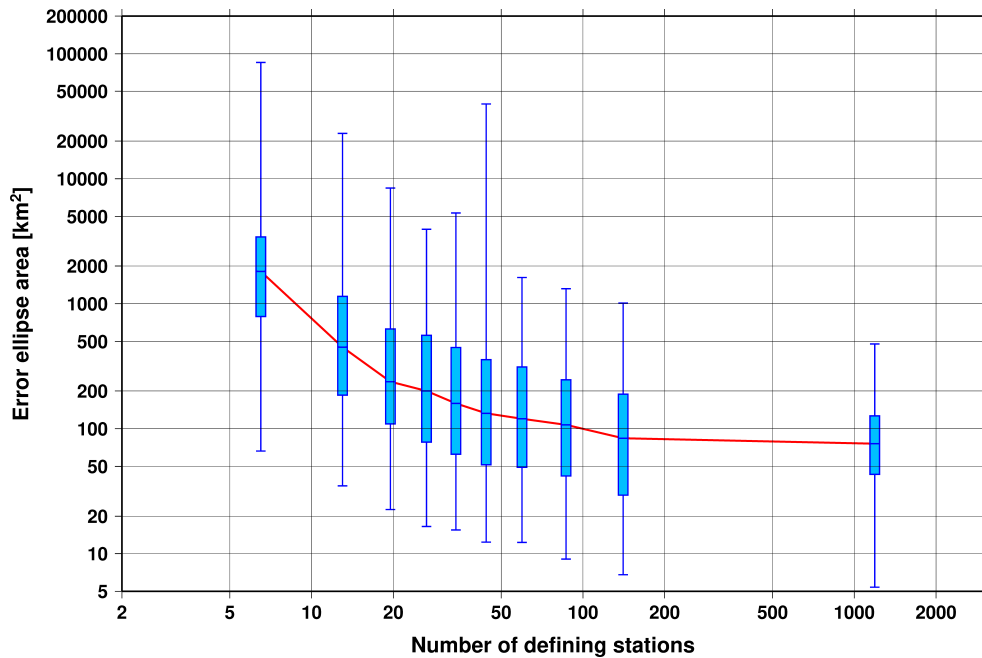


**Figure 8.12:** Box-and-whisker plot of the area of the 90% confidence error ellipse of the ISC-located events as a function of the number of defining stations. Each box represents one-tenth-worth of the total number of data. The red line indicates the median 90% confidence error ellipse area.

## 8.2 Seismic Phases and Travel-Time Residuals

The number of phases that are associated to events over the summary period in the ISC Bulletin is shown in Figure 8.13. Phase types and their total number in the ISC Bulletin is shown in the Appendix, Table 10.3. A summary of phase types is indicated in Figure 8.14.

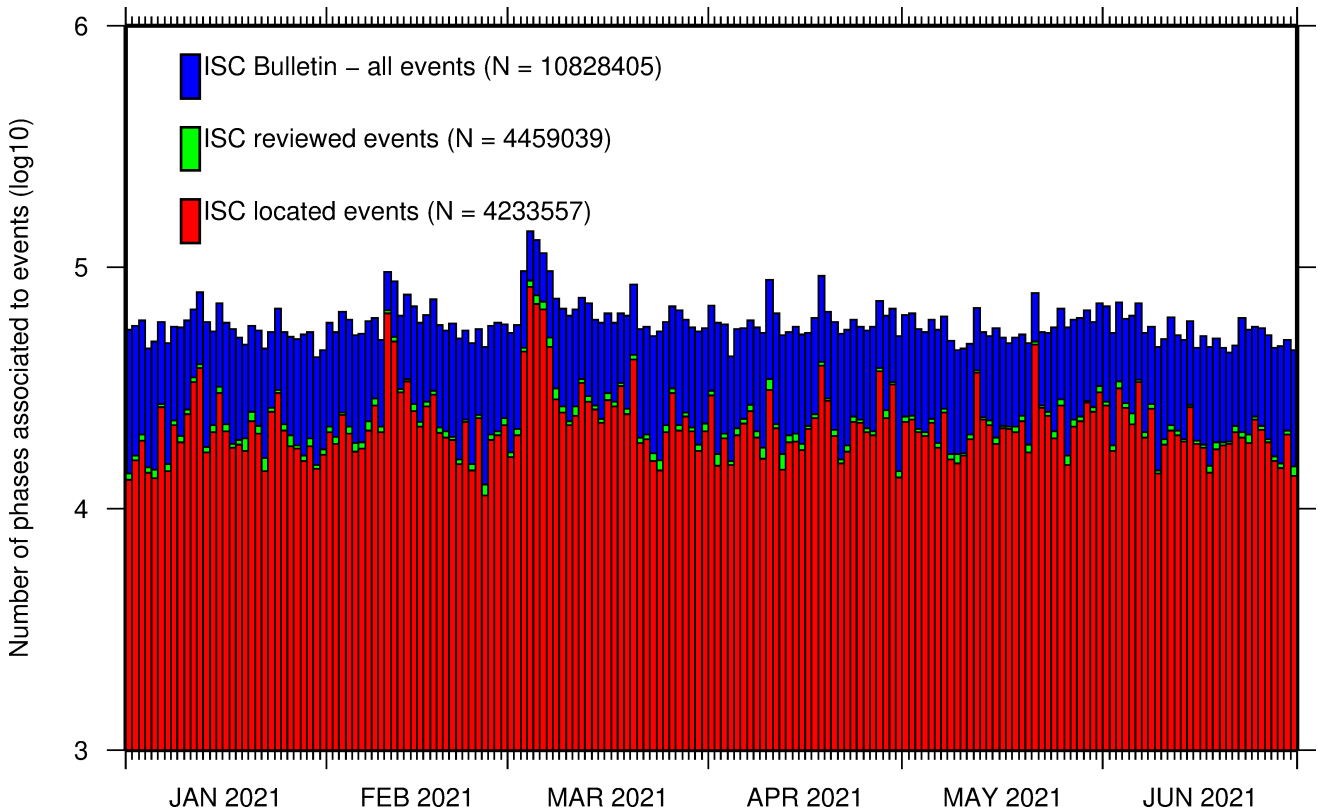


**Figure 8.13:** Histogram showing the number of phases ( $N$ ) that the ISC has associated to events within the ISC Bulletin for the current summary period.

In computing ISC locations, the current (for events since 2009) ISC location algorithm (*Bondár and Storchak, 2011*) uses all *ak135* phases where possible. Within the Bulletin, the phases that contribute to an ISC location are labelled as *time defining*. In this section, we summarise these time defining phases.

In Figure 8.15, the number of defining phases is shown in a histogram over the summary period. Each defining phase is listed in Table 8.1, which also provides a summary of the number of defining phases per event. A pie chart showing the proportion of defining phases is shown in Figure 8.16. Figure 8.17 shows travel times of seismic waves. The distribution of residuals for these defining phases is shown for the top five phases in Figures 8.18 through 8.22.

**Table 8.1:** Numbers of ‘time defining’ phases within the ISC Bulletin for 22515 ISC located events.

Phase	Number of ‘defining’ phases	Number of events	Max per event	Median per event
P	980435	15517	2330	16
Pn	752509	20775	1061	18
Sn	240644	17842	220	7
Pb	131327	10325	135	8
Pg	101586	8055	225	7
PKPdf	81648	5566	972	3
Sb	80979	9509	140	6
Sg	76541	7541	187	6

*Table 8.1: (continued)*

Phase	Number of 'defining' phases	Number of events	Max per event	Median per event
PKiKP	45320	4545	347	2
PKPbc	37984	4611	279	2
S	34631	3488	337	3
PKPab	32069	3726	194	2
PcP	15345	3914	76	2
pP	11681	1556	244	3
PP	9274	1407	160	2
Pdif	8469	1400	297	2
sP	4543	1220	72	2
ScP	4211	1078	51	2
SS	4149	912	71	2
SKSac	3547	518	82	3
pwP	2449	767	28	2
PKKPbc	2436	578	73	2
ScS	999	367	30	1
SKPbc	976	304	34	2
sS	871	453	15	1
PnPn	849	521	9	1
SnSn	844	500	14	1
pPKPdf	742	322	50	1
pPKPab	670	231	38	1
P'P'df	665	188	23	2
PKKPdf	553	290	15	1
SKiKP	541	282	23	1
pPKPbc	435	221	22	1
PKKPab	434	241	21	1
SKPdf	431	163	26	1
sPKPdf	399	245	17	1
SKSdf	353	233	31	1
sPKPab	265	122	18	1
PS	254	150	7	1
SKPab	225	130	13	1
SKKSac	222	155	6	1
P'P'bc	176	110	5	1
SKKSdf	132	119	3	1
sPKPbc	131	103	4	1
pPKiKP	118	53	15	1
PcS	112	92	4	1
pS	106	91	3	1
PnS	101	88	2	1
Sdif	79	56	4	1
SKKPbc	76	28	13	2
SP	72	40	11	1
PKSdf	72	50	5	1
PbPb	61	52	4	1
pPdif	44	28	11	1
SKKPdf	43	19	14	1
P'P'ab	26	21	2	1
SKKPab	17	9	4	1
SbSb	16	16	1	1
sPKiKP	15	14	2	1
SPn	10	10	1	1
sPdif	9	9	1	1
sPn	8	7	2	1
PKSbc	4	4	1	1
S'S'ac	3	3	1	1
pSKSac	2	2	1	1
pPn	2	1	2	2

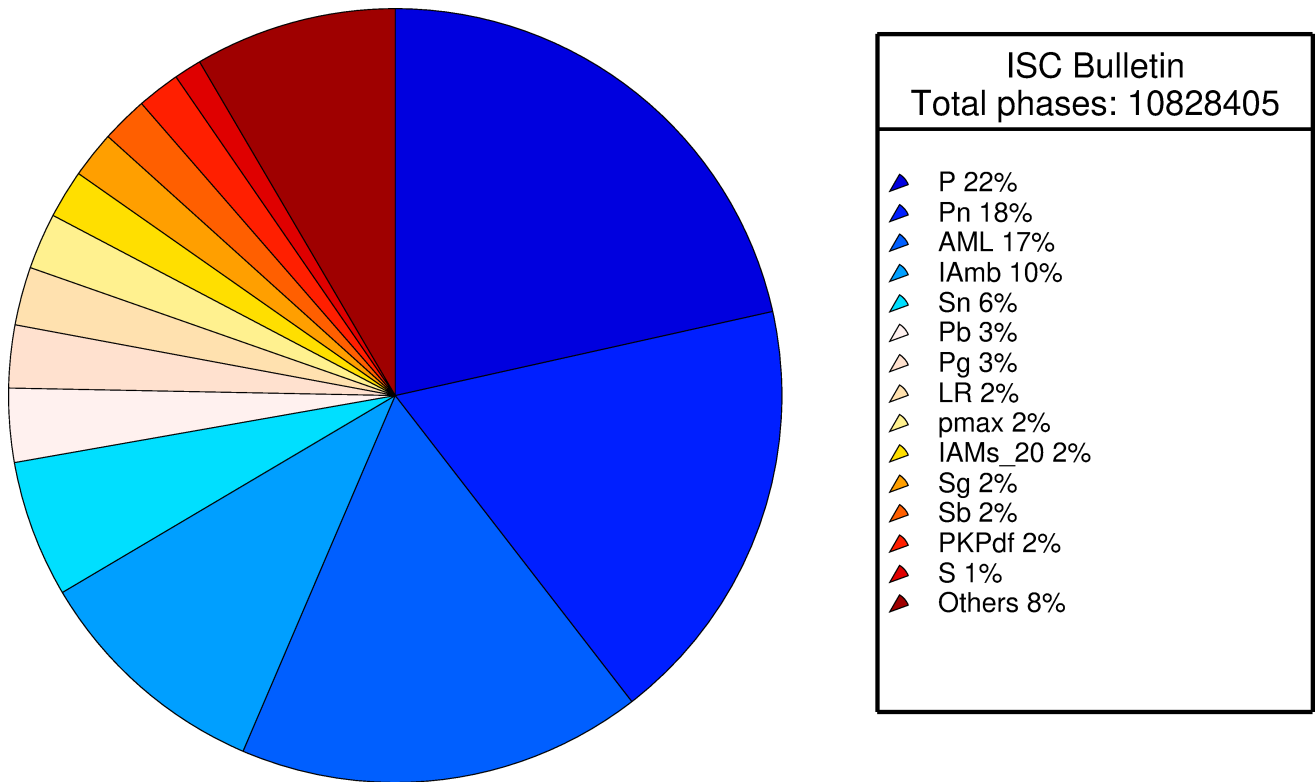


Figure 8.14: Pie chart showing the fraction of various phase types in the ISC Bulletin for this summary period.

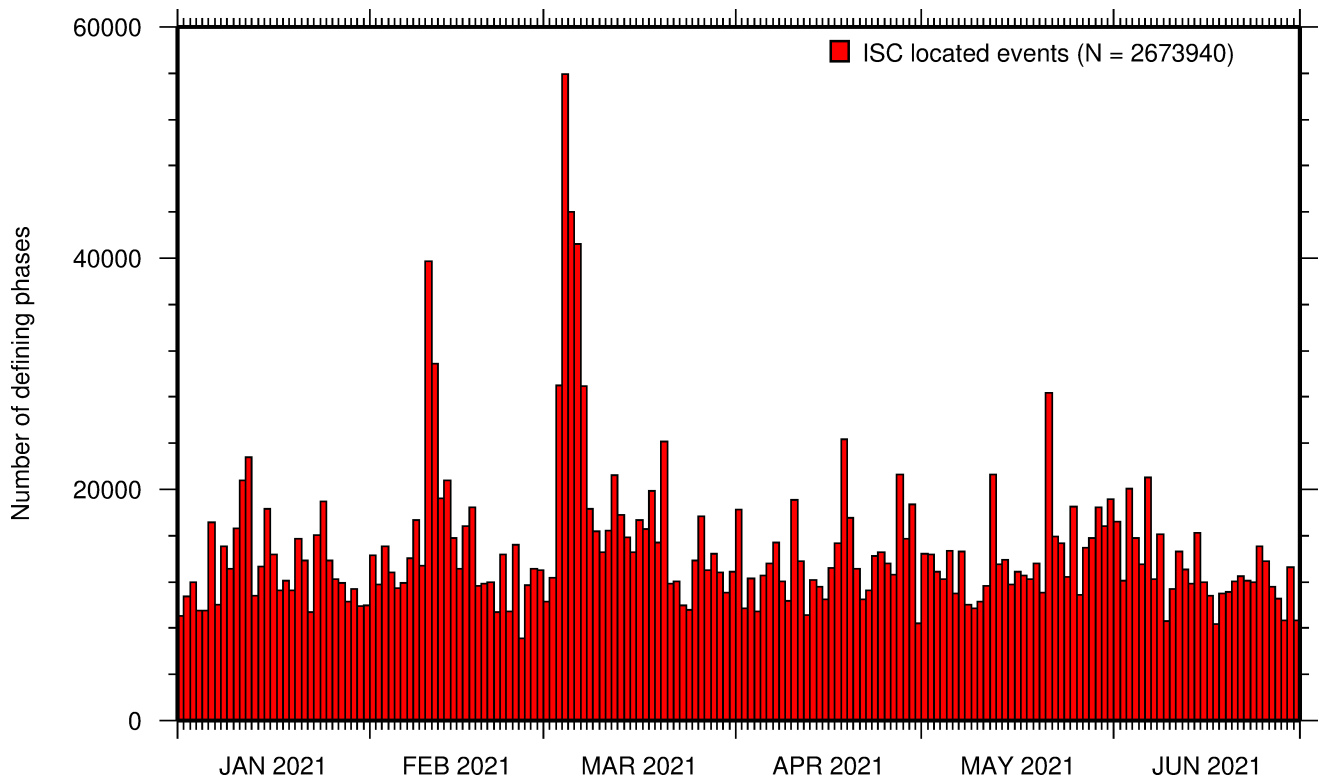


Figure 8.15: Histogram showing the number of defining phases in the ISC Bulletin, for events located by the ISC.

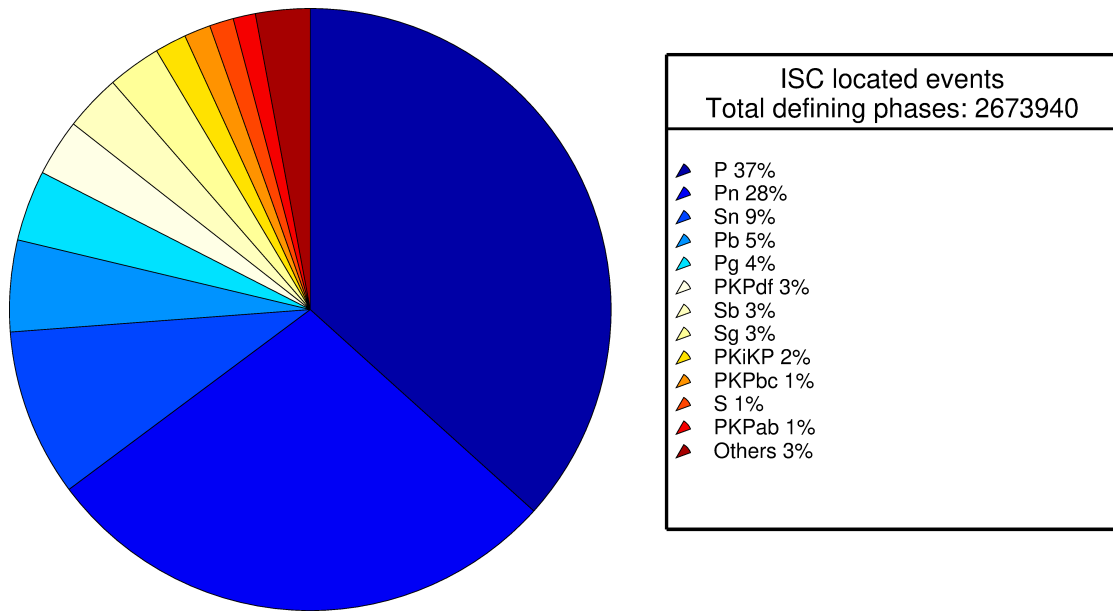


Figure 8.16: Pie chart showing the defining phases in the ISC Bulletin, for events located by the ISC. A complete list of defining phases is shown in Table 8.1.

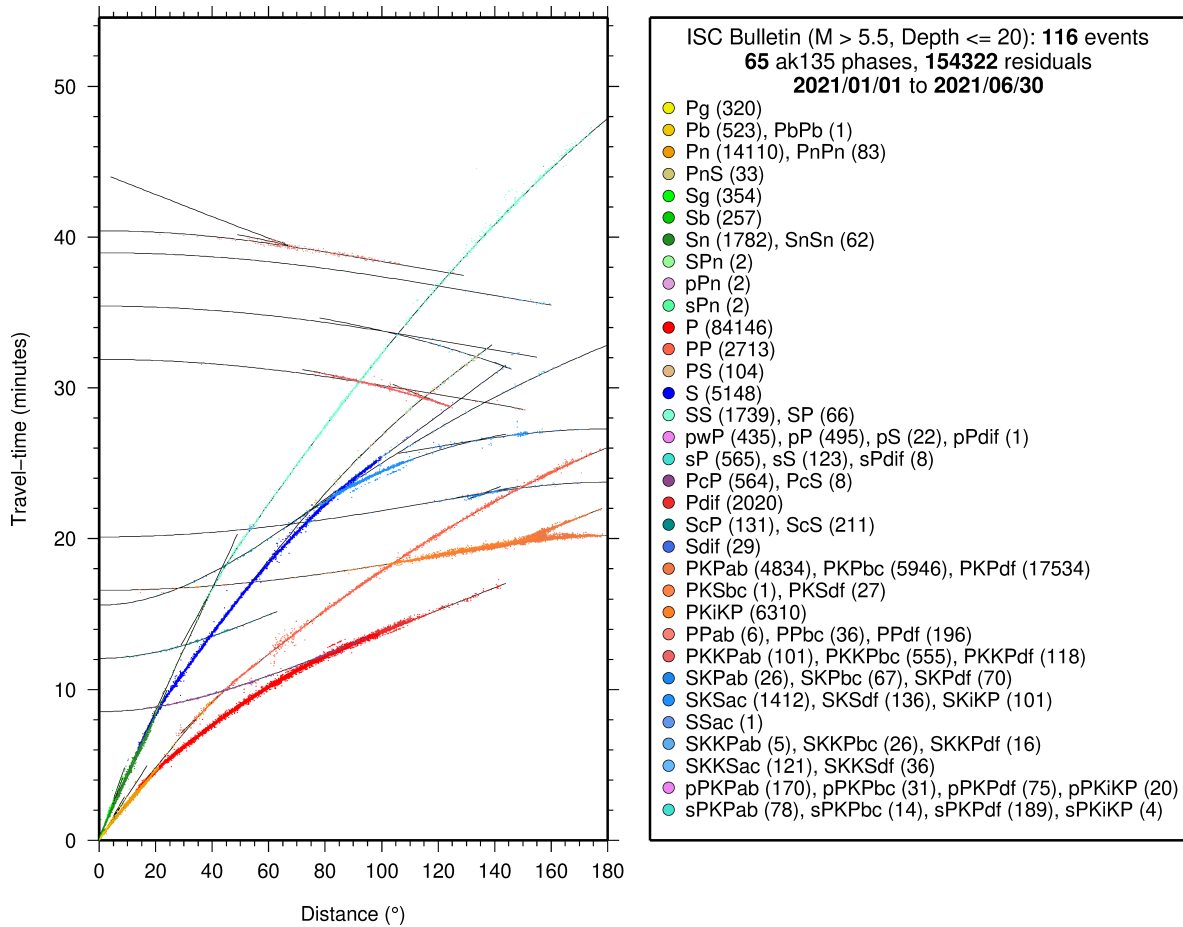
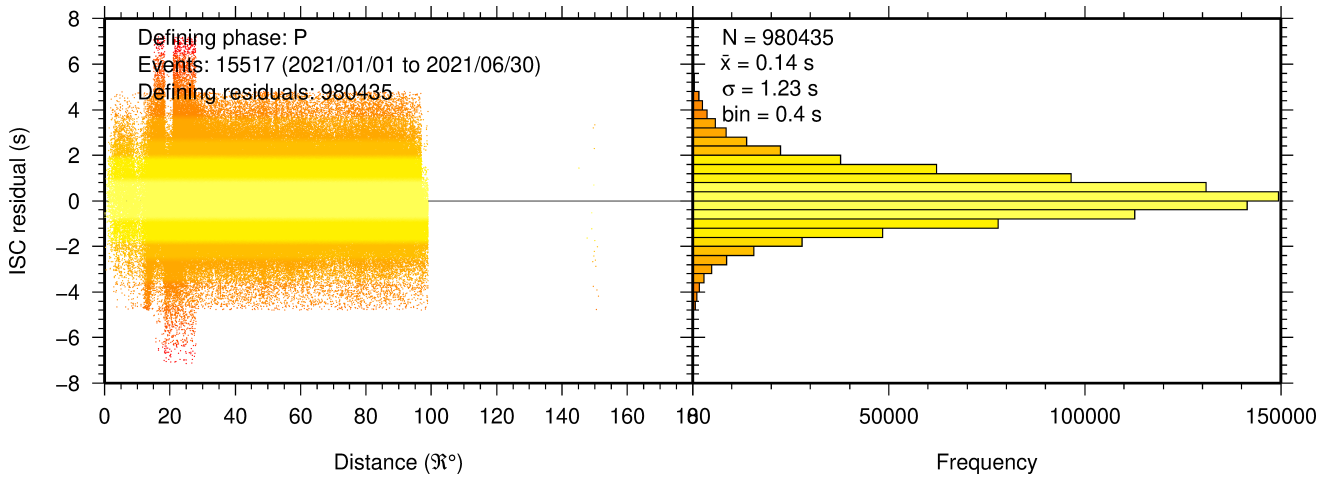
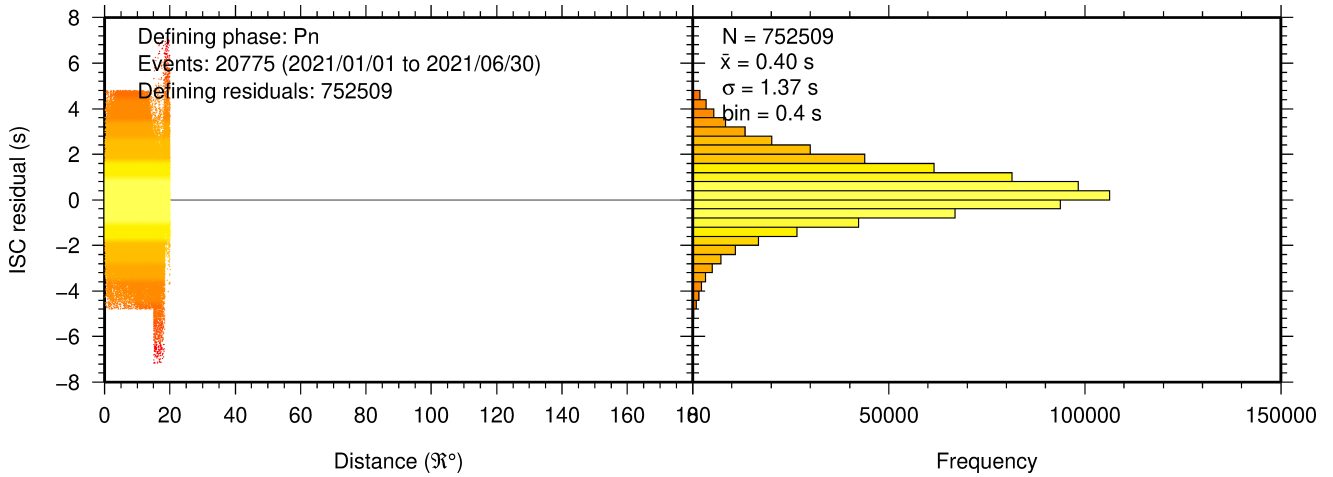


Figure 8.17: Distribution of travel-time observations in the ISC Bulletin for events with  $M > 5.5$  and depth less than 20 km. The travel-time observations are shown relative to a 0 km source and compared with the theoretical ak135 travel-time curves (solid lines). The legend lists the number of each phase plotted.





**Figure 8.18:** Distribution of travel-time residuals for the defining P phases used in the computation of ISC located events in the Bulletin.



**Figure 8.19:** Distribution of travel-time residuals for the defining Pn phases used in the computation of ISC located events in the Bulletin.

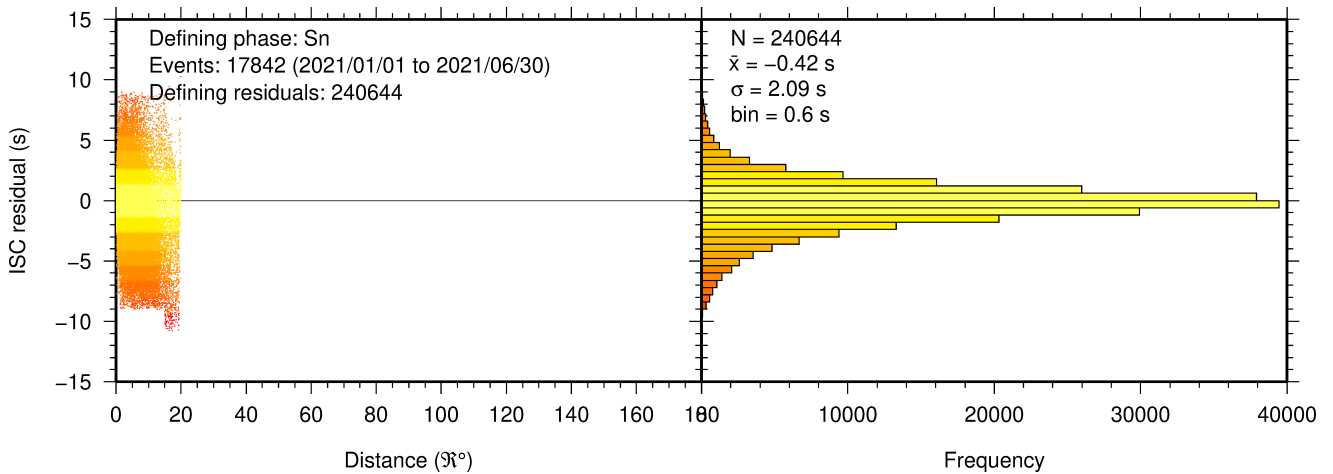


**Figure 8.20:** Distribution of travel-time residuals for the defining Sn phases used in the computation of ISC located events in the Bulletin.

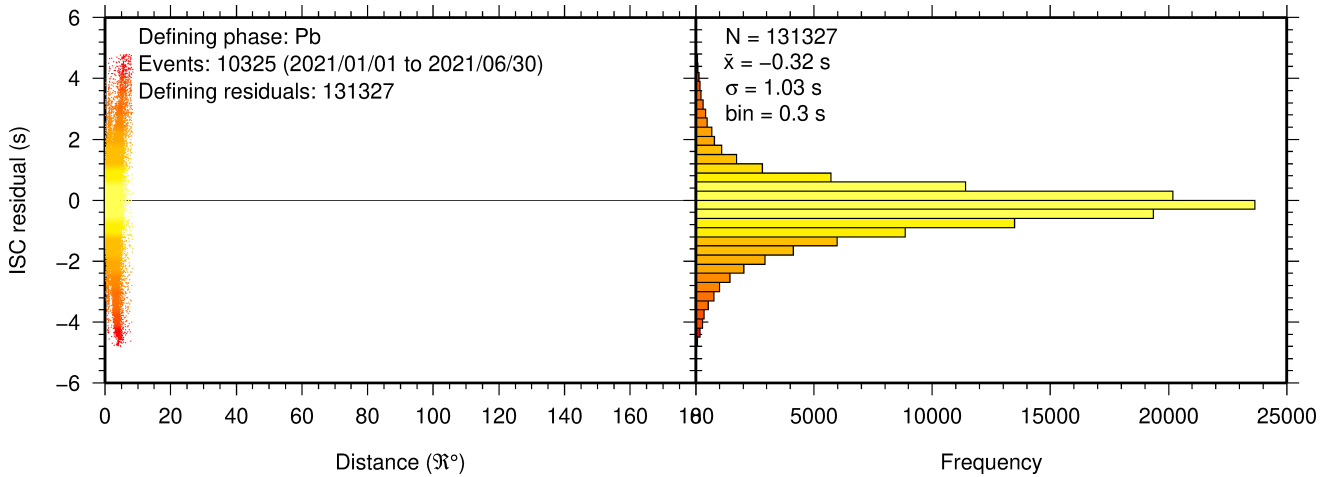


**Figure 8.21:** Distribution of travel-time residuals for the defining Pb phases used in the computation of ISC located events in the Bulletin.

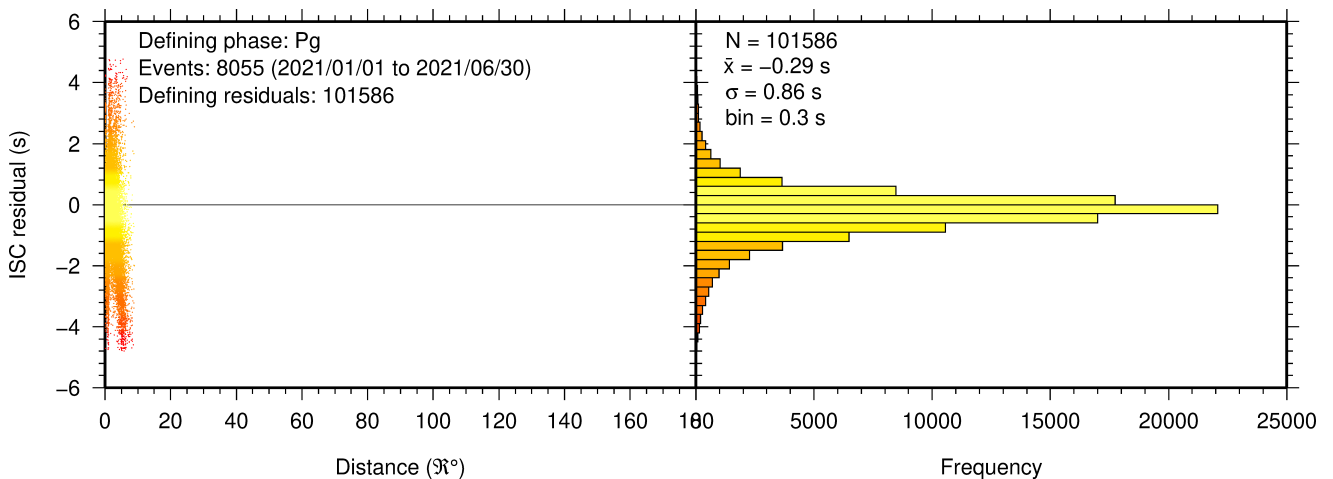


**Figure 8.22:** Distribution of travel-time residuals for the defining Pg phases used in the computation of ISC located events in the Bulletin.

### 8.3 Seismic Wave Amplitudes and Periods

The ISC Bulletin contains a variety of seismic wave amplitudes and periods measured by reporting agencies. For this Bulletin Summary, the total of collected amplitudes and periods is 4,951,951 (see Section 7.3). For the determination of the ISC magnitudes  $M_S$  and  $m_b$ , only a fraction of such data can be used. Indeed, the ISC network magnitudes are computed only for ISC located events. Here we recall the main features of the ISC procedure for  $M_S$  and  $m_b$  computation (see detailed description in Section 10.1.4). For each amplitude-period pair in a reading the ISC algorithm computes the magnitude (a reading can include several amplitude-period measurements) and the reading magnitude is assigned to the maximum A/T in the reading. If more than one reading magnitude is available for a station, the station magnitude is the median of the reading magnitudes. The network magnitude is computed then as the 20% alpha-trimmed median of the station magnitudes (at least three required).  $M_S$  is computed for shallow earthquakes (depth  $\leq 60$  km) only and using amplitudes and periods on all three components (when available) if the period is within 10-60 s and the epicentral distance is between  $20^\circ$  and  $160^\circ$ .  $m_b$  is computed also for deep earthquakes (depth down to 700 km) but only with amplitudes on the vertical

component measured at periods  $\leq 3$  s in the distance range  $21^\circ$ - $100^\circ$ .

Table 8.2 is a summary of the amplitude and period data that contributed to the computation of station and ISC *MS* and *mb* network magnitudes for this Bulletin Summary.

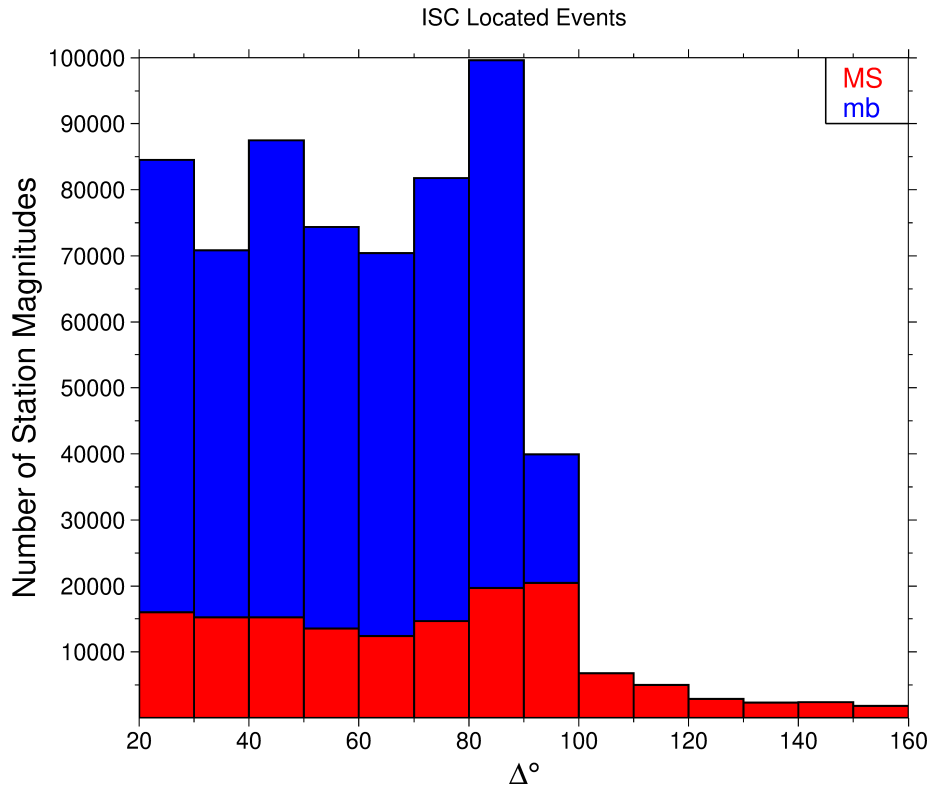
**Table 8.2:** Summary of the amplitude-period data used by the ISC Locator to compute *MS* and *mb*.

	<i>MS</i>	<i>mb</i>
Number of amplitude-period data	172917	680437
Number of readings	151071	673241
Percentage of readings in the ISC located events with qualifying data for magnitude computation	13.7	54.3
Number of station magnitudes	145567	546158
Number of network magnitudes	3994	13993

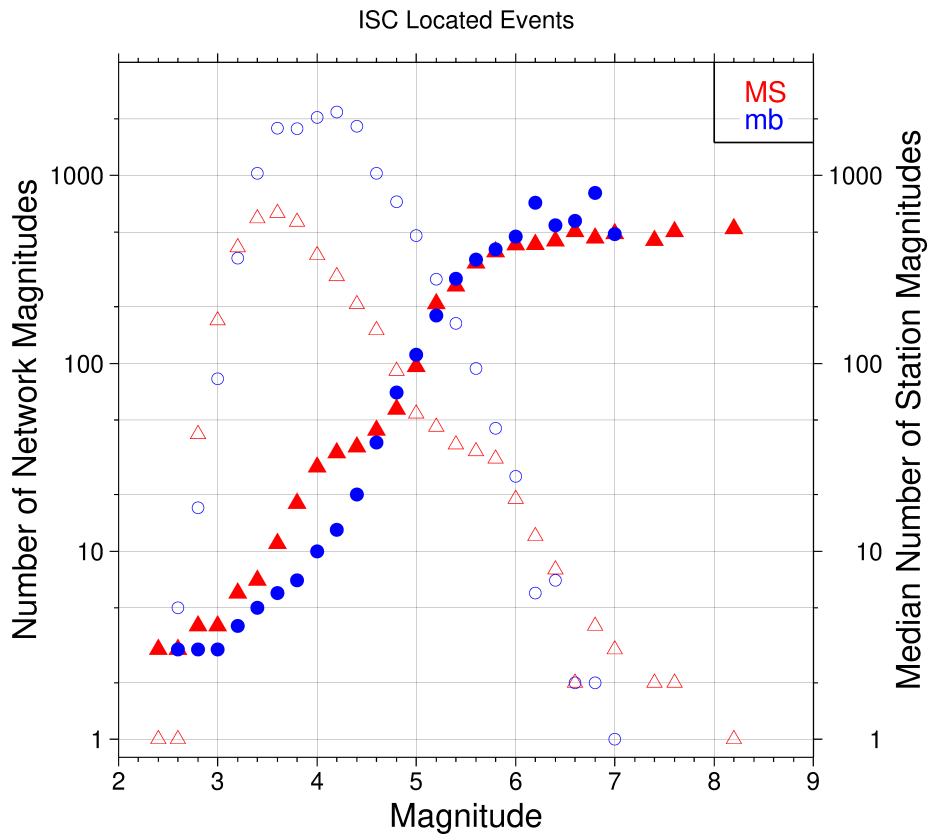
A small percentage of the readings with qualifying data for *MS* and *mb* calculation have more than one amplitude-period pair. Notably, only 14% of the readings for the ISC located (shallow) events included qualifying data for *MS* computation, whereas for *mb* the percentage is much higher at 54%. This is due to the seismological practice of reporting agencies. Agencies contributing systematic reports of amplitude and period data are listed in Appendix Table 10.4. Obviously the ISC Bulletin would benefit if more agencies included surface wave amplitude-period data in their reports.

Figure 8.23 shows the distribution of the number of station magnitudes versus distance. For *mb* there is a significant increase in the distance range  $70^\circ$ - $90^\circ$ , whereas for *MS* most of the contributing stations are below  $100^\circ$ . The increase in number of station magnitude between  $70^\circ$ - $90^\circ$  for *mb* is partly due to the very dense distribution of seismic stations in North America and Europe with respect to earthquake occurring in various subduction zones around the Pacific Ocean.

Finally, Figure 8.24 shows the distribution of network *MS* and *mb* as well as the median number of stations for magnitude bins of 0.2. Clearly with increasing magnitude the number of events is smaller but with a general tendency of having more stations contributing to the network magnitude.



**Figure 8.23:** Distribution of the number of station magnitudes computed by the ISC Locator for mb (blue) and MS (red) versus distance.



**Figure 8.24:** Number of network magnitudes (open symbols) and median number of stations magnitudes (filled symbols). Blue circles refer to mb and red triangles to MS. The width of the magnitude interval  $\delta M$  is 0.2, and each symbol includes data with magnitude in  $M \pm \delta M/2$ .

### 8.4 Completeness of the ISC Bulletin

We define the magnitude of completeness (hereafter  $M_C$ ) as the lowest magnitude threshold above which all events are believed to be recorded. The Bulletin with events bigger than the defined  $M_C$  is assumed to be complete.

Until Issue 53, Volume II (July - December 2016) of the Summary of the ISC an estimation of  $M_C$  was computed only with the maximum curvature technique (*Woessner and Wiemer, 2005*). After the completion of the Rebuild Project and relocation of ISC hypocenters from data years 1964 to 2010 (*Storchak et al., 2017*), the estimate of  $M_C$  for the entire ISC Bulletin is re-computed using four catalogue based methodologies (*Adamaki, 2017*, and references therein): the previously used maximum curvature for comparison (maxC),  $M_C$  based on the b-value stability (MBS technique), the Goodness of Fit Test with a 90% level of fit (GFT90) and the modified Goodness of Fit Test (mGFT). Further details on each of these methodologies and their statistical behaviour can be found in *Leptokaropoulos et al. (2018)*.

The magnitudes of completeness of the ISC Bulletin for this Summary period is shown in Figure 8.25. How  $M_C$  varies for the ISC Bulletin over the years is shown in Figure 8.26. The step change in 1996 corresponds with the inclusion of the Prototype IDC (EIDC) Bulletin, followed by the Reviewed Event Bulletin (REB) of the IDC.

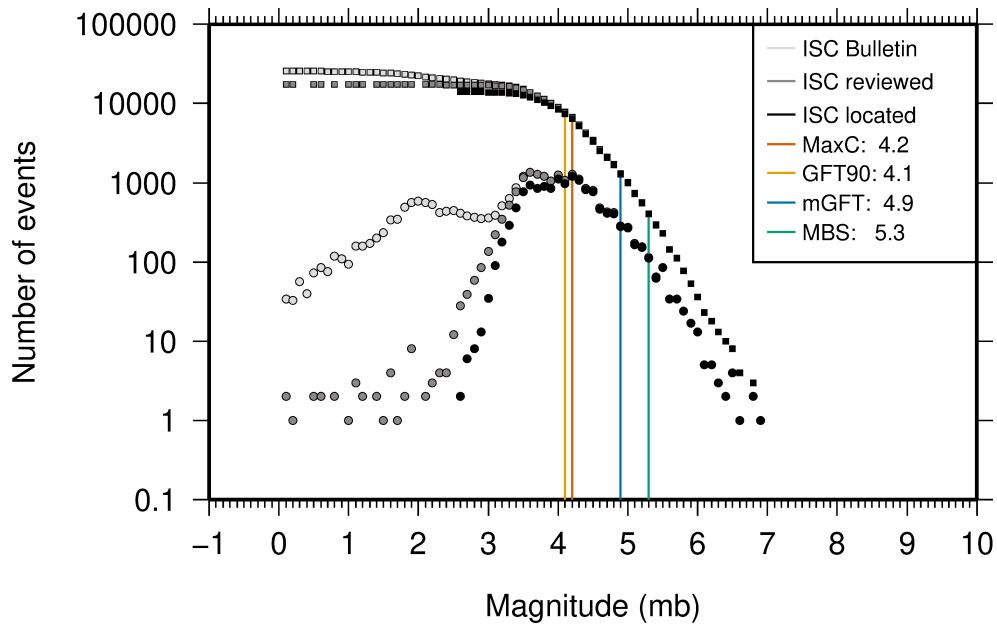


**Figure 8.25:** Frequency and cumulative frequency magnitude distribution for all events in the ISC Bulletin, ISC reviewed events and events located by the ISC. The magnitude of completeness ( $M_C$ ) is shown for the ISC Bulletin. Note: only events with values of mb are represented in the figure.

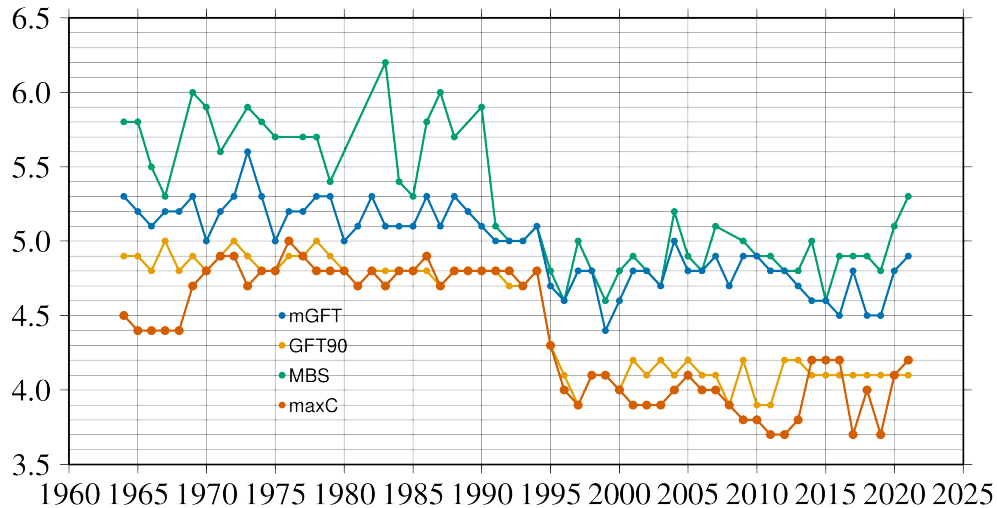


**Figure 8.26:** Variation of magnitude of completeness ( $M_C$ ) for each year in the ISC Bulletin. Note:  $M_C$  is calculated only using those events with values of  $mb$ .

## 8.5 Magnitude Comparisons

The ISC Bulletin publishes network magnitudes reported by multiple agencies to the ISC. For events that have been located by the ISC, where enough amplitude data has been collected, the  $MS$  and  $mb$  magnitudes are calculated by the ISC ( $MS$  is computed only for depths  $\leq 60$  km). In this section, ISC magnitudes and some other reported magnitudes in the ISC Bulletin are compared.

The comparison between  $MS$  and  $mb$  computed by the ISC locator for events in this summary period is shown in Figure 8.27, where the large number of data pairs allows a colour coding of the data density. The scatter in the data reflects the fundamental differences between these magnitude scales.

Similar plots are shown in Figure 8.28 and 8.29, respectively, for comparisons of ISC  $mb$  and ISC  $MS$  with  $M_W$  from the GCMT catalogue. Since  $M_W$  is not often available below magnitude 5, these distributions are mostly for larger, global events. Not surprisingly, the scatter between  $mb$  and  $M_W$  is larger than the scatter between  $MS$  and  $M_W$ . Also, the saturation effect of  $mb$  is clearly visible for earthquakes with  $M_W > 6.5$ . In contrast,  $MS$  scales well with  $M_W > 6$ , whereas for smaller magnitudes  $MS$  appears to be systematically smaller than  $M_W$ .

In Figure 8.30 ISC values of  $mb$  are compared with all reported values of  $mb$ , values of  $mb$  reported by NEIC and values of  $mb$  reported by IDC. Similarly in Figure 8.31, ISC values of  $MS$  are compared with all reported values of  $MS$ , values of  $MS$  reported by NEIC and values of  $MS$  reported by IDC. There is a large scatter between the ISC magnitudes and the  $mb$  and  $MS$  reported by all other agencies.

The scatter decreases both for  $mb$  and  $MS$  when ISC magnitudes are compared just with NEIC and IDC magnitudes. This is not surprising as the latter two agencies provide most of the amplitudes and periods used by the ISC locator to compute  $MS$  and  $mb$ . However, ISC  $mb$  appears to be smaller than NEIC  $mb$  for  $mb < 4$  and larger than IDC  $mb$  for  $mb > 4$ . Since NEIC does not include IDC amplitudes, it seems these features originate from observations at the high-gain, low-noise sites reported by the IDC. A good scaling is generally observed for the  $MS$  comparisons between ISC and IDC.



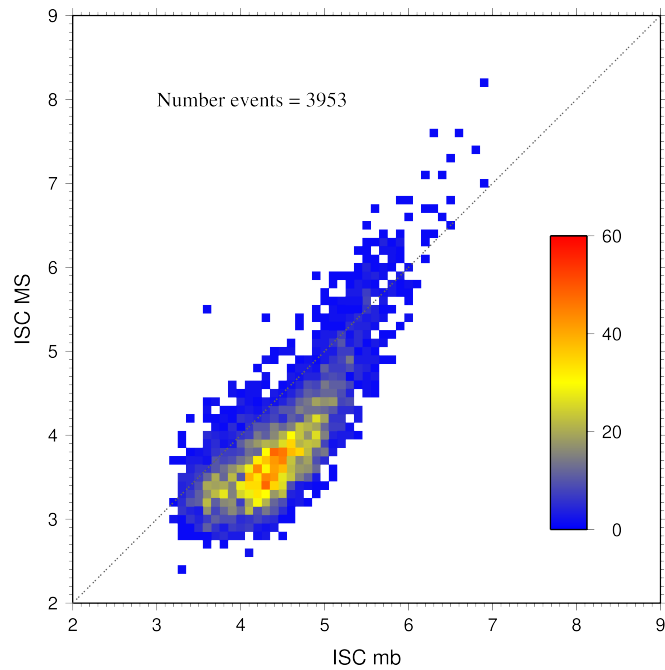


**Figure 8.27:** Comparison of ISC values of MS with mb for common event pairs.

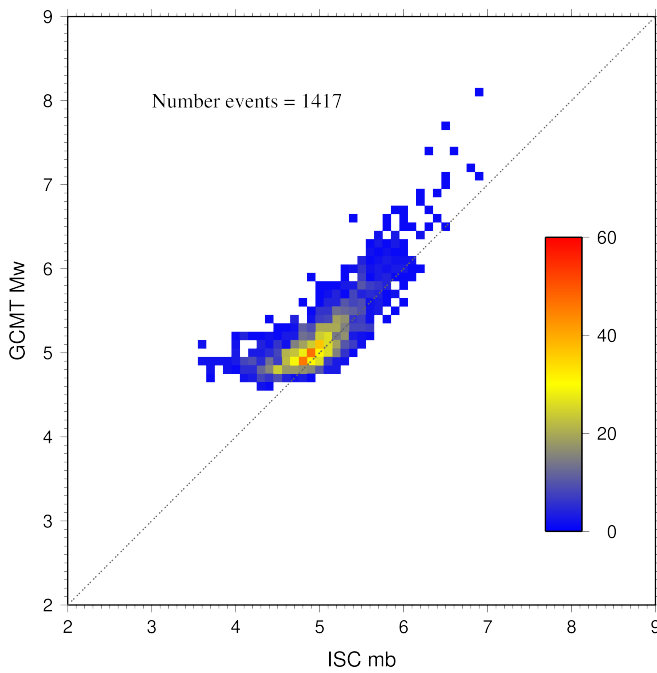


**Figure 8.28:** Comparison of ISC values of mb with GCMT  $M_w$  for common event pairs.

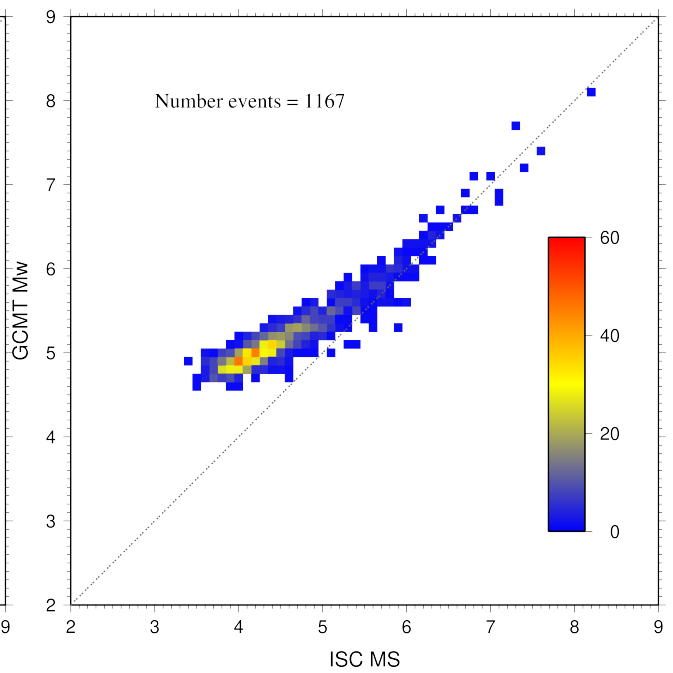


**Figure 8.29:** Comparison of ISC values of MS with GCMT  $M_w$  for common event pairs.

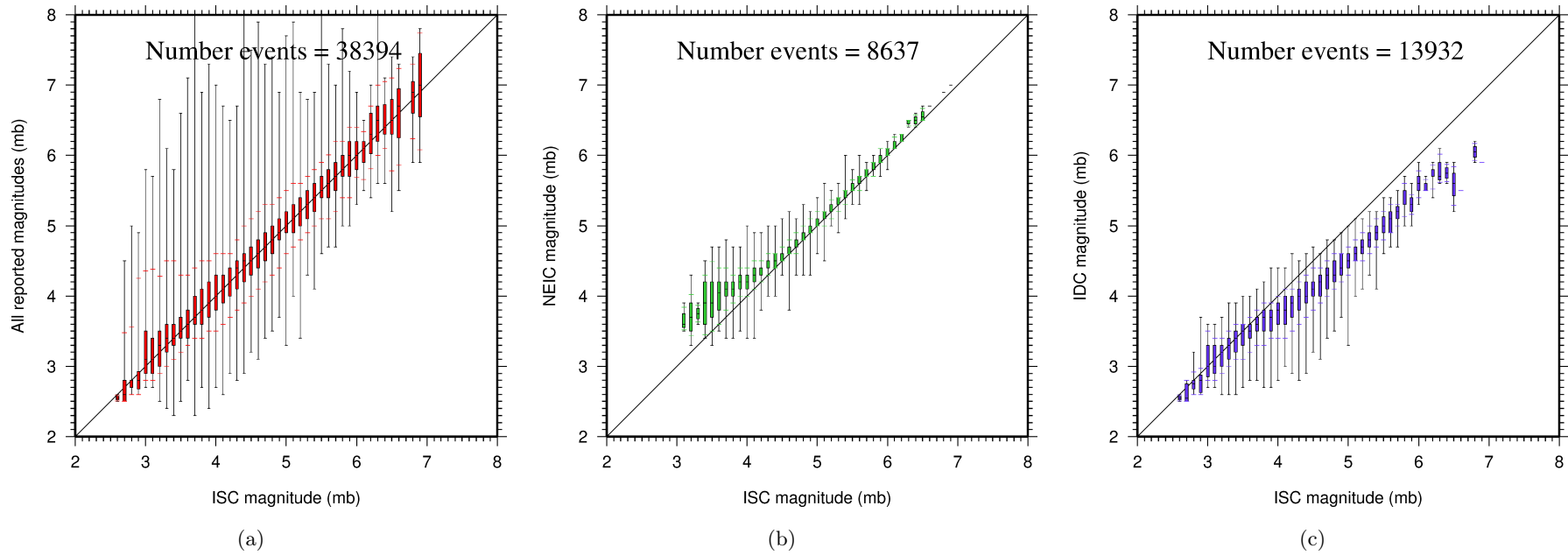


**Figure 8.30:** Comparison of ISC magnitude data (mb) with additional agency magnitudes (mb). The statistical summary is shown in box-and-whisker plots where the 10th and 90th percentiles are shown in addition to the max and min values. (a): All magnitudes reported; (b): NEIC magnitudes; (c): IDC magnitudes.

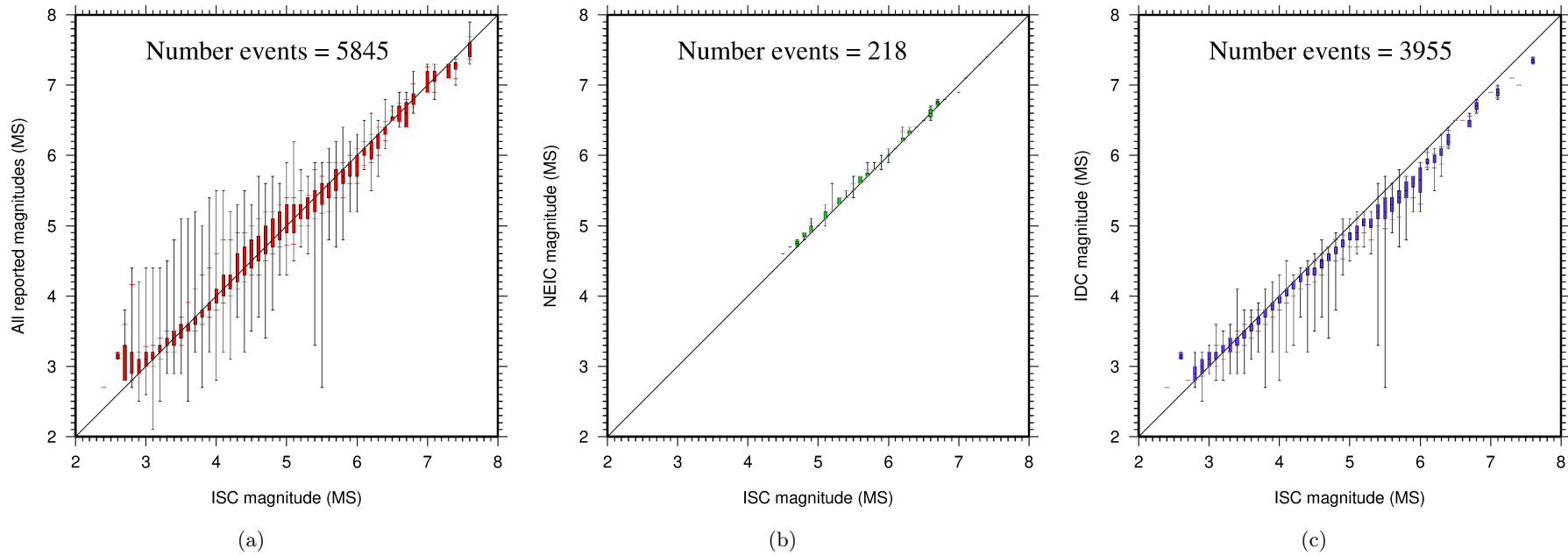


**Figure 8.31:** Comparison of ISC magnitude data ( $MS$ ) with additional agency magnitudes ( $MS$ ). The statistical summary is shown in the box-and-whisker plots where the 10th and 90th percentiles are shown in addition to the max and min values. (a): All magnitudes reported; (b): NEIC magnitudes; (c): IDC magnitudes.

## 9

# The Leading Data Contributors

For the current six-month period, 151 agencies reported related bulletin data. Although we are grateful for every report, we nevertheless would like to acknowledge those agencies that made the most useful or distinct contributions to the contents of the ISC Bulletin. Here we note those agencies that:

- provided a comparatively large volume of parametric data (see Section 9.1),
- reported data that helped quite considerably to improve the quality of the ISC locations or magnitude determinations (see Section 9.2),
- helped the ISC by consistently reporting data in one of the standard recognised formats and in-line with the ISC data collection schedule (see Section 9.3).

We do not aim to discourage those numerous small networks who provide comparatively smaller yet still most essential volumes of regional data regularly, consistently and accurately. Without these reports the ISC Bulletin would not be as comprehensive and complete as it is today.

### 9.1 The Largest Data Contributors

We acknowledge the contribution of IDC, NEIC, GFZ, MOS, BJI, MCSM, CLL and a few others (Figure 9.1) that reported the majority of moderate to large events recorded at teleseismic distances. The contributions of NEIC, IDC, MEX, JMA and several others are also acknowledged with respect to smaller seismic events. The contributions of JMA, AFAD, ISK, RSNC, ATH, TAP, WEL and a number of others are also acknowledged with respect to small seismic events. Note that the NEIC bulletin accumulates a contribution of all regional networks in the USA. Several agencies monitoring highly seismic regions routinely report large volumes of small to moderate magnitude events, such as those in Japan, Chinese Taipei, Turkey, Italy, Greece, New Zealand, Mexico and Columbia. Contributions of small magnitude events by agencies in regions of low seismicity, such as Finland are also gratefully received.

We also would like to acknowledge contributions of those agencies that report a large portion of arrival time and amplitude data (Figure 9.2). For small magnitude events, these are local agencies in charge of monitoring local and regional seismicity. For moderate to large events, contributions of NEIC, GFZ, MOS, IDC are especially acknowledged. Notably, four agencies (NEIC, GFZ, MOS and IDC) together reported over 70% of all amplitude measurements made for teleseismically recorded events. We hope that other agencies would also be able to update their monitoring routines in the future to include the amplitude reports for teleseismic events compliant with the IASPEI standards.

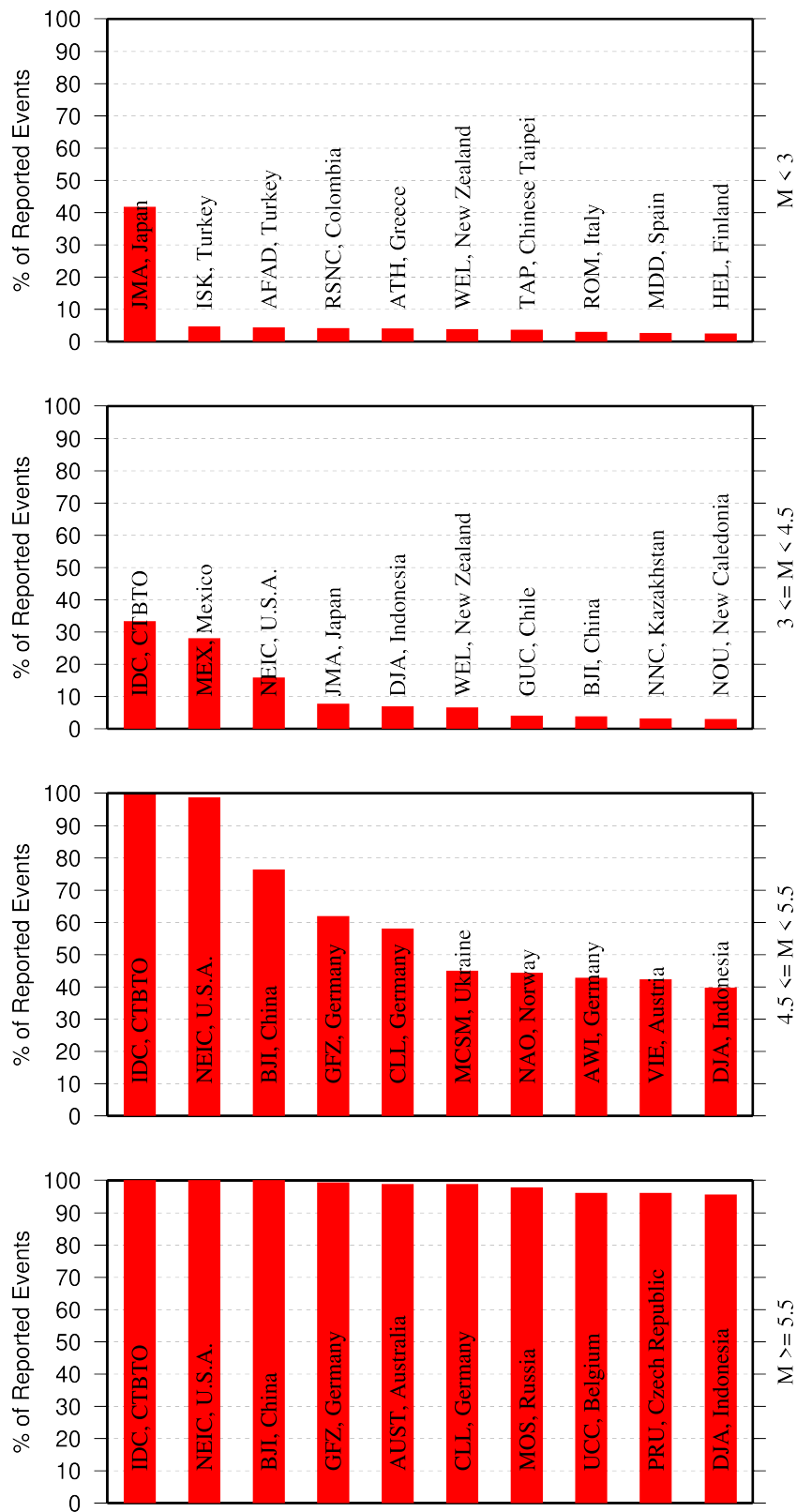


**Figure 9.1:** Frequency of events in the ISC Bulletin for which an agency reported at least one item of data: a moment tensor, a hypocentre, a station arrival time or an amplitude. The top ten agencies are shown for four magnitude intervals.

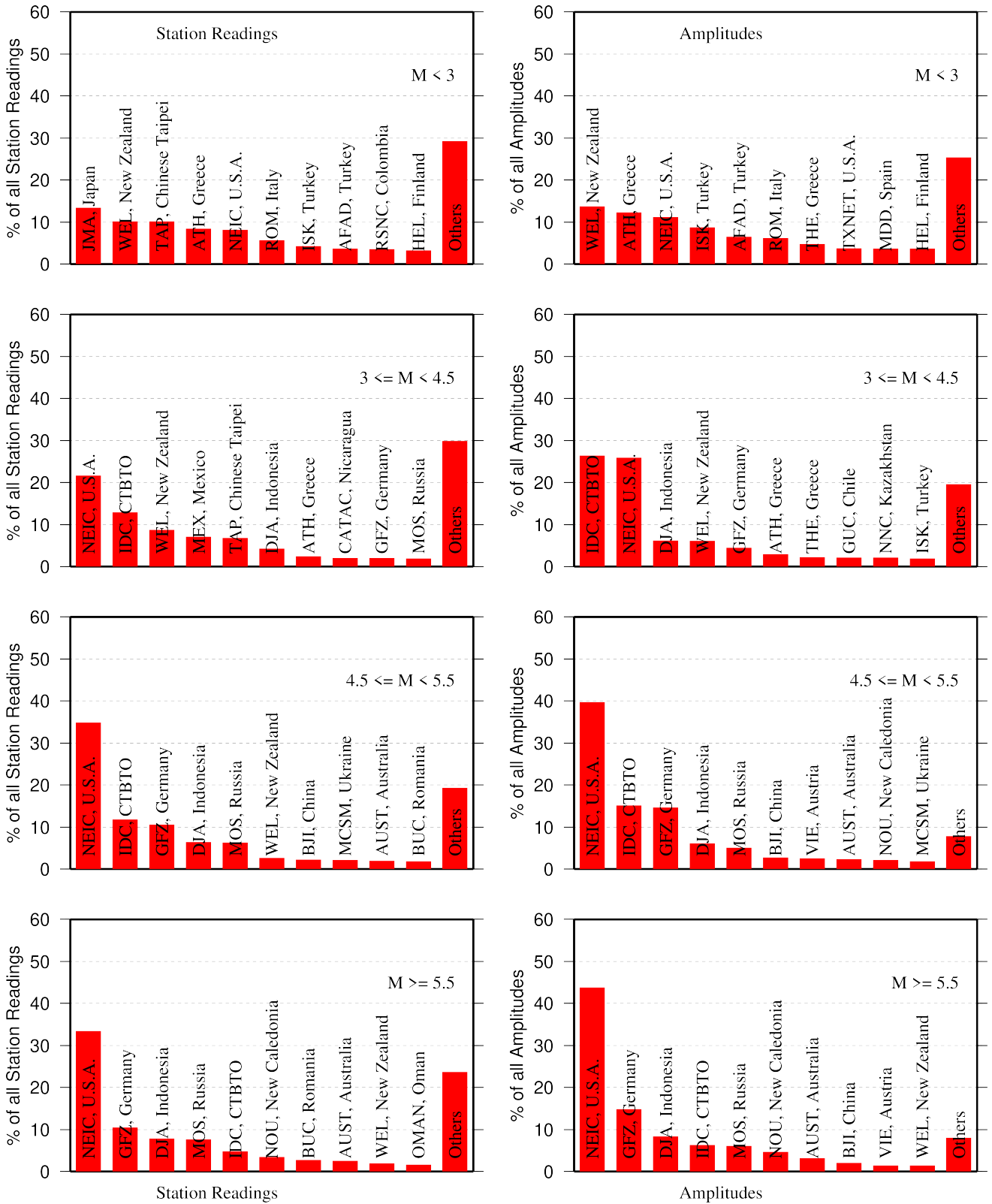


Figure 9.2: Contributions of station arrival time readings (left) and amplitudes (right) of agencies to the ISC Bulletin. Top ten agencies are shown for four magnitude intervals.



## 9.2 Contributors Reporting the Most Valuable Parameters

One of the main ISC duties is to re-calculate hypocentre estimates for those seismic events where a collective wealth of all station reports received from all agencies is likely to improve either the event location or depth compared to the hypocentre solution from each single agency. For areas with a sparse local seismic network or an unfavourable station configuration, readings made by other networks at teleseismic distances are very important. All events near mid-oceanic ridges as well as those in the majority of subduction zones around the world fall into this category. Hence we greatly appreciate the effort made by many agencies that report data for remote earthquakes (Figure 9.3). For some agencies, such as the IDC and the NEIC, it is part of their mission. For instance, the IDC reports almost every seismic event that is large enough to be recorded at teleseismic distance (20 degrees and beyond). This is largely because the International Monitoring System of primary arrays and broadband instruments is distributed at quiet sites around the world in order to be able to detect possible violations of the Comprehensive Nuclear-Test-Ban Treaty. The NEIC reported over 50% of those events as their mission requires them to report events above magnitude 4.5 outside the United States of America. For other agencies reporting distant events it is an extra effort that they undertake to notify their governments and relief agencies as well as to help the ISC and academic research in general. Hence these agencies usually report on the larger magnitude events. BJI, GFZ, CLL, NAO, VIE, AWI, MOS and MCSM each reported individual station arrivals for several percent of all relevant events. We encourage other agencies to report distant events to us.

In addition to the first arriving phase we encourage reporters to contribute observations of secondary seismic phases that help constrain the event location and depth: S, Sn, Sg and pP, sP, PcP (Figure 9.4). We expect though that these observations are actually made from waveforms, rather than just predicted by standard velocity models and modern software programs. It is especially important that these arrivals are manually reviewed by an operator (as we know takes place at the IDC and NEIC), as opposed to some lesser attempts to provide automatic phase readings that are later rejected by the ISC due to a generally poor quality of unreviewed picking.

Another important long-term task that the ISC performs is to compute the most definitive values of

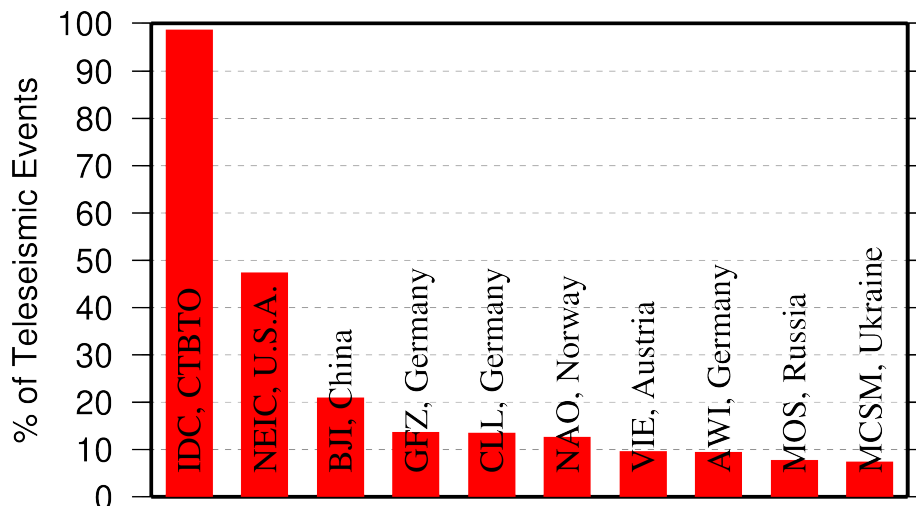


**Figure 9.3:** Top ten agencies that reported teleseismic phase arrivals for a large portion of ISC events.

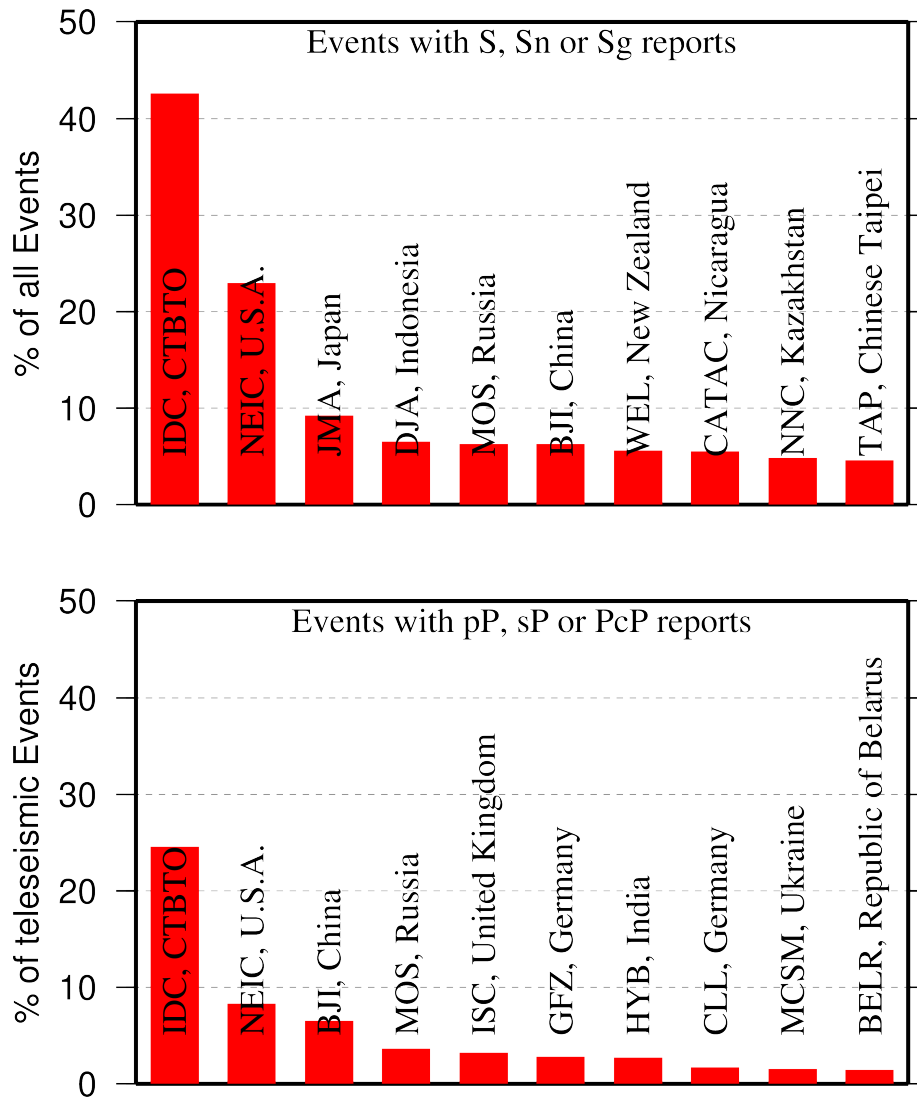


**Figure 9.4:** Top ten agencies that reported secondary phases important for an accurate epicentre location (top) and focal depth determination (bottom).

MS and mb network magnitudes that are considered reliable due to removal of outliers and consequent averaging (using alpha-trimmed median) across the largest network of stations, generally not feasible for a single agency. Despite concern over the bias at the lower end of mb introduced by the body wave amplitude data from the IDC, other agencies are also known to bias the results. This topic is further discussed in Section 8.5.

Notably, the IDC reports almost 100% of all events for which *MS* and *mb* are estimated. This is due to the standard routine that requires determination of body and surface wave magnitudes useful for discrimination purposes. NEIC, BJI, MOS, CLL, GFZ and a few other agencies (Figure 9.5) are also responsible for the majority of the amplitude and period reports that contribute towards the ISC magnitudes.

The top ten agencies that most frequently report seismic moment tensor determinations and moment magnitude are shown in Figure 9.6. The ISC calculates moment tensors, along with the earthquake source time function and depth for moderate magnitude earthquakes ( $M_w$  5.8 - 7.2) using the ISC-PPSM (ISC-Probabilistic Point Source Model) methodology developed in collaboration with the seismology group

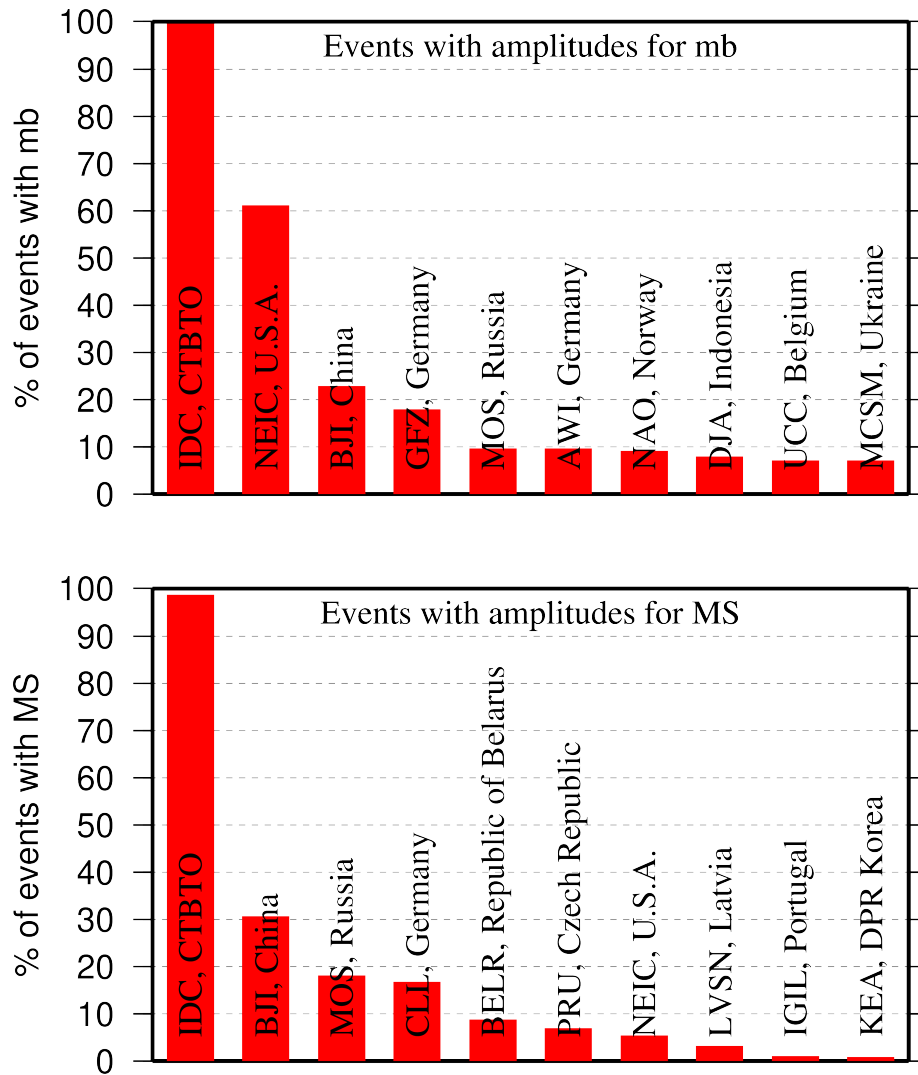


**Figure 9.5:** Agencies that report defining body (top) and surface (bottom) wave amplitudes and periods for the largest fraction of those ISC Bulletin events with MS/mb determinations.

at the University of Oxford (Garth et al 2023).

Among other event parameters the ISC Bulletin also contains information on event type. We cannot independently verify the type of each event in the Bulletin and thus rely on other agencies to report the event type to us. Practices of reporting non-tectonic events vary greatly from country to country. Many agencies do not include anthropogenic events in their reports. Suppression of such events from reports to the ISC may lead to a situation where a neighbouring agency reports the anthropogenic event as an earthquake for which expected data are missing. This in turn is detrimental to ISC Bulletin users studying natural seismic hazard. Hence we encourage all agencies to join the agencies listed on Figure 9.7 and several others in reporting both natural and anthropogenic events to the ISC.

The ISC Bulletin also contains felt and damaging information when local agencies have reported it to us. Agencies listed on Figure 9.8 provide such information for the majority of all felt or damaging events in the ISC Bulletin.

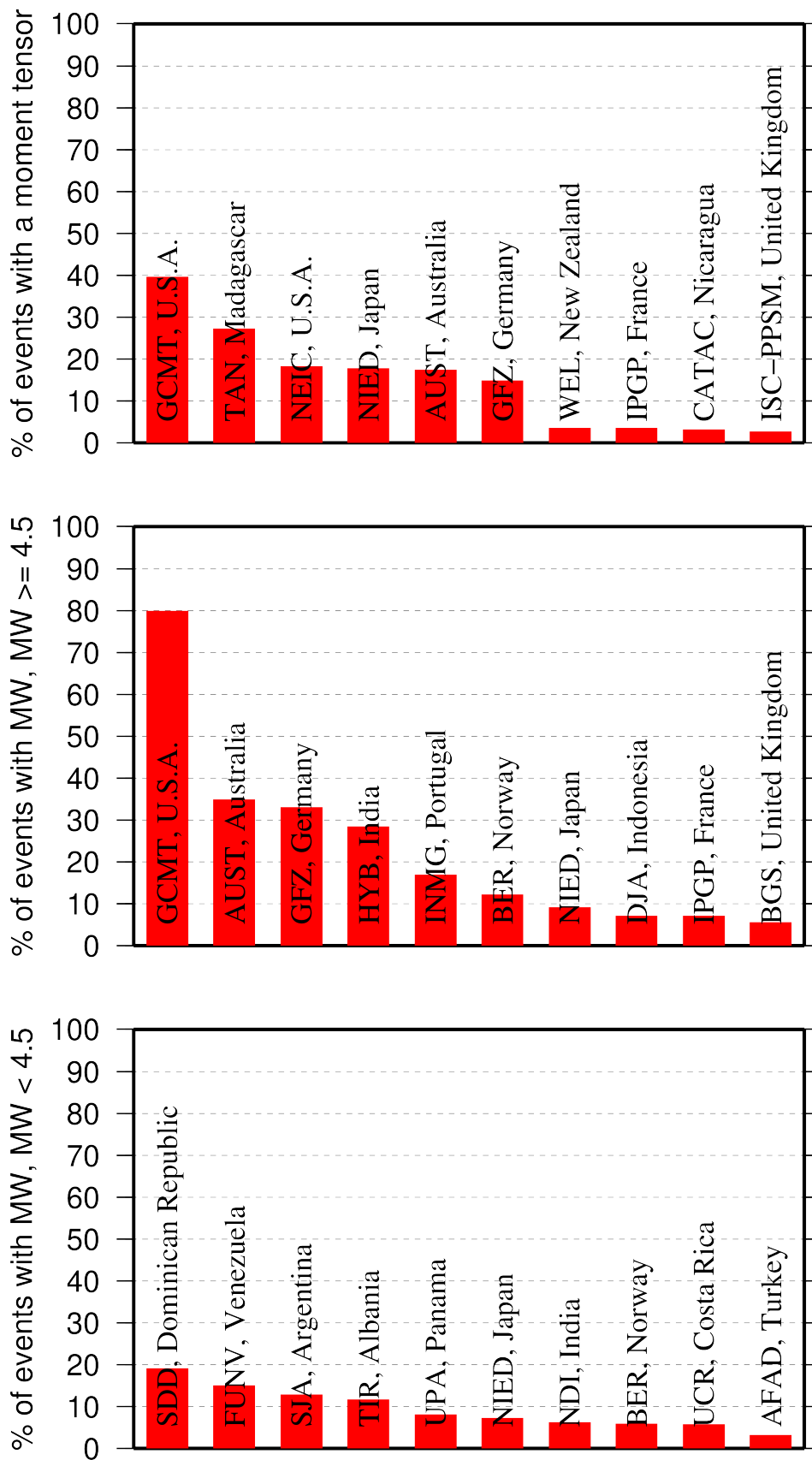


**Figure 9.6:** Top ten agencies that most frequently report determinations of seismic moment tensor (top) and moment magnitude (middle/bottom for  $M$  greater/smaller than 4.5).

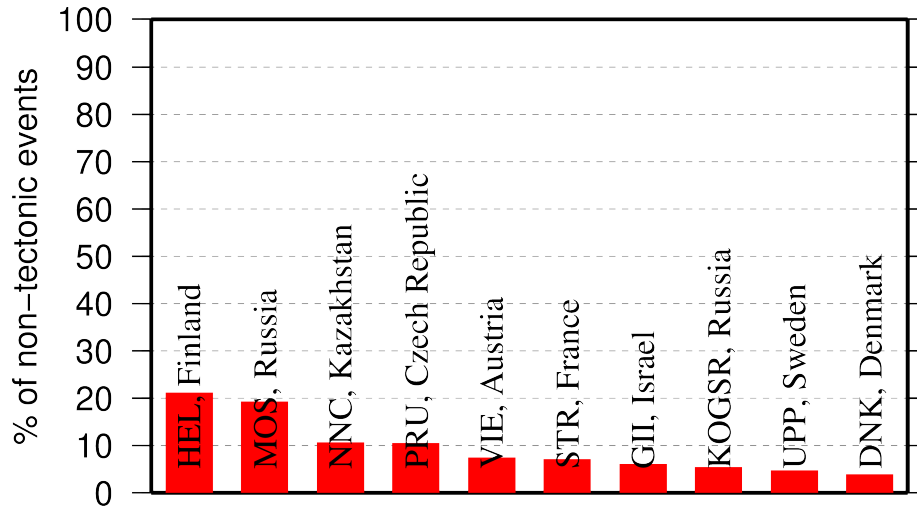


*Figure 9.7: Top ten agencies that most frequently report non-tectonic seismic events to the ISC.*

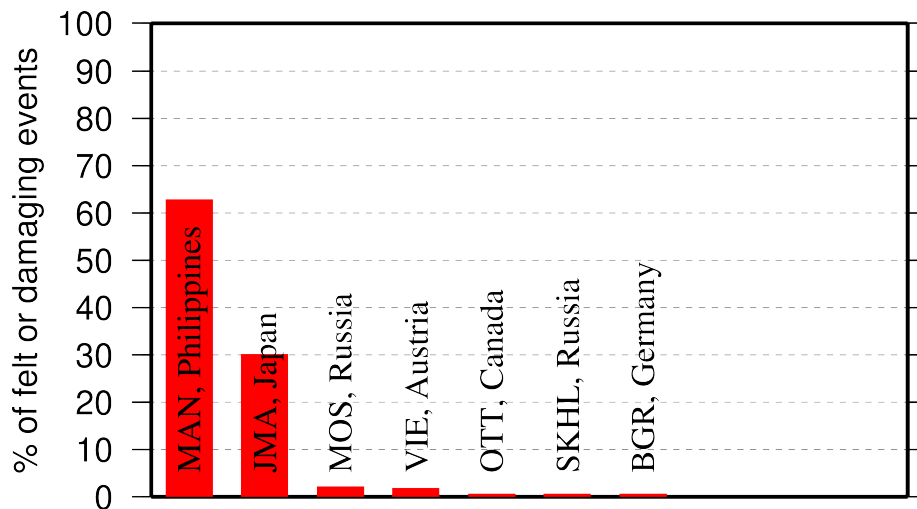


*Figure 9.8: Top agencies that most frequently report macroseismic information to the ISC.*

### 9.3 The Most Consistent and Punctual Contributors

During this six-month period, 27 agencies reported their bulletin data in one of the standard seismic formats (ISF, IMS, GSE, Nordic or QuakeML) and within the current 12-month deadline. Here we must reiterate that the ISC accepts reviewed bulletin data after a final analysis as soon as they are ready. These data, even if they arrive before the deadline, are immediately parsed into the ISC database, grouped with other data and become available to the ISC users on-line as part of the preliminary ISC Bulletin. There is no reason to wait until the deadline to send the data to the ISC. Table 9.1 lists all agencies that have been helpful to the ISC in this respect during the six-month period.

**Table 9.1:** Agencies that contributed reviewed bulletin data to the ISC in one of the standard international formats before the submission deadline.

Agency Code	Country	Average Delay from real time (days)
ZUR	Switzerland	15
AUST	Australia	15
ATH	Greece	18
WEL	New Zealand	20
IDC	Austria	28
IGIL	Portugal	31
NAO	Norway	38
LDG	France	51
ECX	Mexico	61
SVSA	Portugal	61
KNET	Kyrgyzstan	83
BUC	Romania	104
ISK	Turkey	106
UPP	Sweden	115
NAM	Namibia	121
CATAC	Nicaragua	134
STR	France	135
KEA	Democratic People’s Republic of Korea	151
GRAL	Lebanon	154
DSN	United Arab Emirates	166
BJI	China	181
PPT	French Polynesia	196
VIE	Austria	224
TIR	Albania	230
BGS	United Kingdom	252
IPEC	Czech Republic	295
FUNV	Venezuela	302
OMAN	Oman	309
INMG	Portugal	325
NEIC	U.S.A.	329
MOS	Russia	333
SDD	Dominican Republic	341
ISN	Iraq	342
ROM	Italy	358
UCC	Belgium	358

# 10

## Appendix

### 10.1 ISC Operational Procedures

#### 10.1.1 Introduction

The relational database at the ISC is the primary source for the ISC Bulletin. This database is also the source for the ISC web-based search and this printed Summary. The ISC database is also mirrored at several institutions such as the Data Management Center of the Incorporated Research Institutions for Seismology (IRIS DMC), Earthquake Research Institute (ERI) of the University of Tokyo and a few others.

The database holds information about ISC events, both natural and anthropogenic. Information on each event may include hypocentre estimates, moment tensors, event type, felt and damaging reports and associated station observations reported by different agencies and grouped together per physical event.

The majority of the ISC events are small and are not reviewed by the ISC analysts. Those that are reviewed (usually magnitude greater than 3.5) may or may not include an ISC hypocentre solution and magnitude estimates. The decision depends on whether the wealth of combined information from several agencies as compared to the data of each single agency alone warrants the ISC location. The events are called ISC events regardless of whether they have been reviewed or located by the ISC or not.

All events located by the ISC are reviewed by the ISC analysts but not the other way round. Analyst review involves an examination of the integrity of all reported parametric information. It does not involve review of waveforms. Even if waveforms from all of the thousands of stations included in a typical recent month of the ISC Bulletin were freely available, it would be an unmanageable task to inspect them all.

We shall now describe briefly current processes and procedures involved in producing the Bulletin of the International Seismological Centre. These have been developed from former practices described in the Introduction to earlier issues of the ISC Bulletin to account for modern methods and technologies of data collection and analysis.

#### 10.1.2 Data Collection

Parametric data, mainly comprising seismic event hypocentre solutions, phase arrival observations and associated magnitude data, are now mostly emailed to the ISC ([seismo@isc.ac.uk](mailto:seismo@isc.ac.uk)) by agencies around the world. Other macroseismic and source information associated with seismic events may also be incorporated in accordance with modern standards. The process of data collection at the ISC involves the automatic parsing of these data into the ISC relational database. The ISC now has over 200 individual parsers to account for legacy and current bulletin data formats used by data reporters.



Figure 10.1 shows the 313 agencies that have reported bulletin data to the ISC, directly or via regional data centres, during the entire period of the ISC existence: these agencies are also listed in Table 10.2 of the Appendix. In Figure 10.1, corresponding countries are shown shaded in red. Please note that the continent of Antarctica appears white on the map despite a steady stream of bulletin data from Antarctic stations: the agencies that run these stations are based elsewhere.

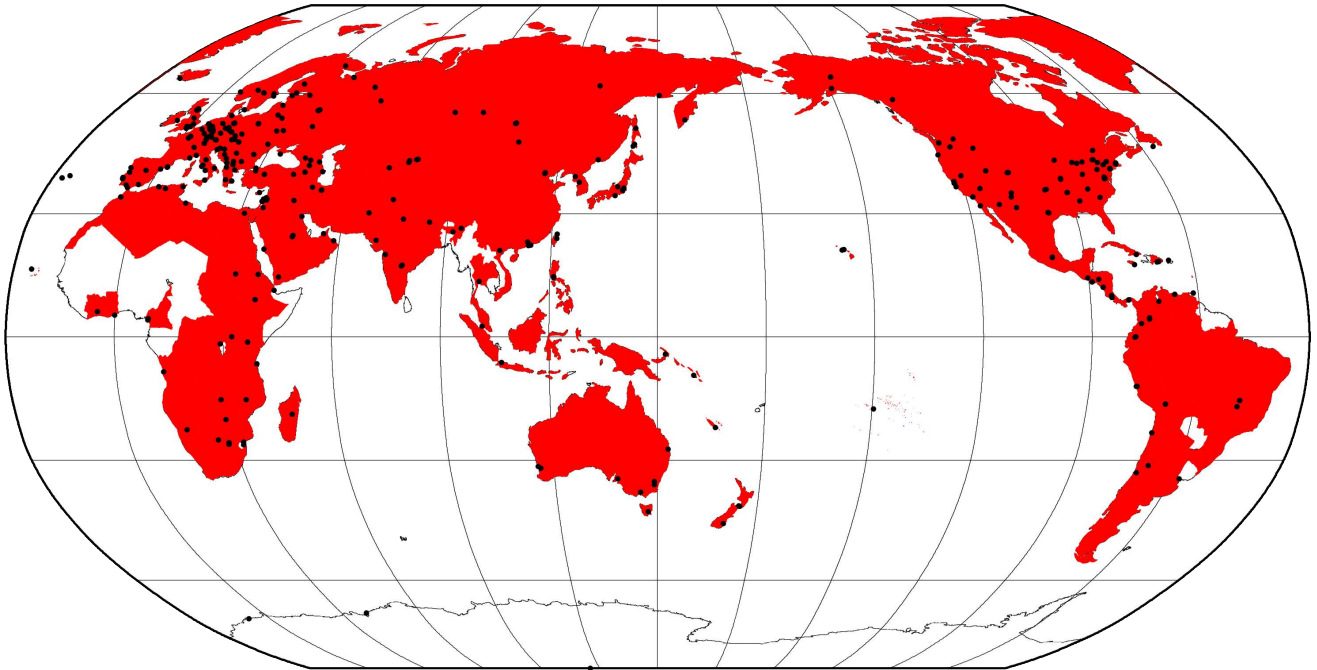


*Figure 10.1: Map of 313 agencies and corresponding countries that have reported seismic bulletin data to the ISC at least once during the entire period of the ISC operations, either directly or via regional data centres. Corresponding countries are shaded in red.*

### 10.1.3 ISC Automatic Procedures

#### Grouping

Grouping is the automatic process by which the many hypocentre solutions sent by the agencies reporting to the ISC for the same physical event are merged together into a single ISC event. This process possibly begins with an alert message and ends before a final review by ISC analysts. The process periodically runs through a set time interval of the input data stream, typically one day, looking for hypocentres in newly received data that are not yet grouped into an ISC event. Thus it considers only data more recent than the last data month reviewed by the ISC analysts. Immediately after grouping the seismic arrival associator is run on the same time interval, dealing with new phase arrival data not associated with any hypocentre.

The first stage of grouping gets a score where possible for each hypocentre to determine whether the reported hypocentre will be considered to be the primary estimate, or prime, for an ISC event. This score is based on the station arrival times reported in association with the hypocentre in four epicentral distance zones that characterise the networks of stations reporting:

1. Whole network

2. Local, 0 - 150 km
3. Near-regional, 3° - 10°
4. Teleseismic, 28° - 180°

For each distance zone, the azimuthal gap, the secondary azimuthal gap (the largest azimuthal gap filled by a single station), the minimum and maximum epicentral distance and number of stations are all used to calculate the value of  $dU$ , the normalised absolute deviation from best fitting uniformly distributed stations (*Bondár and McLaughlin, 2009a*). Clearly, this procedure can only use:

1. Bulletin data with hypocentres and sufficient associated seismic arrivals
2. Data for stations that are in the International Registry (IR)
3. Station data that are actually reported to ISC: CENC (China), for example, reports at most 34 stations, whilst many more may have been used to determine the hypocentre.

The hypocentres are then each considered in turn for grouping using one of two methods, the first by searching for a similar hypocentre, and the second by searching for the best fit of the reported phase arrival data that are associated with the candidate hypocentre. The method chosen for a reporter is based on feedback gained from ISC analysts.

For finding similar hypocentres, three sets of limits for origin-time difference and epicentral separation are used according to the type of bulletin data, be it alert, provisional or final. These limits are, respectively:

- $\pm 2$  minutes and  $10^\circ$
- $\pm 2$  minutes and  $4^\circ$
- $\pm 1$  minutes and  $2^\circ$

If there is no overlap with the hypocentre of an existing ISC event, a new event is formed. For each candidate hypocentre, a proximity score is otherwise calculated based on differences in time,  $t$ , and distance,  $s$ , between the candidate hypocentre and a hypocentre in an event with which it could potentially be grouped.

$$\text{Proximity score} = 2 - (dt/dt_{max}) - (ds/ds_{max})$$

where  $ds_{max}$  is the maximum distance between hypocentres and  $dt_{max}$  the maximum difference in origin time.

As long as there is no duplication of hypocentre (with the same author, origin time and location within tight limits) the candidate hypocentre together with the associated phase data is grouped with the prime hypocentre of the event and the initial  $dU$  score is used to reassess the prime hypocentre designation. Apparent duplicated hypocentre estimations, including preliminary solutions relayed by other agencies, need to be assessed to determine whether they should really be split between different events. Should

there be two or more equally valid events, these can be assessed in turn and may eventually be merged together.

Grouping by fit of the associated phase arrival data is simpler. The residuals of the arrival data are calculated using ak135 travel times for all suitable prime hypocentres within the widest proximity limits given above for similar hypocentres. The hypocentre and associated phase arrival data is then grouped with the event with the best fitting prime hypocentre, which may similarly be re-designated according to the dU scores. Associations of phase arrival data are updated to be with the prime hypocentre estimate of each ISC event.

It follows that a hypocentre and associated phase arrival data submitted by a reporter will have the reported hypocentre set as the prime hypocentre in the ISC event if no other submitted hypocentre estimate is a closer match. It follows also that a hypocentre submitted without phase data can only be grouped with a similar hypocentre. Generally, early arriving data may be superseded by later arriving data: the data will still be in the ISC database but be deprecated, that is, marked as being no longer useful for further processes.

### **Association**

Association is the automatic procedure, run routinely after grouping, that links reported phase arrivals at IR stations with the prime hypocentres of ISC events. As grouping took care of those phases associated with reported hypocentres, by associating the phases to the respective prime hypocentres of the ISC events without further checks, this procedure is only required for phase arrival observations that were sent without any association of event made for them by the reporter. Currently only 5% of arrival data is sent unassociated compared with 25% when the ISC began storing reported data directly to a database for data year 1999.

If a phase arrival is found to be very similar to another already reported, it is placed in the same event, otherwise the procedure below is followed.

For associating a phase arrival, suitable events are sought with prime hypocentre origin-times in the window 40 minutes before and 100 s after the arrival time. For each phase arrival and prime hypocentre an ak135 travel-time residual is calculated for either the reported arrival phase name or an alternative from a default list if appropriate. Possible timing errors that are multiples of 60 s (a minute) are considered if the phase arrival is at a station not known to be digitally recording. A reporting likelihood is then determined based on the reported event magnitude: a magnitude default of 3.0 is used if no magnitude is given.

A final score is calculated from the residuals, from the likelihood of the phase observations for the magnitude of the event and from the S-P misfit. A phase arrival along with all other phase arrivals in that reading for the station is then associated with the prime hypocentre with the best score. If no suitable match is found, the reading remains unassociated but may be used at some later stage.

## Thresholding

Thresholding is the process determining which events are to be reviewed by the ISC analysts. In former times, before email transmission of data was convenient, all events were reviewed, with magnitudes nearly always 3.5 or above. Nowadays, data contributors are encouraged to send all their data, which are stored in the ISC database. The overwhelming amount of data, including that for many more smaller events and from many more seismograph stations, led to the advent of ISC Comprehensive Bulletin, for all events, and the ISC Reviewed Bulletin, for selected events reviewed by ISC analysts. Thresholding has been under constant review since the start of the 1999 data year.

Several criteria are considered to decide which events merit review. Once a decision is made, whether or not an event is to be reviewed, further criteria are not considered.

In this section,  $M$  is the maximum magnitude reported by any agency for the event. The sequence of tests in the automatic decision process for reviewing events is currently:

- All events reported by the International Data Centre (IDC) of the Comprehensive Nuclear-Test-Ban Treaty Organization (CTBTO) are reviewed.
- If  $M$  is greater than or equal to 3.5, the event is reviewed.
- If  $M$  is less than 2.5, the event is not reviewed.
- If  $M$  is unknown, the number of data sources of hypocentres and phase arrivals is used. Care is taken here to avoid counting indirect reports arriving via agencies such as NEIC, which compile regional and global data:
  - If the number of hypocentre authors is greater than two and the maximum epicentral distance of arrival data is greater than  $10^\circ$ , the event is reviewed.
  - If the number of arrival authors is greater than two and the maximum epicentral distance of arrival data is greater than  $10^\circ$ , the event is reviewed.
  - Otherwise the event is not reviewed.
- If  $M$  is between 2.5 and 3.5:
  - If the number of hypocentre and seismic arrival authors is less than two, the event is not reviewed.
  - If any bulletin contributing to the event has at least ten stations within  $3^\circ$  and the secondary azimuthal gap (the largest azimuthal gap filled by a single station) is less than  $135^\circ$ , the event is not reviewed.

## Location by the ISC

The automatic processes group and associate incoming data into ISC events as indicated above. These data are available to users before review by the ISC analysts but there will be no ISC hypocentre solutions for any of the events. The candidate events due for review by the ISC analysts are determined by the

---

thresholding process, which is why many smaller events remain without an ISC hypocentre solution even after the analyst review.

Several further checks of the data are made in preparation for the analyst review, and initial trial estimates for ISC hypocentres are then generated using the accumulated data. If sufficiently robust, the ISC hypocentre estimation will be retained and be made the prime solution for the event, but this, of course, will itself be subject to the analyst review.

It is important to note that not all reviewed events will have an ISC hypocentre. At least one of the criteria listed below must be met for an initial ISC location of a reviewed event to be made:

- All events with an IDC hypocentre, unless IDC is the only hypocentre author and there are less than six associated phases.
- Two or more reporters of data
- Phase data at epicentral distance  $\geq 20^\circ$

The ISC locator also needs an initial seed location; in all events except those with eight or more reporters of data where the existing prime is used, this is calculated using a Neighbourhood Algorithm (NA) (*Sambridge, 1999; Sambridge and Kennett, 2001*). More information about the ISC location algorithm and initial seed is given in the next section.

#### 10.1.4 ISC Location Algorithm

The ISC location algorithm is described in detail in *Bondár and Storchak (2011)* (<https://doi.org/10.1111/j.1365-246X.2011.05107.x>, Manual: [www.isc.ac.uk/iscbulletin/iscloc/](http://www.isc.ac.uk/iscbulletin/iscloc/)); here we give a short summary of the major features. Ever since the ISC came into existence in 1964, it has been committed to providing a homogeneous bulletin that benefits scientific research. Hence the location algorithm used by the ISC then, except for some minor modifications, had remained largely unchanged for 40 years (*Adams et al., 1982; Bolt, 1960*). While the ISC location procedures had served the scientific community well in the past, they could certainly be improved and a new ISC location algorithm was developed and implemented from data year 2010. Since then, the entire ISC Bulletin has been relocated with the new location algorithm as part of the Rebuild project (*Storchak et al., 2017; 2020*).

Linearised location algorithms are very sensitive to the initial starting point for the location. The old procedures made the assumption that a good initial hypocentre is available among the reported hypocentres. However, there is no guarantee that any of the reported hypocentres are close to the global minimum in the search space. Furthermore, attempting to find a free-depth solution was futile when the data had no resolving power for depth (e.g. when the first arrival is not within the inflection point of the P travel-time curve). When there was no depth resolution, the algorithm would simply pick a point on the origin time – depth trade-off curve. The old ISC locator assumed that the observational errors are independent. The recent years have seen a phenomenal growth both in the number of reported events and phases, owing to the ever-increasing number of stations worldwide. Similar ray paths will produce correlated travel-time prediction errors due to unmodelled heterogeneities in the Earth, resulting in

underestimated location uncertainties and for unfavourable network geometries, location bias. Hence, accounting for correlated travel-time prediction errors becomes imperative if we want to improve (or simply maintain) location accuracy as station networks become progressively denser. Finally, publishing network magnitudes that may have been derived from a single station measurement was rather prone to producing erroneous event magnitude estimates.

To meet the challenge imposed by the ever-increasing data volume from heavily unbalanced networks a new ISC location algorithm was introduced to ensure the efficient handling of data and to further improve the location accuracy of events reviewed by the ISC. The ISC location algorithm

- Uses all ak135 (*Kennett et al.*, 1995) predicted phases (including depth phases) in the location;
- Obtains the initial hypocentre guess via the Neighbourhood Algorithm (NA) (*Sambridge*, 1999; *Sambridge and Kennett*, 2001);
- Performs iterative linearised inversion using an *a priori* estimate of the full data covariance matrix to account for correlated model errors (*Bondár and McLaughlin*, 2009b);
- Attempts a free-depth solution if and only if there is depth resolution, otherwise it fixes the depth to a region-dependent default depth;
- Scales uncertainties to 90% confidence level and calculates location quality metrics for various distance ranges;
- Obtains a depth-phase depth estimate based on reported surface reflections via depth-phase stacking (*Murphy and Barker*, 2006);
- Provides robust network magnitude estimates with uncertainties.

## Seismic Phases

One of the major advantages of using the ak135 travel-time predictions (*Kennett et al.*, 1995) is that they do not suffer from the baseline difference between P, S and PKP phases compared with the Jeffreys-Bullen tables (*Jeffreys and Bullen*, 1940). Furthermore, ak135 offers an abundance of phases from the IASPEI Standard Seismic List (*Storchak et al.*, 2003; 2011) that can be used in the location, most notably the PKP branches and depth-sensitive phases. Elevation and ellipticity corrections (*Dziewonski and Gilbert*, 1976; *Engdahl et al.*, 1998; *Kennett et al.*, 1996), using the WG84 ellipsoid parameters, are added to the ak135 predictions. For depth phases, bounce point (elevation correction at the surface reflection point) and water depth (for pwP) corrections are calculated using the algorithm of *Engdahl et al.* (1998). We use the ETOPO1 global relief model (*Amante and Eakins*, 2009) to obtain the elevation or the water depth at the bounce point.

Phase picking errors are described by *a priori* measurement error estimates derived from the inspection of the distribution of ground truth residuals (residuals calculated with respect to the ground truth location) from the IASPEI Reference Event List (*Bondár and McLaughlin*, 2009a). For phases that do not have a sufficient number of observations in the ground truth database we establish *a priori* measurement errors so that the consistency of the relative weighting schema is maintained. First-arriving P-type phases (P,

Pn, Pb, Pg) are picked more accurately than later phases, so their measurement error estimates are the smallest, 0.8 s. The measurement error for first-arriving S-phases (S, Sn, Sb, Sg) is set to 1.5 s. Phases traversing through or reflecting from the inner/outer core of the Earth have somewhat larger (1.3 s for PKP, PKS, PKKP, PKKS and P'P' branches as well as PKiKP, PcP and PcS, and 1.8 s for SKP, SKS, SKKP, SKKS and S'S' branches as well as SKiKP, ScP and ScS) measurement error estimates to account for possible identification errors among the various branches. Free-surface reflections and conversions (PnPn, PbPb, PgPg, PS, PnS, PgS and SnSn, SbSb, SgSg, SP, SPn, SPg) are observed less frequently and with larger uncertainty, and therefore suffer from large, 2.5 s, measurement errors. Similarly, a measurement error of 2.8 s is assigned to the longer period and typically emergent diffracted phases (Pdif, Sdif, PKPdif). The *a priori* measurement error for the commonly observed depth phases (pP, sP, pS, sS and pwP) is set to 1.3 s, while the remaining depth phases (pPKP, sPKP, pSKS, sSKS branches and pPb, sPb, sSb, pPn, sPn, sSn) have the measurement error estimate set to 1.8 s. We set the measurement error estimate to 2.5 s for the less reliable depth phases (pPg, sPg, sSg, pPdif, pSdif, sPdif and sSdif). Note that we also allow for distance-dependent measurement errors. For instance, to account for possible phase identification errors at far-regional distances the *a priori* measurement error for Pn and P is increased from 0.8 s to 1.2 s and for Sn and S from 1.5 s to 1.8 s between 15° and 28°. The measurement errors between 40° and 180° are set to 1.3 s and 1.8 s for the prominent PP and SS arrivals respectively, but they are increased to 1.8 s and 2.5 s between 25° and 40°.

The relative weighting scheme (Figure 10.2) described above ensures that arrivals picked less reliably or prone to phase identification errors are down-weighted in the location algorithm. Since the ISC works with reported parametric data with wildly varying quality, we opted for a rather conservative set of *a priori* measurement error estimates.

### Correlated Travel-Time Prediction Error Structure

Most location algorithms, either linearised or non-linear, assume that all observational errors are independent. This assumption is violated when the separation between stations is less than the scale length of local velocity heterogeneities. When correlated travel-time prediction errors are present, the data covariance matrix is no longer diagonal, and the redundancy in the observations reduces the effective number of degrees of freedom. Thus, ignoring the correlated error structure inevitably results in underestimated location uncertainty estimates. For events located by an unbalanced seismic network this may also lead to a biased location estimate. *Chang et al.* (1983) demonstrated that accounting for correlated error structure in a linearised location algorithm is relatively straightforward once an estimate of the non-diagonal data covariance matrix is available. To determine the data covariance matrix we follow the approach described by *Bondár and McLaughlin* (2009b). They assume that the similarity between ray paths is well approximated by the station separation. This simplifying assumption allows for the estimation of covariances between station pairs from a generic P variogram model derived from ground truth residuals. Because the overwhelming number of phases in the ISC Bulletin is teleseismic P, we expect that the generic variogram model will perform reasonably well anywhere on the globe.

Since in this representation the covariances depend only on station separations, the covariance matrix (and its inverse) needs to be calculated only once. We assume that different phases owing to the different ray paths they travel along as well as station pairs with a separation larger than 1000 km are uncorrelated.





Hence, the data covariance matrix is a sparse, block-diagonal matrix. Furthermore, if the stations in each phase block are ordered by their nearest neighbour distance, the phase blocks themselves become block-diagonal. To reduce the computational time of inverting large matrices we exploit the inherent block-diagonal structure by inverting the covariance matrix block-by-block. The *a priori* measurement error variances are added to the diagonal of the data covariance matrix.

## Depth Resolution

In principle, depth can be resolved if there is a mixture of upgoing and downgoing waves emanating from the source, that is, if there are stations covering the distance range where the vertical partial derivative of the travel-time of the first-arriving phase changes sign (local networks), or if there are phases with vertical slowness of opposite sign (depth phases). Core reflections, such as PcP, and to a lesser extent, secondary phases (S in particular) could also help in resolving the depth.

We developed a number of criteria to test whether the reported data for an event have sufficient depth resolution:

- local network: one or more stations within  $0.2^\circ$  with time-defining phases
- depth phases: five or more time-defining depth phases reported by at least two agencies (to reduce a chance of misinterpretation by a single inexperienced analyst)
- core reflections: five or more time-defining core reflections (PcP, ScS) reported by at least two agencies
- local/near regional S: five or more time-defining S and P pairs within  $3^\circ$

We attempt a free-depth solution if any of the above criteria are satisfied; otherwise we fix the depth to a default depth dependent on the epicentre location. This will preferably be the grid depth based on the ISC default depth grid (Figure 10.3). Where no grid depth is available the default depth is set to either 10 km or 35 km based on the GRN (See Figure 10.4. A list of GRN's can be found in Section 10.2.2). The default depth grid was derived from the EHB (*Engdahl et al., 1998*) free-depth solutions, including the fixed-depth EHB earthquakes that were flagged as having reliable depth estimate (personal communication with Bob Engdahl), as well as from free-depth solutions obtained by the new locator when locating the entire ISC Bulletin data-set. As Figure 10.3 indicates, the default depth grid provides a reasonable depth estimate where seismicity is well established. Note that the depths of known anthropogenic events and landslides are fixed to the surface.

## Depth-Phase Stack

While we use depth phases directly in the location, the depth-phase stacking method (*Murphy and Barker, 2006*) provides an independent means to obtain robust depth estimates. Because the depth obtained from the depth-phase stacking method implicitly depends on the epicentre itself, we perform the depth-phase stack only twice: first, with respect to the initial location in order to obtain a reasonable

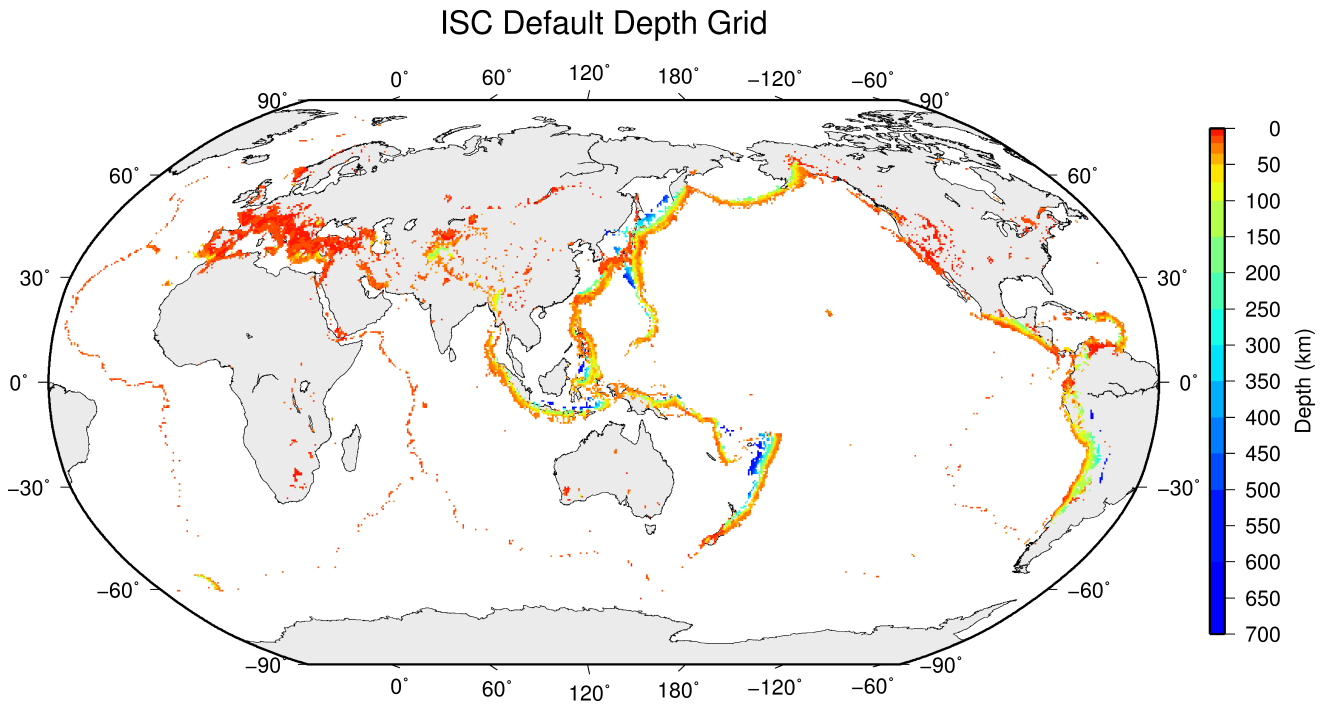


*Figure 10.3: Default depths on a 0.5×0.5 degree grid derived from EHB free-depth solutions and EHB events flagged as reliable depth, as well as free-depth solutions from the entire ISC Bulletin located with the new locator.*

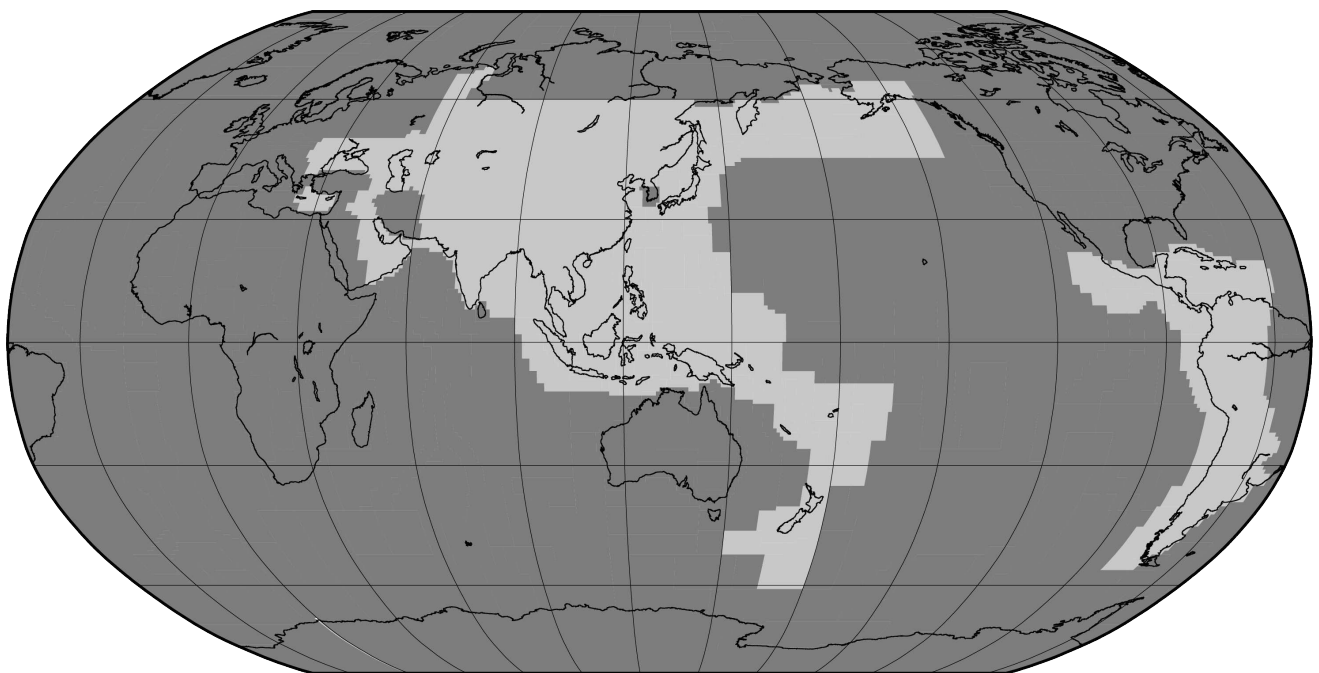


*Figure 10.4: Default depths by Flinn-Engdahl geographic regions. Dark grey regions are set to 10 km and light grey to 35 km*

starting point for the depth in the grid search described in the following section; second, with respect to the final location to obtain the final estimate for the depth-phase constrained depth.

### Initial Hypocentre

For poorly recorded events the reported hypocentres may exhibit a large scatter and they could suffer from large location errors, especially if they are only recorded teleseismically. In order to obtain a good initial hypocentre guess for the linearised location algorithm we employ the Neighbourhood Algorithm (NA) (*Sambridge, 1999; Sambridge and Kennett, 2001*). NA is a nonlinear grid search method capable of exploring a large search space and rapidly closing in on the global optimum. *Kennett (2006)* discusses in detail the NA algorithm and its use for locating earthquakes.

We perform a search around the median of reported hypocentre parameters with a generously defined search region – within a  $2^\circ$  radius circle around the median epicentre, 10 s around the median origin time and 150 km around the median reported depth. These default search parameters were obtained by trial-and-error runs to achieve a compromise between execution time and allowance for gross errors in the median reported hypocentre parameters. Note that if our test for depth resolution fails, we fix the depth to the region-dependent default depth. The initial hypocentre estimate will be the one with the smallest L1-norm misfit among the NA trial hypocentres. Once close to the global optimum, we proceed with the linearised location algorithm to obtain the final solution and corresponding formal uncertainties.

### Iterative Linearised Location Algorithm

We adopt the location algorithm described in detail in *Bondár and McLaughlin (2009b)*. Recall that in the presence of correlated travel-time prediction errors the data covariance matrix is no longer diagonal. Using the singular value decomposition of the data covariance matrix we construct a projection matrix that orthogonalises the data set and projects redundant observations into the null space. In other words, we solve the inversion problem in the eigen coordinate system in which the transformed observations are independent.

The model covariance matrix yields the four-dimensional error ellipsoid whose projections provide the two-dimensional error ellipse and one-dimensional errors for depth and origin time. These uncertainties are scaled to the 90% confidence level. Note that since we projected the system of equations into the eigen coordinate system, the number of independent observations is less than the total number of observations. Hence, the estimated location error ellipses necessarily become larger, providing a more realistic representation of the location uncertainties. The major advantage of this approach is that the projection matrix is calculated only once for each event location.

### Validation Tests

To demonstrate improvements due to the new location procedures, we located some 7,200 GT0-5 events in the IASPEI Reference Event List (*Bondár and McLaughlin, 2009a*) both with the old ISC locator (which constitutes the baseline) and with the new location algorithm. We also located the entire available

(1960-2010) ISC Bulletin, including four years of the International Seismological Summary (ISS, the predecessor of the ISC) catalogue (*Villaseñor and Engdahl, 2005; 2007*).

The location of GT events demonstrated that the new ISC location algorithm provides small but consistent location improvements, considerable improvements in depth determination and significantly more accurate formal uncertainty estimates. Even using a 1-D model and a variogram model that fits teleseismic observations we could achieve realistic uncertainty estimates, as the 90% confidence error ellipses cover the true locations 80-85% of the time. The default depth grid provides reasonable depth estimates where there is seismicity. We have shown that the location and depth accuracy obtained by the new algorithm matches or surpasses the accuracy of the original EHB Bulletin. The EHB Bulletin has since been improved and is replaced by the ISC-EHB Bulletin.

We noted above that the location improvements for the ground truth events are consistent, but minor. This is not surprising as most of the events in the IASPEI Reference Event List are very well-recorded with a small azimuthal gap and dominated by P-type phases. In these circumstances we can expect significant location improvements only for heavily unbalanced networks where large numbers of correlated ray paths conspire to introduce location bias. On the other hand, the ISC Bulletin represents a plethora of station configurations ranging from reasonable to the most unfavourable network geometries. Hence, more dramatic location improvements when locating the ISC Bulletin is expected. Although in this case we cannot measure the improvement in location accuracy due to the lack of ground truth information, we show that with the new locator we obtain significantly better clustering of event locations (Figure 10.5), thus providing an improved view of the seismicity of the Earth.

### **Magnitude Calculation**

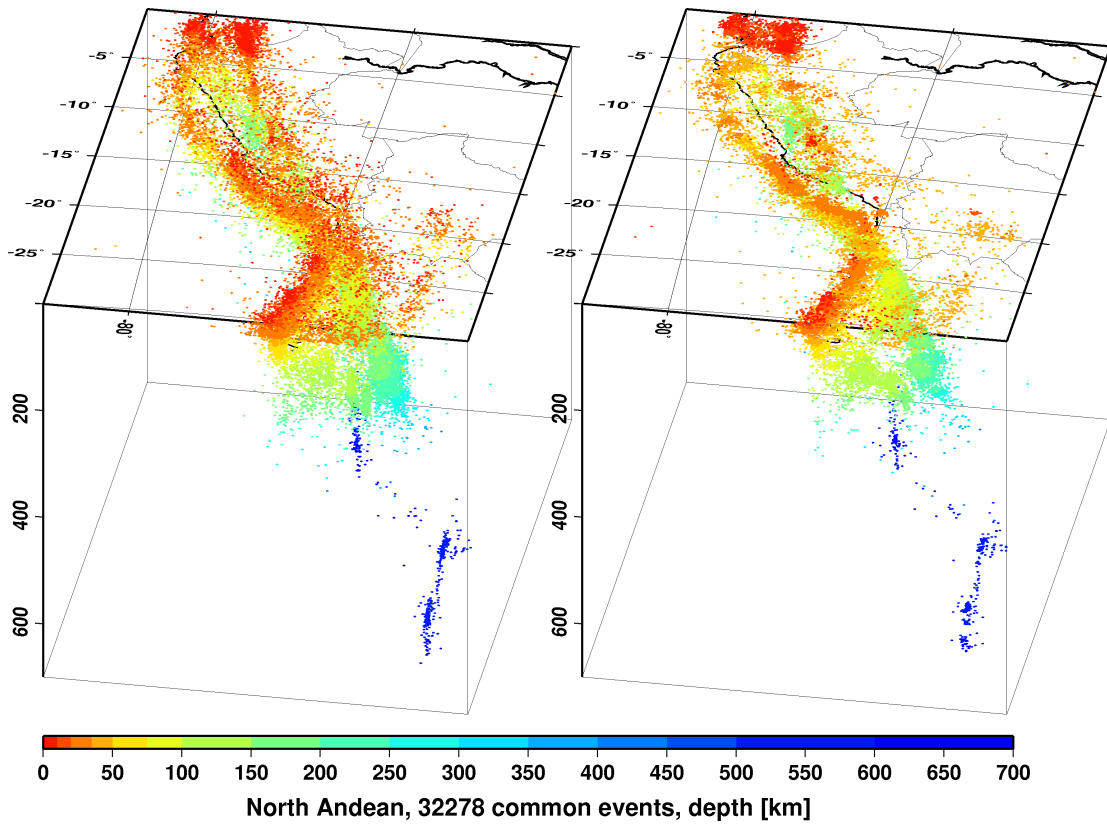
Currently the ISC locator calculates body and surface wave magnitudes.  $MS$  is calculated for shallow events (depth  $< 60$  km) only. At least three station magnitudes are required for a network ( $mb$  or  $MS$ ) magnitude. The network magnitude is defined as the median of the station magnitudes, and its uncertainty is defined as the standard median absolute deviation (SMAD) of the alpha-trimmed ( $\alpha = 20\%$ ) station magnitudes.

The station magnitude is defined as the median of reading magnitudes for a station. The reading magnitude is defined as the magnitude computed from the maximal  $\log(A/T)$  in a reading. Amplitude magnitudes are calculated for each reported amplitude-period pair.

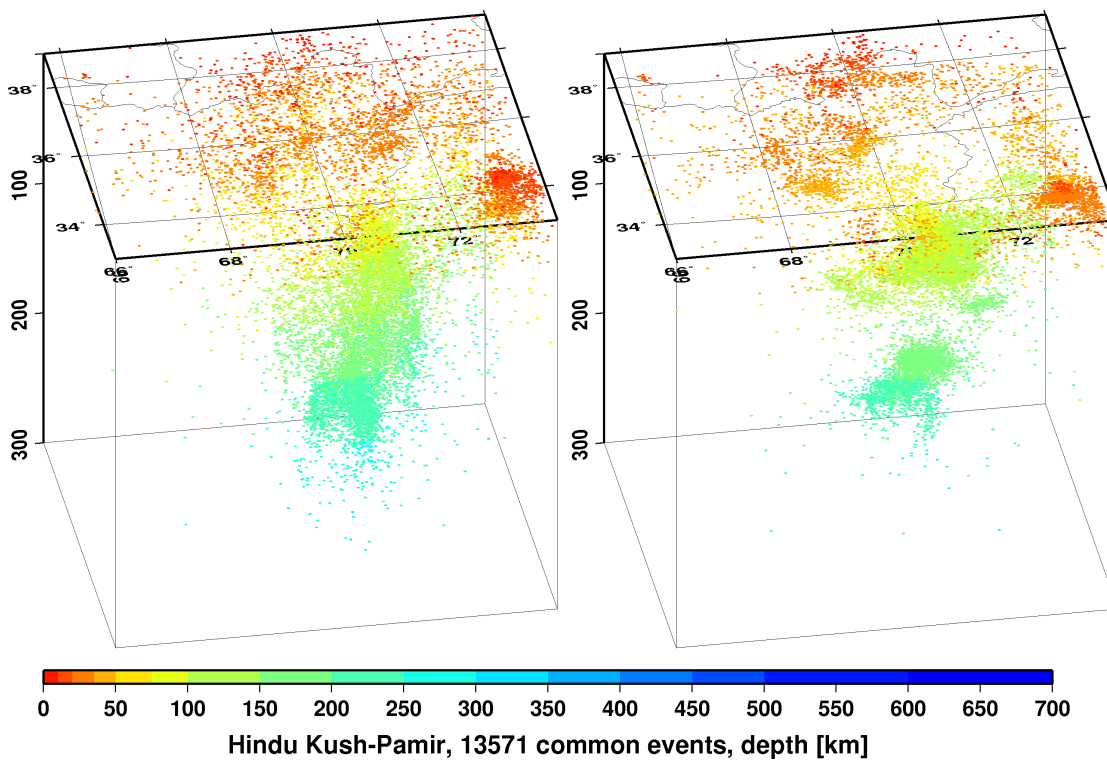
### **Body-Wave Magnitudes**

Body-wave magnitudes are calculated for each reported amplitude-period pair, provided that the phase is in the list of phases that can contribute to  $mb$  (P, pP, sP, AMB, IAmb, pmax), the station is between the epicentral distances  $21 - 100^\circ$  and the period is less than 3 s.

A reading contains all parametric data reported by a single agency for an event at a station, and it may have several reported amplitude and periods. The amplitudes are measured as zero-to-peak values in nanometres. For each pair an amplitude  $mb$  is calculated.



(a)



(b)

**Figure 10.5:** Comparison of seismicity maps for common events in the reviewed ISC Bulletin (old locator, left) and the located ISC Bulletin (new locator, right) for the North Andean (a) and Hindu Kush - Pamir regions (b). The events are better clustered when located with the new locator.

$$mb_{amp} = \log(A/T) + Q(\Delta, h) - 3 \quad (10.1)$$

If no amplitude-period pairs are reported for a reading, the body-wave magnitude is calculated using the reported  $\logat$  values for  $\log(A/T)$ .

$$mb_{amp} = \logat + Q(\Delta, h) - 3 \quad (10.2)$$

where the magnitude attenuation  $Q(\Delta, h)$  value is calculated using the Gutenberg-Richter tables (*Gutenberg and Richter, 1956*).

For each reading the ISC locator finds the reported amplitude-period pair for which  $A/T$  is maximal:

$$mb_{rd} = \log(\max(A/T)) + Q(\Delta, h) - 3 \quad (10.3)$$

Or, if no amplitude-period pairs were reported for the reading:

$$mb_{rd} = \max(\logat) + Q(\Delta, h) - 3 \quad (10.4)$$

Several agencies may report data from the same station. The station magnitude is defined as the median of the reading magnitudes for a station.

$$mb_{sta} = \text{median}(mb_{rd}) \quad (10.5)$$

Once all station  $mb$  values are determined, the station magnitudes are sorted and the lower and upper alpha percentiles are made non-defining. The network  $mb$  and its uncertainty are then calculated as the median and the standard median absolute deviation (SMAD) of the alpha-trimmed station magnitudes, respectively.

### Surface-Wave Magnitudes

Surface-wave magnitudes are calculated for each reported amplitude-period pair, provided that the phase is in the list of phases that can contribute to  $MS$  ( $AMS$ ,  $IAMs\_20$ ,  $LR$ ,  $MLR$ ,  $M$ ,  $L$ ), the station is between the epicentral distances  $20 - 160^\circ$  and the period is between  $10 - 60$  s.

For each reported amplitude-period pair  $MS$  is calculated using the Prague formula (*Vaněk et al., 1962*). Amplitude  $MS$  is calculated for each component (Z, E, N) separately.

$$MS_{amp} = \log(A/T) + 1.66 * \log(\Delta) + 0.3 \quad (10.6)$$

To calculate the reading  $MS$ , the ISC locator first finds the reported amplitude-period pair for which  $A/T$  is maximal on the vertical component.



$$MS_Z = \log(\max(A_Z/T_Z)) + 1.66 * \log(\Delta) + 0.3 \quad (10.7)$$

Then it finds the  $\max(A/T)$  for the E and N components for which the period measured on the horizontal components is within  $\pm 5s$  from the period measured on the vertical component.

$$MS_E = \log(\max(A_E/T_E)) + 1.66 * \log(\Delta) + 0.3 \quad (10.8)$$

$$MS_N = \log(\max(A_N/T_N)) + 1.66 * \log(\Delta) + 0.3 \quad (10.9)$$

The horizontal  $MS$  is calculated as

$$\max(A/T)_h = \begin{cases} \sqrt{2(\max(A_E/T_E))^2} & \text{if } MS_N \text{ does not exist} \\ \sqrt{(\max(A_E/T_E))^2 + (\max(A_N/T_N))^2} & \text{if } MS_E \text{ and } MS_N \text{ exist} \\ \sqrt{2(\max(A_N/T_N))^2} & \text{if } MS_E \text{ does not exist} \end{cases} \quad (10.10)$$

$$MS_H = \log(\max(A/T)_H) + 1.66 * \log(\Delta) + 0.3 \quad (10.11)$$

The reading  $MS$  is defined as

$$MS = \begin{cases} (MS_Z + MS_H)/2 & \text{if } MS_Z \text{ and } MS_H \text{ exist} \\ MS_H & \text{if } MS_Z \text{ does not exist} \\ MS_Z & \text{if } MS_H \text{ does not exist} \end{cases} \quad (10.12)$$

Several agencies may report data from the same station. The station magnitude is defined as the median of the reading magnitudes for a station.

$$MS_{sta} = \text{median}(MS_{rd}) \quad (10.13)$$

Once all station  $MS$  values are determined, the station magnitudes are sorted and the lower and upper alpha percentiles are made non-defining. The network  $MS$  and its uncertainty are calculated as the median and the standard median absolute deviation (SMAD) of the alpha-trimmed station magnitudes, respectively.

### 10.1.5 Review Process

Typically, for each month, the ISC analysts now review approximately 10-20% of the events in the ISC database, currently 3,500-5,000 per data month. This review is done about 24 months behind real time to allow for the comprehensive collection of data from networks and data centres worldwide.

Users of the ISC Bulletin can be assured that all ISC Bulletin events with an ISC hypocentre solution have been reviewed by the ISC analysts. Not all reviewed events will end up having an ISC hypocentre solution, but events that have not been reviewed are flagged accordingly.

At the beginning of analysis of each data month, events that need to be reviewed by an analyst are flagged based on the thresholding procedure described in Section 10.1.3. These events are split into daily blocks on average consisting of 100 – 150 events. They are then analysed and if necessary edited by an analyst. After all blocks in a data month have been reviewed, they are being assessed again by a different analyst to spot any potential inconsistencies that might have been overlooked in the first run.

Analysis is done with the help of the Visual Bulletin Analysis System (VBAS) developed at the ISC. For each event it shows the reported hypocentres, magnitudes and phase arrivals as well as an ISC solution for the hypocentre, if there is one, along with phase arrival-time residuals and error estimates. Amongst other visual aids, VBAS plots graphs of travel time curves, seismicity maps, depth distributions of reported hypocentres and station geometry.

The analysts have the capability to execute a variety of commands that can be used to merge or split events, to move phase arrivals or hypocentres from one event to another or to modify the reported phase names. There are also several commands to change the starting depth or location in the location algorithm.

The main tasks in reviewing the ISC Bulletin are to:

1. Check that the grouping of hypocentres and association of phase arrivals is appropriate.
2. Check that the depth and location is appropriate for the region and reported phase arrivals.
3. Check that no data are missing for an event, given the region and magnitude, and that included data are appropriate.
4. Examine the phase arrival-time residuals to check that the ISC hypocentre solution is appropriate.
5. Look for outliers in the observations and for misassociated phases.
6. Check that the station azimuthal coverage for ISC hypocentres is at least 45 deg.

As well as examining each event closely, it is also important to scan the hypocentres and phase arrivals of adjacent events, close in time and space, to ensure that there is uniformity in the composition of the events. In some cases, two events should be merged into one event, as apparent in some other case. In other cases, one apparent event needs to be split into two events, when the automatic grouping has erroneously created one event with more than one reported hypocentre out of the observations for two real events that are distinct but closely occurring.

Misassociated phase arrivals are returned to the unassociated data stream, if not immediately placed by the analyst in another event where they belong. These unassociated phases are then available to be associated with some other event if the time and location is appropriate. The analysts also check that no phase is associated to more than one event.

Towards the end of the monthly analysis, the ISC ‘Search’ procedure runs, attempting to build events from the remaining set of unassociated phase arrivals. The algorithm is based on the methodology of *Engdahl and Gunst* (1966). Candidate events are validated or rejected by attempting to find ISC hypocentres for them using the ISC locator. The surviving events are then reviewed. Those events

with phase arrival observations reported by stations from at least two networks are added to the ISC Bulletin if the solutions meet the standards set by the ISC analysts. These events have only an ISC determination of hypocentre.

At the end of analysis for a data month, a set of final checks is run for quality control, with the results reviewed by an analyst and the defects rectified. These are checks for inconsistencies and errors to ensure the general integrity of the ISC Bulletin.

### 10.1.6 Probabilistic Point Source Model (ISC-PPSM)

From data month January 2019 we have begun routinely calculating the earthquake moment tensor, source time function (STF) and depth for moderate magnitude ( $M_W$  5.8 – 7.2) earthquakes. The resulting catalogue is referred to as ISC-PPSM (International Seismological Centre - Probabilistic Point Source Model). This point source calculation is performed using a Bayesian inversion technique based on the methods proposed by *Stähler and Sigloch* (2014; 2016). There are three main purposes of the ISC-PPSM catalogue:

1. Quantifying the uncertainties in the earthquake moment tensor.
2. Providing new constraints on the earthquake STF, along with full error estimation.
3. Adding new depth resolution, especially for relatively shallow ( $< 40$  km depth) moderate magnitude earthquakes, where surface reflected depth phases are subsumed into the earthquake STF.

The first purpose is motivated by the range of moment tensor solutions that can be reported by different agencies or methods for the same earthquake (e.g., *Lentas et al.* (2019)). It is clear that given the variability in the data and methods these different earthquake mechanisms may not be reconciled in all cases. Instead, we aim to quantify the full range of plausible earthquake mechanisms for a given event.

The second role of the ISC-PPSM catalogue is to provide new parameterised estimates of the earthquake STF. By parameterising the STF, we allow the range of plausible STFs to be assessed, but also reduce the sensitivity to near source reverberations (such as water depth phases). It is hoped that this will provide a new resource for full waveform tomographic studies, as well as earthquake physics studies.

Thirdly, and of most significance to the wider ISC operations, ISC-PPSM offers new depth resolution for remote shallow moderate magnitude earthquakes, where the depth of an ISC hypocentre would otherwise be fixed to a default or grid depth (e.g., Section 10.1.4 and *Bondár and Storchak* (2011)). As ISC-PPSM solves for both the earthquake depth and STF, the tradeoffs between depth and STF length are directly addressed. In cases where no free depth solution is possible, the ISC-PPSM depth can be fixed to by an analyst during the review process.

To allow the ISC-PPSM depth to be used in the main ISC review process, we calculate preliminary ISC-PPSM results ahead of the review process. For the preliminary ISC-PPSM result, the earthquake latitude and longitude are fixed to the USGS-PDE epicenter. After the main ISC review process, we recalculate the ISC-PPSM solution at the location of the reviewed ISC epicenter. After checking that the revised ISC-PPSM depths are consistent with any earthquake depths that were fixed to preliminary

ISC-PPSM, we publish the revised ISC-PPSM solution. If the depths are not consistent to within 1 km, we relocate the ISC hypocentre at the revised ISC-PPSM depth.

### 10.1.7 The use of Network code for Arrivals at the ISC and in ISCLoc

The ISC has implemented the use of the IASPEI station coding standard ADSL (Agency Deployment Station Location) from data year 2021.

This allows the use of many additional stations and complements the increasing usage of reporting formats, such as QuakeML, where more extensive station information is a requirement. As of 2024, 27 agencies report data to the ISC, in a format that includes a network code (this is the equivalent of deployment in ADSL standard). Currently we use stations that are included in the FDSN registry, <https://www.fdsn.org/>, in addition to the International Station Registry (IR) which is hosted by the ISC, both are the equivalent of Agency in ADSL. Any agencies established in the future will be able to fit within this framework as required. To ensure users can utilise all station information contained within the ISC Bulletin, station coordinates and agency/network codes are included in ISF 2.1. It also allows for greater attribution of the data reported in the ISC Bulletin.

Figure 10.6 shows the location of FDSN registered stations (1848) that are not in or very near to an IR registered station that the ISC has arrivals for 2021. These are counted in a similar way to the IR, that is, the new stations are positions that are at least 2 km from any other station. The number would be much higher if multiple networks and channels were included in the count.

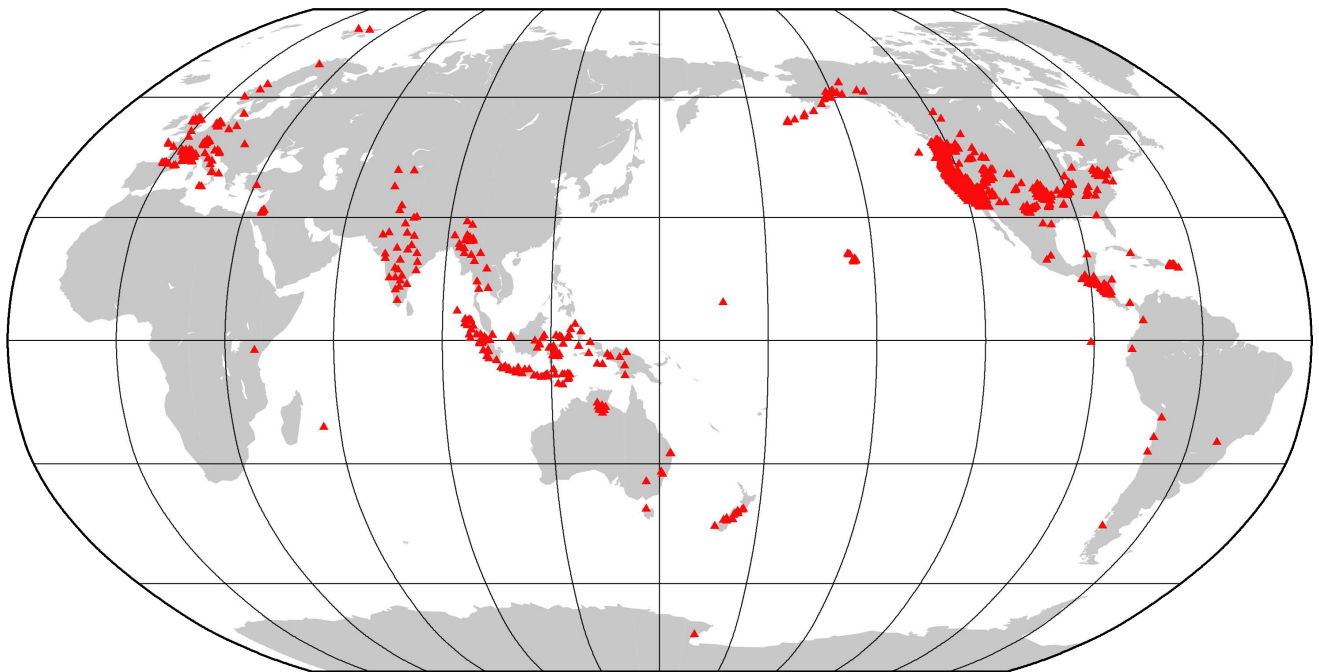


*Figure 10.6: Non-IR registered stations in the ISC Bulletin 2021*

Figure 10.7 shows a step change in secondary azimuthal gaps of the ISC hypocentres from 2021 onwards, this improvement is a direct result of the switch to ADSL.

All the programs used by the ISC, the locator ISCLoc, database and public search tools have all had to be changed to deal with network codes. A new public version of the locator will be released in 2025.

## ISC Hypocentre Median Secondary Gaps

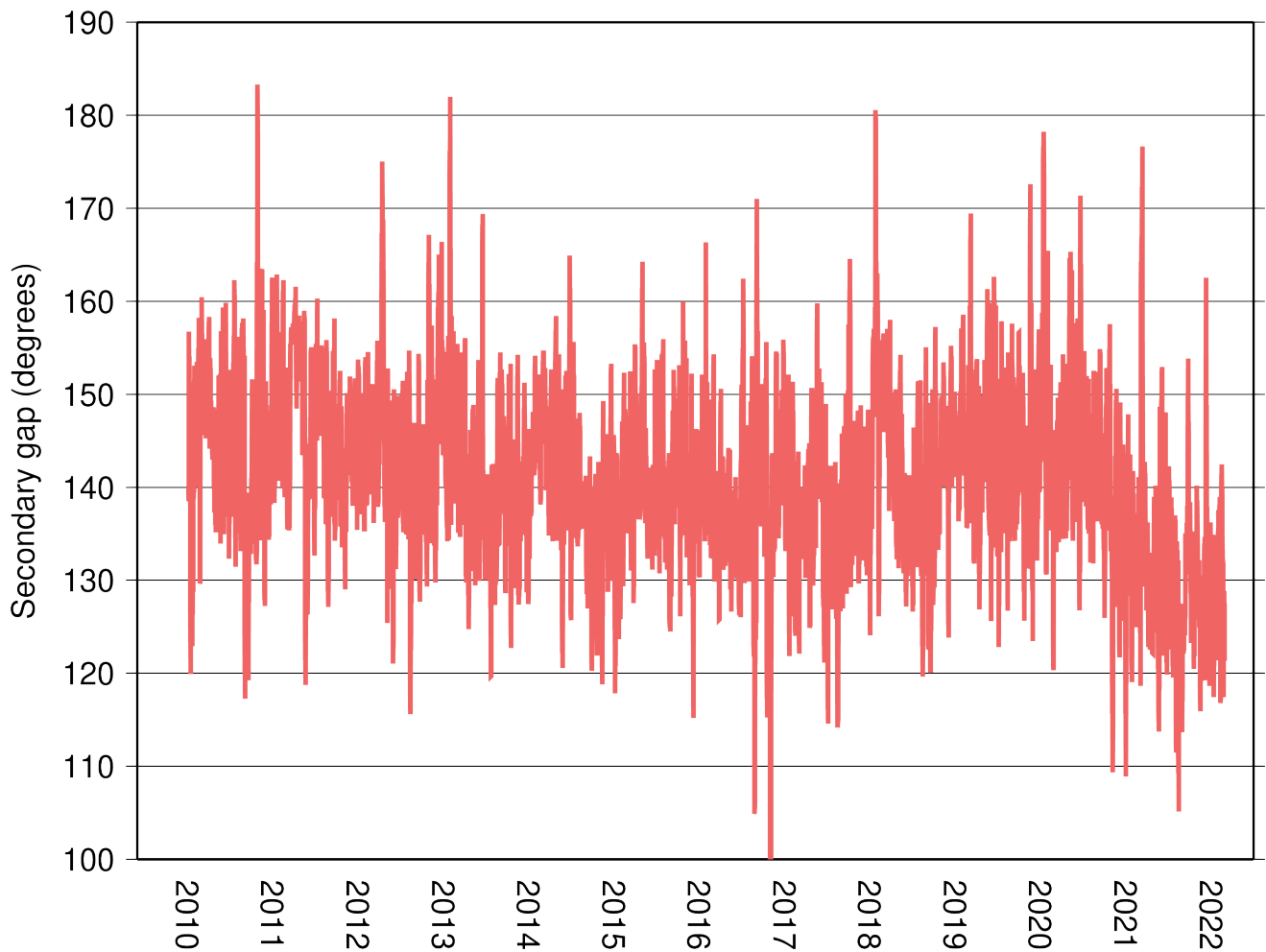


*Figure 10.7: Secondary gap of ISC hypocentres*

Details of all stations used in the ISC Bulletin can be found here <https://www.isc.ac.uk/stations/>.

### 10.1.8 History of Operational Changes

The following operational changes are listed here for historical archiving purpose. Some of them have effectively become irrelevant as a result of further changes.

- From data-month January 2001 onwards, both P and S groups of arrival times are used in location.
- From data-month September 2002 onwards, the printed ISC Bulletins have been generated directly from the ISC Relational Database.
- From data-month October 2002, a new location program ISCloc has been used in operations. Also, the IASPEI standard phase list has now been adopted by the ISC. Please see Section 10.2.1 for details.
- From data-month January 2003 onwards, an updated regionalisation scheme has been adopted (*Young et al.*, 1996).

- From data-month January 2006 the ISC hypocentres are computed using the *ak135* earth velocity model (*Kennett et al.*, 1995) and then reviewed by ISC seismologists. The ISC still produces the hypocentre solutions based on Jeffreys-Bullen travel time tables (agency code ISCJB), yet these solutions are no longer reviewed.

Currently, the ISC is re-computing the entire ISC Bulletin as part of the Rebuild Project using *ak135* and the new location program (Section 10.1.4) in order to assure homogeneity and consistency of the data in the ISC Bulletin.

- From data-month January 2009, a new location program (*Bondár and Storchak*, 2011) has been used in operations. The new program uses all predicted *ak135* phases and accounts for correlated model errors. An overview of the location algorithm is provided in this volume (Section 10.1.4).
- As of February 2020, the ISC Bulletin for the period 1964-2010 has been completely rebuilt (*Storchak et al.*, 2017; 2020): all ISC hypocentres and magnitude have been recalculated using the algorithm by *Bondár and Storchak* (2011); many new previously unavailable datasets added based on extensive international correspondence with networks, data centres, temporary deployment managers and individual researchers; the Bulletin has been cleaned from phantom and poorly constrained events; many station readings have been added or corrected.
- From data-month January 2021 the ISC Bulletin will be using data from stations with network codes.

## 10.2 IASPEI Standards

### 10.2.1 Standard Nomenclature of Seismic Phases

The following list of seismic phases was approved by the IASPEI Commission on Seismological Observation and Interpretation (CoSOI) and adopted by IASPEI on 9th July 2003. More details can be found in *Storchak et al.* (2003) and *Storchak et al.* (2011). Ray paths for some of these phases are shown in Figures 10.8–10.13.

#### Crustal Phases

Pg	At short distances, either an upgoing P wave from a source in the upper crust or a P wave bottoming in the upper crust. At larger distances also, arrivals caused by multiple P-wave reverberations inside the whole crust with a group velocity around 5.8 km/s.
Pb	Either an upgoing P wave from a source in the lower crust or a P wave bottoming in the lower crust (alt: P*)
Pn	Any P wave bottoming in the uppermost mantle or an upgoing P wave from a source in the uppermost mantle
PnPn	Pn free-surface reflection
PgPg	Pg free-surface reflection
PmP	P reflection from the outer side of the Moho
PmPN	PmP multiple free surface reflection; <i>N</i> is a positive integer. For example, PmP2 is PmPPmP.
PmS	P to S reflection/conversion from the outer side of the Moho

Sg	At short distances, either an upgoing S wave from a source in the upper crust or an S wave bottoming in the upper crust. At larger distances also, arrivals caused by superposition of multiple S-wave reverberations and SV to P and/or P to SV conversions inside the whole crust.
Sb	Either an upgoing S wave from a source in the lower crust or an S wave bottoming in the lower crust (alt: S*)
Sn	Any S wave bottoming in the uppermost mantle or an upgoing S wave from a source in the uppermost mantle
SnSn	Sn free-surface reflection
SgSg	Sg free-surface reflection
SmS	S reflection from the outer side of the Moho
SmSN	SmS multiple free-surface reflection; $N$ is a positive integer. For example, SmS2 is SmSSmS.
SmP	S to P reflection/conversion from the outer side of the Moho
Lg	A wave group observed at larger regional distances and caused by superposition of multiple S-wave reverberations and SV to P and/or P to SV conversions inside the whole crust. The maximum energy travels with a group velocity of approximately 3.5 km/s
Rg	Short-period crustal Rayleigh wave

**Mantle Phases**

P	A longitudinal wave, bottoming below the uppermost mantle; also an upgoing longitudinal wave from a source below the uppermost mantle
PP	Free-surface reflection of P wave leaving a source downward
PS	P, leaving a source downward, reflected as an S at the free surface. At shorter distances the first leg is represented by a crustal P wave.
PPP	Analogous to PP
PPS	PP which is converted to S at the second reflection point on the free surface; travel time matches that of PSP
PSS	PS reflected at the free surface
PcP	P reflection from the core-mantle boundary (CMB)
PcS	P converted to S when reflected from the CMB
PcPN	PcP reflected from the free surface $N - 1$ times; $N$ is a positive integer. For example PcP2 is PcPPcP.
Pz+P	(alt: PzP) P reflection from outer side of a discontinuity at depth $z$ ; $z$ may be a positive numerical value in km. For example, P660+P is a P reflection from the top of the 660 km discontinuity.
Pz-P	P reflection from inner side of a discontinuity at depth $z$ . For example, P660-P is a P reflection from below the 660 km discontinuity, which means it is precursory to PP.
Pz+S	(alt:PzS) P converted to S when reflected from outer side of discontinuity at depth $z$
Pz-S	P converted to S when reflected from inner side of discontinuity at depth $z$
PScS	P (leaving a source downward) to ScS reflection at the free surface
Pdif	P diffracted along the CMB in the mantle (old: Pdiff)
S	Shear wave, bottoming below the uppermost mantle; also an upgoing shear wave from a source below the uppermost mantle
SS	Free-surface reflection of an S wave leaving a source downward
SP	S, leaving a source downward, reflected as P at the free surface. At shorter distances the second leg is represented by a crustal P wave.
SSS	Analogous to SS
SSP	SS converted to P when reflected from the free surface; travel time matches that of SPS
SPP	SP reflected at the free surface
ScS	S reflection from the CMB
ScP	S converted to P when reflected from the CMB
ScSN	ScS multiple free-surface reflection; $N$ is a positive integer. For example ScS2 is ScSScS.



Sz+S	S reflection from outer side of a discontinuity at depth $z$ ; $z$ may be a positive numerical value in km. For example S660+S is an S reflection from the top of the 660 km discontinuity. (alt: SzS)
Sz-S	S reflection from inner side of discontinuity at depth $z$ . For example, S660-S is an S reflection from below the 660 km discontinuity, which means it is precursory to SS.
Sz+P	(alt: SzP) S converted to P when reflected from outer side of discontinuity at depth $z$
Sz-P	S converted to P when reflected from inner side of discontinuity at depth $z$
ScSP	ScS to P reflection at the free surface
Sdif	S diffracted along the CMB in the mantle (old: Sdiff)

**Core Phases**

PKP	Unspecified P wave bottoming in the core (alt: P')
PKPab	P wave bottoming in the upper outer core; ab indicates the retrograde branch of the PKP caustic (old: PKP2)
PKPbc	P wave bottoming in the lower outer core; bc indicates the prograde branch of the PKP caustic (old: PKP1)
PKPdf	P wave bottoming in the inner core (alt: PKIKP)
PKPpre	A precursor to PKPdf due to scattering near or at the CMB (old: PKhKP)
PKPdif	P wave diffracted at the inner core boundary (ICB) in the outer core
PKS	Unspecified P wave bottoming in the core and converting to S at the CMB
PKSab	PKS bottoming in the upper outer core
PKSbc	PKS bottoming in the lower outer core
PKSdf	PKS bottoming in the inner core
P'P'	Free-surface reflection of PKP (alt: PKPPKP)
P'N	PKP reflected at the free surface $N - 1$ times; $N$ is a positive integer. For example, P'3 is P'P'P'. (alt: PKPN)
P' <sub>z</sub> -P'	PKP reflected from inner side of a discontinuity at depth $z$ outside the core, which means it is precursory to P'P'; $z$ may be a positive numerical value in km
P'S'	(alt: PKPSKS) PKP converted to SKS when reflected from the free surface; other examples are P'PKS, P'SKP
PS'	P (leaving a source downward) to SKS reflection at the free surface (alt: PSKS)
PKKP	Unspecified P wave reflected once from the inner side of the CMB
PKKPab	PKKP bottoming in the upper outer core
PKKPbc	PKKP bottoming in the lower outer core
PKKPdf	PKKP bottoming in the inner core
PNKP	P wave reflected $N - 1$ times from inner side of the CMB; $N$ is a positive integer.
PKKPpre	A precursor to PKKP due to scattering near the CMB
PKiKP	P wave reflected from the inner core boundary (ICB)
PKNIKP	P wave reflected $N - 1$ times from the inner side of the ICB
PKJKP	P wave traversing the outer core as P and the inner core as S
PKKS	P wave reflected once from inner side of the CMB and converted to S at the CMB
PKKSab	PKKS bottoming in the upper outer core
PKKSbc	PKKS bottoming in the lower outer core
PKKSdf	PKKS bottoming in the inner core
PcPP'	PcP to PKP reflection at the free surface; other examples are PcPS', PcSP', PcSS', PcPSKP, PcSSKP. (alt: PcPPKP)
SKS	unspecified S wave traversing the core as P (alt: S')
SKSac	SKS bottoming in the outer core
SKSdf	SKS bottoming in the inner core (alt: SKIKS)
SPdifKS	SKS wave with a segment of mantle side Pdif at the source and/or the receiver side of the ray path (alt: SKPdifS)
SKP	Unspecified S wave traversing the core and then the mantle as P
SKPab	SKP bottoming in the upper outer core
SKPbc	SKP bottoming in the lower outer core
SKPdf	SKP bottoming in the inner core
S'S'	Free-surface reflection of SKS (alt: SKSSKS)
S'N	SKS reflected at the free surface $N - 1$ times; $N$ is a positive integer
S' <sub>z</sub> -S'	SKS reflected from inner side of discontinuity at depth $z$ outside the core, which means it is precursory to S'S'; $z$ may be a positive numerical value in km.
S'P'	(alt: SKSPKP) SKS converted to PKP when reflected from the free surface; other examples are S'SKP, S'PKS.
S'P	(alt: SKSP) SKS to P reflection at the free surface
SKKS	Unspecified S wave reflected once from inner side of the CMB
SKKSac	SKKS bottoming in the outer core
SKKSdf	SKKS bottoming in the inner core
SNKS	S wave reflected $N - 1$ times from inner side of the CMB; $N$ is a positive integer.

SKiKS	S wave traversing the outer core as P and reflected from the ICB
SKJKS	S wave traversing the outer core as P and the inner core as S
SKKP	S wave traversing the core as P with one reflection from the inner side of the CMB and then continuing as P in the mantle
SKKPab	SKKP bottoming in the upper outer core
SKKPbc	SKKP bottoming in the lower outer core
SKKPdf	SKKP bottoming in the inner core
ScSS'	ScS to SKS reflection at the free surface; other examples are ScPS', ScSP', ScPP', ScSSKP, ScPSKP. (alt: ScSSKS)

**Near-source Surface reflections (Depth Phases)**

pPy	All P-type onsets (Py), as defined above, which resulted from reflection of an upgoing P wave at the free surface or an ocean bottom. <b>WARNING:</b> The character <i>y</i> is only a wild card for any seismic phase, which could be generated at the free surface. Examples are pP, pPKP, pPP, pPcP, etc.
sPy	All Py resulting from reflection of an upgoing S wave at the free surface or an ocean bottom; for example, sP, sPKP, sPP, sPcP, etc.
pSy	All S-type onsets (Sy), as defined above, which resulted from reflection of an upgoing P wave at the free surface or an ocean bottom; for example, pS, pSKS, pSS, pScP, etc.
sSy	All Sy resulting from reflection of an upgoing S wave at the free surface or an ocean bottom; for example, sSn, sSS, sScS, sSdif, etc.
pwPy	All Py resulting from reflection of an upgoing P wave at the ocean's free surface
pmPy	All Py resulting from reflection of an upgoing P wave from the inner side of the Moho

**Surface Waves**

L	Unspecified long-period surface wave
LQ	Love wave
LR	Rayleigh wave
G	Mantle wave of Love type
GN	Mantle wave of Love type; <i>N</i> is integer and indicates wave packets traveling along the minor arcs (odd numbers) or major arc (even numbers) of the great circle
R	Mantle wave of Rayleigh type
RN	Mantle wave of Rayleigh type; <i>N</i> is integer and indicates wave packets traveling along the minor arcs (odd numbers) or major arc (even numbers) of the great circle
PL	Fundamental leaking mode following P onsets generated by coupling of P energy into the waveguide formed by the crust and upper mantle SPL S wave coupling into the PL waveguide; other examples are SSPL, SSSPL.

**Acoustic Phases**

H	A hydroacoustic wave from a source in the water, which couples in the ground
HPg	H phase converted to Pg at the receiver side
HSg	H phase converted to Sg at the receiver side
HRg	H phase converted to Rg at the receiver side
I	An atmospheric sound arrival which couples in the ground
IPg	I phase converted to Pg at the receiver side
ISg	I phase converted to Sg at the receiver side
IRg	I phase converted to Rg at the receiver side
T	A tertiary wave. This is an acoustic wave from a source in the solid earth, usually trapped in a low-velocity oceanic water layer called the SOFAR channel (SOund Fixing And Ranging).
TPg	T phase converted to Pg at the receiver side
TSg	T phase converted to Sg at the receiver side
TRg	T phase converted to Rg at the receiver side

### Amplitude Measurement Phases

The following set of amplitude measurement names refers to the IASPEI Magnitude Standard (see [http://www.iaspei.org/commissions/commission-on-seismological-observation-and-interpretation/Summary\\_WG\\_recommendations\\_20130327.pdf](http://www.iaspei.org/commissions/commission-on-seismological-observation-and-interpretation/Summary_WG_recommendations_20130327.pdf)), compliance to which is indicated by the presence of leading letter I. The absence of leading letter I indicates that a measurement is non-standard. Letter A indicates a measurement in *nm* made on a displacement seismogram, whereas letter V indicates a measurement in *nm/s* made on a velocity seismogram.

IAML	Displacement amplitude measured according to the IASPEI standard for local magnitude <i>ML</i>
IAMs_20	Displacement amplitude measured according to IASPEI standard for surface-wave magnitude <i>MS(20)</i>
IVMs_BB	Velocity amplitude measured according to IASPEI standard for broadband surface-wave magnitude <i>MS(BB)</i>
IAmb	Displacement amplitude measured according to IASPEI standard for short-period teleseismic body-wave magnitude <i>mb</i>
IVmB_BB	Velocity amplitude measured according to IASPEI standard for broadband teleseismic body-wave magnitude <i>mB(BB)</i>
AX_IN	Displacement amplitude of phase of type <i>X</i> (e.g., PP, S, etc), measured on an instrument of type IN (e.g., SP - short-period, LP - long-period, BB - broadband)
VX_IN	Velocity amplitude of phase of type <i>X</i> and instrument of type IN (as above)
A	Unspecified displacement amplitude measurement
V	Unspecified velocity amplitude measurement
AML	Displacement amplitude measurement for nonstandard local magnitude
AMs	Displacement amplitude measurement for nonstandard surface-wave magnitude
Amb	Displacement amplitude measurement for nonstandard short-period body-wave magnitude
AmB	Displacement amplitude measurement for nonstandard medium to long-period body-wave magnitude
END	Time of visible end of record for duration magnitude

### Unidentified Arrivals

x	unidentified arrival (old: i, e, NULL)
rx	unidentified regional arrival (old: i, e, NULL)
tx	unidentified teleseismic arrival (old: i, e, NULL)
Px	unidentified arrival of P type (old: i, e, NULL, (P), P?)
Sx	unidentified arrival of S type (old: i, e, NULL, (S), S?)

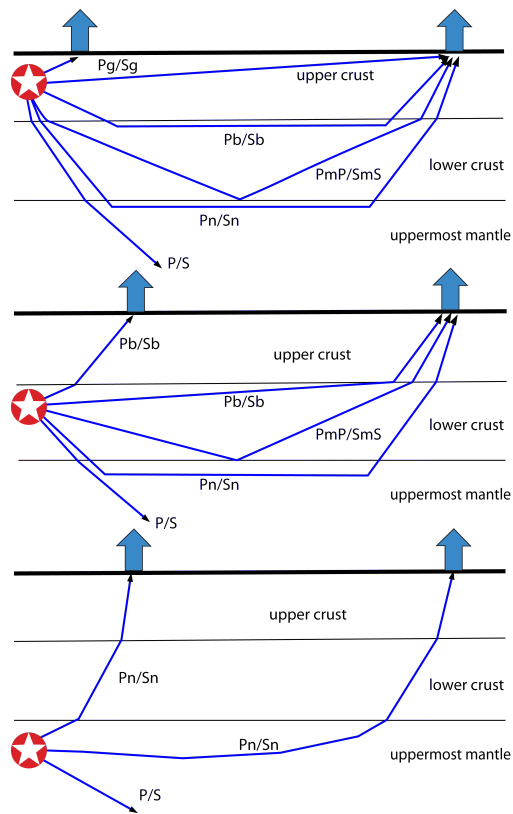


**Figure 10.8:** Seismic ‘crustal phases’ observed in the case of a two-layer crust in local and regional distance ranges ( $0^\circ < D < \text{about } 20^\circ$ ) from the seismic source in the: upper crust (top); lower crust (middle); and uppermost mantle (bottom).

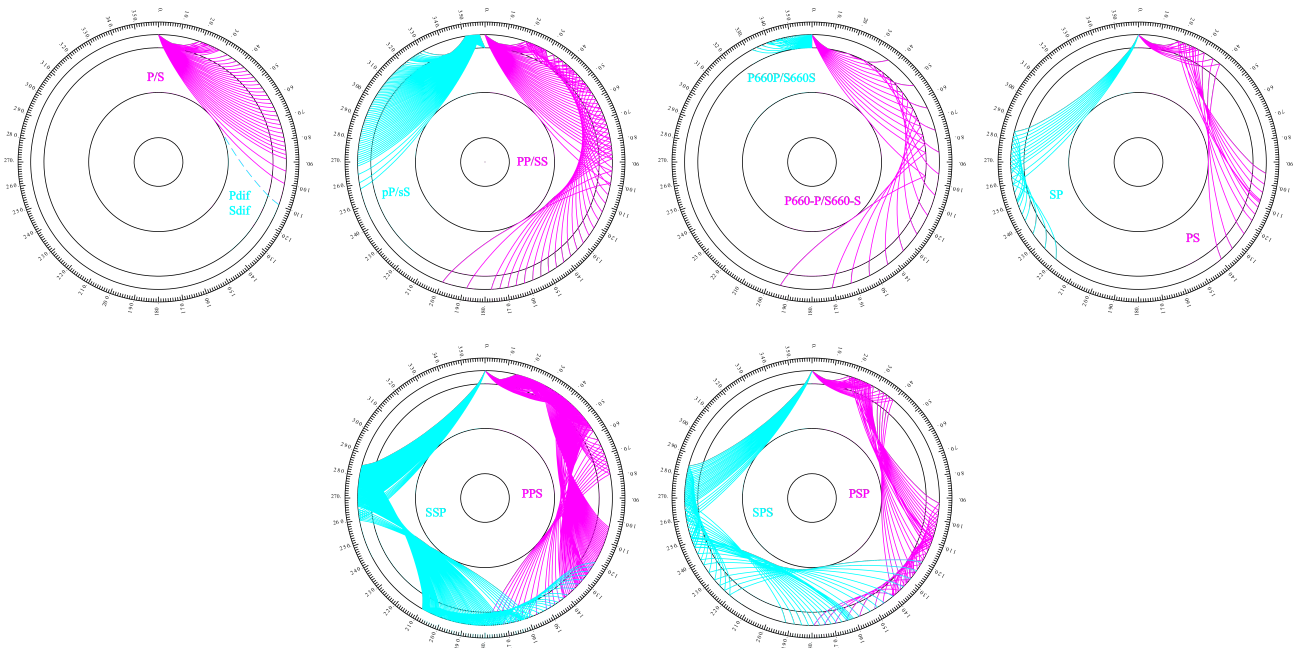


**Figure 10.9:** Mantle phases observed at the teleseismic distance range  $D > \text{about } 20^\circ$ .

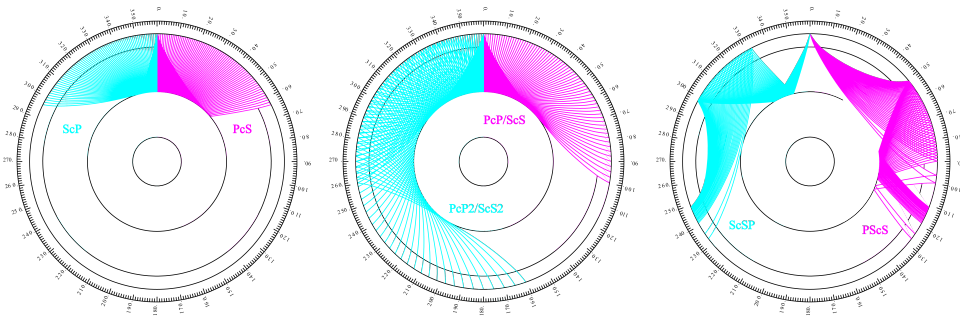


*Figure 10.10: Reflections from the Earth's core.*

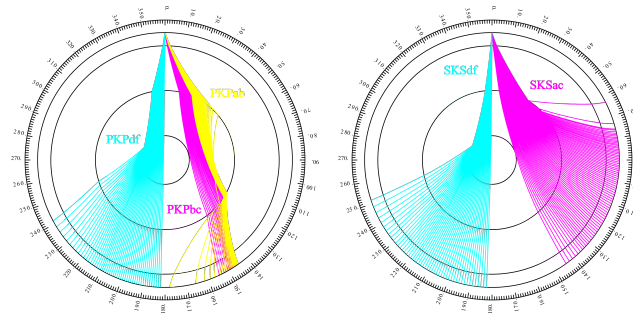


*Figure 10.11: Seismic rays of direct core phases.*

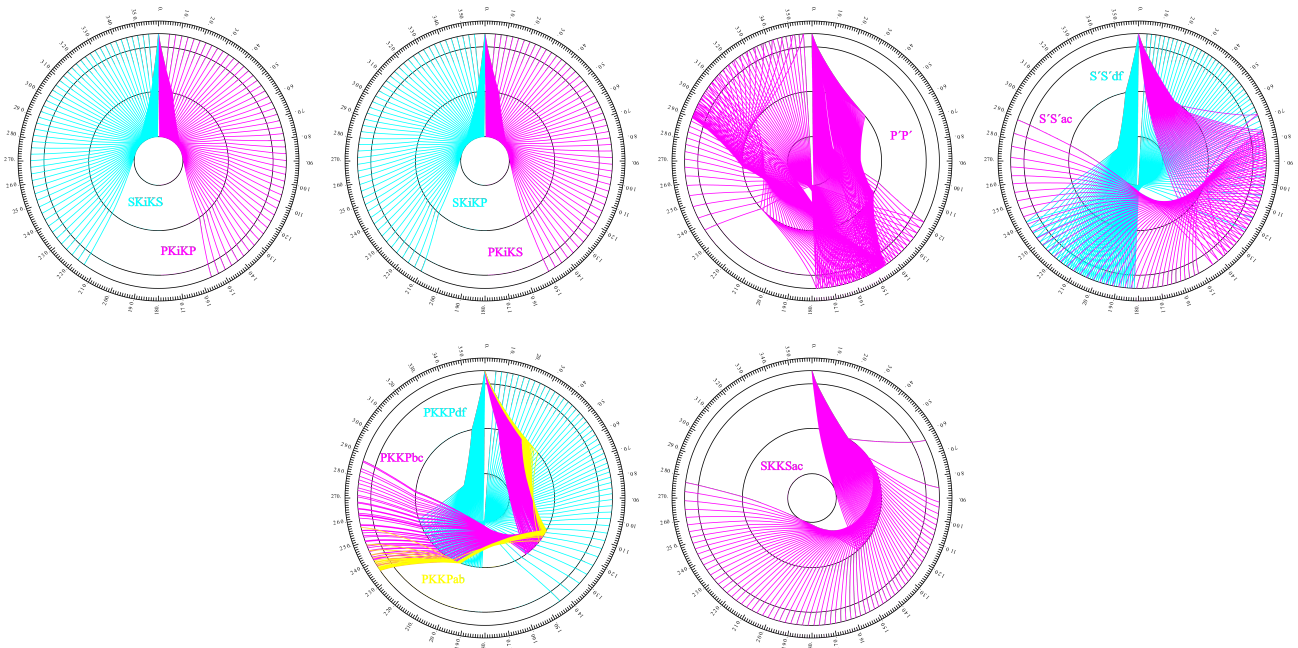


*Figure 10.12: Seismic rays of single-reflected core phases.*

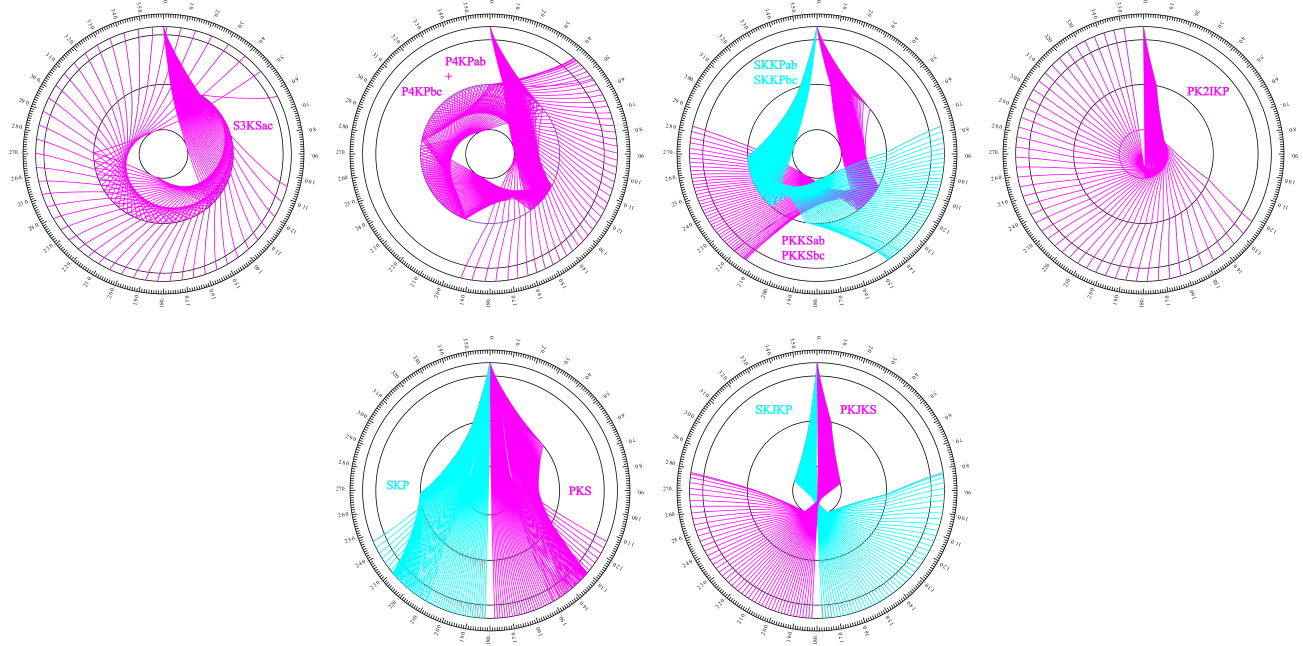


Figure 10.13: Seismic rays of multiple-reflected and converted core phases.

### 10.2.2 Flinn-Engdahl Regions

The Flinn-Engdahl regions were first proposed by *Flinn and Engdahl* (1965), with the standard defined by *Flinn et al.* (1974). The latest version of the schema, published by *Young et al.* (1996), divides the Earth into 50 seismic regions (Figure 10.14), which are further subdivided producing a total of 754 geographical regions (listed below). The geographic regions are numbered 1 to 757 with regions 172, 299 and 550 no longer in use. The boundaries of these regions are defined at one-degree intervals.

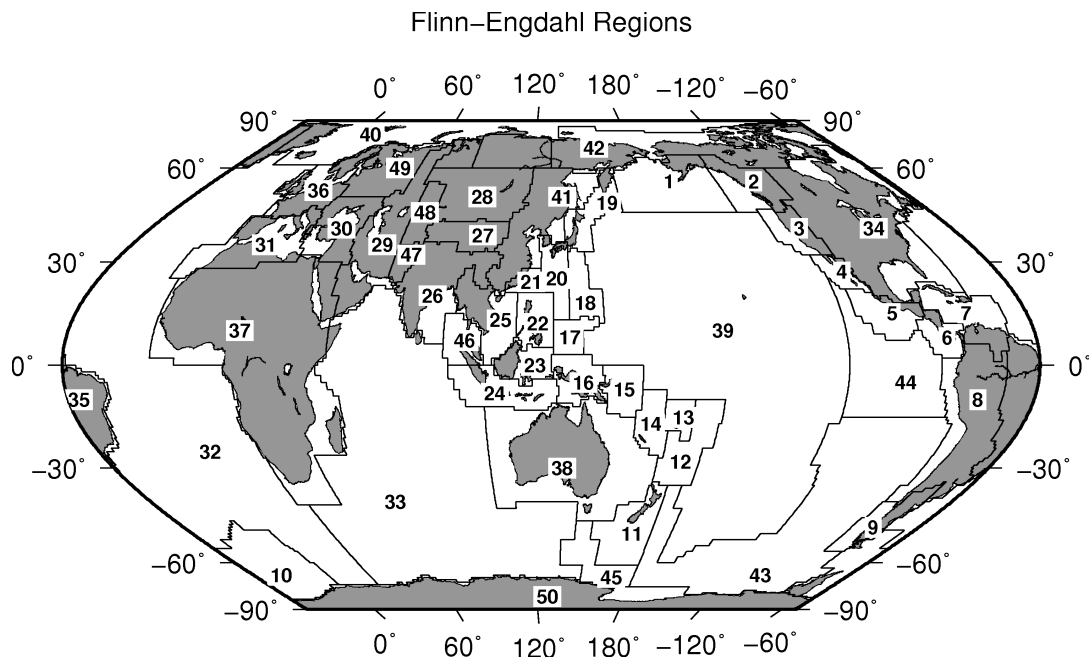


Figure 10.14: Map of all Flinn-Engdahl seismic regions.



**Seismic Region 1**

**Alaska-Aleutian Arc**

1. Central Alaska
2. Southern Alaska
3. Bering Sea
4. Komandorsky Islands region
5. Near Islands
6. Rat Islands
7. Andreanof Islands
8. Pribilof Islands
9. Fox Islands
10. Unimak Island region
11. Bristol Bay
12. Alaska Peninsula
13. Kodiak Island region
14. Kenai Peninsula
15. Gulf of Alaska
16. South of Aleutian Islands
17. South of Alaska

**Seismic Region 2**

**Eastern Alaska to Vancouver Island**

18. Southern Yukon Territory
19. Southeastern Alaska
20. Off coast of southeastern Alaska
21. West of Vancouver Island
22. Queen Charlotte Islands region
23. British Columbia
24. Alberta
25. Vancouver Island region
26. Off coast of Washington
27. Near coast of Washington
28. Washington-Oregon border region
29. Washington

**Seismic Region 3**

**California-Nevada Region**

30. Off coast of Oregon
31. Near coast of Oregon
32. Oregon
33. Western Idaho
34. Off coast of northern California
35. Near coast of northern California
36. Northern California
37. Nevada
38. Off coast of California
39. Central California
40. California-Nevada border region
41. Southern Nevada
42. Western Arizona
43. Southern California
44. California-Arizona border region
45. California-Baja California border region
46. Western Arizona-Sonora border

region

**Seismic Region 4**

**Lower California and Gulf of California**

47. Off west coast of Baja California
48. Baja California
49. Gulf of California
50. Sonora
51. Off coast of central Mexico
52. Near coast of central Mexico

**Seismic Region 5**

**Mexico-Guatemala Area**

53. Revilla Gigedo Islands region
54. Off coast of Jalisco
55. Near coast of Jalisco
56. Near coast of Michoacan
57. Michoacan
58. Near coast of Guerrero
59. Guerrero
60. Oaxaca
61. Chiapas
62. Mexico-Guatemala border region
63. Off coast of Mexico
64. Off coast of Michoacan
65. Off coast of Guerrero
66. Near coast of Oaxaca
67. Off coast of Oaxaca
68. Off coast of Chiapas
69. Near coast of Chiapas
70. Guatemala
71. Near coast of Guatemala
730. Northern East Pacific Rise

**Seismic Region 6**

**Central America**

72. Honduras
73. El Salvador
74. Near coast of Nicaragua
75. Nicaragua
76. Off coast of central America
77. Off coast of Costa Rica
78. Costa Rica
79. North of Panama
80. Panama-Costa Rica border region
81. Panama
82. Panama-Colombia border region
83. South of Panama

**Seismic Region 7**

**Caribbean Loop**

84. Yucatan Peninsula
85. Cuba region
86. Jamaica region

87. Haiti region
88. Dominican Republic region
89. Mona Passage
90. Puerto Rico region
91. Virgin Islands
92. Leeward Islands
93. Belize
94. Caribbean Sea
95. Windward Islands
96. Near north coast of Colombia
97. Near coast of Venezuela
98. Trinidad
99. Northern Colombia
100. Lake Maracaibo
101. Venezuela
731. North of Honduras

**Seismic Region 8**

**Andean South America**

102. Near west coast of Colombia
103. Colombia
104. Off coast of Ecuador
105. Near coast of Ecuador
106. Colombia-Ecuador border region
107. Ecuador
108. Off coast of northern Peru
109. Near coast of northern Peru
110. Peru-Ecuador border region
111. Northern Peru
112. Peru-Brazil border region
113. Western Brazil
114. Off coast of Peru
115. Near coast of Peru
116. Central Peru
117. Southern Peru
118. Peru-Bolivia border region
119. Northern Bolivia
120. Central Bolivia
121. Off coast of northern Chile
122. Near coast of northern Chile
123. Northern Chile
124. Chile-Bolivia border region
125. Southern Bolivia
126. Paraguay
127. Chile-Argentina border region
128. Jujuy Province
129. Salta Province
130. Catamarca Province
131. Tucuman Province
132. Santiago del Estero Province
133. Northeastern Argentina
134. Off coast of central Chile
135. Near coast of central Chile
136. Central Chile
137. San Juan Province
138. La Rioja Province
139. Mendoza Province

- 140. San Luis Province
- 141. Cordoba Province
- 142. Uruguay

**Seismic Region 9**

**Extreme South America**

- 143. Off coast of southern Chile
- 144. Southern Chile
- 145. Southern Chile-Argentina border region
- 146. Southern Argentina

**Seismic Region 10**

**Southern Antilles**

- 147. Tierra del Fuego
- 148. Falkland Islands region
- 149. Drake Passage
- 150. Scotia Sea
- 151. South Georgia Island region
- 152. South Georgia Rise
- 153. South Sandwich Islands region
- 154. South Shetland Islands
- 155. Antarctic Peninsula
- 156. Southwestern Atlantic Ocean
- 157. Weddell Sea
- 732. East of South Sandwich Islands

**Seismic Region 11**

**New Zealand Region**

- 158. Off west coast of North Island
- 159. North Island
- 160. Off east coast of North Island
- 161. Off west coast of South Island
- 162. South Island
- 163. Cook Strait
- 164. Off east coast of South Island
- 165. North of Macquarie Island
- 166. Auckland Islands region
- 167. Macquarie Island region
- 168. South of New Zealand

**Seismic Region 12**

**Kermadec-Tonga-Samoa Area**

- 169. Samoa Islands region
- 170. Samoa Islands
- 171. South of Fiji Islands
- 172. West of Tonga Islands (REGION NOT IN USE)
- 173. Tonga Islands
- 174. Tonga Islands region
- 175. South of Tonga Islands
- 176. North of New Zealand
- 177. Kermadec Islands region
- 178. Kermadec Islands
- 179. South of Kermadec Islands

**Seismic Region 13**

**Fiji Area**

- 180. North of Fiji Islands
- 181. Fiji Islands region
- 182. Fiji Islands

**Seismic Region 14**

**Vanuatu (New Hebrides)**

- 183. Santa Cruz Islands region
- 184. Santa Cruz Islands
- 185. Vanuatu Islands region
- 186. Vanuatu Islands
- 187. New Caledonia
- 188. Loyalty Islands
- 189. Southeast of Loyalty Islands

**Seismic Region 15**

**Bismarck and Solomon Islands**

- 190. New Ireland region
- 191. North of Solomon Islands
- 192. New Britain region
- 193. Bougainville-Solomon Islands region
- 194. D'Entrecasteaux Islands region
- 195. South of Solomon Islands

**Seismic Region 16**

**New Guinea**

- 196. Irian Jaya region
- 197. Near north coast of Irian Jaya
- 198. Ninigo Islands region
- 199. Admiralty Islands region
- 200. Near north coast of New Guinea
- 201. Irian Jaya
- 202. New Guinea
- 203. Bismarck Sea
- 204. Aru Islands region
- 205. Near south coast of Irian Jaya
- 206. Near south coast of New Guinea
- 207. Eastern New Guinea region
- 208. Arafura Sea

**Seismic Region 17**

**Caroline Islands to Guam**

- 209. Western Caroline Islands
- 210. South of Mariana Islands

**Seismic Region 18**

**Guam to Japan**

- 211. Southeast of Honshu
- 212. Bonin Islands region
- 213. Volcano Islands region
- 214. West of Mariana Islands
- 215. Mariana Islands region
- 216. Mariana Islands

**Seismic Region 19**

**Japan-Kurils-Kamchatka**

- 217. Kamchatka Peninsula
- 218. Near east coast of Kamchatka Peninsula
- 219. Off east coast of Kamchatka Peninsula
- 220. Northwest of Kuril Islands
- 221. Kuril Islands
- 222. East of Kuril Islands
- 223. Eastern Sea of Japan
- 224. Hokkaido region
- 225. Off southeast coast of Hokkaido
- 226. Near west coast of eastern Honshu
- 227. Eastern Honshu
- 228. Near east coast of eastern Honshu
- 229. Off east coast of Honshu
- 230. Near south coast of eastern Honshu

**Seismic Region 20**

**Southwestern Japan and Ryukyu Islands**

- 231. South Korea
- 232. Western Honshu
- 233. Near south coast of western Honshu
- 234. Northwest of Ryukyu Islands
- 235. Kyushu
- 236. Shikoku
- 237. Southeast of Shikoku
- 238. Ryukyu Islands
- 239. Southeast of Ryukyu Islands
- 240. West of Bonin Islands
- 241. Philippine Sea

**Seismic Region 21**

**Taiwan**

- 242. Near coast of southeastern China
- 243. Taiwan region
- 244. Taiwan
- 245. Northeast of Taiwan
- 246. Southwestern Ryukyu Islands
- 247. Southeast of Taiwan

**Seismic Region 22**

**Philippines**

- 248. Philippine Islands region
- 249. Luzon
- 250. Mindoro
- 251. Samar
- 252. Palawan
- 253. Sulu Sea
- 254. Panay

255. Cebu  
256. Leyte  
257. Negros  
258. Sulu Archipelago  
259. Mindanao  
260. East of Philippine Islands

**Seismic Region 23**

**Borneo-Sulawesi**

261. Borneo  
262. Celebes Sea  
263. Talaud Islands  
264. North of Halmahera  
265. Minahassa Peninsula, Sulawesi  
266. Northern Molucca Sea  
267. Halmahera  
268. Sulawesi  
269. Southern Molucca Sea  
270. Ceram Sea  
271. Buru  
272. Seram

**Seismic Region 24**

**Sunda Arc**

273. Southwest of Sumatera  
274. Southern Sumatera  
275. Java Sea  
276. Sunda Strait  
277. Jawa  
278. Bali Sea  
279. Flores Sea  
280. Banda Sea  
281. Tanimbar Islands region  
282. South of Jawa  
283. Bali region  
284. South of Bali  
285. Sumbawa region  
286. Flores region  
287. Sumba region  
288. Savu Sea  
289. Timor region  
290. Timor Sea  
291. South of Sumbawa  
292. South of Sumba  
293. South of Timor

**Seismic Region 25**

**Myanmar and Southeast Asia**

294. Myanmar-India border region  
295. Myanmar-Bangladesh border region  
296. Myanmar  
297. Myanmar-China border region  
298. Near south coast of Myanmar  
299. Southeast Asia (REGION NOT IN USE)  
300. Hainan Island

301. South China Sea  
733. Thailand  
734. Laos  
735. Kampuchea  
736. Vietnam  
737. Gulf of Tongking

**Seismic Region 26**

**India-Xizang-Szechwan-Yunnan**

302. Eastern Kashmir  
303. Kashmir-India border region  
304. Kashmir-Xizang border region  
305. Western Xizang-India border region  
306. Xizang  
307. Sichuan  
308. Northern India  
309. Nepal-India border region  
310. Nepal  
311. Sikkim  
312. Bhutan  
313. Eastern Xizang-India border region  
314. Southern India  
315. India-Bangladesh border region  
316. Bangladesh  
317. Northeastern India  
318. Yunnan  
319. Bay of Bengal

**Seismic Region 27**

**Southern Xinjiang to Gansu**

320. Kyrgyzstan-Xinjiang border region  
321. Southern Xinjiang  
322. Gansu  
323. Western Nei Mongol  
324. Kashmir-Xinjiang border region  
325. Qinghai

**Seismic Region 28**

**Alma-Ata to Lake Baikal**

326. Southwestern Siberia  
327. Lake Baykal region  
328. East of Lake Baykal  
329. Eastern Kazakhstan  
330. Lake Issyk-Kul region  
331. Kazakhstan-Xinjiang border region  
332. Northern Xinjiang  
333. Tuva-Buryatia-Mongolia border region  
334. Mongolia

**Seismic Region 29**

**Western Asia**

335. Ural Mountains region  
336. Western Kazakhstan  
337. Eastern Caucasus  
338. Caspian Sea  
339. Northwestern Uzbekistan  
340. Turkmenistan  
341. Iran-Turkmenistan border region  
342. Turkmenistan-Afghanistan border region  
343. Turkey-Iran border region  
344. Iran-Armenia-Azerbaijan border region  
345. Northwestern Iran  
346. Iran-Iraq border region  
347. Western Iran  
348. Northern and central Iran  
349. Northwestern Afghanistan  
350. Southwestern Afghanistan  
351. Eastern Arabian Peninsula  
352. Persian Gulf  
353. Southern Iran  
354. Southwestern Pakistan  
355. Gulf of Oman  
356. Off coast of Pakistan

**Seismic Region 30**

**Middle East-Crimea-Eastern Balkans**

357. Ukraine-Moldova-Southwestern Russia region  
358. Romania  
359. Bulgaria  
360. Black Sea  
361. Crimea region  
362. Western Caucasus  
363. Greece-Bulgaria border region  
364. Greece  
365. Aegean Sea  
366. Turkey  
367. Turkey-Georgia-Armenia border region  
368. Southern Greece  
369. Dodecanese Islands  
370. Crete  
371. Eastern Mediterranean Sea  
372. Cyprus region  
373. Dead Sea region  
374. Jordan-Syria region  
375. Iraq

**Seismic Region 31**

**Western Mediterranean Area**

376. Portugal  
377. Spain

- 378. Pyrenees
- 379. Near south coast of France
- 380. Corsica
- 381. Central Italy
- 382. Adriatic Sea
- 383. Northwestern Balkan Peninsula
- 384. West of Gibraltar
- 385. Strait of Gibraltar
- 386. Balearic Islands
- 387. Western Mediterranean Sea
- 388. Sardinia
- 389. Tyrrhenian Sea
- 390. Southern Italy
- 391. Albania
- 392. Greece-Albania border region
- 393. Madeira Islands region
- 394. Canary Islands region
- 395. Morocco
- 396. Northern Algeria
- 397. Tunisia
- 398. Sicily
- 399. Ionian Sea
- 400. Central Mediterranean Sea
- 401. Near coast of Libya

**Seismic Region 32**

**Atlantic Ocean**

- 402. North Atlantic Ocean
- 403. Northern Mid-Atlantic Ridge
- 404. Azores Islands region
- 405. Azores Islands
- 406. Central Mid-Atlantic Ridge
- 407. North of Ascension Island
- 408. Ascension Island region
- 409. South Atlantic Ocean
- 410. Southern Mid-Atlantic Ridge
- 411. Tristan da Cunha region
- 412. Bouvet Island region
- 413. Southwest of Africa
- 414. Southeastern Atlantic Ocean
- 738. Reykjanes Ridge
- 739. Azores-Cape St. Vincent Ridge

**Seismic Region 33**

**Indian Ocean**

- 415. Eastern Gulf of Aden
- 416. Socotra region
- 417. Arabian Sea
- 418. Lakshadweep region
- 419. Northeastern Somalia
- 420. North Indian Ocean
- 421. Carlsberg Ridge
- 422. Maldive Islands region
- 423. Laccadive Sea
- 424. Sri Lanka
- 425. South Indian Ocean
- 426. Chagos Archipelago region

- 427. Mauritius-Reunion region
- 428. Southwest Indian Ridge
- 429. Mid-Indian Ridge
- 430. South of Africa
- 431. Prince Edward Islands region
- 432. Crozet Islands region
- 433. Kerguelen Islands region
- 434. Broken Ridge
- 435. Southeast Indian Ridge
- 436. Southern Kerguelen Plateau
- 437. South of Australia
- 740. Owen Fracture Zone region
- 741. Indian Ocean Triple Junction
- 742. Western Indian-Antarctic Ridge

**Seismic Region 34**  
**Eastern North America**

- 438. Saskatchewan
- 439. Manitoba
- 440. Hudson Bay
- 441. Ontario
- 442. Hudson Strait region
- 443. Northern Quebec
- 444. Davis Strait
- 445. Labrador
- 446. Labrador Sea
- 447. Southern Quebec
- 448. Gaspé Peninsula
- 449. Eastern Quebec
- 450. Anticosti Island
- 451. New Brunswick
- 452. Nova Scotia
- 453. Prince Edward Island
- 454. Gulf of St. Lawrence
- 455. Newfoundland
- 456. Montana
- 457. Eastern Idaho
- 458. Hebgen Lake region, Montana
- 459. Yellowstone region
- 460. Wyoming
- 461. North Dakota
- 462. South Dakota
- 463. Nebraska
- 464. Minnesota
- 465. Iowa
- 466. Wisconsin
- 467. Illinois
- 468. Michigan
- 469. Indiana
- 470. Southern Ontario
- 471. Ohio
- 472. New York
- 473. Pennsylvania
- 474. Vermont-New Hampshire region
- 475. Maine
- 476. Southern New England

- 477. Gulf of Maine
- 478. Utah
- 479. Colorado
- 480. Kansas
- 481. Iowa-Missouri border region
- 482. Missouri-Kansas border region
- 483. Missouri
- 484. Missouri-Arkansas border region
- 485. Missouri-Illinois border region
- 486. New Madrid region, Missouri
- 487. Cape Girardeau region, Missouri
- 488. Southern Illinois
- 489. Southern Indiana
- 490. Kentucky
- 491. West Virginia
- 492. Virginia
- 493. Chesapeake Bay region
- 494. New Jersey
- 495. Eastern Arizona
- 496. New Mexico
- 497. Northwestern Texas-Oklahoma border region
- 498. Western Texas
- 499. Oklahoma
- 500. Central Texas
- 501. Arkansas-Oklahoma border region
- 502. Arkansas
- 503. Louisiana-Texas border region
- 504. Louisiana
- 505. Mississippi
- 506. Tennessee
- 507. Alabama
- 508. Western Florida
- 509. Georgia
- 510. Florida-Georgia border region
- 511. South Carolina
- 512. North Carolina
- 513. Off east coast of United States
- 514. Florida Peninsula
- 515. Bahama Islands
- 516. Eastern Arizona-Sonora border region
- 517. New Mexico-Chihuahua border region
- 518. Texas-Mexico border region
- 519. Southern Texas
- 520. Near coast of Texas
- 521. Chihuahua
- 522. Northern Mexico
- 523. Central Mexico
- 524. Jalisco
- 525. Veracruz
- 526. Gulf of Mexico
- 527. Bay of Campeche



**Seismic Region 35**

**Eastern South America**

- 528. Brazil
- 529. Guyana
- 530. Suriname
- 531. French Guiana

**Seismic Region 36**

**Northwestern Europe**

- 532. Eire
- 533. United Kingdom
- 534. North Sea
- 535. Southern Norway
- 536. Sweden
- 537. Baltic Sea
- 538. France
- 539. Bay of Biscay
- 540. The Netherlands
- 541. Belgium
- 542. Denmark
- 543. Germany
- 544. Switzerland
- 545. Northern Italy
- 546. Austria
- 547. Czech and Slovak Republics
- 548. Poland
- 549. Hungary

**Seismic Region 37**

**Africa**

- 550. Northwest Africa (REGION NOT IN USE)
- 551. Southern Algeria
- 552. Libya
- 553. Egypt
- 554. Red Sea
- 555. Western Arabian Peninsula
- 556. Chad region
- 557. Sudan
- 558. Ethiopia
- 559. Western Gulf of Aden
- 560. Northwestern Somalia
- 561. Off south coast of northwest Africa
- 562. Cameroon
- 563. Equatorial Guinea
- 564. Central African Republic
- 565. Gabon
- 566. Congo
- 567. Zaire
- 568. Uganda
- 569. Lake Victoria region
- 570. Kenya
- 571. Southern Somalia
- 572. Lake Tanganyika region
- 573. Tanzania
- 574. Northwest of Madagascar

- 575. Angola
- 576. Zambia
- 577. Malawi
- 578. Namibia
- 579. Botswana
- 580. Zimbabwe
- 581. Mozambique
- 582. Mozambique Channel
- 583. Madagascar
- 584. South Africa
- 585. Lesotho
- 586. Swaziland
- 587. Off coast of South Africa
- 743. Western Sahara
- 744. Mauritania
- 745. Mali
- 746. Senegal-Gambia region
- 747. Guinea region
- 748. Sierra Leone
- 749. Liberia region
- 750. Cote d'Ivoire
- 751. Burkina Faso
- 752. Ghana
- 753. Benin-Togo region
- 754. Niger
- 755. Nigeria

**Seismic Region 38**

**Australia**

- 588. Northwest of Australia
- 589. West of Australia
- 590. Western Australia
- 591. Northern Territory
- 592. South Australia
- 593. Gulf of Carpentaria
- 594. Queensland
- 595. Coral Sea
- 596. Northwest of New Caledonia
- 597. New Caledonia region
- 598. Southwest of Australia
- 599. Off south coast of Australia
- 600. Near coast of South Australia
- 601. New South Wales
- 602. Victoria
- 603. Near southeast coast of Australia
- 604. Near east coast of Australia
- 605. East of Australia
- 606. Norfolk Island region
- 607. Northwest of New Zealand
- 608. Bass Strait
- 609. Tasmania region
- 610. Southeast of Australia

**Seismic Region 39**

**Pacific Basin**

- 611. North Pacific Ocean

- 612. Hawaiian Islands region
- 613. Hawaiian Islands
- 614. Eastern Caroline Islands region
- 615. Marshall Islands region
- 616. Enewetak Atoll region
- 617. Bikini Atoll region
- 618. Gilbert Islands region
- 619. Johnston Island region
- 620. Line Islands region
- 621. Palmyra Island region
- 622. Kiritimati region
- 623. Tuvalu region
- 624. Phoenix Islands region
- 625. Tokelau Islands region
- 626. Northern Cook Islands
- 627. Cook Islands region
- 628. Society Islands region
- 629. Tubuai Islands region
- 630. Marquesas Islands region
- 631. Tuamotu Archipelago region
- 632. South Pacific Ocean

**Seismic Region 40**

**Arctic Zone**

- 633. Lomonosov Ridge
- 634. Arctic Ocean
- 635. Near north coast of Kalaallit Nunaat
- 636. Eastern Kalaallit Nunaat
- 637. Iceland region
- 638. Iceland
- 639. Jan Mayen Island region
- 640. Greenland Sea
- 641. North of Svalbard
- 642. Norwegian Sea
- 643. Svalbard region
- 644. North of Franz Josef Land
- 645. Franz Josef Land
- 646. Northern Norway
- 647. Barents Sea
- 648. Novaya Zemlya
- 649. Kara Sea
- 650. Near coast of northwestern Siberia
- 651. North of Severnaya Zemlya
- 652. Severnaya Zemlya
- 653. Near coast of northern Siberia
- 654. East of Severnaya Zemlya
- 655. Laptev Sea

**Seismic Region 41**

**Eastern Asia**

- 656. Southeastern Siberia
- 657. Priamurye-Northeastern China border region
- 658. Northeastern China
- 659. North Korea

660. Sea of Japan  
661. Primorye  
662. Sakhalin Island  
663. Sea of Okhotsk  
664. Southeastern China  
665. Yellow Sea  
666. Off east coast of southeastern China

**Seismic Region 42**

**Northeastern Asia, Northern Alaska to Greenland**

667. North of New Siberian Islands  
668. New Siberian Islands  
669. Eastern Siberian Sea  
670. Near north coast of eastern Siberia  
671. Eastern Siberia  
672. Chukchi Sea  
673. Bering Strait  
674. St. Lawrence Island region  
675. Beaufort Sea  
676. Northern Alaska  
677. Northern Yukon Territory  
678. Queen Elizabeth Islands  
679. Northwest Territories  
680. Western Kalaallit Nunaat  
681. Baffin Bay  
682. Baffin Island region

**Seismic Region 43**

**Southeastern and Antarctic Pacific Ocean**

683. Southeastcentral Pacific Ocean  
684. Southern East Pacific Rise  
685. Easter Island region  
686. West Chile Rise

687. Juan Fernandez Islands region  
688. East of North Island  
689. Chatham Islands region  
690. South of Chatham Islands  
691. Pacific-Antarctic Ridge  
692. Southern Pacific Ocean  
756. Southeast of Easter Island

**Seismic Region 44**

**Galapagos Area**

693. Eastcentral Pacific Ocean  
694. Central East Pacific Rise  
695. West of Galapagos Islands  
696. Galapagos Islands region  
697. Galapagos Islands  
698. Southwest of Galapagos Islands  
699. Southeast of Galapagos Islands  
757. Galapagos Triple Junction region

**Seismic Region 45**

**Macquarie Loop**

700. South of Tasmania  
701. West of Macquarie Island  
702. Balleny Islands region

**Seismic Region 46**

**Andaman Islands to Sumatera**

703. Andaman Islands region  
704. Nicobar Islands region  
705. Off west coast of northern Sumatera  
706. Northern Sumatera  
707. Malay Peninsula  
708. Gulf of Thailand

**Seismic Region 47**

**Baluchistan**

709. Southeastern Afghanistan  
710. Pakistan  
711. Southwestern Kashmir  
712. India-Pakistan border region

**Seismic Region 48**

**Hindu Kush and Pamir**

713. Central Kazakhstan  
714. Southeastern Uzbekistan  
715. Tajikistan  
716. Kyrgyzstan  
717. Afghanistan-Tajikistan border region  
718. Hindu Kush region  
719. Tajikistan-Xinjiang border region  
720. Northwestern Kashmir

**Seismic Region 49**

**Northern Eurasia**

721. Finland  
722. Norway-Murmansk border region  
723. Finland-Karelia border region  
724. Baltic States-Belarus-Northwestern Russia  
725. Northwestern Siberia  
726. Northern and central Siberia

**Seismic Region 50**

**Antarctica**

727. Victoria Land  
728. Ross Sea  
729. Antarctica

### 10.2.3 IASPEI Magnitudes

The ISC publishes a diversity of magnitude data. Although trying to be as complete and specific as possible, preference is now given to magnitudes determined according to standard procedures recommended by the Working Group on Magnitude Measurements of the IASPEI Commission on Seismological Observation and Interpretation (CoSOI). So far, such standards have been agreed upon for the local magnitude  $ML$ , the local-regional  $mb\_Lg$ , and for two types each of body-wave ( $mb$  and  $mB\_BB$ ) and surface-wave magnitudes ( $Ms\_20$  and  $Ms\_BB$ ). With the exception of  $ML$ , all other standard magnitudes are measured on vertical-component records only.  $BB$  stands for direct measurement on unfiltered velocity broadband records in a wide range of periods, provided that their passband covers at least the period range within which  $mB\_BB$  and  $Ms\_BB$  are supposed to be measured. Otherwise, a deconvolution has to be applied prior to the amplitude and period measurement so as to assure that this specification is met. In contrast,  $mb\_Lg$ ,  $mb$  and  $Ms\_20$  are based on narrowband amplitude measurements around periods of 1 s and 20 s, respectively.

$ML$  is consistent with the original definition of the local magnitude by *Richter* (1935) and  $mB\_BB$  in close agreement with the original definition of medium-period body-wave magnitude  $mB$  measured in a wide range of periods between some 2 to 20 s and calibrated with the *Gutenberg and Richter* (1956) Q-function for vertical-component P waves. Similarly,  $Ms\_BB$  is best tuned to the unbiased use of the IASPEI (1967) recommended standard magnitude formula for surface-wave amplitudes in a wide range of periods and distances, as proposed by its authors *Vaněk et al.* (1962). In contrast,  $mb$  and  $Ms\_20$  are chiefly based on measurement standards defined by US agencies in the 1960s in conjunction with the global deployment of the World-Wide Standard Seismograph Network (WWSSN), which did not include medium or broadband recordings. Some modifications were made in the 1970s to account for IASPEI recommendations on extended measurement time windows for  $mb$ . Although not optimal for calibrating narrow-band spectral amplitudes measured around 1 s and 20 s only,  $mb$  and  $Ms\_20$  use the same original calibrations functions as  $mB\_BB$  and  $Ms\_BB$ . But  $mb$  and  $Ms\_20$  data constitute by far the largest available magnitude data sets. Therefore they continue to be used, with appreciation for their advantages (e.g.,  $mb$  is by far the most frequently measured teleseismic magnitude and often the only available and reasonably good magnitude estimator for small earthquakes) and their shortcomings (see section 3.2.5.2 of Chapter 3 in NMSOP-2).

Abbreviated descriptions of the standard procedures for  $ML$ ,  $mb\_Lg$ ,  $mb$ ,  $mB\_BB$  and  $Ms\_BB$  are summarised below. For more details, including also the transfer functions of the simulation filters to be used, see [http://www.iaspei.org/commissions/commission-on-seismological-observation-and-interpretation/Summary\\_WG\\_recommendations\\_20130327.pdf](http://www.iaspei.org/commissions/commission-on-seismological-observation-and-interpretation/Summary_WG_recommendations_20130327.pdf).

All amplitudes used in the magnitude formulas below are in most circumstances to be measured as one-half the maximum deflection of the seismogram trace, peak-to-adjacent-trough or trough-to-adjacent-peak, where the peak and trough are separated by one crossing of the zero-line: this measurement is sometimes described as “one-half peak-to-peak amplitude.” The periods are to be measured as twice the time-intervals separating the peak and adjacent-trough from which the amplitudes are measured. The amplitude-phase arrival-times are to be measured and reported too as the time of the zero-crossing between the peak and adjacent-trough from which the amplitudes are measured. The issue of amplitude and period measuring procedures, and circumstances under which alternative procedures are acceptable



or preferable, is discussed further in Section 5 of IS 3.3 and in section 3.2.3.3 of Chapter 3 of NMSOP-2.

Amplitudes measured according to recommended IASPEI standard procedures should be reported with the following ISF amplitude “phase names”: IAML, IAmb\_Lg, IAmb, IAMs\_20, IVmB\_BB and IVMs\_BB. “I” stands for “International” or “IASPEI”, “A” for displacement amplitude, measured in nm, and “V” for velocity amplitude, measured in nm/s. Although the ISC will calculate standard surface-wave magnitudes only for earthquakes shallower than 60 km, contributing agencies or stations are encouraged to report standard amplitude measurements of IAMs\_20 and IVMs\_BB for deeper earthquakes as well.

Note that the commonly known classical calibration relationships have been modified in the following to be consistent with displacements measured in nm, and velocities in nm/s, which is now common with high-resolution digital data and analysis tools. With these general definitions of the measurement parameters, where  $R$  is hypocentral distance in km (typically less than 1000 km),  $\Delta$  is epicentral distance in degrees and  $h$  is hypocentre depth in km, the standard formulas and procedures read as follows:

$ML$ :

$$ML = \log_{10}(A) + 1.11 \log_{10} R + 0.00189R - 2.09 \quad (10.14)$$

for crustal earthquakes in regions with attenuative properties similar to those of southern California, and with  $A$  being the maximum trace amplitude in nm that is measured on output from a horizontal-component instrument that is filtered so that the response of the seismograph/filter system replicates that of a Wood-Anderson standard seismograph (but with a static magnification of 1). For the normalised simulated response curve and related poles and zeros see Figure 1 and Table 1 in IS 3.3 of NMSOP-2.

Equation (10.14) is an expansion of that of *Hutton and Boore (1987)*. The constant term in equation (10.14),  $-2.09$ , is based on an experimentally determined static magnification of the Wood-Anderson of 2080 (see *Uhrhammer and Collins (1990)*), rather than the theoretical magnification of 2800 that was specified by the seismograph’s manufacturer. The formulation of equation (10.14) assures that reported  $ML$  amplitude data are not affected by uncertainty in the static magnification of the Wood-Anderson seismograph.

For seismographic stations containing two horizontal components, amplitudes are measured independently from each horizontal component and each amplitude is treated as a single datum. There is no effort to measure the two observations at the same time, and there is no attempt to compute a vector average. For crustal earthquakes in regions with attenuative properties that are different from those of coastal California and for measuring magnitudes with vertical-component seismographs the constants in the above equation have to be re-determined to adjust for the different regional attenuation and travel paths as well as for systematic differences between amplitudes measured on horizontal and vertical seismographs.

$mb\_Lg$ :

$$mb\_Lg = \log_{10}(A) + 0.833 \log_{10} R + 0.434\gamma(R - 10) - 0.87 \quad (10.15)$$

where  $A$  = “sustained ground-motion amplitude” in nm, defined as the third largest amplitude in the

---

time window corresponding to group velocities of 3.6 to 3.2 km/s, in the period ( $T$ ) range 0.7 s to 1.3 s;  $R$  = epicentral distance in km,  $\gamma$  = coefficient of attenuation in  $\text{km}^{-1}$ .  $\gamma$  is related to the quality factor  $Q$  through the equation  $\gamma = \pi/(QU T)$ , where  $U$  is group velocity and  $T$  is the wave period of the  $L_g$  wave.  $\gamma$  is a strong function of crustal structure and should be determined specifically for the region in which the  $mb\_Lg$  is to be used.  $A$  and  $T$  are measured on output from a vertical-component instrument that is filtered so that the frequency response of the seismograph/filter system replicates that of a WWSSN short-period seismograph (see Figure 1 and Table 1 in IS 3.3 of NMSOP-2). Arrival times with respect to the origin of the seismic disturbance are used, along with epicentral distance, to compute group velocity  $U$ .

$mb$ :

$$mb = \log_{10}(A/T) + Q(\Delta, h) - 3.0 \quad (10.16)$$

where  $A$  = vertical component P-wave ground amplitude in nm measured at distances  $20^\circ \leq \Delta \leq 100^\circ$  and calculated from the maximum trace-amplitude with  $T < 3$  s in the entire P-phase train (time spanned by P, pP, sP, and possibly PcP and their codas, and ending preferably before PP).  $A$  and  $T$  are measured on output from an instrument that is filtered so that the frequency response of the seismograph/filter system replicates that of a WWSSN short-period seismograph (see Figure 1 and Table 1 in IS 3.3 of NMSOP-2).  $A$  is determined by dividing the maximum trace amplitude by the magnification of the simulated WWSSN-SP response at period  $T$ .

$Q(\Delta, h)$  = attenuation function for PZ (P-waves recorded on vertical component seismographs) established by *Gutenberg and Richter* (1956) in the tabulated or algorithmic form as used by the U.S. Geological Survey/National Earthquake Information Center (USGS/NEIC) (see Table 2 in IS 3.3 and program description PD 3.1 in NMSOP-2);

$mB\_BB$ :

$$mB\_BB = \log_{10}(Vmax/2\pi) + Q(\Delta, h) - 3.0 \quad (10.17)$$

where  $Vmax$  = vertical component ground velocity in nm/s at periods between  $0.2 \text{ s} < T < 30 \text{ s}$ , measured in the range  $20^\circ \leq \Delta \leq 100^\circ$ .  $Vmax$  is calculated from the maximum trace-amplitude in the entire P-phase train (see  $mb$ ), as recorded on a seismogram that is proportional to velocity at least in the period range of measurements.  $Q(\Delta, h)$  = attenuation function for PZ established by *Gutenberg and Richter* (1956) (see 10.16). Equation (10.16) differs from the equation for  $mB$  of *Gutenberg and Richter* (1956) by virtue of the  $\log_{10}(Vmax/2\pi)$  term, which replaces the classical  $\log_{10}(A/T)_{max}$  term. Contributors should continue to send observations of  $A$  and  $T$  to ISC.

$Ms\_20$ :

$$Ms\_20 = \log_{10}(A/T) + 1.66 \log_{10} \Delta + 0.3 \quad (10.18)$$

where  $A$  = vertical-component ground displacement in nm at  $20^\circ \leq \Delta \leq 160^\circ$  epicentral distance measured from the maximum trace amplitude of a surface-wave phase having a period  $T$  between 18 s

---

and 22 s on a waveform that has been filtered so that the frequency response of the seismograph/filter replicates that of a WWSSN long-period seismograph (see Figure 1 and Table 1 in IS 3.3 of NMSOP-2).  $A$  is determined by dividing the maximum trace amplitude by the magnification of the simulated WWSSN-LP response at period  $T$ . Equation (10.18) is formally equivalent to the  $M_s$  equation proposed by *Vaněk et al.* (1962) but is here applied to vertical motion measurements in a narrow range of periods.

$M_s\_BB$ :

$$M_s\_BB = \log_{10}(Vmax/2\pi) + 1.66 \log_{10} \Delta + 0.3 \quad (10.19)$$

where  $Vmax$  = vertical-component ground velocity in nm/s associated with the maximum trace-amplitude in the surface-wave train at periods between  $3 \text{ s} < T < 60 \text{ s}$  as recorded at distances  $2^\circ \leq \Delta \leq 160^\circ$  on a seismogram that is proportional to velocity in that range of considered periods. Equation (10.19) is based on the  $M_s$  equation proposed by *Vaněk et al.* (1962), but is here applied to vertical motion measurements and is used with the  $\log_{10}(Vmax/2\pi)$  term replacing the  $\log_{10}(A/T)_{max}$  term of the original. As for  $mB\_BB$ , observations of  $A$  and  $T$  should be reported to ISC.

$Mw$ :

$$Mw = (\log_{10} M_0 - 9.1) / 1.5 \quad (10.20)$$

Moment magnitude  $Mw$  is calculated from data of the scalar seismic moment  $M_0$  (when given in Nm), or

$$Mw = (\log_{10} M_0 - 16.1) / 1.5 \quad (10.21)$$

its CGS equivalent when  $M_0$  is in dyne-cm.

Please note that the magnitude nomenclature used in this Section uses the IASPEI standards as the reference. However, the magnitude type is typically written in plain text in most typical data reports and so it is in this document. Moreover, writing magnitude types in plain text allows us to reproduce the magnitude type as stored in the database and provides a more direct identification of the magnitude type reported by different agencies. A short description of the common magnitude types available in this Summary is given in table 7.6.

#### 10.2.4 The IASPEI Seismic Format (ISF)

The ISF is the IASPEI approved standard format for the exchange of parametric seismological data (hypocentres, magnitudes, phase arrivals, moment tensors etc.) and is one of the formats used by the ISC. It was adopted as standard in August 2001 and is an extension of the International Monitoring System 1.0 (IMS1.0) standard, which was developed for exchanging data used to monitor the Comprehensive Nuclear-Test-Ban Treaty. An example of the ISF is shown in Listing 10.1.

Bulletins which use the ISF are comprised of origin and arrival information, provided in a series of data blocks. These include: a bulletin title block; an event title block; an origin block; a magnitude sub-block; an effect block; a reference block; and a phase block.

Within these blocks an important extension of the IMS1.0 standard is the ability to add additional comments and thus provide further parametric information. The ISF comments are distinguishable within the open parentheses required for IMS1.0 comments by beginning with a hash mark (#) followed by a keyword identifying the type of formatted comment. Each additional line required in the ISF comment begins with the hash (within the comment parentheses) followed by blank spaces at least as long as the keyword. Optional lines within the comment are signified with a plus sign (+) instead of a hash mark. The keywords include **PRIME** (to designate a prime origin of a hypocentre); **CENTROID** (to indicate the centroid origin); **MOMTENS** (moment tensor solution); **FAULT\_PLANE** (fault plane solution); **PRINAX** (principal axes); **PARAM** (an origin parameter e.g. hypocentre depth given by a depth phase).

The ISC has now moved to ISF 2.1 as the default format for searches, this provides more detail primarily for the identification of arrivals. An essential change with the implemented use of network codes from data year 2021.

The full documentation for the ISF 1 and 2.1 is maintained at the ISC and can be downloaded from:

[www.isc.ac.uk/standards/isf/download/isf21.pdf](http://www.isc.ac.uk/standards/isf/download/isf21.pdf)

[www.isc.ac.uk/standards/isf/download/isf.pdf](http://www.isc.ac.uk/standards/isf/download/isf.pdf)

The documentation for the IMS1.0 standard can be downloaded from:

[www.isc.ac.uk/standards/isf/download/ims1\\_0.pdf](http://www.isc.ac.uk/standards/isf/download/ims1_0.pdf)



### 10.2.5 Ground Truth (GT) Events

Accurate locations are crucial in testing Earth models derived from body and surface wave tomography as well as in location calibration studies. ‘Ground Truth’ (GT) events are well-established source locations and origin times. A database of IASPEI reference events (GT earthquakes and explosions) is hosted at the ISC ([www.isc.ac.uk](http://www.isc.ac.uk)). A full description of GT selection criteria can be found in *Bondár and McLaughlin (2009a)*.

The events are coded by category GT0, GT1, GT2 or GT5, where the epicentre of a GT $X$  event is known to within  $X$  km to a 95% confidence level. A map of all IASPEI reference events is shown in Figure 10.15 and the types of event are categorised in Figure 10.16. GT0 are explosions with announced locations and origin times. GT1 and GT2 are typically explosions, mine blasts or rock bursts either associated to explosion phenomenology located upon overhead imagery with seismically determined origin times, or precisely located by in-mine seismic networks. GT1-2 events are assumed to be shallow, but depth is unknown.

The database consists of nuclear explosions of GT0–5 quality, adopted from the Nuclear Explosion Database (*Bennett et al., 2010*); GT0–5 chemical explosions, rock bursts, mine-induced events, as well as a few earthquakes, inherited from the reference event set by *Bondár et al. (2004)*; GT5 events (typically earthquakes with crustal depths) which have been identified using either the method of *Bondár et al. (2008)* (2,275 events) or *Bondár and McLaughlin (2009a)* (updated regularly from the EHB catalogue (*Engdahl et al., 1998*)), which uses the following criteria:

- 10 or more stations within 150 km from the epicentre
- one or more stations within 10 km
- $\Delta U \leq 0.35$
- a secondary azimuthal gap  $\leq 160^\circ$

where  $\Delta U$  is the network quality metric defined as the mean absolute deviation between the best-fitting uniformly distributed network of stations and the actual network:

$$\Delta U = \frac{4 \sum |esaz_i - (unif_i + b)|}{360N}, 0 \leq \Delta U \leq 1 \quad (10.22)$$

where  $N$  is the number of stations,  $esaz_i$  is the  $i$ th event-to-station azimuth,  $unif_i = 360i/N$  for  $i = 0, \dots, N - 1$ , and  $b = avg(esaz_i) - avg(unif_i)$ .  $\Delta U$  is normalised so that it is 0 when the stations are uniformly distributed in azimuth and 1 when all the stations are at the same azimuth.

The seismological community is invited to participate in this project by nominating seismic events for the reference event database. Submitters may be contacted for further confirmation and for arrival time data. The IASPEI Reference Event List will be periodically published both in written and electronic form with proper acknowledgement of all submitters.

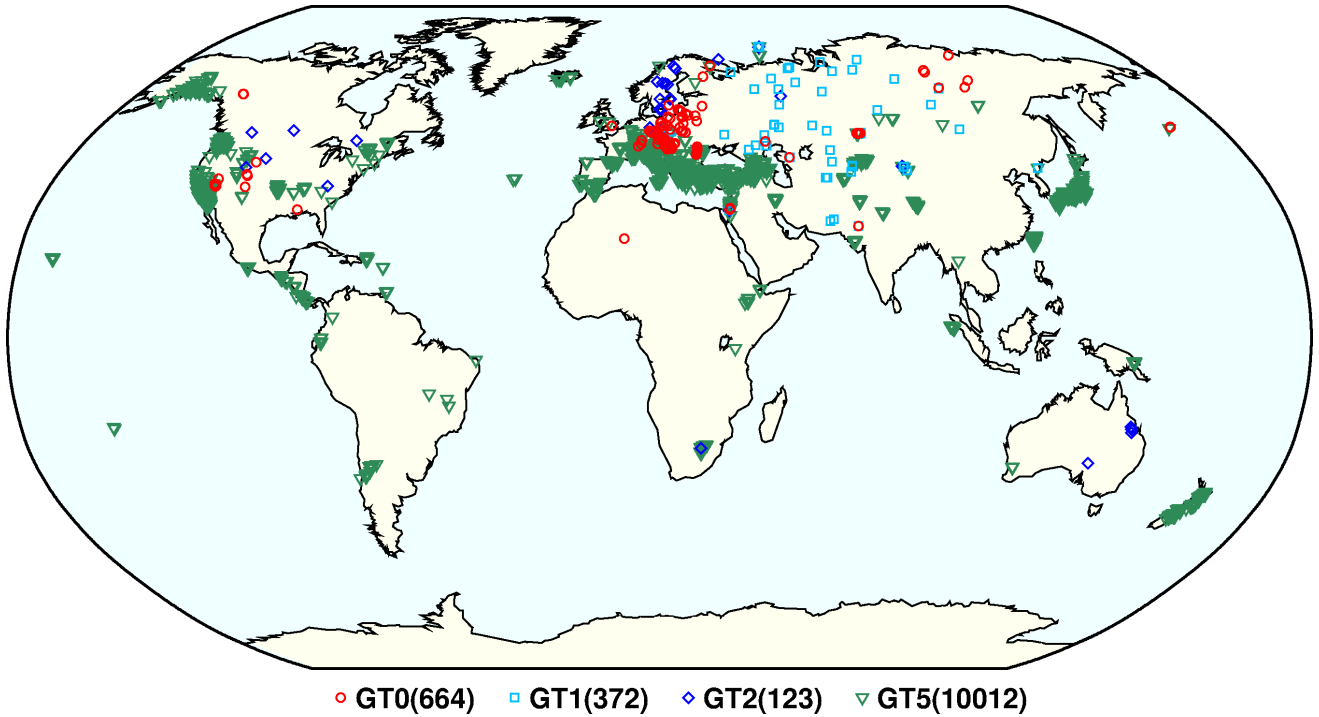


Figure 10.15: Map of all IASPEI Reference Events as of January 2023.

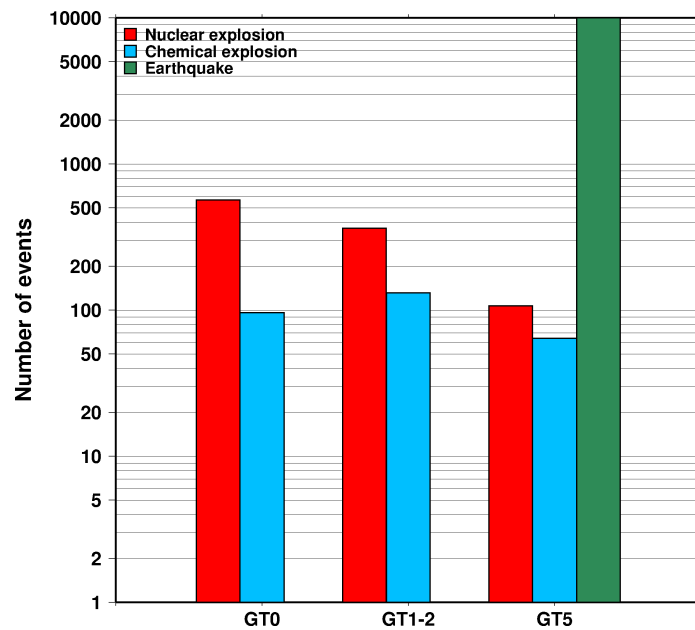


Figure 10.16: Histogram showing the event types within the IASPEI Reference Event list as of January 2023.



### 10.2.6 Nomenclature of Event Types

The nomenclature of event types currently used in the ISC Bulletin takes its origin from the IASPEI International Seismic Format (ISF).

Event type codes are composed of a leading character that generally indicates the confidence with which the type of the event is asserted and a trailing character that generally gives the type of the event. The leading and trailing characters may be used in any combination.

The **leading** characters are:

- s = suspected
- k = known
- f = felt (implies known)
- d = damaging (implies felt and known)

The **trailing** characters are:

- c = meteoritic event
- e = earthquake
- h = chemical explosion
- i = induced event
- l = landslide
- m = mining explosion
- n = nuclear explosion
- r = rock burst
- x = experimental explosion

A chemical explosion might be for mining or experimental purposes, and it is conceivable that other types of event might be assigned two or more different event type codes. This is deliberate, and matches the ambiguous identification of events in existing databases.

In addition, the code **uk** is used for events of unknown type and **ls** is used for known landslides.

The frequency of the different event types designated in the ISC Bulletin since 1964 is indicated in Figure 10.17.

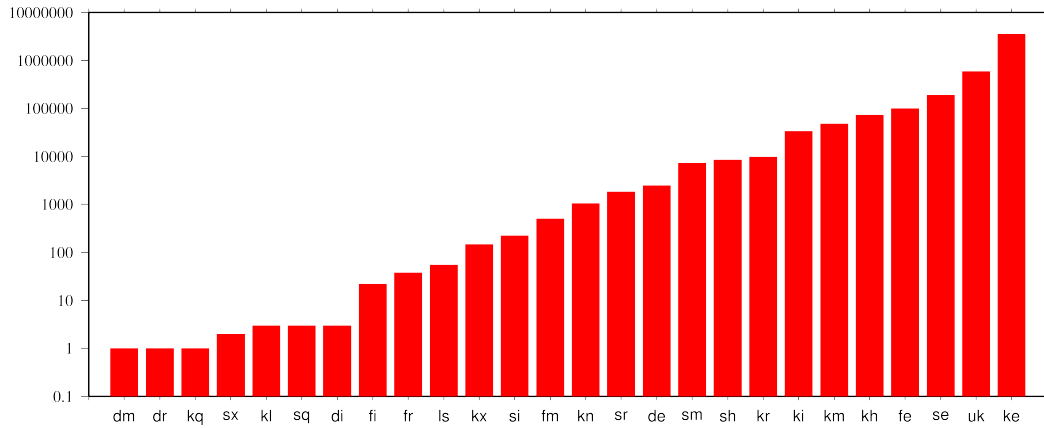


Figure 10.17: Event types in the ISC Bulletin

There are currently plans to revise this nomenclature as part of the joint IASPEI Commission on Seismological Observation and Interpretation (CoSOI) and FDSN working group.

### 10.3 Tables

Table 10.2: Listing of all 396 agencies that have directly reported to the ISC. The 151 agencies highlighted in bold have reported data to the ISC Bulletin for the period of this Bulletin Summary.

Agency Code	Agency Name
AAA	Alma-ata, Kazakhstan
AAE	University of Addis Ababa, Ethiopia
AAM	University of Michigan, USA
ADE	Primary Industries and Resources SA, Australia
ADH	Observatorio Afonso Chaves, Portugal
AEIC	Alaska Earthquake Information Center, USA
<b>AFAD</b>	<b>Disaster and Emergency Management Presidency, Turkey</b>
AFAR	The Afar Depression: Interpretation of the 1960-2000 Earthquakes, Israel
AFUA	University of Alabama, USA
ALG	Algiers University, Algeria
ANDRE	USSR
ANF	USArray Array Network Facility, USA
ANT	Antofagasta, Chile
ARE	Instituto Geofisico del Peru, Peru
ARO	Observatoire Géophysique d'Arta, Djibouti
<b>ASGSR</b>	<b>Altay-Sayan Branch, Geophysical Survey, Russian Academy of Sciences, Russia</b>
<b>ASIES</b>	<b>Institute of Earth Sciences, Academia Sinica, Chinese Taipei</b>
ASL	Albuquerque Seismological Laboratory, USA
ASM	University of Asmara, Eritrea
ATA	The Earthquake Research Center Ataturk University, Turkey
<b>ATH</b>	<b>National Observatory of Athens, Greece</b>
<b>AUST</b>	<b>Geoscience Australia, Australia</b>
AVETI	USSR
<b>AWI</b>	<b>Alfred Wegener Institute for Polar and Marine Research, Germany</b>

*Table 10.2: Continued.*

Agency Code	Agency Name
<b>AZER</b>	<b>Republican Seismic Survey Center of Azerbaijan National Academy of Sciences, Azerbaijan</b>
BCIS	Bureau Central International de Sismologie, France
BDF	Observatório Sismológico da Universidade de Brasília, Brazil
<b>BELR</b>	<b>Centre of Geophysical Monitoring of the National Academy of Sciences of Belarus, Republic of Belarus</b>
<b>BEO</b>	<b>Republički seizmološki zavod, Serbia</b>
<b>BER</b>	<b>University of Bergen, Norway</b>
BERK	Berkheimer H, Germany
<b>BGR</b>	<b>Bundesanstalt für Geowissenschaften und Rohstoffe, Germany</b>
<b>BGS</b>	<b>British Geological Survey, United Kingdom</b>
<b>BGSI</b>	<b>Botswana Geoscience Institute, Botswana</b>
BHJ2	Study of Aftershocks of the Bhuj Earthquake by Japanese Research Team, Japan
BIAK	Biak earthquake aftershocks (17-Feb-1996), USA
<b>BJI</b>	<b>China Earthquake Networks Center, China</b>
<b>BKK</b>	<b>Thai Meteorological Department, Thailand</b>
BNS	Erdbebenstation, Geologisches Institut der Universität, Köl, Germany
BOG	Universidad Javeriana, Colombia
<b>BRA</b>	<b>Geophysical Institute, Slovak Academy of Sciences, Slovakia</b>
<b>BRG</b>	<b>Seismological Observatory Berggießhübel, TU Bergakademie Freiberg, Germany</b>
BRK	Berkeley Seismological Laboratory, USA
BRS	Brisbane Seismograph Station, Australia
<b>BUC</b>	<b>National Institute for Earth Physics, Romania</b>
BUD	Geodetic and Geophysical Research Institute, Hungary
BUEE	Earth & Environment, USA
BUG	Institute of Geology, Mineralogy & Geophysics, Germany
<b>BUL</b>	<b>Goetz Observatory, Zimbabwe</b>
BUT	Montana Bureau of Mines and Geology, USA
<b>BYKL</b>	<b>Baykal Regional Seismological Centre, GS SB RAS, Russia</b>
CADCG	Central America Data Centre, Costa Rica
CAN	Australian National University, Australia
CANSK	Canadian and Scandinavian Networks, Sweden
CAR	Instituto Sismologico de Caracas, Venezuela
CASC	Central American Seismic Center, Costa Rica
<b>CATAC</b>	<b>Central American Tsunami Advisory Center, Nicaragua</b>
CENT	Centennial Earthquake Catalog, USA
CERI	Center for Earthquake Research and Information, USA
<b>CFUSG</b>	<b>Inst. of Seismology and Geodynamics, V.I. Vernadsky Crimean Federal University, Republic of Crimea</b>
<b>CLL</b>	<b>Geophysikalisches Observatorium Collm, Germany</b>
CNG	Seismographic Station Chagalane, Mozambique
<b>CNRM</b>	<b>Centre National de Recherche, Morocco</b>
COSMOS	Consortium of Organizations for Strong Motion Observations, USA
<b>CRAAG</b>	<b>Centre de Recherche en Astronomie, Astrophysique et Géophysique, Algeria</b>
CSC	University of South Carolina, USA
CSEM	Centre Sismologique Euro-Méditerranéen (CSEM/EMSC), France

*Table 10.2: Continued.*

Agency Code	Agency Name
<b>CUPWA</b>	<b>Curtin University, Australia</b>
DAGSR	Dagestan Branch, Geophysical Survey, Russian Academy of Sciences, Russia
DASA	Defense Atomic Support Agency, USA
DBN	Koninklijk Nederlands Meteorologisch Instituut, Netherlands
DDA	General Directorate of Disaster Affairs, Turkey
DHMR	Yemen National Seismological Center, Yemen
<b>DIAS</b>	<b>Dublin Institute for Advanced Studies, Ireland</b>
<b>DJA</b>	<b>Badan Meteorologi, Klimatologi dan Geofisika, Indonesia</b>
<b>DMN</b>	<b>National Seismological Centre, Nepal, Nepal</b>
DNAG	USA
<b>DNK</b>	<b>Geological Survey of Denmark and Greenland, Denmark</b>
<b>DSN</b>	<b>Dubai Seismic Network, United Arab Emirates</b>
DUSS	Damascus University, Syria, Syria
<b>EAF</b>	<b>East African Network, Unknown</b>
EAGLE	Ethiopia-Afar Geoscientific Lithospheric Experiment, Unknown
EBR	Observatori de l'Ebre, Spain
EBSE	Ethiopian Broadband Seismic Experiment, Unknown
ECGS	European Center for Geodynamics and Seismology, Luxembourg
<b>ECX</b>	<b>Centro de Investigación Científica y de Educación Superior de Ensenada, Mexico</b>
EFATE	OBS Experiment near Efate, Vanuatu, USA
EHB	Engdahl, van der Hilst and Buland, USA
EIDC	Experimental (GSETT3) International Data Center, USA
EKA	Eskdalemuir Array Station, United Kingdom
ENT	Geological Survey and Mines Department, Uganda
EPSI	Reference events computed by the ISC for EPSI project, United Kingdom
ERDA	Energy Research and Development Administration, USA
EST	Geological Survey of Estonia, Estonia
EUROP	Unknown
EVIBIB	Data from publications listed in the ISC Event Bibliography, Unknown
FBR	Fabra Observatory, Spain
<b>FCIAR</b>	<b>Federal Center for Integrated Arctic Research, Russia</b>
FDF	Fort de France, Martinique
FIA0	Finessa Array, Finland
FOR	Unknown Historical Agency, Unknown - historical agency
FUBES	Earth Science Dept., Geophysics Section, Germany
<b>FUNV</b>	<b>Fundación Venezolana de Investigaciones Sismológicas, Venezuela</b>
FUR	Geophysikalisches Observatorium der Universität München, Germany
GBZT	Marmara Research Center, Turkey
<b>GCG</b>	<b>INSIVUMEH, Guatemala</b>
<b>GCMT</b>	<b>The Global CMT Project, USA</b>
GDNRW	Geologischer Dienst Nordrhein-Westfalen, Germany
<b>GEN</b>	<b>Dipartimento per lo Studio del Territorio e delle sue Risorse (RSNI), Italy</b>
GEOAZ	UMR Géoazur, France
GEOMR	GEOMAR, Germany

*Table 10.2: Continued.*

Agency Code	Agency Name
<b>GFZ</b>	<b>Helmholtz Centre Potsdam GFZ German Research Centre For Geosciences, Germany</b>
<b>GII</b>	<b>The Geophysical Institute of Israel, Israel</b>
GOM	Observatoire Volcanologique de Goma, Democratic Republic of the Congo
<b>GRAL</b>	<b>National Council for Scientific Research, Lebanon</b>
<b>GSDM</b>	<b>Geological Survey Department Malawi, Malawi</b>
GSET2	Group of Scientific Experts Second Technical Test 1991, April 22 - June 2, Unknown
GTFE	German Task Force for Earthquakes, Germany
<b>GUC</b>	<b>Centro Sismológico Nacional, Universidad de Chile, Chile</b>
HAN	Hannover, Germany
HDC	Observatorio Vulcanológico y Sismológico de Costa Rica, Costa Rica
<b>HEL</b>	<b>Institute of Seismology, University of Helsinki, Finland</b>
HFS	Hagfors Observatory, Sweden
HFS1	Hagfors Observatory, Sweden
HFS2	Hagfors Observatory, Sweden
HIMNT	Himalayan Nepal Tibet Experiment, USA
<b>HKC</b>	<b>Hong Kong Observatory, Hong Kong</b>
HLUG	Hessisches Landesamt für Umwelt und Geologie, Germany
<b>HLW</b>	<b>National Research Institute of Astronomy and Geophysics, Egypt</b>
HNR	Ministry of Mines, Energy and Rural Electrification, Solomon Islands
HON	Pacific Tsunami Warning Center - NOAA, USA
HRVD	Harvard University, USA
HRVD_LR	Department of Geological Sciences, Harvard University, USA
HVO	Hawaiian Volcano Observatory, USA
<b>HYB</b>	<b>National Geophysical Research Institute, India</b>
HYD	National Geophysical Research Institute, India
IAG	Instituto Andaluz de Geofísica, Spain
IASBS	Institute for Advanced Studies in Basic Sciences, Iran
IASPEI	IASPEI Working Group on Reference Events, USA
ICE	Instituto Costarricense de Electricidad, Costa Rica
<b>IDC</b>	<b>International Data Centre, CTBTO, Austria</b>
IDG	Institute of Dynamics of Geosphere, Russian Academy of Sciences, Russia
IEC	Institute of the Earth Crust, SB RAS, Russia
IEPN	Institute of Environmental Problems of the North, Russian Academy of Sciences, Russia
IFREE	Institute For Research on Earth Evolution, Japan
IGGSL	Seismology Lab, Institute of Geology & Geophysics, Chinese Academy of Sciences, China
<b>IGIL</b>	<b>Instituto Dom Luiz, University of Lisbon, Portugal</b>
IGKR	Institute of Geology, Komi Science Centre, Ural Branch, Russian Academy of Sciences, Russia
IGKRC	Institute of Geology, Karelian Research Centre, Russian Academy of Sciences, Russia
<b>IGQ</b>	<b>Servicio Nacional de Sismología y Vulcanología, Ecuador</b>
IGS	Institute of Geological Sciences, United Kingdom

Table 10.2: Continued.

Agency Code	Agency Name
INAM	Instituto Nacional de Meteorologia e Geofisica - INAMET, Angola
INDEPTH3	International Deep Profiling of Tibet and the Himalayas, USA
INET	Instituto Nicaraguense de Estudios Territoriales - INETER, Nicaragua
<b>INMG</b>	<b>Instituto Português do Mar e da Atmosfera, I.P., Portugal</b>
INMGC	Instituto Nacional de Meteorologia e Geofísica, Cape Verde
<b>IPEC</b>	<b>The Institute of Physics of the Earth (IPEC), Czech Republic</b>
IPER	Institute of Physics of the Earth, Academy of Sciences, Moscow, Russia
<b>IPGP</b>	<b>Institut de Physique du Globe de Paris, France</b>
IPRG	Institute for Petroleum Research and Geophysics, Israel
IRIS	IRIS Data Management Center, USA
IRSM	Institute of Rock Structure and Mechanics, Czech Republic
<b>ISC</b>	<b>International Seismological Centre, United Kingdom</b>
<b>ISC-PPSM</b>	<b>International Seismological Centre Probabilistic Point Source Model, United Kingdom</b>
<b>ISK</b>	<b>Kandilli Observatory and Earthquake Research Institute, Turkey</b>
<b>ISN</b>	<b>Iraqi Meteorological and Seismology Organisation, Iraq</b>
ISS	International Seismological Summary, United Kingdom
IST	Institute of Physics of the Earth, Technical University of Istanbul, Turkey
<b>ISU</b>	<b>Institute of Seismology, Academy of Sciences, Republic of Uzbekistan, Uzbekistan</b>
ITU	Faculty of Mines, Department of Geophysical Engineering, Turkey
JEN	Geodynamisches Observatorium Moxa, Germany
<b>JMA</b>	<b>Japan Meteorological Agency, Japan</b>
JOH	Bernard Price Institute of Geophysics, South Africa
<b>JSN</b>	<b>Jamaica Seismic Network, Jamaica</b>
<b>JSO</b>	<b>Jordan Seismological Observatory, Jordan</b>
KBC	Institut de Recherches Géologiques et Minières, Cameroon
<b>KEA</b>	<b>Korea Earthquake Administration, Democratic People's Republic of Korea</b>
KEW	Kew Observatory, United Kingdom
KHC	Institute of Geophysics, Czech Academy of Sciences, Czech Republic
KISR	Kuwait Institute for Scientific Research, Kuwait
KLM	Malaysian Meteorological Service, Malaysia
<b>KMA</b>	<b>Korea Meteorological Administration, Republic of Korea</b>
KMGRS	Kavkazskie Mineralnye Vody Branch, Geophysical Survey, RAS, Russia
<b>KNET</b>	<b>Kyrgyz Seismic Network, Kyrgyzstan</b>
<b>KOGSR</b>	<b>Kola Branch, Geophysical Survey, Russian Academy of Sciences, Russia</b>
KRAR	Krasnoyarsk Scientific Research Inst. of Geology and Mineral Resources, Russia, Russia
KRL	Geodätisches Institut der Universität Karlsruhe, Germany
<b>KRNET</b>	<b>Institute of Seismology, Academy of Sciences of Kyrgyz Republic, Kyrgyzstan</b>
<b>KRSC</b>	<b>Kamchatka Branch of the Geophysical Survey of the RAS, Russia</b>
<b>KRSZO</b>	<b>Geodetic and Geophysical Research Institute, Hungarian Academy of Sciences, Hungary</b>
KSA	Observatoire de Ksara, Lebanon

*Table 10.2: Continued.*

Agency Code	Agency Name
KUK	Geological Survey Department of Ghana, Ghana
LAO	Large Aperture Seismic Array, USA
<b>LDG</b>	<b>Laboratoire de Détection et de Géophysique/CEA, France</b>
LDN	University of Western Ontario, Canada
LDO	Lamont-Doherty Earth Observatory, USA
LED	Landeserdbebendienst Baden-Württemberg, Germany
LEDBW	Landeserdbebendienst Baden-Württemberg, Germany
LER	Besucherbergwerk Binweide Station, Germany
LIB	Tripoli, Libya
LIC	Station Géophysique de Lamto, Ivory Coast
LIM	Lima, Peru
LIS	Instituto de Meteorologia, Portugal
<b>LIT</b>	<b>Geological Survey of Lithuania, Lithuania</b>
<b>LJU</b>	<b>Slovenian Environment Agency, Slovenia</b>
<b>LPA</b>	<b>Universidad Nacional de La Plata, Argentina</b>
LPZ	Observatorio San Calixto, Bolivia
LRSM	Long Range Seismic Measurements Project, Unknown
LSZ	Geological Survey Department of Zambia, Zambia
<b>LVSN</b>	<b>Latvian Seismic Network, Latvia</b>
<b>MAN</b>	<b>Philippine Institute of Volcanology and Seismology, Philippines</b>
MAT	The Matsushiro Seismological Observatory, Japan
MATSS	USSR
<b>MCO</b>	<b>Macao Meteorological and Geophysical Bureau, Macao, China</b>
<b>MCSM</b>	<b>Main Centre for Special Monitoring, Ukraine</b>
<b>MDD</b>	<b>Instituto Geográfico Nacional, Spain</b>
<b>MED_RCMT</b>	<b>MedNet Regional Centroid - Moment Tensors, Italy</b>
MERI	Maharashtra Engineering Research Institute, India
MES	Messina Seismological Observatory, Italy
<b>MEX</b>	<b>Instituto de Geofísica de la UNAM, Mexico</b>
<b>MIRAS</b>	<b>Mining Institute of the Ural Branch of the Russian Academy of Sciences, Russia</b>
MNH	Institut für Angewandte Geophysik der Universität München, Germany
MOLD	Institute of Geophysics and Geology, Moldova
<b>MOS</b>	<b>Geophysical Survey of Russian Academy of Sciences, Russia</b>
MOZ	Direccao Nacional de Geologia, Mozambique
MOZAR	Mozambique
<b>MRB</b>	<b>Institut Cartogràfic i Geològic de Catalunya, Spain</b>
MSI	Messina Seismological Observatory, Italy
MSSP	Micro Seismic Studies Programme, PINSTECH, Pakistan
MSUGS	Michigan State University, Department of Geological Sciences, USA
MUN	Mundaring Observatory, Australia
NAI	University of Nairobi, Kenya
<b>NAM</b>	<b>The Geological Survey of Namibia, Namibia</b>
<b>NAO</b>	<b>Stiftelsen NORSAR, Norway</b>
NCEDC	Northern California Earthquake Data Center, USA
<b>NDI</b>	<b>National Centre for Seismology of the Ministry of Earth Sciences of India, India</b>
NEGSR	North East (Magadan) Branch, Geophysical Survey, Russian Academy of Sciences, Russia



Table 10.2: Continued.

Agency Code	Agency Name
<b>NEIC</b>	<b>National Earthquake Information Center, USA</b>
NEIS	National Earthquake Information Service, USA
<b>NERS</b>	<b>North Eastern Regional Seismological Centre, Magadan, GS RAS, Russia</b>
<b>NIC</b>	<b>Cyprus Geological Survey Department, Cyprus</b>
<b>NIED</b>	<b>National Research Institute for Earth Science and Disaster Re- siliience, Japan</b>
NKSZ	USSR
<b>NNC</b>	<b>National Nuclear Center, Kazakhstan</b>
NOGSR	North Ossetia (Alania) Branch, Geophysical Survey, Russian Academy of Sciences, Russia
<b>NOU</b>	<b>IRD Centre de Nouméa, New Caledonia</b>
NSSC	National Syrian Seismological Center, Syria
<b>NSSP</b>	<b>National Survey of Seismic Protection, Armenia</b>
OBGSR	Central (Obninsk) Branch, Geophysical Survey, Russian Academy of Sci- ences, Russia
OBM	Institute of Astronomy and Geophysics, Mongolian Academy of Sciences, Mongolia
OGAUC	Centro de Investigação da Terra e do Espaço da Universidade de Coim- bra, Portugal
OGSO	Ohio Geological Survey, USA
<b>OMAN</b>	<b>Sultan Qaboos University, Oman</b>
ORF	Orfeus Data Center, Netherlands
<b>OSPL</b>	<b>Observatorio Sismologico Politecnico Loyola, Dominican Re- public</b>
OSUB	Osservatorio Sismologico Universita di Bari, Italy
<b>OSUNB</b>	<b>Observatory Seismological of the University of Brasilia, Brazil</b>
<b>OTT</b>	<b>Canadian Hazards Information Service, Natural Resources Canada, Canada</b>
PAL	Palisades, USA
PAS	California Institute of Technology, USA
PDA	Universidade dos Açores, Portugal
<b>PDG</b>	<b>Institute of Hydrometeorology and Seismology of Montenegro, Montenegro</b>
PEK	Peking, China
PGC	Pacific Geoscience Centre, Canada
<b>PJWWP</b>	<b>Private Observatory of Pawel Jacek Wiejacz, D.Sc., Poland</b>
<b>PLV</b>	<b>Institute of Geophysics, Viet Nam Academy of Science and Technology, Viet Nam</b>
PMEL	Pacific seismicity from hydrophones, USA
PMR	Alaska Tsunami Warning Center,, USA
PNNL	Pacific Northwest National Laboratory, USA
<b>PNSN</b>	<b>Pacific Northwest Seismic Network, USA</b>
<b>PPT</b>	<b>Laboratoire de Géophysique/CEA, French Polynesia</b>
<b>PRE</b>	<b>Council for Geoscience, South Africa</b>
<b>PRU</b>	<b>Institute of Geophysics, Czech Academy of Sciences, Czech Re- public</b>
PTO	Instituto Geofísico da Universidade do Porto, Portugal
<b>PTWC</b>	<b>Pacific Tsunami Warning Center, USA</b>

*Table 10.2: Continued.*

Agency Code	Agency Name
<b>QCP</b>	<b>Manila Observatory, Philippines</b>
QUE	Pakistan Meteorological Department, Pakistan
QUI	Escuela Politécnica Nacional, Ecuador
RAB	Rabaul Volcanological Observatory, Papua New Guinea
RBA	Université Mohammed V, Morocco
REN	MacKay School of Mines, USA
<b>REY</b>	<b>Icelandic Meteorological Office, Iceland</b>
<b>RHSSO</b>	<b>Republic Hydrometeorological Service, Seismological Observatory, Banja Luka, Bosnia and Herzegovina</b>
<b>RISSC</b>	<b>Laboratory of Research on Experimental and Computational Seimology, Italy</b>
RMIT	Royal Melbourne Institute of Technology, Australia
ROC	Odenbach Seismic Observatory, USA
<b>ROM</b>	<b>Istituto Nazionale di Geofisica e Vulcanologia, Italy</b>
RRLJ	Regional Research Laboratory Jorhat, India
RSMAC	Red Sísmica Mexicana de Apertura Continental, Mexico
<b>RSNC</b>	<b>Red Sismológica Nacional de Colombia, Colombia</b>
<b>RSPR</b>	<b>Red Sísmica de Puerto Rico, USA</b>
RYD	King Saud University, Saudi Arabia
SAGSR	Sakhalin Branch, Geophysical Survey, Russian Academy of Sciences, Russia
SAPSE	Southern Alps Passive Seismic Experiment, New Zealand
SAR	Sarajevo Seismological Station, Bosnia and Herzegovina
<b>SARA</b>	<b>SARA Electronic Instrument s.r.l., Italy</b>
SBDV	USSR
<b>SCB</b>	<b>Observatorio San Calixto, Bolivia</b>
SCEDC	Southern California Earthquake Data Center, USA
SCSIO	Key Laboratory of Ocean and Marginal Sea Geology, South China Sea, China
<b>SDD</b>	<b>Universidad Autonoma de Santo Domingo, Dominican Republic</b>
SEA	Geophysics Program AK-50, USA
SET	Setif Observatory, Algeria
<b>SFS</b>	<b>Real Instituto y Observatorio de la Armada, Spain</b>
<b>SGS</b>	<b>Saudi Geological Survey, Saudi Arabia</b>
SHL	Central Seismological Observatory, India
<b>SIGU</b>	<b>Subbotin Institute of Geophysics, National Academy of Sciences, Ukraine</b>
SIK	Seismic Institute of Kosovo, Unknown
SIO	Scripps Institution of Oceanography, USA
<b>SJA</b>	<b>Instituto Nacional de Prevención Sísmica, Argentina</b>
SJS	Instituto Costarricense de Electricidad, Costa Rica
<b>SKHL</b>	<b>Sakhalin Experimental and Methodological Seismological Expedition, GS RAS, Russia</b>
SKL	Sakhalin Complex Scientific Research Institute, Russia
<b>SKO</b>	<b>Seismological Observatory Skopje, North Macedonia</b>
SLC	Salt Lake City, USA
SLM	Saint Louis University, USA
SLUB	Seismological Laboratory of University of Basrah, Iraq

Table 10.2: Continued.

Agency Code	Agency Name
<b>SNET</b>	<b>Servicio Nacional de Estudios Territoriales, El Salvador</b>
SNM	New Mexico Institute of Mining and Technology, USA
SNSN	Saudi National Seismic Network, Saudi Arabia
<b>SOF</b>	<b>National Institute of Geophysics, Geology and Geography, Bulgaria</b>
SOMC	Seismological Observatory of Mount Cameroon, Cameroon
<b>SOME</b>	<b>Seismological Experimental Methodological Expedition, Kazakhstan</b>
SPA	USGS - South Pole, Antarctica
SPGM	Service de Physique du Globe, Morocco
SPITAK	Armenia
SRI	Stanford Research Institute, USA
SSN	Sudan Seismic Network, Sudan
<b>SSNC</b>	<b>Servicio Sismológico Nacional Cubano, Cuba</b>
SSS	Centro de Estudios y Investigaciones Geotecnicas del San Salvador, El Salvador
STK	Stockholm Seismological Station, Sweden
<b>STR</b>	<b>EOST / RéNaSS, France</b>
STU	Stuttgart Seismological Station, Germany
<b>SVSA</b>	<b>Sistema de Vigilância Sismológica dos Açores, Portugal</b>
<b>SYO</b>	<b>National Institute of Polar Research, Japan</b>
SZGRF	Seismologisches Zentralobservatorium Gräfenberg, Germany
TAC	Estación Central de Tacubaya, Mexico
<b>TAN</b>	<b>Antananarivo, Madagascar</b>
TANZANIA	Tanzania Broadband Seismic Experiment, USA
<b>TAP</b>	<b>Central Weather Bureau (CWB), Chinese Taipei</b>
TAU	University of Tasmania, Australia
<b>TEH</b>	<b>Tehran University, Iran</b>
TEIC	Center for Earthquake Research and Information, USA
<b>THE</b>	<b>Department of Geophysics, Aristotle University of Thessaloniki, Greece</b>
<b>THR</b>	<b>International Institute of Earthquake Engineering and Seismology (IIEES), Iran</b>
<b>TIF</b>	<b>Institute of Earth Sciences/ National Seismic Monitoring Center, Georgia</b>
<b>TIR</b>	<b>Institute of Geosciences, Polytechnic University of Tirana, Albania</b>
<b>TRI</b>	<b>Istituto Nazionale di Oceanografia e di Geofisica Sperimentale (OGS), Italy</b>
<b>TRN</b>	<b>The Seismic Research Centre, Trinidad and Tobago</b>
TTG	Titograd Seismological Station, Montenegro
TUL	Oklahoma Geological Survey, USA
<b>TUN</b>	<b>Institut National de la Météorologie, Tunisia</b>
TVA	Tennessee Valley Authority, USA
<b>TXNET</b>	<b>Texas Seismological Network, University of Texas at Austin, USA</b>
TZN	University of Dar Es Salaam, Tanzania
UAF	Department of Geosciences, USA
UATDG	The University of Arizona, Department of Geosciences, USA

*Table 10.2: Continued.*

Agency Code	Agency Name
UAV	Red Sismológica de Los Andes Venezolanos, Venezuela
UCB	University of Colorado, Boulder, USA
<b>UCC</b>	<b>Royal Observatory of Belgium, Belgium</b>
UCDES	Department of Earth Sciences, United Kingdom
<b>UCR</b>	<b>Sección de Sismología, Vulcanología y Exploración Geofísica, Costa Rica</b>
UCSC	Earth & Planetary Sciences, USA
UESG	School of Geosciences, United Kingdom
UGN	Institute of Geonics AS CR, Czech Republic
ULE	University of Leeds, United Kingdom
UNAH	Universidad Nacional Autonoma de Honduras, Honduras
<b>UPA</b>	<b>Universidad de Panama, Panama</b>
UPIES	Institute of Earth- and Environmental Science, Germany
<b>UPP</b>	<b>University of Uppsala, Sweden</b>
<b>UPSL</b>	<b>University of Patras, Department of Geology, Greece</b>
UREES	Department of Earth and Environmental Science, USA
USAEC	United States Atomic Energy Commission, USA
USCGS	United States Coast and Geodetic Survey, USA
USGS	United States Geological Survey, USA
UTEP	Department of Geological Sciences, USA
UUSS	The University of Utah Seismograph Stations, USA
UVC	Universidad del Valle, Colombia
UWMDG	University of Wisconsin-Madison, Department of Geoscience, USA
<b>VAO</b>	<b>Instituto Astronomico e Geofisico, Brazil</b>
<b>VIE</b>	<b>Zentralanstalt für Meteorologie und Geodynamik (ZAMG), Austria</b>
VMGSR	Voronezh Crystalline Massif Branch, Geophysical Survey, RAS, Russia
VSI	University of Athens, Greece
VUW	Victoria University of Wellington, New Zealand
<b>WAR</b>	<b>Institute of Geophysics, Polish Academy of Sciences, Poland</b>
WASN	USA
<b>WBNET</b>	<b>Institute of Geophysics, Czech Academy of Sciences, Czech Republic</b>
<b>WEL</b>	<b>Institute of Geological and Nuclear Sciences, New Zealand</b>
WES	Weston Observatory, USA
WUSTL	Washington University Earth and Planetary Sciences, USA
YAGSR	Yakut (Saha) Branch, Geophysical Survey, Russian Academy of Sciences, Russia
<b>YARS</b>	<b>Yakutiya Regional Seismological Center, GS SB RAS, Russia</b>
<b>ZAG</b>	<b>Seismological Survey of the Republic of Croatia, Croatia</b>
ZEMSU	USSR
<b>ZUR</b>	<b>Swiss Seismological Service (SED), Switzerland</b>
ZUR_RMT	Zurich Moment Tensors, Switzerland

**Table 10.3:** Phases reported to the ISC. These include phases that could not be matched to an appropriate ak135 phases. Those agencies that reported at least 10% of a particular phase are also shown.

Reported Phase	Total	Agencies reporting
P	4864824	
S	2176271	JMA (15%), TAP (15%)
AML	1269050	ROM (39%), WEL (21%), ATH (11%)
NULL	619092	IDC (32%), NEIC (31%), AEIC (12%)
IAML	590066	NEIC (49%), AFAD (19%)
IAmb	477719	NEIC (98%)
Pg	344703	ISK (22%), STR (11%), ZAG (11%)
Pn	309260	NEIC (28%), ISK (21%)
Sg	286237	ZAG (14%), ISK (14%), MDD (11%), STR (11%)
LR	115952	IDC (91%)
pmax	111865	MOS (65%), BJI (35%)
Sn	110145	MDD (14%), IDC (11%), NEIC (11%)
IAMs_20	96986	NEIC (98%)
SG	78764	HEL (51%), PRU (30%)
PG	72240	HEL (57%), PRU (21%), IPEC (11%)
PKP	68564	IDC (32%), VIE (21%), MCSM (12%)
L	40705	BJI (95%)
IVmb_Lg	39439	MDD (100%)
Lg	35987	NNC (58%), IDC (22%), KRSZO (15%)
PN	33642	MOS (36%), HEL (32%), IPEC (11%)
IAmb_Lg	31100	NEIC (100%)
T	26675	IDC (99%)
smax	26489	HEL (70%), MOS (22%)
SN	24186	HEL (73%), OTT (11%)
A	23067	TEH (56%), JMA (27%), SKHL (17%)
PKPbc	22076	IDC (73%)
pP	20630	BJI (25%), ISC (16%), IDC (14%), GFZ (11%)
PKIKP	18149	MOS (99%)
MSG	17213	HEL (100%)
PcP	14201	IDC (62%), ISC (12%)
MLR	13512	MOS (100%)
PP	12852	IDC (20%), BJI (19%), BELR (16%)
SB	12708	HEL (100%)
PKPdf	11229	NEIC (41%), INMG (14%), BER (11%)
PB	10328	HEL (100%)
AMS	9694	LVSN (39%), PRU (33%), CLL (25%)
SS	9046	MOS (31%), BELR (26%), BJI (20%)
PKPab	8551	IDC (48%), INMG (17%), BGR (12%)
x	7515	CLL (31%), BRG (29%), TRN (14%), PRU (12%), NDI (11%)
sP	6705	BJI (67%), ISC (18%)
PKiKP	6511	VIE (34%), IDC (31%), BELR (17%)
Smax	5884	BYKL (100%)
Trac	5132	OTT (100%)
Pmax	4947	BYKL (99%)
Amp	4700	BRG (100%)
PKP2	4051	MOS (99%)
PPP	3972	MOS (49%), BELR (45%)
ScP	3731	IDC (74%), ISC (12%)
SSS	3513	BELR (56%), MOS (33%)
LQ	2929	BELR (51%), PPT (40%)
LRM	2911	BELR (100%)
PKKPbc	2908	IDC (98%)
pPKP	2621	VIE (64%), IDC (12%)
*PP	2462	MOS (100%)
LG	2236	BRA (75%), OTT (25%)
I	2221	IDC (100%)
AMB	2188	SKHL (98%)
IVmb_VC	2065	MDD (100%)
SKS	2054	BJI (48%), BELR (38%)
PKhKP	2051	IDC (100%)
PKPAB	1819	PRU (100%)
sS	1705	BJI (73%), BELR (20%)
PKPBC	1599	PRU (100%)
Pdiff	1460	IDC (55%), VIE (30%)
IVmB_BB	1165	BER (83%), SSNC (12%)
max	1105	BYKL (100%)
Sgmax	1104	NERS (100%)
SKPbc	1026	IDC (89%)
IVMs_BB	956	BER (81%)
PKPPKP	849	IDC (97%)

*Table 10.3: (continued)*

Reported Phase	Total	Agencies reporting
PKKP	826	IDC (47%), VIE (38%)
PKPDF	789	PRU (99%)
PKHKP	780	MOS (100%)
ScS	727	BJI (58%), HYB (16%)
PS	659	MOS (41%), BELR (26%), CLL (19%)
SKP	650	IDC (35%), VIE (27%), BELR (19%), PRU (11%)
END	605	ROM (93%)
SKS <sub>ac</sub>	577	HYB (29%), BER (25%), AWI (15%)
Pd <sub>if</sub>	568	NEIC (20%), INMG (13%), BJI (12%)
LH	550	CLL (100%)
SKKS	519	BELR (69%), BJI (27%)
pPKP <sub>bc</sub>	502	IDC (50%), BGR (28%)
pPKiKP	453	VIE (58%), BELR (29%)
*SS	447	MOS (100%)
AMs_VX	433	NEIC (100%)
tx	423	INMG (97%)
AMP	410	BER (85%)
LV	403	CLL (100%)
*SP	394	MOS (100%)
PPMZ	385	BJI (100%)
PD <sub>IFF</sub>	374	PRU (47%), BRA (29%), IPEC (22%)
AmB	358	KEA (100%)
SP	356	MOS (24%), BER (20%), BGR (13%)
P <sub>gmax</sub>	352	NERS (99%)
PPS	328	CLL (55%), BELR (27%)
pPKP <sub>df</sub>	291	BER (52%), CLL (19%)
PKKP <sub>ab</sub>	261	IDC (97%)
sPKP	252	BJI (68%), BELR (26%)
L <sub>m</sub>	242	CLL (100%)
PKP <sub>2bc</sub>	242	IDC (100%)
PKS	227	BELR (75%), BJI (17%)
SKP <sub>df</sub>	221	BER (51%), CLL (30%)
AM <sub>b</sub>	211	L <sub>VSN</sub> (100%)
p	198	ROM (66%), MAN (33%)
SKKP <sub>bc</sub>	193	IDC (99%)
SKKS <sub>ac</sub>	188	HYB (54%), CLL (36%)
SSSS	188	CLL (99%)
pPKP <sub>ab</sub>	183	CLL (51%), IDC (22%)
SKKP	176	BELR (68%), VIE (12%), IDC (11%)
S <sub>b</sub>	172	BYKL (47%), NAO (24%), CLL (22%)
S <sub>mS</sub>	164	BGR (71%), ZUR (29%)
P <sub>mP</sub>	152	ZUR (53%), BGR (47%)
P <sub>b</sub>	151	BYKL (64%), NAO (17%)
P <sub>3KPbc</sub>	148	IDC (100%)
H	136	IDC (100%)
PKP <sub>pre</sub>	136	NEIC (54%), PRU (31%), CLL (15%)
PKP <sub>dif</sub>	126	CLL (96%)
AM <sub>WP</sub>	123	NEIC (100%)
P <sub>cS</sub>	117	BJI (93%)
P <sub>gPg</sub>	116	BYKL (100%)
L <sub>mV</sub>	115	CLL (100%)
L <sub>mH</sub>	110	CLL (100%)
PSKS	101	CLL (80%), BRG (20%)
BAZ	100	DNK (97%)
P <sub>4KPbc</sub>	97	IDC (100%)
PCP	88	LPA (41%), PRU (30%), MOS (15%)
BAZ-P	79	DNK (100%)
sPP	77	CLL (87%), BRG (13%)
pPP	75	LPA (45%), CLL (43%)
rx	74	SVSA (42%), SKHL (30%), INMG (28%)
S <sub>dif</sub>	72	CLL (61%), BRG (31%)
P'P'	69	VIE (96%)
SKS <sub>df</sub>	68	HYB (51%), BER (21%), CLL (21%)
(PKP <sub>ab</sub> )	65	CLL (100%)
S <sub>gSg</sub>	65	BYKL (100%)
SME	64	BJI (100%)
SMN	64	BJI (100%)
s	64	MAN (100%)
SKP <sub>ab</sub>	63	IDC (78%), INMG (16%)
P <sub>x</sub>	62	CLL (100%)
sPKiKP	62	BELR (65%), HYB (11%)

*Table 10.3: (continued)*

Reported Phase	Total	Agencies reporting
m	58	SIGU (100%)
ASPG	55	OSPL (80%), BER (20%)
ATPG	55	OSPL (80%), BER (20%)
X	54	SYO (63%), BGR (31%)
ASSG	53	OSPL (79%), BER (21%)
ATSG	53	OSPL (79%), BER (21%)
PKPmax	52	CLL (100%)
PKKS	50	BELR (96%)
pPcP	49	IDC (90%)
SPP	49	BELR (49%), BRG (24%), MOS (14%)
PPPP	47	CLL (96%)
SKIKS	41	LPA (100%)
PKP2ab	41	IDC (100%)
pPdiff	38	VIE (92%)
(sP)	38	CLL (100%)
IAMLHF	37	BER (100%)
sSKS	37	BELR (100%)
r	36	BRG (100%)
(PKiKP)	36	CLL (100%)
SKIKP	35	LPA (100%)
SKKSdf	35	CLL (86%), HYB (11%)
PKIKS	34	LPA (100%)
SCS	34	LPA (100%)
SKPa	33	NAO (97%)
PKP1	30	PPT (100%)
PSP	29	LPA (100%)
(pP)	27	CLL (100%)
PKSdf	25	BER (76%), CLL (16%)
(PKPdf)	25	CLL (100%)
sSS	24	CLL (92%)
SKiKP	24	IDC (88%)
BAZ-Pn	22	DNK (100%)
cP	21	DMN (100%)
P3KP	21	IDC (100%)
Rg	20	IDC (90%)
PKKPdf	19	WAR (32%), CLL (21%), HYB (16%), BRG (16%), OMAN (16%)
sPKPbc	19	BGR (74%), CLL (26%)
(PKPbc)	18	CLL (100%)
Plp	18	CLL (100%)
R2	18	CLL (100%)
sPKPdf	17	CLL (59%), BRG (18%)
Sdiff	16	LJU (50%), VIE (31%), OMAN (19%)
pPdif	15	BRG (47%), CLL (27%), BELR (20%)
(Sg)	15	CLL (87%), CFUSG (13%)
BAZ-Sn	15	DNK (100%)
(SSS)	15	CLL (100%)
PKPlp	14	CLL (100%)
(PKPdif)	14	CLL (100%)
Lmax	14	CLL (100%)
E	14	YARS (50%), INMG (36%), SSNC (14%)
P*	13	BGR (92%)
PSPS	13	CLL (100%)
(SSSS)	13	CLL (100%)
Sglp	13	CLL (100%)
sSSS	12	CLL (100%)
pwP	12	NEIC (92%)
MSN	12	HEL (75%), BER (25%)
PPPrev	12	CLL (100%)
PSS	11	CLL (91%)
(SS)	11	CLL (100%)
sPPP	11	CLL (100%)
SKSP	11	CLL (82%), BRG (18%)
sPdif	10	CLL (50%), BELR (30%), BRG (20%)
(PP)	10	CLL (100%)
PSSrev	10	CLL (100%)
Sm	10	CFUSG (100%)
P'P'df	9	AWI (67%), HYB (22%), NEIC (11%)
AP	9	MOS (100%)
AMPN	9	SJA (100%)
(Pg)	8	CLL (100%)
AMSN	8	SJA (100%)



*Table 10.3: (continued)*

Reported Phase	Total	Agencies reporting
(PPS)	8	CLL (100%)
(S)	8	CFUSG (100%)
Sx	8	CLL (100%)
RG	8	HEL (100%)
SDIFF	8	LPA (75%), BRA (25%)
sPS	8	CLL (88%), BRG (12%)
Pg_3	7	ATH (100%)
PKPPKpdf	7	CLL (100%)
Pn_2	7	ATH (100%)
(PKP)	7	CLL (100%)
pS	7	BRG (57%), CLL (29%), BELR (14%)
rg	7	BRG (100%)
SDIF	7	PRU (100%)
SKKPdf	7	BRG (57%), CLL (29%), HYB (14%)
(PPP)	6	CLL (100%)
PnA	6	THR (100%)
sSSS	6	CLL (100%)
PKPdfc	6	PJWWP (100%)
(Sn)	6	CLL (100%)
sPKPab	6	CLL (67%), BRG (33%)
SKSSKSac	6	CLL (67%), BRG (33%)
pPPS	6	CLL (100%)
M	6	LJU (100%)
SH	6	SYO (100%)
pPn	5	AWI (80%), BJI (20%)
(sPP)	5	CLL (100%)
(pPKPab)	5	CLL (100%)
PSKSrev	5	CLL (100%)
sPPS	5	CLL (100%)
sSP	5	CLL (60%), BRG (40%)
sSKPdf	5	CLL (100%)
PKPdfd	5	PJWWP (100%)
PKPPcP	5	BRG (100%)
(P)	5	CFUSG (100%)
BAZ-Sg	4	DNK (100%)
Pm	4	CFUSG (100%)
sPn	4	AWI (75%), HYB (25%)
R3	4	CLL (100%)
SKKSacre	4	CLL (100%)
SgL	4	CLL (100%)
P'P'bc	4	AWI (100%)
PKSbc	4	CLL (100%)
PPPPrev	3	CLL (100%)
(Pn)	3	CLL (100%)
(pPKiKP)	3	CLL (100%)
AMPG	3	SJA (100%)
XS	3	PRU (100%)
P9	3	MEX (67%), BER (33%)
PKPpB	3	WAR (100%)
(SKPdf)	3	CLL (100%)
PPlp	3	CLL (100%)
pSKSac	3	CLL (100%)
P3	3	EAF (100%)
PKPPKpbc	3	CLL (100%)
(SP)	3	CLL (100%)
SA	3	SJA (100%)
sSdif	3	CLL (67%), BRG (33%)
IAML_BB	3	THR (100%)
AMSG	3	SJA (100%)
Pg_4	3	ATH (100%)
PKPdf(2)	2	CLL (100%)
PPmax	2	CLL (100%)
(pPKPdf)	2	CLL (100%)
sPKKPbc	2	CLL (100%)
(SKSP)	2	CLL (100%)
SKSSKS	2	BRG (100%)
sPcP	2	CLL (100%)
(PSPS)	2	CLL (100%)
(sPPP)	2	CLL (100%)
PSPSrev	2	CLL (100%)
(SKSac)	2	CLL (100%)

**Table 10.3:** (continued)

Reported Phase	Total	Agencies reporting
ES	2	EAF (50%), INMG (50%)
PKPdfmax	2	CLL (100%)
SSP	2	CLL (100%)
(SKKSac)	2	CLL (100%)
pPS	2	CLL (100%)
(SKSdf)	2	CLL (100%)
(Sdif)	2	CLL (100%)
pPPmax	2	CLL (100%)
PPP(2)	2	LPA (100%)
PKPabmax	2	CLL (100%)
(PS)	2	CLL (100%)
(PSKS)	2	CLL (100%)
SNE	2	BRA (100%)
(pPKPbc)	2	CLL (100%)
PKPc	2	PJWWP (100%)
pPKSbc	2	CLL (100%)
S*	2	BJI (50%), BGR (50%)
(P	2	CFUSG (100%)
pPmax	2	CLL (100%)
P(2)	2	CLL (100%)
Pn_1	2	ATH (100%)
pPKPdif	2	CLL (100%)
(SKKSdf)	2	CLL (100%)
PKPabd	2	PJWWP (100%)
(Pdif)	2	CLL (100%)
sPKP3ab	1	CLL (100%)
S'S'ac	1	HYB (100%)
Sg_2	1	ATH (100%)
(sPKPdf)	1	CLL (100%)
(PKKPab)	1	CLL (100%)
Sg_3	1	ATH (100%)
pSKPab	1	CLL (100%)
SS(2)	1	LPA (100%)
pSKKSac	1	CLL (100%)
sPKSab	1	CLL (100%)
PKKSbc	1	CLL (100%)
sPmax	1	CLL (100%)
po	1	KRSC (100%)
SPS	1	CLL (100%)
sPPPP	1	CLL (100%)
pSKSP	1	CLL (100%)
PKiK	1	HYB (100%)
pPdifmax	1	CLL (100%)
XP	1	MOS (100%)
pPKPPKPb	1	CLL (100%)
PP2	1	BER (100%)
SCP	1	IPEC (100%)
(sPKPbc)	1	CLL (100%)
SKSab	1	BER (100%)
pPKSdf	1	CLL (100%)
Pdifmax	1	CLL (100%)
pP5	1	BER (100%)
(PcP)	1	CLL (100%)
pPKKPdf	1	CLL (100%)
sSKKSacr	1	CLL (100%)
(PSS)	1	CLL (100%)
sSKKSac	1	CLL (100%)
(PKSdf)	1	CLL (100%)
KP	1	IPEC (100%)
sPSS	1	CLL (100%)
PKPab(2)	1	CLL (100%)
(sS)	1	CLL (100%)
(sPcP)	1	CLL (100%)
pPKPlp	1	CLL (100%)
P4KP	1	IDC (100%)
SKPPKPdf	1	CLL (100%)
S3	1	EAF (100%)
SN5	1	ISN (100%)
pPPPmax	1	CLL (100%)
S5	1	INMG (100%)
EP	1	EAF (100%)

**Table 10.3:** (continued)

Reported Phase	Total	Agencies reporting
SSP <sub>rev</sub>	1	CLL (100%)
P <sub>diff</sub> X	1	SYO (100%)
P <sub>1</sub>	1	DNK (100%)
S <sub>r</sub>	1	MEX (100%)
EN	1	INMG (100%)
(sSKP <sub>bc</sub> )	1	CLL (100%)
IVM <sub>s</sub> BB	1	MEX (100%)
PKKS <sub>df</sub>	1	CLL (100%)
(PKS <sub>bc</sub> )	1	CLL (100%)
PPP <sub>lp</sub>	1	CLL (100%)
SKPPK <sub>Pbc</sub>	1	CLL (100%)
PKPPK <sub>Pab</sub>	1	CLL (100%)
pPKPPK <sub>Pd</sub>	1	CLL (100%)
pP <sub>9</sub>	1	BER (100%)
SSS(2)	1	LPA (100%)
PKP <sub>diff</sub> 2	1	CLL (100%)
(sPKiKP)	1	CLL (100%)
SSS <sub>rev</sub>	1	CLL (100%)
(sSKP <sub>df</sub> )	1	CLL (100%)
pSP	1	CLL (100%)
(SKP <sub>bc</sub> )	1	CLL (100%)
SS <sub>rev</sub>	1	CLL (100%)
pZP	1	SYO (100%)
(sSSS)	1	CLL (100%)
S'S' <sub>df</sub>	1	HYB (100%)
sPKK <sub>Pdf</sub>	1	CLL (100%)
pKPPK <sub>Pdf</sub>	1	CLL (100%)
sPKPPK <sub>Pd</sub>	1	CLL (100%)
(PPP <sub>rev</sub> )	1	CLL (100%)
P <sub>diff</sub> lp	1	CLL (100%)
S <sub>s</sub>	1	TRI (100%)
SSS <sub>max</sub>	1	CLL (100%)
pPPK <sub>Pdf</sub>	1	CLL (100%)
PP(2)	1	CLL (100%)
sPKS <sub>bc</sub>	1	CLL (100%)
pPPP	1	CLL (100%)
BAZ-P <sub>g</sub>	1	DNK (100%)
(sPKP <sub>ab</sub> )	1	CLL (100%)
sP <sub>diff</sub> ma	1	CLL (100%)
pPKK <sub>Pab</sub>	1	CLL (100%)
pPPP <sub>rev</sub>	1	CLL (100%)
sScS	1	CLL (100%)
P <sub>n</sub> 3	1	ATH (100%)
PKP <sub>bc</sub> (2)	1	CLL (100%)
sSPS	1	CLL (100%)
(sS <sub>df</sub> )	1	CLL (100%)
KPP	1	IPEC (100%)
Scs	1	PJWWP (100%)
(S)	1	CFUSG (100%)
pP <sub>7</sub>	1	BER (100%)
(SKK <sub>Pdf</sub> )	1	CLL (100%)
pPKP <sub>ab</sub> ma	1	CLL (100%)
BAZ-P <sub>1</sub>	1	DNK (100%)
P <sub>n</sub> 4	1	ATH (100%)
sK <sub>Pbc</sub>	1	BGR (100%)
PKP <sub>3ab</sub>	1	CLL (100%)
sPSKS	1	CLL (100%)
SKS <sub>d</sub>	1	HYB (100%)
SbSb	1	UCC (100%)

**Table 10.4:** Reporters of amplitude data

Agency	Number of reported amplitudes	Number of amplitudes in ISC located events	Number used for ISC <i>mb</i>	Number used for ISC <i>MS</i>
NEIC	980298	681846	227993	42282
IDC	576160	551897	129769	81245
ROM	504065	23325	0	0
AUST	292724	25286	10452	0
WEL	233100	25981	0	0
GFZ	215883	215029	87452	0
ATH	142751	16386	0	0
DJA	137764	105967	21712	0
MCSM	133435	100827	45879	0
MDD	116297	15542	0	0
AFAD	104999	12034	0	0
ISK	95561	17866	0	0
MOS	93370	90088	35424	9913
THE	93191	24561	0	0
RSNC	76901	24145	3968	0
BJI	76007	73402	18991	26555
NNC	73307	25908	76	0
VIE	59393	32694	11552	0
INMG	53600	28198	3191	0
SJA	42615	16621	0	0
SOME	38920	15882	2242	0
GUC	37850	9799	0	0
HEL	33941	1641	0	0
NOU	31921	31534	14336	0
TXNET	30458	730	0	0
SSNC	26311	3821	88	0
AWI	23189	8733	1793	0
DMN	16428	15362	0	0
JMA	15304	15200	0	0
PRU	14778	6201	213	3707
SVSA	13068	1196	463	0
PPT	13052	8437	456	0
TIR	12020	3792	328	0
LDG	11156	1361	0	0
TEH	10870	4880	0	0
PRE	9993	596	0	0
ZUR	9737	1364	0	0
NDI	8754	6746	1715	44
MRB	7897	240	0	0
BER	7735	2233	18	0
BUC	7713	2504	0	0
DNK	7536	3613	2639	15
OSPL	7309	2034	0	0
LJU	6893	639	6	2
SKHL	6804	2554	0	0
BKK	6179	4069	21	0

*Table 10.4: Continued.*

Agency	Number of reported amplitudes	Number of amplitudes in ISC located events	Number used for ISC <i>mb</i>	Number used for ISC <i>MS</i>
BYKL	6110	3911	0	0
ECX	6078	1303	0	0
KRSZO	5983	349	22	0
BELR	5969	3663	625	795
BGR	5530	5464	4005	0
CLL	5195	4955	348	1856
BGS	5091	3330	2607	460
PDG	4999	2567	0	0
NIC	4713	1329	0	0
KNET	3597	1362	0	0
YARS	3136	200	0	0
JSO	3120	1921	566	0
LVSN	3111	1669	6	892
BRG	3067	1632	0	0
ASGSR	2990	1379	0	0
BGSI	2688	573	0	0
UCC	2589	2415	1959	0
BRA	2557	1400	1094	0
IPEC	2349	560	0	0
NAO	2332	2288	1267	0
MIRAS	2293	72	0	0
WBNET	2188	24	0	0
SKO	2053	368	0	0
OTT	2024	100	0	0
SCB	1753	448	0	0
CFUSG	1354	1108	0	0
NERS	1207	207	0	0
MAN	1154	1050	0	0
KEA	911	538	0	75
IGIL	909	505	111	135
NAM	861	62	0	0
PLV	484	194	0	0
GCG	461	332	0	0
SIGU	423	334	0	0
ISN	399	389	0	0
THR	355	355	0	0
FCIAR	257	180	42	0
EAF	237	57	0	2
WAR	176	160	0	113
UPA	61	0	0	0
HYB	34	28	0	5
PJWWP	16	16	0	0

# 11

## Glossary of ISC Terminology

- **ADSL**

An acronym for Agency.Deployment.Station.Location, a method of describing a seismic station. Allowing station coordinates to be distinguished by many more parameters.
- **Agency/ISC data contributor**

An academic or government institute, seismological organisation or company, geological/meteorological survey, station operator or author that reports or contributed data in the past to the ISC or one of its predecessors. Agencies may contribute data to the ISC directly, or indirectly through other ISC data contributors.
- **Agency code**

A unique, maximum eight-character code for a data reporting agency (e.g. NEIC, GFZ, BUD) or author (e.g. ISC, ISC-EHB, IASPEI). Often the agency code is the commonly used acronym of the reporting institute.
- **Arrival**

A phase pick at a station is characterised by a phase name and an arrival time.
- **Associated phase**

Associated phase arrival or amplitude measurements represent a collection of observations belonging to (i.e. generated by) an event. The complete set of observations are associated to the prime hypocentre.
- **Azimuthal gap/Secondary azimuthal gap**

The azimuthal gap for an event is defined as the largest angle between two stations with defining phases when the stations are ordered by their event-to-station azimuths. The secondary azimuthal gap is the largest azimuthal gap a single station closes.
- **BAAS**

Seismological bulletins published by the British Association for the Advancement of Science (1913-1917) under the leadership of H.H. Turner. These bulletins are the predecessors of the ISS Bulletins and include reports from stations distributed worldwide.
- **Bulletin**

An ordered list of event hypocentres, uncertainties, focal mechanisms, network magnitudes, as well as phase arrival and amplitude observations associated to each event. An event bulletin may list all the reported hypocentres for an event. The convention in the ISC Bulletin is that the preferred (prime) hypocentre appears last in the list of reported hypocentres for an event.

- Catalogue

An ordered list of event hypocentres, uncertainties and magnitudes. An event catalogue typically lists only the preferred (prime) hypocentres and network magnitudes.

- CoSOI/IASPEI

Commission on Seismological Observation and Interpretation, a commission of IASPEI that prepares and discusses international standards and procedures in seismological observation and interpretation.

- Defining/Non-defining phase

A defining phase is used in the location of the event (time-defining) or in the calculation of the network magnitude (magnitude-defining). Non-defining phases are not used in the calculations because they suffer from large residuals or could not be identified.

- Direct/Indirect report

A data report sent (e-mailed) directly to the ISC, or indirectly through another ISC data contributor.

- Duplicates

Nearly identical phase arrival time data reported by one or more agencies for the same station. Duplicates may be created by agencies reporting observations from other agencies, or several agencies independently analysing the waveforms from the same station.

- Event

A natural (e.g. earthquake, landslide, asteroid impact) or anthropogenic (e.g. explosion) phenomenon that generates seismic waves and its source can be identified by an event location algorithm.

- Grouping

The ISC algorithm that organises reported hypocentres into groups of events. Phases associated to any of the reported hypocentres will also be associated to the preferred (prime) hypocentre. The grouping algorithm also attempts to associate phases that were reported without an accompanying hypocentre to events.

- Ground Truth

An event with a hypocentre known to certain accuracy at a high confidence level. For instance, GT0 stands for events with exactly known location, depth and origin time (typically explosions); GT5 stands for events with their epicentre known to 5 km accuracy at the 95% confidence level, while their depth and origin time may be known with less accuracy.

- Ground Truth database

On behalf of IASPEI, the ISC hosts and maintains the IASPEI Reference Event List, a bulletin of ground truth events.



- IASPEI

International Association of Seismology and Physics of the Earth Interior, [www.iaspei.org](http://www.iaspei.org).

- International Registry of Seismograph Stations (IR)

Registry of seismographic stations, jointly run by the ISC and the World Data Center for Seismology, Denver (NEIC). The registry provides and maintains unique five-letter codes for stations participating in the international parametric and waveform data exchange.

- ISC Bulletin

The comprehensive bulletin of the seismicity of the Earth stored in the ISC database and accessible through the ISC website. The bulletin contains both natural and anthropogenic events. Currently the ISC Bulletin spans more than 60 years (1960-to date) and it is constantly extended by adding both recent and past data. Eventually the ISC Bulletin will contain all instrumentally recorded events since 1900.

- ISC Governing Council

According to the ISC Bye-laws: The Governing Council of the ISC is the forum of the Formal Representatives of all Members of the ISC.

- ISC-located events

A subset of the events selected for ISC review are located by the ISC. The rules for selecting an event for location are described in Section 10.1.3; ISC-located events are denoted by the author ISC.

- ISC Member

An academic or government institute, seismological organisation or company, geological/meteorological survey, station operator, national/international scientific organisation that contribute to the ISC budget by paying membership fees. ISC members have voting rights in the ISC Governing Council.

- ISC-PPSM

ISC-PPSM (ISC - Probabilistic Point Source Model) is a catalogue of probabilistic point source models, comprising an earthquake depth, moment tensor and source time function, calculated at the ISC to address shallow moderate magnitude earthquake depths and moment tensor uncertainties, as well as adding new constraints on earthquake source time functions.

- ISC-reviewed events

A subset of the events reported to the ISC are selected for ISC analyst review. These events may or may not be located by the ISC. The rules for selecting an event for review are described in Section 10.1.3. Non-reviewed events are explicitly marked in the ISC Bulletin by the comment following the prime hypocentre "Event not reviewed by the ISC".

- ISF

International Seismic Format ([www.isc.ac.uk/standards/isf](http://www.isc.ac.uk/standards/isf)). A standard bulletin format approved by IASPEI. The ISC Bulletin is presented in this format at the ISC website.

- ISS

International Seismological Summary (1918-1963). These bulletins are the predecessors of the ISC Bulletin and represent the major source of instrumental seismological data before the digital era. The ISS contains regionally and teleseismically recorded events from several hundreds of globally distributed stations.

- Network magnitude

The event magnitude reported by an agency or computed by the ISC locator. An agency can report several network magnitudes for the same event and also several values for the same magnitude type. The network magnitude obtained with the ISC locator is defined as the median of station magnitudes of the same magnitude type.

- Phase

A maximum eight-character code for a seismic, infrasonic, or hydroacoustic phase. During the ISC processing, reported phases are mapped to standard IASPEI phase names. Amplitude measurements are identified by specific phase names to facilitate the computation of body-wave and surface-wave magnitudes.

- Prime hypocentre

The preferred hypocentre solution for an event from a list of hypocentres reported by various agencies or calculated by the ISC.

- Reading

Parametric data that are associated to a single event and reported by a single agency from a single station. A reading typically includes one or more phase names, arrival time and/or amplitude/period measurements.

- Report/Data report

All data that are reported to the ISC are parsed and stored in the ISC database. These may include event bulletins, focal mechanisms, moment tensor solutions, macroseismic descriptions and other event comments, as well as phase arrival data that are not associated to events. Every single report sent to the ISC can be traced back in the ISC database via its unique report identifier.

- Shide Circulars

Collections of station reports for large earthquakes occurring in the period 1899-1912. These reports were compiled through the efforts of J. Milne. The reports are mainly for stations of the British Empire equipped with Milne seismographs. After Milne's death, the Shide Circulars were replaced by the Seismological Bulletins of the BAAS.

- Station code

A unique, maximum five-character code for a seismic station.

## 12

# Acknowledgements

We thank our colleagues at the Yakutia Branch of the Geophysical Survey of the Russian Academy of Sciences for kindly accepting our invitation and preparing an article for this issue of the Summary.

We are also grateful to the developers of the Generic Mapping Tools (GMT) suite of software (*Wessel et al.*, 2019) that was used extensively for producing the figures.

Finally, we thank the ISC Member Institutions, Data Contributors, Funding Agencies (including NSF Award 2414178 and Royal Society Award INT004) and Sponsors for supporting the long-term operation of the ISC.

## References

- Adamaki, A. (2017), Seismicity Analysis Using Dense Network Data : Catalogue Statistics and Possible Foreshocks Investigated Using Empirical and Synthetic Data, Ph.D. thesis, Uppsala University, urn:nbn:se:uu:diva-328057.
- Adams, R. D., A. A. Hughes, and D. M. McGregor (1982), Analysis procedures at the International Seismological Centre, *Physics of the Earth and Planetary Interiors*, 30, 85–93.
- Amante, C., and B. W. Eakins (2009), ETOPO1 1 arc-minute global relief model: procedures, data sources and analysis, *NOAA Technical Memorandum NESDIS NGDC-24*, NOAA.
- Balfour, N., R. Baldwin, and A. Bird (2008), Magnitude calculations in Antelope 4.10, *Analysis Group Note of Geological Survey of Canada*, pp. 1–13.
- Bennett, T. J., V. Oancea, B. W. Barker, Y.-L. Kung, M. Bahavar, B. C. Kohl, J. . Murphy, and I. K. Bondár (2010), The nuclear explosion database NEDB: a new database and web site for accessing nuclear explosion source information and waveforms, *Seismological Research Letters*, 81, <https://doi.org/10.1785/gssrl.81.1.12>.
- Bisztricsany, E. A. (1958), A new method for the determination of the magnitude of earthquakes, *Geofiz. Kozl*, pp. 69–76.
- Bolt, B. A. (1960), The revision of earthquake epicentres, focal depths and origin time using a high-speed computer, *Geophysical Journal of the Royal Astronomical Society*, 3, 434–440.
- Bondár, I., and K. McLaughlin (2009a), A new ground truth data set for seismic studies, *Seismological Research Letters*, 80, 465–472.
- Bondár, I., and K. McLaughlin (2009b), Seismic location bias and uncertainty in the presence of correlated and non-Gaussian travel-time errors, *Bulletin of the Seismological Society of America*, 99, 172–193.
- Bondár, I., and D. Storchak (2011), Improved location procedures at the International Seismological Centre, *Geophysical Journal International*, 186, 1220–1244.
- Bondár, I., E. R. Engdahl, X. Yang, H. A. A. Ghalib, A. Hofstetter, V. Kirchenko, R. Wagner, I. Gupta, G. Ekström, E. Bergman, H. Israelsson, and K. McLaughlin (2004), Collection of a reference event set for regional and teleseismic location calibration, *Bulletin of the Seismological Society of America*, 94, 1528–1545.
- Bondár, I., E. Bergman, E. R. Engdahl, B. Kohl, Y.-L. Kung, and K. McLaughlin (2008), A hybrid multiple event location technique to obtain ground truth event locations, *Geophysical Journal International*, 175, <https://doi.org/10.1111/j.1365246X.2008.03867x>.
- Bormann, P., and J. W. Dewey (2012), The new IASPEI standards for determining magnitudes from digital data and their relation to classical magnitudes, IS 3.3, *New Manual of Seismological Observatory Practice 2 (NMSOP-2)*, P. Bormann (Ed.), pp. 1–44, [https://doi.org/10.2312/GFZ.NMSOP-2](https://doi.org/10.2312/GFZ.NMSOP-2_IS_3.3), <http://nmsop.gfz-postsdam.de>.
- Bormann, P., and J. Saul (2008), The new IASPEI standard broadband magnitude mB, *Seism. Res. Lett*, 79(5), 698–705.
- Bormann, P., R. Liu, X. Ren, R. Gutdeutsch, D. Kaiser, and S. Castellaro (2007), Chinese national network magnitudes, their Relation to NEIC magnitudes and recommendations for new IASPEI magnitude standards, *Bulletin of the Seismological Society of America*, 97(1B), 114–127, <https://doi.org/10.1785/012006007835>.

- Bormann, P., R. Liu, Z. Xu, R. Ren, and S. Wendt (2009), First application of the new IASPEI teleseismic magnitude standards to data of the China National Seismographic Network, *Bulletin of the Seismological Society of America*, *99*, 1868–1891, <https://doi.org/10.1785/0120080010>.
- Chang, A. C., R. H. Shumway, R. R. Blandford, and B. W. Barker (1983), Two methods to improve location estimates - preliminary results, *Bulletin of the Seismological Society of America*, *73*, 281–295.
- Choy, G. L., and J. L. Boatwright (1995), Global patterns of radiated seismic energy and apparent stress, *J. Geophys. Res.*, *100*(B9), 18,205–18,228.
- Dziewonski, A. M., and F. Gilbert (1976), The effect of small, aspherical perturbations on travel times and a re-examination of the correction for ellipticity, *Geophysical Journal of the Royal Astronomical Society*, *44*, 7–17.
- Dziewonski, A. M., T.-A. Chou, and J. H. Woodhouse (1981), Determination of earthquake source parameters from waveform data for studies of global and regional seismicity, *J. Geophys. Res.*, *86*, 2825–2852.
- Engdahl, E. R., and R. H. Gunst (1966), Use of a high speed computer for the preliminary determination of earthquake hypocentres, *Bulletin of the Seismological Society of America*, *56*, 325–336.
- Engdahl, E. R., and A. Villaseñor (2002), Global seismicity: 1900–1999, *International Handbook of Earthquake Engineering and Seismology, International Geophysics series*, *81A*, 665–690.
- Engdahl, E. R., D. Di Giacomo, B. Sakarya, C. G. Gkarlaoui, J. Harris, and D. A. Storchak (2020), ISC-EHB 1964–2016, an Improved Data Set for Studies of Earth Structure and Global Seismicity, *Earth and Space Science*, *7*(1), <https://doi.org/10.1029/2019EA000897>.
- Engdahl, E. R., R. van der Hilst, and R. Buland (1998), Global teleseismic earthquake relocation with improved travel times and procedures for depth determination, *Bulletin of the Seismological Society of America*, *88*, 722–743.
- Flinn, E. A., and E. R. Engdahl (1965), Proposed basis for geographical and seismic regionalization, *Reviews of Geophysics*, *3*(1), 123–149.
- Flinn, E. A., E. R. Engdahl, and A. R. Hill (1974), Seismic and geographical regionalization, *Bulletin of the Seismological Society of America*, *64*, 771–993.
- Gutenberg, B. (1945a), Amplitudes of P, PP and S and magnitude of shallow earthquakes, *Bulletin of the Seismological Society of America*, *35*, 57–69.
- Gutenberg, B. (1945b), Magnitude determination of deep-focus earthquakes, *Bulletin of the Seismological Society of America*, *35*, 117–130.
- Gutenberg, B. (1945c), Amplitudes of surface waves and magnitudes of shallow earthquakes, *Bulletin of the Seismological Society of America*, *35*, 3–12.
- Gutenberg, B., and C. F. Richter (1956), Magnitude and Energy of earthquakes, *Ann. Geof.*, *9*, 1–5.
- Hutton, L. K., and D. M. Boore (1987), The ML scale in southern California, *Bulletin of the Seismological Society of America*, *77*, 2074–2094.
- IASPEI (2005), Summary of Magnitude Working group recommendations on standard procedures for determining earthquake magnitudes from digital data, <http://www.iaspei.org/commissions/CSOI.html#wgmm>, [http://www.iaspei.org/commissions/CSOI/summary\\_of\\_WG\\_recommendations\\_2005.pdf](http://www.iaspei.org/commissions/CSOI/summary_of_WG_recommendations_2005.pdf).
- IASPEI (2013), Summary of magnitude working group recommendations on standard procedures for determining earthquake magnitudes from digital data, [http://www.iaspei.org/commissions/CSOI/Summary\\_of\\_WG\\_recommendations\\_20130327.pdf](http://www.iaspei.org/commissions/CSOI/Summary_of_WG_recommendations_20130327.pdf).
- IDC (1999), IDC processing of seismic, hydroacoustic and infrasonic data, *IDC Documentation*.
- Jeffreys, H., and K. E. Bullen (1940), *Seismological Tables*, British Association for the Advancement of Science.
- Kanamori, H. (1977), The energy release in great earthquakes, *J. Geophys. Res.*, *82*, 2981–2987.

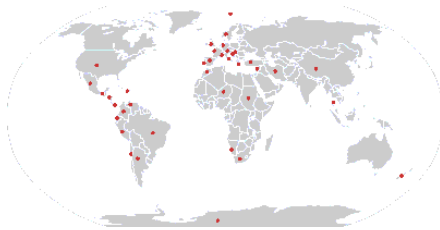
- Kennett, B. L. N. (2006), Non-linear methods for event location in a global context, *Physics of the Earth and Planetary Interiors*, 158, 45–64.
- Kennett, B. L. N., E. R. Engdahl, and R. Buland (1995), Constraints on seismic velocities in the Earth from traveltimes, *Geophysical Journal International*, 122, 108–124.
- Kennett, B. L. N., E. R. Engdahl, and R. Buland (1996), Ellipticity corrections for seismic phases, *Geophysical Journal International*, 127, 40–48.
- Lee, W. H. K., R. Bennet, and K. Meagher (1972), A method of estimating magnitude of local earthquakes from signal duration, *U.S. Geol. Surv.*, Open-File Rep.
- Lentas, K., D. D. Giacomo, J. Harris, and D. A. Storchak (2019), The ISC Bulletin as a comprehensive source of earthquake source mechanisms, *Earth System Science Data*, 11(2), 565–578, <https://doi.org/10.5194/essd-11-565-2019>.
- Leptokaropoulos, K. M., A. K. Adamaki, R. G. Roberts, C. G. Gkarlaouni, and P. M. Paradisopoulou (2018), Impact of magnitude uncertainties on seismic catalogue properties, *Geophysical Journal International*, 213(2), 940–951, <https://doi.org/10.1093/gji/ggy023>.
- Murphy, J. R., and B. W. Barker (2006), Improved focal-depth determination through automated identification of the seismic depth phases pP and sP, *Bulletin of the Seismological Society of America*, 96, 1213–1229.
- NMSOP-2 (2012), *New Manual of Seismological Observatory Practice (NMSOP-2)*, IASPEI, GFZ, German Research Centre for Geosciences, Potsdam, <https://doi.org/10.2312/GFZ.NMSOP-2>, <http://nmsop.gfz-potsdam.de>, urn:nbn:de:kobv:b103-NMSOP-2.
- Nuttli, O. W. (1973), Seismic wave attenuation and magnitude relations for eastern North America, *J. Geophys. Res.*, 78, 876–885.
- Richter, C. F. (1935), An instrumental earthquake magnitude scale, *Bulletin of the Seismological Society of America*, 25, 1–32.
- Ringdal, F. (1976), Maximum-likelihood estimation of seismic magnitude, *Bulletin of the Seismological Society of America*, 66(3), 789–802.
- Sambridge, M. (1999), Geophysical inversion with a neighbourhood algorithm, *Geophysical Journal International*, 138, 479–494.
- Sambridge, M., and B. L. N. Kennett (2001), Seismic event location: non-linear inversion using a neighbourhood algorithm, *Pure and Applied Geophysics*, 158, 241–257.
- Storchak, D. A., J. Schweitzer, and P. Bormann (2003), The IASPEI standard seismic phases list, *Seismological Research Letters*, 74(6), 761–772.
- Storchak, D. A., J. Schweitzer, and P. Bormann (2011), Seismic phase names: IASPEI Standard, in *Encyclopedia of Solid Earth Geophysics*, edited by H.K. Gupta, pp. 1162–1173, Springer.
- Storchak, D. A., J. Harris, L. Brown, K. Lieser, B. Shumba, R. Verney, D. Di Giacomo, and E. I. M. Korger (2017), Rebuild of the Bulletin of the International Seismological Centre (ISC), part 1: 1964–1979, *Geoscience Letters*, 4(32), <https://doi.org/10.1186/s40562-017-0098-z>.
- Storchak, D. A., J. Harris, L. Brown, K. Lieser, B. Shumba, and D. Di Giacomo (2020), Rebuild of the Bulletin of the International Seismological Centre (ISC)-part 2: 1980–2010, *Geoscience Letters*, 7(18), <https://doi.org/10.1186/s40562-020-00164-6>.
- Stähler, S., and K. Sigloch (2014), Fully probabilistic seismic source inversion—Part 1: Efficient parameterisation, *Solid Earth*, 5(2), 1055–1069, <https://doi.org/10.5194/se-5-1055-2014>.
- Stähler, S., and K. Sigloch (2016), Fully probabilistic seismic source inversion—Part 2: Modelling errors and station covariances, *Solid Earth*, 7(6), 1521–1536, <https://doi.org/10.5194/se-7-1521-2016>.
- Tsuboi, C. (1954), Determination of the Gutenberg-Richter’s magnitude of earthquakes occurring in and near Japan, *Zisin (J. Seism. Soc. Japan)*, Ser. II(7), 185–193.
- Tsuboi, S., K. Abe, K. Takano, and Y. Yamanaka (1995), Rapid determination of Mw from broadband P waveforms, *Bulletin of the Seismological Society of America*, 85(2), 606–613.

- Uhrhammer, R. A., and E. R. Collins (1990), Synthesis of Wood-Anderson Seismograms from Broadband Digital Records, *Bulletin of the Seismological Society of America*, *80*(3), 702–716.
- Vaněk, J., A. Zapotek, V. Karnik, N. V. Kondorskaya, Y. V. Riznichenko, E. F. Savarensky, S. L. Solov'yov, and N. V. Shebalin (1962), Standardization of magnitude scales, *Izvestiya Akad. SSSR., Ser. Geofiz.*(2), 153–158, Pages 108–111 in the English translation.
- Villaseñor, A., and E. R. Engdahl (2005), A digital hypocenter catalog for the International Seismological Summary, *Seismological Research Letters*, *76*, 554–559.
- Villaseñor, A., and E. R. Engdahl (2007), Systematic relocation of early instrumental seismicity: Earthquakes in the International Seismological Summary for 1960–1963, *Bulletin of the Seismological Society of America*, *97*, 1820–1832.
- Wessel, P., J. F. Luis, L. Uieda, R. Scharroo, F. Wobbe, W. H. F. Smith, and D. Tian (2019), The Generic Mapping Tools version 6, *Geochemistry, Geophysics, Geosystems*, *20*, 5556–5564, <https://doi.org/10.1029/2019GC008515>.
- Weston, J., E. Engdahl, J. Harris, D. Di Giacomo, and D. Storchack (2018), ISC-EHB: Reconstruction of a robust earthquake dataset, *Geophys. J. Int.*, *214*(1), 474–484, <https://doi.org/10.1093/gji/ggy155>.
- Woessner, J., and S. Wiemer (2005), Assessing the quality of earthquake catalogues: estimating the magnitude of completeness and its uncertainty, *Bulletin of the Seismological Society of America*, *95*(2), <https://doi.org/10.1785/0120400007>.
- Young, J. B., B. W. Presgrave, H. Aichele, D. A. Wiens, and E. A. Flinn (1996), The Flinn-Engdahl regionalisation scheme: the 1995 revision, *Physics of the Earth and Planetary Interiors*, *96*, 223–297.





**SARA electronic instruments s.r.l.** your reliable and friendly partner in earthquake monitoring and geophysical exploration.



Since 2000 SARA is specialized in the design and production of instruments and software for applied geophysics, seismological and structural monitoring, devices with high technological content and best price-quality ratio.



Broad band seismometers  
- Observatory grade  
- Compact  
- Borehole



DoReMi  
digital telemetry  
exploration  
seismograph.



Strong motion  
AceBox



Modal analysis  
Digital Array



Seismic stations  
VelBox



## GEOEXPLORER

Processing software suite to perform fast and reliable quality data check and analysis of elasto-mechanical properties of soil before construction or before deploying a seismic station.

- MASW
- HVSr
- REFRACT
- MARW
- DH
- SSV

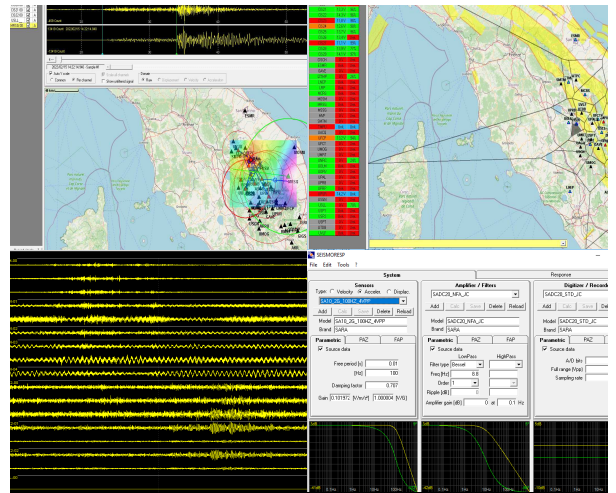
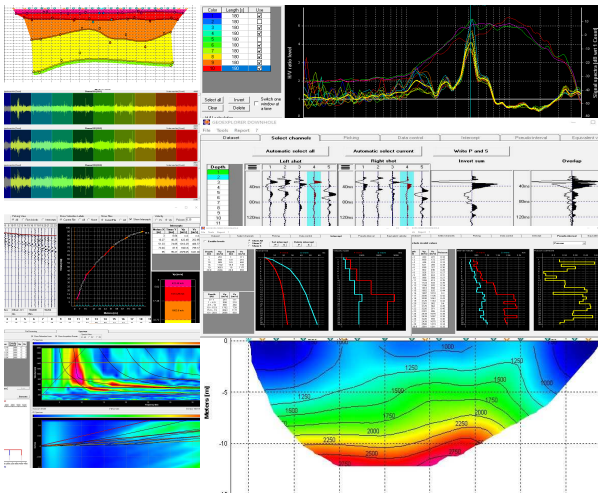


## SEISMOWIN

Modules for earthquakes, seismic and microseismic monitoring.

Capable to:

- Handle hundreds of channels
- Maintain and design networks
- Locate and analyse earthquakes
- Calculate transfer functions
- Plot all events location
- Monitor stations status of health
- Send alerts
- And more...



Via Angelo Morettini, 11 06128 Perugia  
 +39 075 5051014  
 www.sara.pg.it - info@sara.pg.it





# PERFECTLY PAIRED



**arolla** + **nair<sup>slim</sup>**  
VE series broadband seismometer      GMS series recorder / digitiser

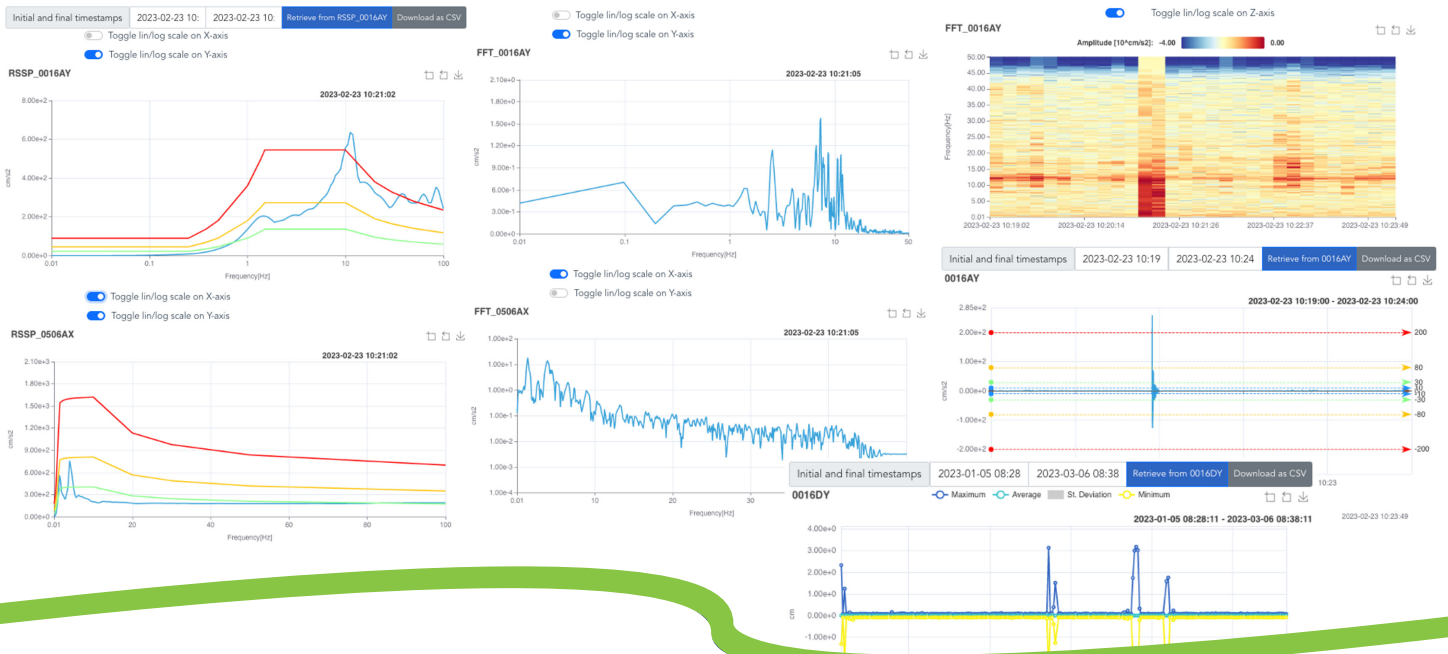
The **arolla** broadband seismometer features a compact and lightweight design, yet it is rugged and versatile, making it an ideal choice for many applications. Weak-motion, broadband seismometers have the highest sensitivity among seismometers over long periods, and are able to pick up even small tremors at great distances.

The culmination of years of experience designing reliable, high-precision, low-noise seismic equipment enabled the creation of **arolla**.

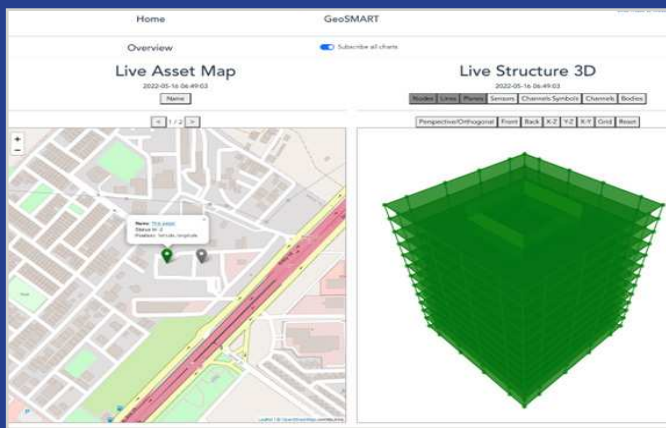
Best paired with **arolla** is **nair<sup>slim</sup>**—GeoSIG’s latest generation seismic recorder that offers highest performance, excellent operational flexibility and enhanced connectivity. GeoSIG’s **nair<sup>slim</sup>** is a self-contained instrument that acquires and processes data in real time. It boasts an impressive 146db (0.01-30Hz), making it suitable for weak motion precision recording. A set comprising **arolla** and **nair<sup>slim</sup>** is fully compatible with existing GeoSIG systems that may already be in place. Also, its simple upgrade path makes **nair<sup>slim</sup>** “future proof.”

A winning combination: **arolla** and **nair<sup>slim</sup>**!

**GeoSIG**  
swiss made to measure 



**GeoSIG**  
swiss made to measure



## GeoSMART Offers Peak Performance

GeoSMART is an innovative graphical application that provides **tools** for realtime structural health monitoring for civil engineering structures. GeoSMART, with its “smart” features, can **monitor** and display the status of a structure that is equipped with GeoSIG measuring instruments. GeoSMART is S2HM in a Box; it has been designed to meet fundamental engineering requirements with respect to **structural health** monitoring applications.

## Main Features of GeoSMART

- ◆ Support for any type of sensor such as acceleration, velocity, displacement, tilt, wind, temperature, strain, and many more.
- ◆ User-friendly web-interface for an intuitive experience.
- ◆ 3D representation of any structure with live status.
- ◆ Interactive zoom, rotate, pan, visibility and projection.
- ◆ Multiple structures on live interactive map.
- ◆ Real-time continuous data acquisition and processing.
- ◆ Storage and direct download of all data and graphics.
- ◆ Data export for long-term storage.
- ◆ Sliding window-based continuous frequency analyses: Amplitude, Spectrogram and Response Spectra.
- ◆ Rigid body motions in translations and rotations.
- ◆ Interpolations for non-instrumented areas.
- ◆ Interstory drift ratios and torsion.
- ◆ Exceedance of predefined threshold levels or curves.
- ◆ Plot of archive data and statistical information.
- ◆ Live screen indicators and HTML formatted emails.
- ◆ Individualised notifications to users / user groups.
- ◆ Customisable messages such as action plans.
- ◆ Reports including actual images of plotted graphics.
- ◆ Hardware relays to start or shutdown any process.
- ◆ Advanced user accessible powerful database.
- ◆ API to fetch and externally manipulate the stored data.

GeoSIG Ltd | Wiesenstrasse 39  
8952 Schlieren, Switzerland  
T: +41 44 810 2150 | F: +41 44 810 2350  
[www.geosig.com](http://www.geosig.com)

For more information, contact us at [info@geosig.com](mailto:info@geosig.com)





[www.gaiacode.com](http://www.gaiacode.com)

### **The World's First Hybrid Seismometer from Gaiacode**

With the newly designed PICO three component broadband feedback instrument Gaiacode is introducing the first hybrid seismometer in the world. Small, lightweight, versatile and easy to install, PICO sets a new standard for all seismic measurements at higher frequencies, without compromising the performance in the longer period teleseismic band.

Suited for rapid deployments in temporary installations, PICO can also be used in array configurations or in more permanent networks.



### **What is a hybrid seismometer?**

Typically, the output of seismic instruments is proportional either to the velocity or the acceleration of ground motions. Seismometers with velocity outputs are mostly used for measuring weak motions like seismic waves stemming from earthquakes at regional or teleseismic distances. On the other hand, instruments with acceleration output record strong motions and are commonly called accelerometers.

PICO's hybrid response combines the best of both worlds, by simultaneously providing two analogue outputs: one proportional to the velocity, the other to the acceleration of the ground motion. This approach has the advantage that over the whole passband both the rich information content of a typical acceleration response can be recorded without losing the sensitivity of a velocity proportional weak motion signal.

### **How do we get the hybrid response of the PICO?**

Gaiacode achieves this unique response characteristic by adding specially designed circuitry to the mechanical side of the PICO before its signal gets processed in its feedback loop. Adding such circuitry allows us also to remotely change the low frequency cutoff (3dB) points without having to physically remove the seismometer from the installation. We offer eight different responses with low frequency cutoff points between 120 sec and 1 sec.

The instruments are delivered with a Gaiacode designed rotatable, waterproof connector (<https://www.gaiacode.com/news/item/95-a-new-type-of-connector>). Its position can be adjusted over a wide range of angles up to 270 degrees. This flexibility allows for easy installation even in postholes or other tight locations.

